

POLITECNICO DI MILANO

Scuola di Ingegneria Industriale e dell'Informazione

Corso di Laurea Magistrale in Ingegneria Biomedica



**VALUTAZIONE SPERIMENTALE E
COMPUTAZIONALE DEL RISCHIO DI
RIFRATTURA DEL RADIO IN SEGUITO ALLA
RIMOZIONE DELLE VITI DA OSTEOSINTESI**

Relatore: Ing. Tomaso Villa

Correlatori: Dr. Stefano Brianza

Dr. Ing. Christian Wissner

Tesi di laurea di:
FEDERICO VICENZI

Matricola: **786682**

Anno Accademico 2013-2014

Index

| | |
|-----------------------------------|-----------|
| INDEX | 3 |
| ABSTRACT - ENGLISH | 5 |
| ABSTRACT - ITALIAN | 6 |
| 1. BACKGROUND..... | 7 |
| 1.1 Radius and forearm | 7 |
| 1.2 Fractures..... | 13 |
| 1.2.1 Bone Healing..... | 21 |
| 1.3 Fracture management | 23 |
| 1.3.1 Surgical Approaches | 29 |
| 1.4 Screw removal..... | 31 |
| 1.5 Re-fractures..... | 34 |
| 2. EXPERIMENTAL TEST | 36 |
| 2.1 Material and Methods | 36 |
| 2.1.1 Clinical Decisions | 36 |
| 2.1.2 Test Definition | 41 |
| 2.2 Experimental test 1..... | 57 |
| 2.2.1 Sample definition | 57 |
| 2.2.2 Test Performance | 64 |
| 2.2.3 Results..... | 70 |
| 2.3 Experimental test 2..... | 73 |
| 2.3.1 Sample definition | 73 |
| 2.3.2 Test Performance | 74 |
| 2.3.3 Results..... | 78 |
| 3. COMPUTATIONAL TEST..... | 83 |
| 3.1 Materials and Methods..... | 83 |
| 3.1.1 Convergence Analysis..... | 88 |
| 3.1.2 Validation..... | 94 |
| 3.2 Computational Results | 97 |

| | |
|--|------------|
| 4. DISCUSSION AND CONCLUSIONS | 99 |
| 4.1 Discussion | 99 |
| 4.1.1 Experimental Test | 99 |
| 4.1.2 Computational Test | 101 |
| 4.2 Conclusions | 114 |
| 4.3 Future developments | 117 |
| | |
| ATTACHMENT 1 | 119 |
| ATTACHMENT 2 | 122 |
| ATTACHMENT 3 | 123 |
| ATTACHMENT 4 | 125 |
| ATTACHMENT 5 | 126 |
| ATTACHMENT 6 | 133 |
| | |
| BIBLIOGRAPHY | 138 |

Abstract - English

Introduction Literature analysis showed that re-fracture of forearm bones has 1 – 35% clinical incidence and one of its main causes is the presence of holes, after the removal of plate and screws, which act as stress risers. The aim of this work was the quantitative evaluation of the influence that different holes left by screw removal have on the re-fracture risk of the radius during mechanical loading.

Test definition The design of the specimens to test and of the type of test to be performed required various considerations to be made. From a clinical point of view the fracture type for which plate implant was simulated was a transverse fracture, the surgical approach was the Henry approach, the plates used were 7 hole plates (Stryker VariAx straight narrow plate and DePuy Synthes LCP plates) with six screws (bone and locking screws). The biomechanical analysis of the forearm in supinated position with a 90° elbow flexion (most common biomechanical model of the forearm) led to the decision of performing a 4-point bending test on the radius bone with tensioning of the volar surface. This appeared to be the worst case loading of the forearm bones and in particular of the radius.

The experimental test was performed on Sawbones® radius samples on which the Stryker VariAx plate with 3.5mm and 2.7 mm screws was implanted and removed and on samples with no holes, which were taken as reference sample. The samples were loaded until failure and the energy to failure of each group was calculated.

The computational test was performed on radius models with no holes, single holes (2.7mm, 3.5mm and 4.5 mm) and multiple holes (simulation of the previous presence of a plate). The radius models were virtually loaded until failure which was reached when the maximum principal stress equaled the σ_{\max} defined for the cortical bone. After the plot of the force-displacement curve the energy to failure was calculated.

The comparisons between different groups were performed calculating the ratio between the energy to failure of the samples with no holes and the samples with holes ($\alpha = E_{\text{NoHoles}} / E_{\text{Holes}}$). Groups which show higher values of α represent a safer situation in terms of re-fracture risk of the bone in correspondence of a bending loading.

Results and conclusions The analysis of the results showed that the safer situation was given by the presence of smaller holes (2.7mm) even if not a great difference was noticed in comparison to the other groups. The statistical analysis performed on the results of the experimental test showed in fact a non-statistical difference between the samples with 2.7mm and with the 3.5mm multiple holes.

The main output of both experimental and computational tests highlighted an important reduction of the energy to failure (max reduction = -80%) when holes were present on the structure suggesting particular care of the forearm during the period immediately after hardware removal until the defects are filled with newly formed bone.

Abstract - Italian

Introduzione Una ricerca bibliografica ha evidenziato come la ri-frattura delle ossa dell'avambraccio presenti un'incidenza che varia nell'intervallo 1-35% e come una delle cause di tale problematica sia la presenza di fori, dopo la rimozione di placca e viti, che agiscono da concentratori di stress. L'obiettivo del presente lavoro è di valutare da un punto di vista quantitativo l'influenza che fori diversi hanno sul rischio di ri-frattura del radio in corrispondenza dell'applicazione di specifici carichi.

Definizione dei test La progettazione dei campioni da testare e del tipo di test da eseguire ha richiesto la considerazione di diversi aspetti. Da un punto di vista clinico la tipologia di frattura per la quale si è scelta di simulare l'impianto della placca è stata la frattura trasversale, l'approccio chirurgico è stato l'approccio di Henry, le placche usate presentavano 7 fori (Stryker VariAx straight narrow plate e DePuy Synthes LCP plate) con sei viti (bone screws e locking screws). L'analisi biomeccanica dell'avambraccio in posizione supina con il gomito flesso di 90° (modello comune per quanto riguarda lo studio dell'avambraccio) ha portato alla decisione di realizzare una flessione a 4 punti sul modello di radio con tensionamento della superficie anteriore dell'osso. Questa tipologia di carico è stata scelta perché ritenuta il caso peggiore per quanto riguarda le sollecitazioni presenti fisiologicamente sull'avambraccio stesso.

Il test sperimentale è stato realizzato su modelli di radio dell'azienda Sawbones® sui quali sono state impiantate e rimosse placche VariAx Stryker con viti 3.5 mm e 2.7 mm e su modelli senza fori, che sono stati presi come campioni di riferimento. Ciascun campione è stato testato fino a fallimento ed è stata calcolata l'energia necessaria per portare a cedimento la struttura.

Le simulazioni computazionali sono state eseguite, invece, su modelli di radio senza fori, con fori singoli (2.7 mm, 3.5 mm e 4.5 mm) e con fori multipli (riproduzione della rimozione di placche da osteosintesi). I modelli computazionali sono stati virtualmente caricati fino a fallimento che avviene nel momento in cui il massimo stress principale raggiunge σ_{max} definito per l'osso corticale. Si è quindi realizzato il grafico forza – spostamento da cui si è calcolata l'energia necessaria per portare a fallimento l'osso.

Il confronto tra i diversi gruppi è stato eseguito calcolando il rapporto tra energia a rottura dei campioni senza fori e con fori ($\alpha = E_{NoHoles} / E_{Holes}$). I gruppi che mostrano valori maggiori di α rappresentano una situazione più sicura per quando riguarda il rischio di ri-frattura del radio in corrispondenza di carichi flessionali.

Risultati e conclusioni L'analisi dei risultati ha mostrato che la situazione migliore (più sicura) per quanto riguarda l'energia a rottura è data dalla presenza delle viti da 2.7 mm anche se la differenza con gli altri gruppi soggetti ai test non è marcata. L'analisi statistica dei dati ottenuti dal test sperimentale ha mostrato, infatti, una differenza statisticamente non significativa tra i gruppi con fori multipli da 2.7mm e da 3.5mm.

Il risultato principale ottenuto sia dal test computazionale sia dal test sperimentale è quello di aver evidenziato la notevole riduzione dell'energia a rottura (massima riduzione = -80%) quando fori sono presenti sull'osso. Questo risultato suggerisce di prestare particolare attenzione nel periodo immediatamente successivo alla rimozione di placca e viti, fino al momento in cui i fori vengono riempiti da nuovo tessuto osseo.

1. Background

1.1 Radius and forearm

The **radius** is one of the two large bones of the forearm. It extends from the lateral side of the elbow to the thumb side of the wrist and runs, during supinated or neutral position, parallel to the ulna, which is the second bone of the forearm [1]. The radius is therefore the most lateral of the two bones while the ulna is the most medial one, when the arms are in anatomical position.

The radius is named for its action, a turning movement about the capitulum of the humerus, which allows the bone to rotate relative to the more fixed ulna. [2] It can be divided in a proximal end, a shaft and a distal end. The proximal end has a head which is disk-shaped and a tuberosity which gives attachment to the biceps muscle. The shaft possesses three borders (interosseous, anterior and posterior) and three surfaces (anterior, posterior and lateral). [3] The distal end forms two palpable points, laterally the styloid process and medially the Lister's tubercle. [4] The radius usually carries two-thirds of the loads on the forearm while the ulna the remaining one-third. [5]

The interosseous membrane is a thick sheet of collagenous tissue between the interosseous borders of the two bones. Its main functions are helping spreading correctly the compression forces between the radius and the ulna, increasing the area of origin of two forearm muscles (deep flexor and extensor of the forearm), stabilizing the forearm bones and allowing smooth forearm rotation. [6] [7] The described bones are shown in Figure 1.

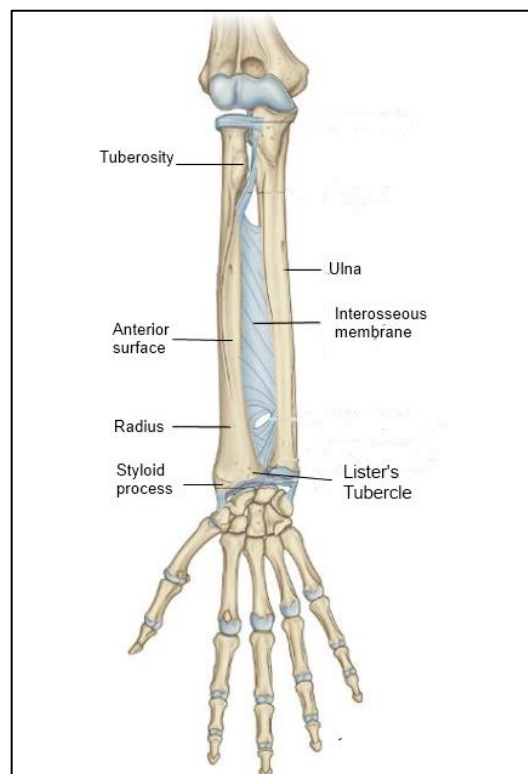


Figure 1: Forearm and hand bones [8]

The radius articulates with the humerus (humero-radial joint), with the carpal bones (radio-carpal joint or wrist joint) and with the ulna (superior, middle and inferior radio-ulnar joints).

The **humero-radial joint** is the joint between the head of the radius and the capitulum of the humerus. It is an arthrodiar joint and is one of the two joints forming the elbow articulation.

It is not directly involved in the hinge movement at the elbow, since the ends of the respective bones are scarcely in contact during flexion. The humero-radial articulation is only passively involved in the pivot movement of the proximal radio-ulnar joint, since the radius rotates in the socket about its long axis, and the actual rotation takes place in the proximal and distal radio-ulnar articulations.

However, the main articulation of the elbow is the **humero-ulnar joint** which is classified as a simple hinge-joint and allows movements of flexion, extension and circumduction but does not involve the radius bone, which is of major interest for this work. [9]

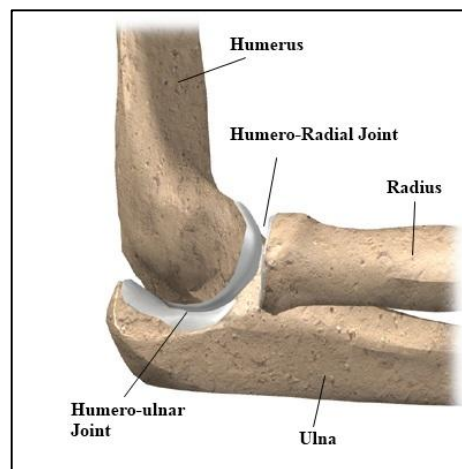


Figure 2: Humero-radial joint [10]

The **radio-carpal joint** is a condyloid articulation. It is formed by the lower end of the radius and the navicular, lunate, and triangular bones. The radius and the three involved carpal bones are separated by an articular disk. The articular surface of the radius and the under surface of the articular disk form together a transversely elliptical concave surface, the receiving cavity.

The superior articular surfaces of the navicular, lunate and triangular form a smooth convex surface, the condyle, which is received into the concavity. [9]

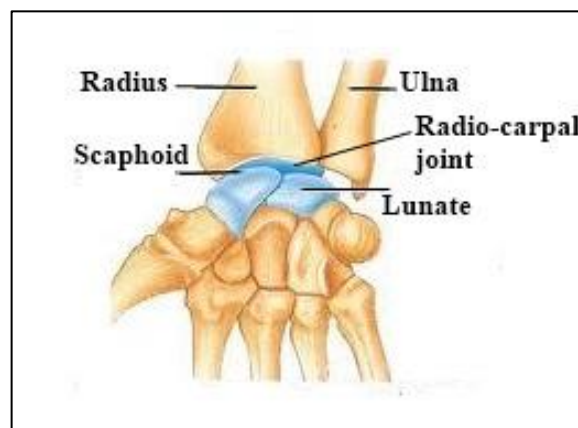


Figure 3: Radio-carpal joint [11]

The **superior (or proximal) radio-ulnar joint** is a pivot type of synovial joint between the disc-like head of the radius and the radial notch on the upper end of the ulna. The head of the radius is held against the radial notch of the ulna by a strong band called the annular ligament. Together, the annular ligament and the radial notch provide stability for the head of the radius during pronation and supination of the forearm. [6] [7] (Figure 4 left)

The **middle radio-ulnar joint (or interosseous membrane)** is a complex structure actually formed by various portions. The interosseous membrane was briefly described in the previous pages and in Figure 1. [6]

The **inferior radio-ulnar joint** is a pivot type of synovial joint between the head of the ulna and the ulnar notch on the lower end of the radius. An articular disc is attached between the styloid process of the ulna and the ulnar notch of the radius. It excludes the ulna from the wrist joint and provides the ulnar head a platform to rotate during movements of supination and pronation. [6] (Figure 4 - right).

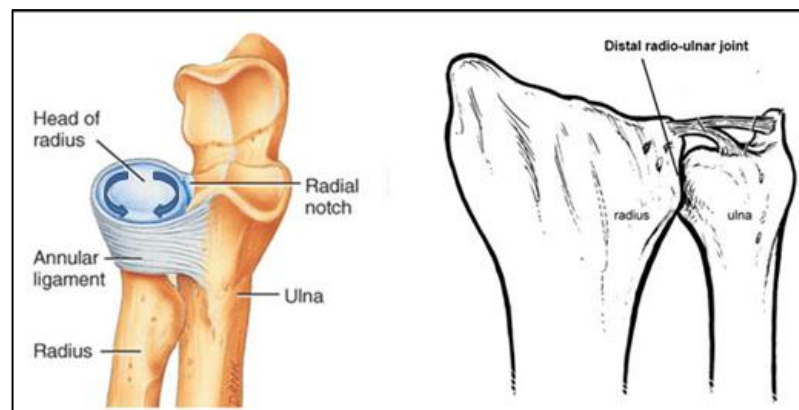


Figure 4: Left: Proximal radio-ulnar joint [11] ; Right: Distal radio-ulnar joint [12]

Various muscles find insertion on the radius bone and each one of them accomplishes one or more specific functions.

The **biceps brachii** muscle is a muscle of the anterior compartment of the arm and it originates from two tendinous heads attached to the scapula. These heads fuse to form one unique body and find insertion in the posterior part of the radial tuberosity. An expansion of the medial border of the tendon (bicipital aponeurosis) is attached to the deep fascia of the forearm and through it to the posterior border of the ulna.

The biceps brachii, therefore, crosses three joints (shoulder, elbow and superior radio-ulnar joint) on which it can exert its action. In particular, on the radio-ulnar joint it acts as a supinator of the forearm and on the elbow and shoulder as a flexor. [6]

The **pronator teres** muscle originates with two heads: a humeral head which is larger and more superficial and an ulnar head which is deeper and smaller. The two heads join each other and the combined muscle passes obliquely across the proximal forearm and inserts in the area of maximum convexity on the lateral surface of the radius. The functions of the pronator teres are primarily of forearm pronator and secondarily of elbow flexor. [6]

The **pronator quadratus** muscle is a flat muscle that arises from the anterior surface of the lower shaft of the ulna and inserts on the lower portion of the radius. This muscle is the chief pronator of the forearm and is assisted by the above described pronator teres. [6]

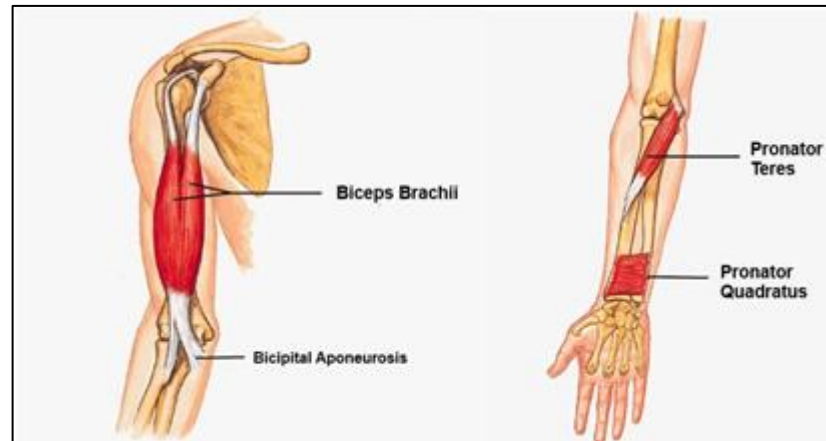
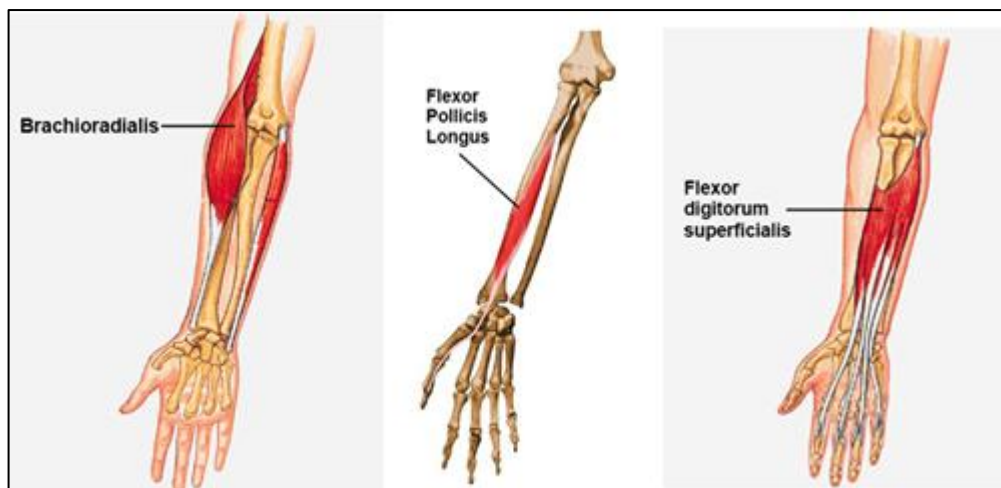


Figure 5: Left: Biceps brachii; Right: Pronator teres and pronator quadratus [8]

The **brachioradialis** originates from the upper two-thirds of the lateral supracondylar ridge of the humerus and is inserted in the radius just above the styloid process. This muscle acts as a flexor of the elbow joint especially when the forearm is in midprone position. [6] The **flexor pollicis longus** muscle arises from the anterior surface of the radius and from the adjacent interosseous membrane and inserts at the base of the distal phalanx of the thumb. This muscle is a flexor of the phalanx of the thumb and when this is flexed it also assists the flexion of the wrist. [9]

The **flexor digitorum superficialis** is a broad muscle that lies under the flexor muscles. It originates with two heads (humero-ulnar and radial heads) and reaches the base of the proximal phalanxes with four independent tendons. This muscle acts as a flexor of the middle phalanxes and as a weak flexor of the proximal phalanxes. [6] These three described muscles are shown in Figure 6



*Figure 6: Left: Brachioradialis muscle [8]; Center: Flexor pollicis longus [13]
Right: Flexor digitorum superficialis muscles [8]*

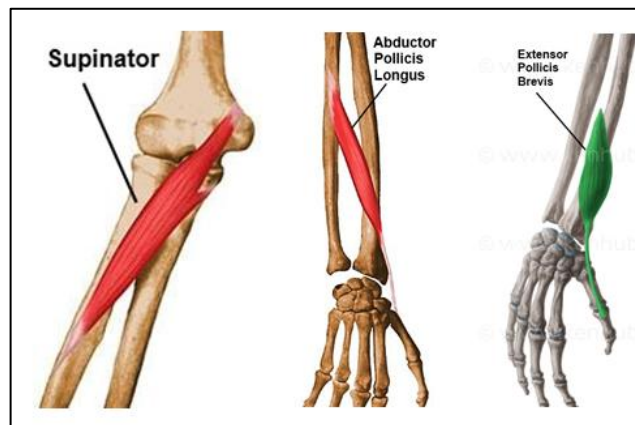
The **supinator** muscle belongs to the extensor compartment of the forearm. It is attached to three bones (humerus, radius and ulna) and is disposed in two laminae which both insert on the lateral proximal radius shaft. [6] The supinator acts, as suggested by its name, to bring the hand into the supinated position. [14] The **abductor pollicis longus** lies immediately below the supinator and is sometimes united with it. It arises from the lateral part of the dorsal surface of the body of the ulna,

from the interosseous membrane, and from the middle third of the dorsal surface of the body of the radius. [9] [14]

The insertion is divided into two parts: the superficial part is inserted into the base of the first metacarpal bone and the deep part is variably inserted into the trapezium, the joint capsule and its ligaments, and into the belly of the abductor pollicis brevis. [15]

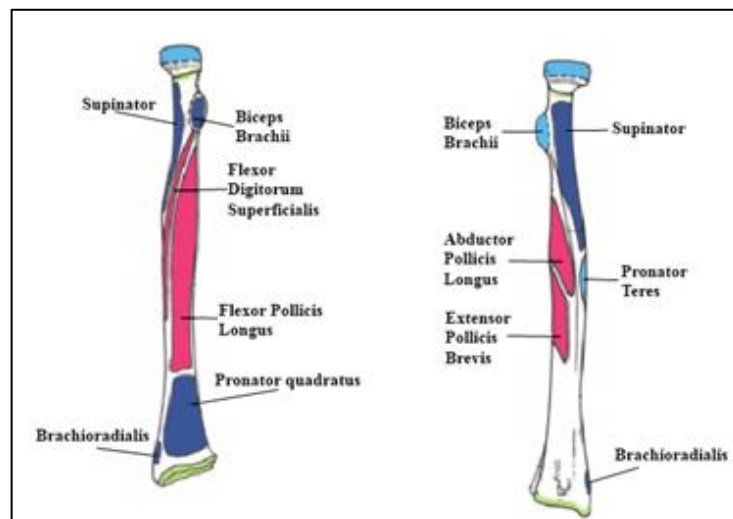
The **extensor pollicis brevis** arises from the dorsal distal portion of the radius and from the interosseous membrane. Its direction is similar to the one of the abductor pollicis longus and is inserted into the base of the first phalanx of the thumb.

In a close relationship to the abductor pollicis longus, the function of the extensor pollicis brevis is to both extend and abduct the thumb. [14] The above presented muscles are shown in Figure 7.



*Figure 7: Left: Supinator; Center: Abductor Pollicis Longus [13]
Right: Extensor Pollicis Brevis muscles [16]*

The complete overview of the muscle attachment sites on the radius is shown, for the right radius bone, in Figure 8.



*Figure 8: Muscle attachments on the radius.
Left:Anterior surface; Right:Posterior/Lateral surface [3]*

One of the most important functions of the forearm complex is permitting the rotation of the hand in space (pronation and supination). Every day activities, in fact, can be carried out only if the interactions between the proximal radio-ulnar joint, the interosseous membrane and the distal radio-ulnar joint are coordinated. Damages or malfunctioning of any of these regions may lead to limitations in forearm rotation which is fundamental for performing correctly even the most common and simple actions. [7]

The mechanism which leads to forearm pronation and supination is quite complex: the ulnar head moves in a rolling and sliding motion in the rim of the sigmoid notch while the radius rotates around the ulnar head in the most distal compartments.

This kind of movement allows the radius to cross the ulna when the hand is in pronation and causes the two bones to be parallel when the hand is in supination.

The rotation of the forearm permits directing the palm of the hand upwards, neutrally and downwards. The maximum range of motion is 82° in supination and 75° in pronation, referring to the neutral position and with the elbow flexed. [17] [18] Figure 9 shows the forearm bones and the main muscles involved during pronation and supination.

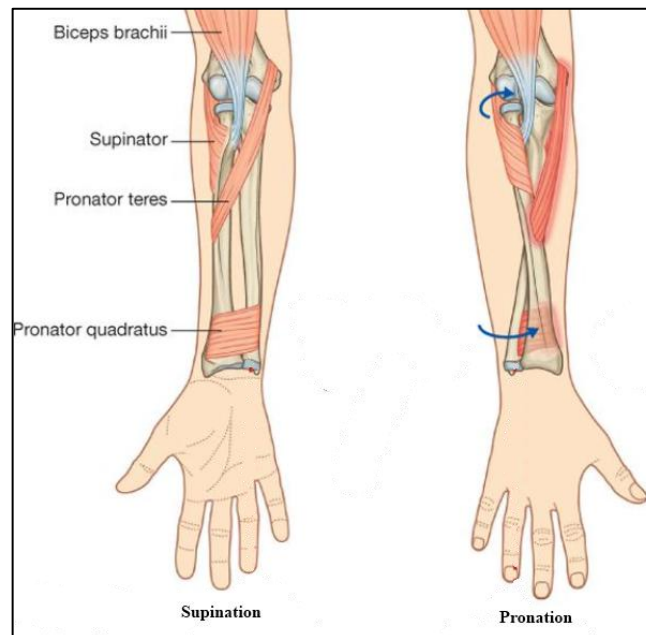


Figure 9: Forearm in supinated and pronated position [11]

1.2 Fractures

A bone fracture is defined as a medical condition in which there is a break in the continuity of the bone. It can be the result of high force impact or stress and can be favored by certain medical conditions that weaken the bone structure, such as osteoporosis, presence of holes and defects, bone cancer or other pathological situations [19] The fracture of a bone usually occurs in a fraction of second. [20]

Fractures can be of various types in terms of location, shape, severity, etc. A classification system of all the fractures was needed in order to facilitate communication between clinicians and permit a better management of the patient's clinical cases. Various classification systems were proposed during the years but with small success.

The combined efforts of the OTA and of Prof. Müller gave birth to the "Muller AO/OTA Classification" which had the major aim to develop a universally applicable and universally acceptable terminology.

This classification is still the most used and is based on an alpha-numerical coding system which allows the localization and the morphological characterization of fractures. Each major long bone or anatomical region as well as each bone segment (bone region) is named and numbered. The fractures of each bone segment are then divided in three types with a further subdivision into three groups and subgroups, generating a hierarchical organization.

Each type of fracture can be characterized by a specific code, formed by 5 parts, which is shortly described below. [21] [20]

- 1) The fractured bone or anatomical region is identified by the first number of the code as can be seen in Figure 10. It should be noted that the radius and ulna bones are identified by the same number (#2)

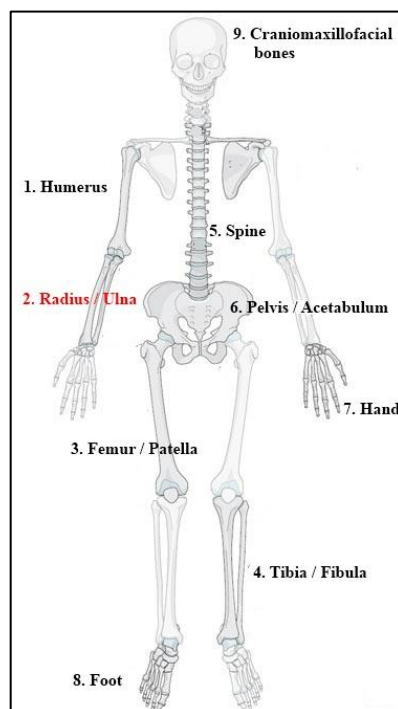


Figure 10: Bone numbering according to AO/OTA classification [22]

- 2) The second part of the code identifies the segment of the long bone subject to the fracture as shown in Figure 11. (#1: proximal epiphysis; #2: diaphysis; #3: distal epiphysis)

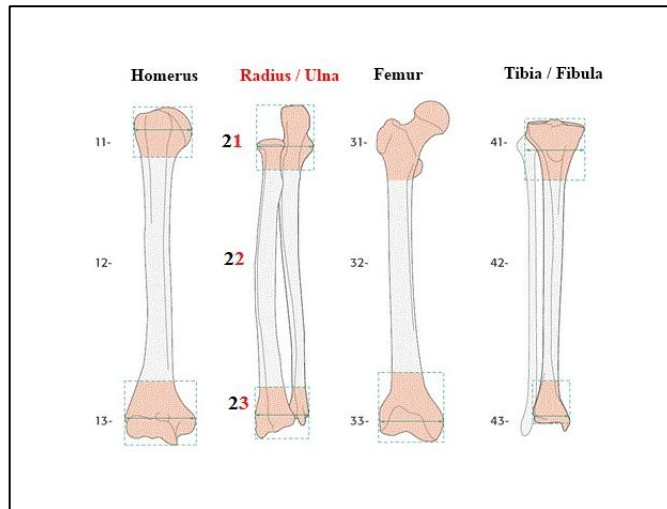


Figure 11: Bone segment numbering according to AO/OTA classification [22]

- 3) The third part of the code is represented by a letter (A, B or C) which indicates the type of fracture. The description of the type of fractures differs between diaphyseal fractures and proximal or distal epiphyseal fractures as shown in Figure 12.

| Segment | Type | | |
|--------------|--|--|--|
| | A | B | C |
| 1 Proximal | <p>Extraarticular</p> <p>No involvement of displaced fractures extending into the articular surface</p> | <p>Partial articular</p> <p>Part of the articular component is involved, leaving the other part attached to the meta-/diaphysis</p> | <p>Complete articular</p> <p>Articular surface involved, metaphyseal fracture completely separates articular component from the diaphysis</p> |
| 2 Diaphyseal | <p>Simple</p> <p>One fracture line, cortical contact between fragments exceeds 90% after reduction</p> | <p>Wedge</p> <p>Three or more fragments, main fragments have contact after reduction</p> | <p>Complex</p> <p>Three or more fragments, main fragments have no contact after reduction</p> |
| 3 Distal | <p>Extraarticular</p> <p>No involvement of displaced fractures extending into the articular surface</p> | <p>Partial articular</p> <p>Part of the articular component is involved, leaving the other part attached to the meta-/diaphysis</p> | <p>Complete articular</p> <p>Articular surface involved, metaphyseal fracture completely separates articular component from the diaphysis</p> |

Figure 12: Fracture type definition according to AO/OTA classification [22]
The fracture types of interest for this study (diaphyseal) are highlighted

- 4) Once a fracture has been recognized as one of the three types presented above (A, B, C) it may be further divided into three fracture groups as shown in Figure 13 for diaphysis fractures and in Figure 14 for epiphysis fractures. The groups which describe in more detail the diaphyseal fractures are of major interest for the purpose of this work










| Type | Group | | |
|------------------|--|---|---|
| | 1 | 2 | 3 |
| A Simple |  Spiral |  Oblique |  Transverse |
| B Wedge |  Spiral |  Bending |  Multifragmentary |
| C Complex |  Spiral |  Segmental |  Irregular |

Figure 13: Classification of diaphysis fractures into 3 fracture groups [22]

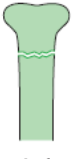


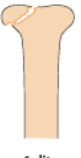
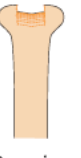
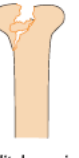
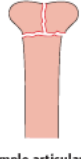

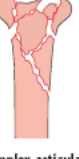
| Type | Group | | |
|----------------------------|--|--|--|
| | 1 | 2 | 3 |
| A Extraarticular |  Simple |  Wedge |  Complex |
| B Partial articular |  Split |  Depression |  Split-depression |
| C Articular |  Simple articular, simple metaphyseal |  Simple articular, complex metaphyseal |  Complex articular, complex metaphyseal |

Figure 14: Classification of epiphysis fractures into 3 fracture groups [22]

- 5) For more specialized requirements and more precise fracture definition, each one of these groups is further divided into three subgroups, based on fracture exact location or fracture morphology.

This gives 81 further subgroups for each bone. [20]

Since the present work focuses on the radius shaft region, in Figure 15 and Table 1 the various possible diaphyseal radial fractures are presented, together with the AO/OTA code used for uniquely defining them.

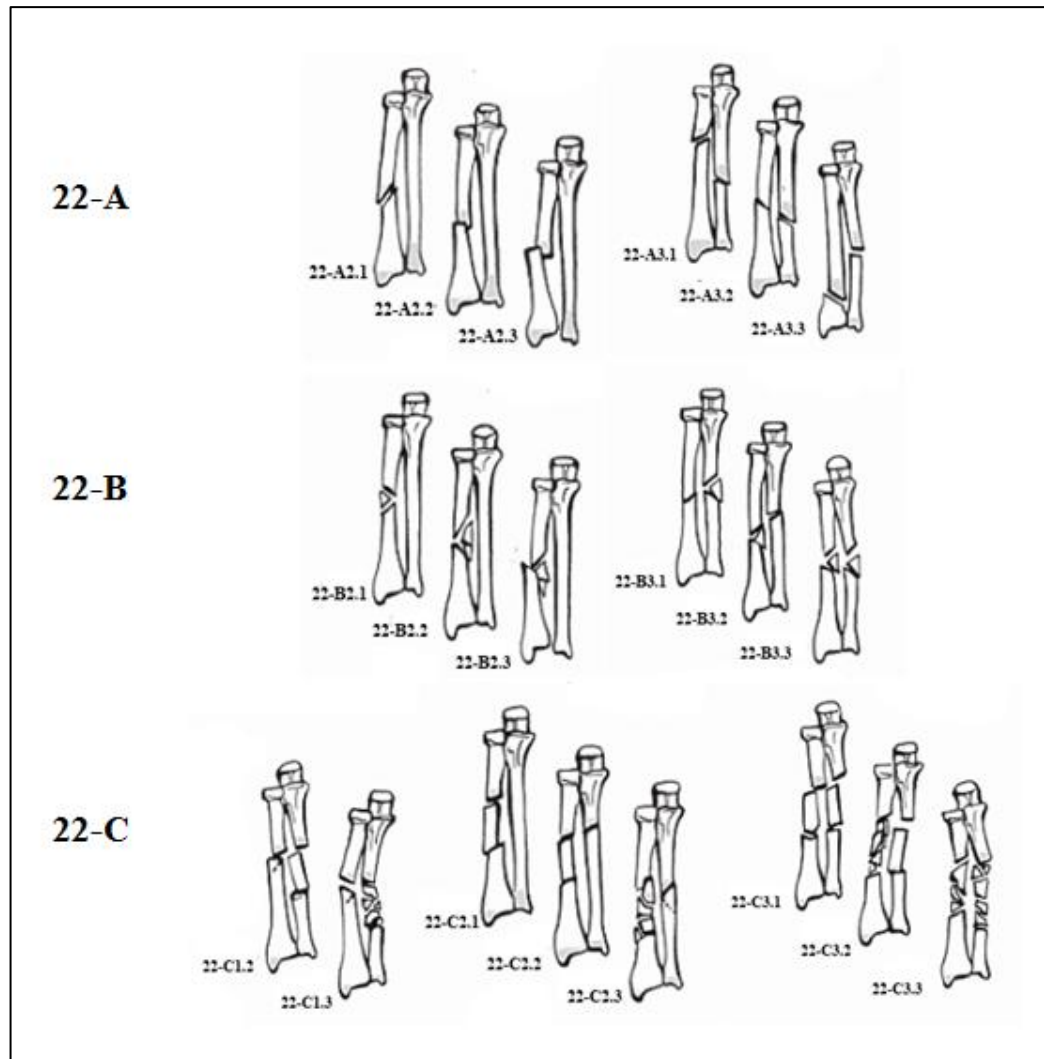


Figure 15: Possible radius diaphysis fracture according to AO/OTA classification [23]

| Fractured Bone | Fracture Location | Type of Fracture | Fracture Groups | Subgroups | AO/ASIF code | Additional sub-divisions | |
|------------------------|---|--|-----------------|---|--------------|--------------------------|---|
| Radius/Ulna (2) | Diaphysis (2) | Simple (A) | Radius (2) | Oblique (1) | 22-A2.1 | - | |
| | | | | Transverse (2) | 22-A2.2 | | |
| | | | | = dislocation of distal radio-ulnar joint (3) | 22-A2.3 | | |
| | | | Both Bones (3) | Radius – proximal zone (1) | 22-A3.1 | | (1) Without dislocation (2) = Dislocation of Radial head (Monteggia) (3) = Dislocation of distal radio-ulnar joint (Galeazzi) |
| | | | | Radius – middle zone (2) | 22-A3.2 | | |
| | | | | Radius – distal zone (3) | 22-A3.3 | | |
| | | Wedge (B) | Radius (2) | Intact Wedge (1) | 22-B2.1 | - | |
| | | | | Fragmented Wedge (2) | 22-B2.2 | | |
| | | | | = dislocation of distal radio-ulnar joint (3) | 22-B2.3 | | |
| | | | Both Bones (3) | Simple radius – wedged ulna (1) | 22-B3.1 | | (1) Without dislocation (2) = Dislocation of Radial head (Monteggia) (3) = Dislocation of distal radio-ulnar joint (Galeazzi) |
| | | | | Radial wedged – simple ulna (2) | 22-B3.2 | | |
| | | | | Radial and ulnar wedged (3) | 22-B3.3 | | |
| Complex (C) | Ulna Complex + eventual Radius simple (1) | Ulna bifocal (2) | 22-C1.2 | (1) = Radius simple (2) = Radius wedged | | | |
| | | Ulna Irregular (3) | 22-C1.3 | (2) = Radius simple (3) = Radius wedged | | | |
| | | Radius bifocal + intact ulna (1) | 22-C2.1 | (1) Without dislocation (3) = Dislocation of distal radio-ulnar joint (Galeazzi) | | | |
| | Both Bones Complex (3) | Radius Complex (2) | 22-C2.2 | - | | | |
| | | Radius bifocal + simple ulna (2) | 22-C2.3 | - | | | |
| | | Bifocal (1) | 22-C3.1 | - | | | |
| Both Bones Complex (3) | Both Bones Complex (3) | Bifocal of one, irregular of the other (2) | 22-C3.2 | (1) Bifocal Radius (2) Irregular Radius | | | |
| | | Irregular (3) | 22-C3.3 | - | | | |

Table 1: Description of the possible radius diaphysis fractures according to AO/OTA classification [24]

Some of the above described radius fractures are presented in the following radiographies.

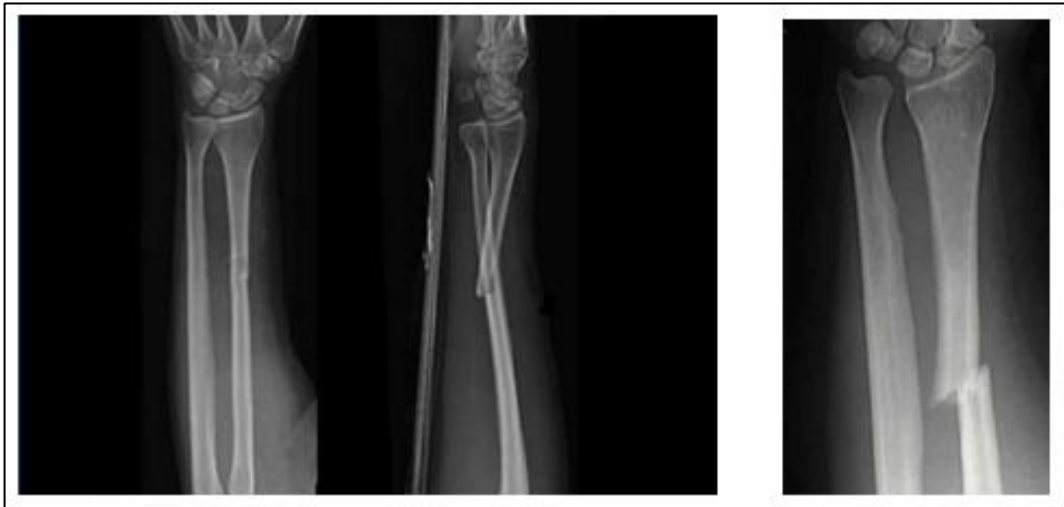


Figure 16: 22-A2 fractures radiographies
Left: 22-A2.2 (obliquity $< 30^\circ$); Right : 22-A2.1 (obliquity $> 30^\circ$) [25]



Figure 17: 22-A3 fractures radiographies. Left: 22-A3.2; Right: 22-A3.3 [25]

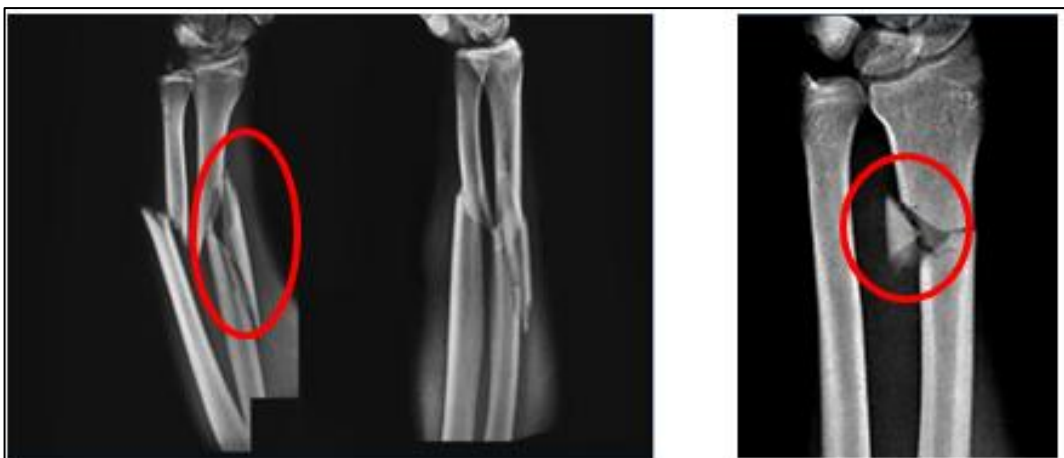


Figure 18: Left: 22-B2.1 fracture; Right: 22-B3.2. Wedges are highlighted [25]

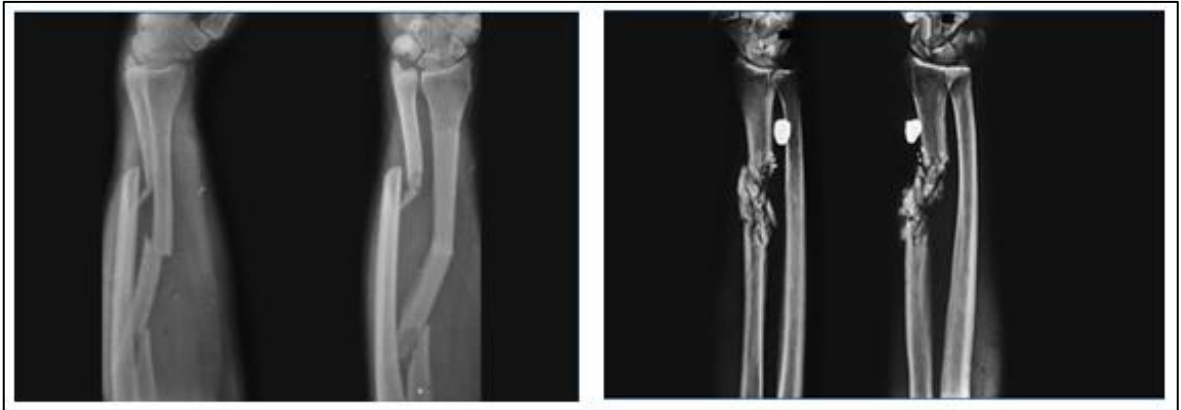


Figure 19: 22-C2 fractures radiographies. Left: 22-C2.2; Right: 22-C2.3 [25]

Multiple mechanisms can be involved in leading to fractures of the forearm bones. The common aspect to all the fractures is usually the high energy involved before reaching the failure point. Fractures of the shaft of the radius and ulna are often displaced and this is caused by the significant amount of force that causes this kind of fractures in adults and by the fact that the muscles attached to the forearm bones pull the fractured fragments and accentuate the displacement. [23]

Referring to the data presented by Bucholz et al., 2009 the forearm fractures are commonly caused by falls (28%), direct blow or assault (21.6%), sport (18.3%) or motor vehicle accident (13.3%). In particular, the most common types of forearm diaphyseal fractures noticed are type A –simple fractures- (86.4%), followed by type B – wedged fractures - (11.9%) and type C – complex fractures - (1.7%). The most common subgroups are A1.2 (25%), A1.1 (25%), A1.3 (6.7%), A2.2 (6.7%), B1.1 (6.7%). The radius appeared to be fractured very limitedly compared to the ulna. Only in fractures A2.2 there was in fact a radius fracture. The ulna was instead the bone which was more commonly broken, mainly because it is the most outer bone when trying to defend from a direct blow or assault. [23] [26] The isolated ulna fracture is in fact commonly called “night-stick fracture” [27].

De Luca et al. 1988 and Wang et al., 2005 reported that injuries to the forearm are mainly caused by motor vehicle accidents and falls or sever crushes [28] [29] confirming the epidemiology presented in the previously cited work.

Hertel et al., 1996 presented the most common forearm fractures in patients which took part to the clinical evaluation. It appeared that 20.6 % (27 cases) had 22-A2 and 22-B2 fractures (only radius), 55% (72 cases) were 22-A3, 22-B3 and 22-C1.3 (both bones involved), 25.2% (33 cases) were 22-A.1 and 22-B.1 fractures (only ulna) and 16.8% (22 cases) presented 22-C.1-3 fractures. [30] These data appear different if compared with the numbers presented by Bucholz et al., 2009 since the radius bone resulted to be much more involved in forearm fractures.

Chapman et al., 1989 presented the data regarding forearm diaphysis fractures in patients treated during a five year period with plate fixation. In total 63 fractures of the radius and 66 fractures of the ulna were reported for a total of 129 fractures. The presented numbers did not refer only to individual fractures of a bone but included also cases where both bones were injured or where a single bone presented more than one fracture (segmented fracture). The classification of the

fractures was given according to the original OTA system which is different from the previously described and more used AO/OTA system. The treated radius and ulna fractures were 23.2% (30 cases) type I, 13.1% (17 cases) type II, 10.8% (14 cases) type III, 23% (29 cases) type IVa and IVb, 15.5% (20 cases) type Va and Vb, 10.8% (14 cases) VIa and VIb, 3.87% (5 cases) VIIa and VIIb. The OTA classification used by Chapman et al., 1989 to classify the shaft fractures is shown in Figure 20. [31]

Wei et al., 1999 analyzed 32 radius and 32 ulna fractures for a total of 64 fractures caused by motor vehicle accidents or motorcycle accident, falls, gunshots, assaults and crushes.

The classification adopted in this work was as well the OTA classification presented in Figure 20. The incidence of the various types of fractures was 26.5% (27 cases) type I, 6.25% (4 cases) type II, 2% (1 case) type III, 13% (8 cases) type IV, 39% (25 cases) type V, 13% (8 cases) type VI, 2% (1 fracture) type VII. [32]

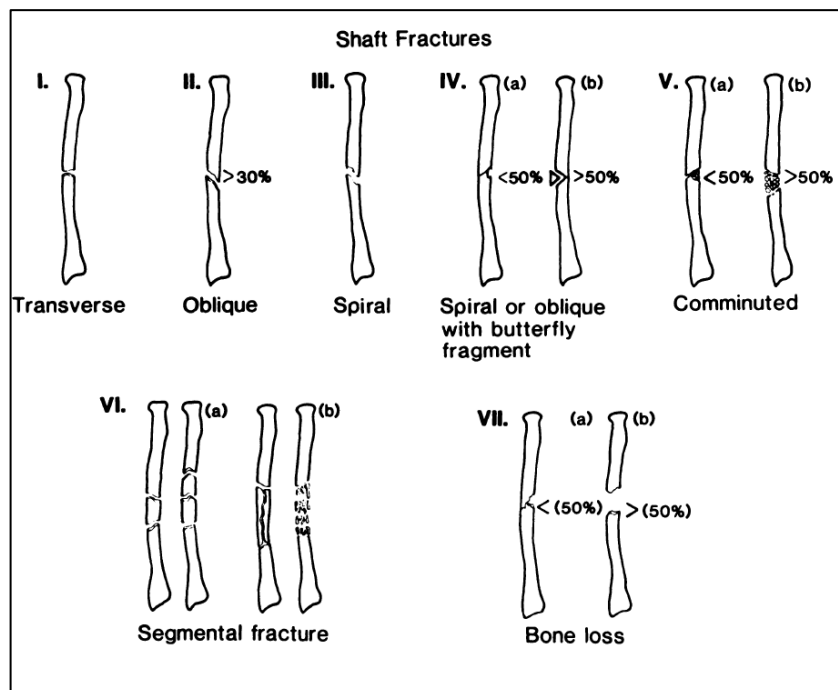


Figure 20: OTA fracture classification for shaft fractures [31]

The shaft of the radius and of the ulna are usually further divided in three regions, a distal region, a middle region and a proximal region as can be noticed from the AO/OTA fracture types 22-A3.1, 22-A3.2 and 22-A3.3 of Table 1.

Fractures were most frequently noticed in the middle third of the forearm bones (Figure 21). [31]

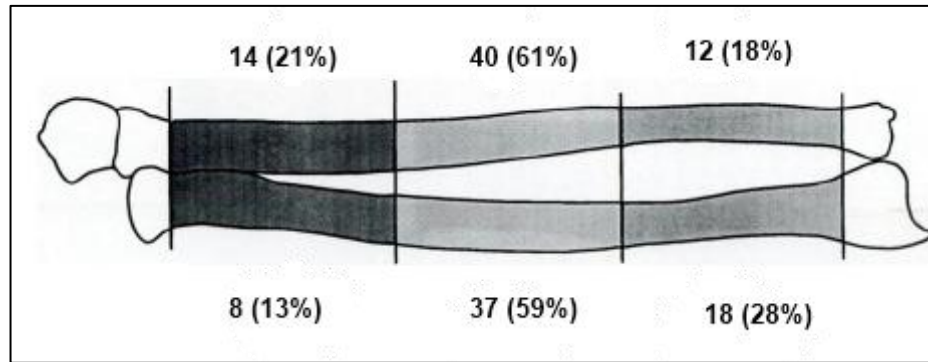


Figure 21: Distribution of fractures on radius and ulna shafts [31]

The recovery of the correct function after fractures of the forearm bones is dependent on the return to a correct rotation of the forearm, to the maintenance of a functional range of motion of the elbow and wrist and to the recovery of grip strength.

The main parameters which influence such aspects are the restoration of a correct rotational and axial alignment, of normal length and of the normal radial bow. The radial bow is a very important factor in obtaining a positive functional outcome after fracture healing. Schemitsch et al., 1992 showed that if the location of the radial bow was within 4-5 % of the one of the normal arm 80% of normal forearm rotation and grip strength could be restored. Overcorrection, undercorrection and a change in the location of the radial bow were all associated with a reduced grip strength and forearm rotation. These findings suggested that the radius has a certain morphology which optimizes function and which should be tried to be restored after fractures and injuries. [33]

1.2.1 Bone Healing

The process that follows the fracture of a bone has the aim of achieving a complete structural and functional restoration of the injured segment. In general, fracture healing is completed by 6-8 weeks after the initial injury. Fracture healing can be divided in two main categories:

- **PRIMARY BONE HEALING**
Primary bone healing requires rigid stabilization with or without compression of the bone ends. This rigid stabilization suppresses the formation of callus in either cancellous or cortical bone. This type of healing is not the most common since most fractures are treated in a way that a small degree of motion is allowed (for example fracture treatment with casts, external or intramedullary fixation allow some limited movement between bone ends). [34]
- **SECONDARY BONE HEALING**
Secondary bone healing is characterized by spontaneous fracture healing in absence of rigid fixation of the fracture site. Commonly, secondary bone healing is divided in 3 main phases which are briefly described below and shown in Figure 22.

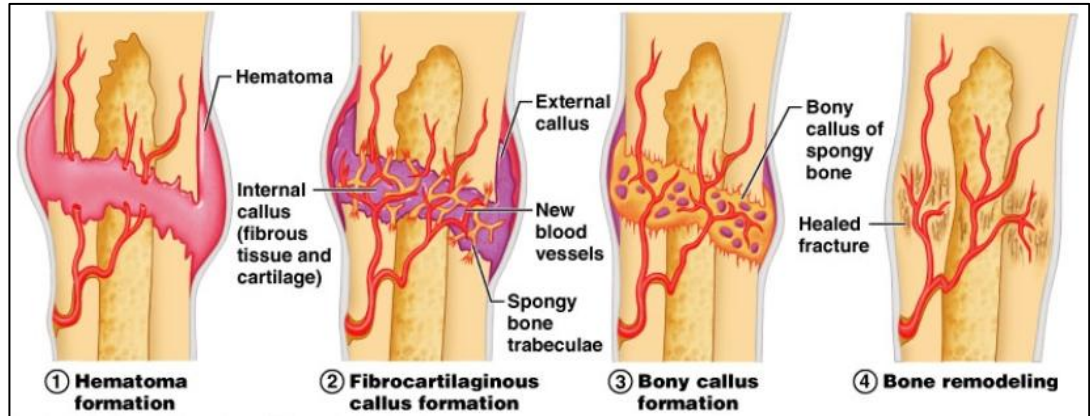


Figure 22: Phases of the secondary fracture healing process [8]

1. **Inflammatory phase:** Immediately following the injury an inflammatory response is generated and can protract up to 1 week post-fracture. This reaction causes pain and swelling which are responses that induce a protection of the fractured site. During the fracture event there is also a damage of the vascular structures, therefore the clotting cascade is activated with the aim of limiting hemorrhage as well as helping building a fibrin network that provides a pathway for cellular migration. The result of this phase is the production of a reparative granuloma. [34]
2. **Reparative phase:** This phase occurs within the first few days and lasts for several weeks with the result of developing a reparative callus tissue in and around the fracture site. The role of the callus is to enhance mechanical stability of the zone involved by the injury by supporting it laterally. As first step of the reparative phase fibrous tissue and cartilage begin to form and revascularization of the fractured site takes place. A soft callus is formed and it represents a first bridging of the fractured zone. In a second moment calcification and mineralization of the soft tissue begin, giving as result a rigid callus, formed by woven bone, which connects the two fracture ends. [34]
3. **Remodeling phase:** This phase is the final part of fracture healing and begins with the replacement of woven bone with lamellar bone and the resorption of excess callus until the restoration of the normal bone architecture is achieved. This phase can last several years and is mainly driven by the mechanical loads which are applied on the structure. [34]

1.3 Fracture management

Diaphyseal fractures of the radius and ulna are considered injuries which bring a high risk of functional limitation. The more proximal the injury is (proximal 1/3 shaft, proximal epiphysis and proximal radio-ulnar joint) the greater the blockage of prono-supination can be. [35]

Therefore, as stated previously, the goal of the treatment must be the restoration of the length, of the axial alignment and of the rotation of the involved bones in order to ensure full capacity of pronation and supination of the forearm. The reduction of fractures of the forearm bones is generally performed by open reduction and plate fixation when the fracture is displaced or the fracture type is complex. [20] In case of undisplaced simple or wedged fractures the treatment can be non-surgical and a cast or brace may be used. [25]

Various decisions have to be taken by the surgeon when reducing a forearm shaft fracture. Choices are necessary in terms of surgical approach, number of screws, type of screws, length of the plate, etc. The decisions are made considering various factors such as condition and type of fracture, personal preference of the surgeon, etc.

An ideal and unique construct for diaphyseal forearm plating is probably not known and could not even exist since each choice made will inevitably carry positive and negative aspects with it. [36]

Multiple devices, in terms of plates, can be used for forearm diaphysis fracture reduction:

Compression plates comprehend plates which feature a hole design that allows axial compression, and therefore fracture reduction, by eccentric screw insertion. The screw holes of the compression plates can be described as a portion of an inclined and angled cylinder. The head of the screws can slide down the inclined shoulder of the cylinder so that when the screw is inserted and tightened the result is a movement of the bone fragment relative to the plate and compression of the fracture is achieved (Figure 23). The design of the screw holes allows obtaining a bone displacement up to 1mm. [20] This plating technique requires pre-contouring of the plate in order to match the anatomy of the bone and the screws are tightened for compressing the plate on the bone surface since the actual stability results from the friction between the plate and the bone. The mentioned compression unfortunately can lead to a disturbance of the blood supply of the bone which can produce for example delayed healing, especially if the treated bone is not of good quality. [44] Compression plates generally work well for simple fractures but they appear not advantageous in comminuted, metaphyseal and/or osteoporotic fractures. [45] This type of plates can permit a primary bone healing since no motion is present at the fracture site (Chapter 1.2.1)[46]

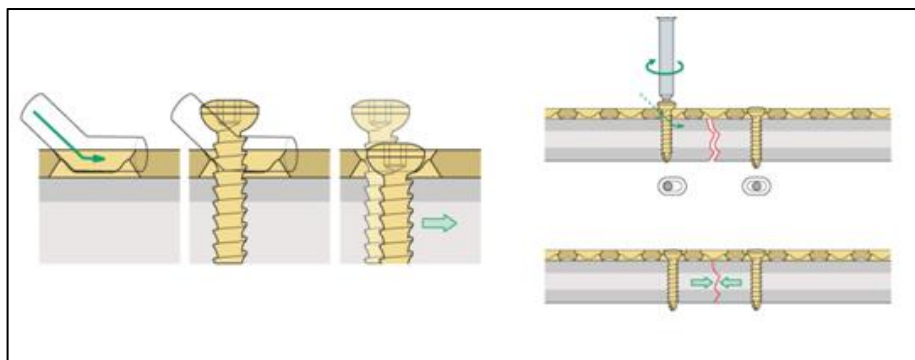


Figure 23: Compression Plates. The screw head slides down the inclined wall of the hole allowing the relative movement of the fragments and compression to be achieved. [25]

Locking plates are devices which use so called locking screws. These screws are characterized by a threaded head that matches and couples directly with the motherthread on the body of the plate in a position which is usually perpendicular to the long axis of the fixator (Figure 24). This provides great stability to the construct since the possibility for the screw of being toggled off is eliminated. The locking plates aim at flexible elastic fixation to initiate spontaneous healing and act more like “internal fixators” than plates, so they are used in order to bridge the fractured area (just like the external fixators). They produce axial forces which are minimal if compared with the ones given by standard compression plates. [20] [44] This plate concept allows a secondary bone healing since relative motion exists at the fractured site (Chapter 1.2.1)

The big advantage of such devices is the reduced contact between the plate and the bone which is possible because the screws lock directly on the plate with the application of a small torque. These plates do not need to be compressed on the bone. This property limits the risk of bone damage, bone necrosis, preserves vascularity and allows a rapid fracture healing with callus formation which is not usually present when using dynamic compression plates.

No precise anatomical contouring is needed, preventing primary dislocation of the fracture caused by an inexact one. [47] The usage of this kind of plates is suggested especially for high comminuted fractures, fractures with bone loss or fractures where anatomic reduction is impossible [46]

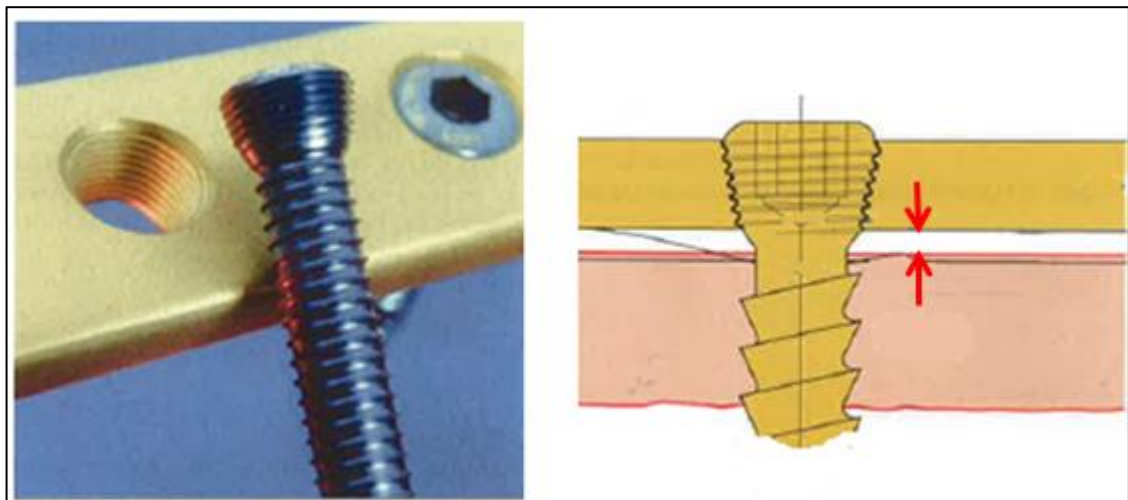


Figure 24: Locking screw technology.

The red arrows show the absence of contact between plate and bone [25]

The **locking-compression plates** combine the use of conventional screws (compression technology) with locking screws. [20] These devices can be used, depending on the fracture situation, as a compression plate, a locked plate (bridging technique) or as an internal fixation system which presents both components and unites compression and bridging techniques.

This versatility is very important since it allows the surgeon to decide intra-operatively whether to use it in the compression mode, in the locking mode or in the hybrid configuration without the need of having two/three diverse types of plates. The choice to use a locking-compression plate in one specific configuration depends on various factors such as fracture location and configuration, condition of the patient, presence of other implants, surgeon’s personal preference, etc.

The usage of standard screws and locking screws in the same application is usually made for increasing stability since the screws are locked to the plate and the possibility of the screw to

toggle, slide or be dislodged is minimized without eliminating the compression of the two bone ends in the fracture site. [44]. Typically, conventional screws are inserted first to reduce the fracture. Once this is achieved locking screws are placed to optimize strength and stability of the construct. [48]

The locking and compression screws are shown for the Stryker VariAx system in Figure 25. Grey screws are locking screws while yellow screws represent bone screws.



Figure 25: Locking-Compression plate in hybrid configuration [49]

The **LC-DCP (Limited Contact-Dynamic Compression Plates)** and **PC-Fix plates (Point Contact Fixator)** represent a development of the conventional compression plate. The most important modifications resulted in a greatly reduced plate-bone area of contact. As mentioned before, the fact that DC plates were compressed on the bone to properly fulfill their work led to damages to the surface of the bone and to slower restoration of the integrity of it. With this improvement the capillaries of the periosteum of the bone are less damaged and slower bone healing is avoided.

The differences regarding the contact area between the standard DCP, the LC-DCP and the PC-Fix are shown in Figure 26. [20]

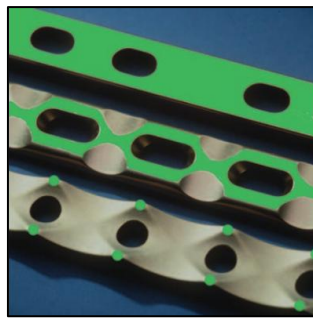


Figure 26: Area of contact: Conventional DCP (top); LC-DCP (middle); PC-Fix(bottom) [47]

Other plates reported in scientific works for the treatment of long bone fractures are **semi-tubular plates** which allow achieving axial compression by inserting eccentrically the screws through the oval holes (usually 4.5mm screws are used with it) and **one-third-tubular plates** which are very similar to the above presented ones but are designed for usage with 3.5 mm and 2.7 mm screws. These systems, especially the semi-tubular plates, were indicated for radius and ulna fractures but are not used so frequently any more since they were replaced by compression plates. [20] [50] These last plates described are presented in Figure 27.



Figure 27: Right: Semi-tubular plate; Left: One-Third Tubular plate [51]

The most used products have been extracted from literature data and are Dynamic Compression Plates (DCP) [29] [36] [37] [30] [38] [20] [39] or Low Contact-Dynamic Compression Plates (LC-DCP) [20] [39] [40]

However, Hidaka et al., 1984 reported the analysis of fracture fixation in patients with radius, ulna or radius and ulna fractures treated with Dynamic Compression Plates DCP (26/32 cases), semitubular plates (5/32 cases) and non-compression plates (1/32 cases). [41]

The clinical study performed by Rosson et al., 1991 showed as well the usage of other kind plates for such types of fractures. The author reported the use of compression plates (29/65 cases) and one-third tubular plates (36/65 cases). He also stated that compression plates were becoming more used at the time of the article writing. [42]

The work of Rumball et al., 1990 also showed the usage of both DCP and semitubular plates even if the number of cases treated with each type of device was not reported. [43]

DeLuca et al., 1988 reported the adoption of compression in 30/42 cases and semitubular plates in 12/42 cases of fractures of forearm bones. [28]

Chapmann et al., 1989 presented the cases of 129 patients which had a plate implanted on the radius or ulna shaft. For 120 patients DCP were used, for 5 cases semitubular plates were adopted and for 4 patients a one-third-tubular plate was chosen. [31]

It is evident that the most frequently used plates are in general compression plates even if various cases are present in which fractures of the forearm bones were treated with other types of devices. All the articles reporting a use of such plates (semitubular plates, one-third-tubular, etc) were written before 1991. In the more recent works analyzed it appeared common practice to use compression plates for treatment of radial and ulnar fractures.

The choice of plate length and number of screws to use is an important aspect of fracture management in order to ensure the generation of a construct with sufficient stability, an environment for adequate bone healing and a minimized damage to the soft tissues involved in the procedure.

There is not a unique way to approach the fractures and different theories and ideas are present in literature and in the scientific world.

The optimal construct can be defined as the one which is stable enough to allow fracture healing and does not result in excessive complications during and after removal. [36]

Commonly, most of the orthopedic surgeons tend to choose the shortest plate possible and to fill all screw holes until a desired number of cortices of fixation is achieved. [39]

However, the most performed procedure for forearm diaphyseal fixation is the one using at least six cortices of fixation, corresponding to three screws inserted in each main fragment, in order to achieve enough stability in the forearm. 7- or 8-hole plates, with one or two holes left empty, should be used for transverse or short oblique fractures and 9-, 10-hole or longer plates for fractures where a third fragment is present. This approach showed excellent results and union rates of 95% - 98%. [20] [36] [52] [36]

These considerations were confirmed by Mehdi Nassab et al., 2012 who state that the most common fixation technique for forearm bones requires 6 screws to be used. The length of the plate, instead, is largely dependent on the grade of comminution of the fracture. Simple fractures of the diaphysis of the radius and ulna for example allow the usage of 7-hole plates while more complex cases require usually the adoption of longer plates. [53]

Various studies, however, reported that the length of the plate is one of the most important parameters in terms of resistance to screw pullout and maximal load applicable before failure and state that there is an advantage when using longer plates. [39]

The idea of utilizing less screws was carried out by Lindvall et al., 2006 since previous studies seemed to show that when inserting three screws per bone fragment the central screw did not really have a specific and important function. In fact the results obtained using plates of different length, always 4 screws and always the same number of available holes outside the fracture zone (6 holes) showed equivalent union rates (no statistical comparison performed) compared with the cases where two more screws were used. These results were accepted and confirmed by various works which as well reported that the usage of fewer screws, more spaced between each other, even led to the creation of a more stable construct. [36]

Analogous conclusions were presented in the work performed by Sanders et al., 2002 where it appeared that once the working length (= fracture zone) is minimized and the plate length is maximized no more than four screws are needed. [52]

Another aspect to be considered is the fact that short plates with all the holes filled by screws form a more rigid construct compared to when longer plates with some free holes are implanted. This can lead to increased risk of stress shielding and weakening of the bone cortex. [36]

The increased number of holes when using six screws instead of four also results in a more weakened bone (more drilled holes and therefore more removed material) and in a greater number of sites of stress rising.

However, various other articles suggested that 4 cortices of fixation per each side of the forearm shaft fracture are not sufficient since failure rates were reported to be higher than when six total screws were used.

In forearm shaft fractures, in addition to the plates, mainly when oblique or spiral fractures are present, the use of a lag screw is suggested in order to compress together the bone fragments.

The plate implanted together with the lag screw can act in “stress neutralization mode” since the lag screw cannot withstand high degrees of axial loads or in “compression mode” with the successive addition of the lag screw through the plate to help this function. [25]

The lag screw can be inserted through a screw hole or independently as shown in Figure 28. When 3.5 mm screws are used in the plate usually 2.7 mm bone screws are suggested as lag screws for forearm shaft fractures. [54] [20]

The lag screw is inserted perpendicularly to the fracture plane in order to work in the most effective way possible and avoid fracture displacement when the screw is tightened. [25]

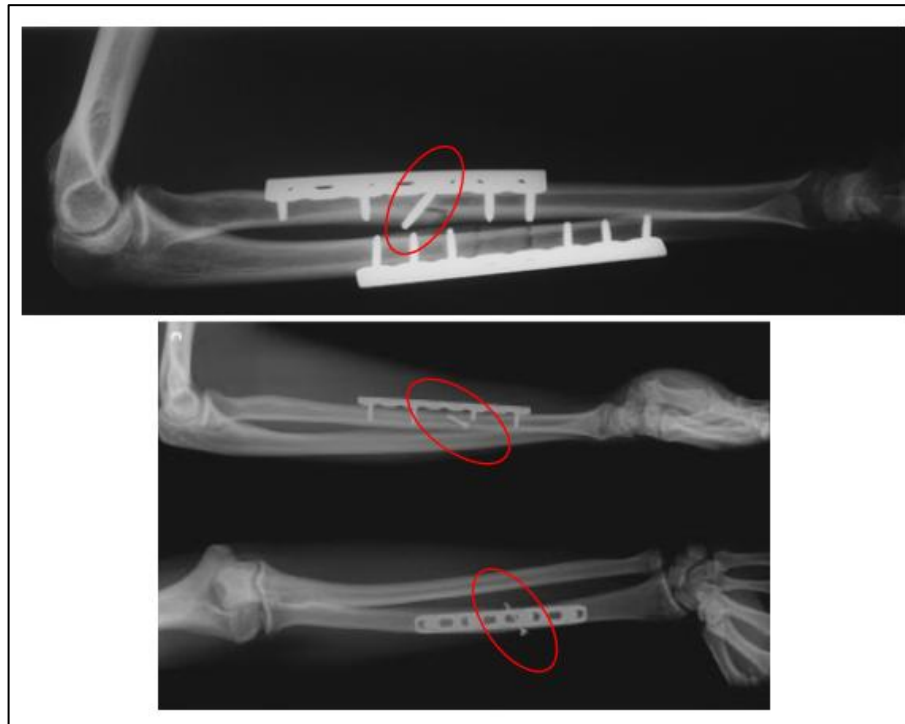


Figure 28: Forearm shaft fractures managed with lag screws and plates.
Top: Lag screw inserted through the plate; Bottom: Lag screw inserted independently [8]

In Figure 29 the two possible types of lag screws are shown.

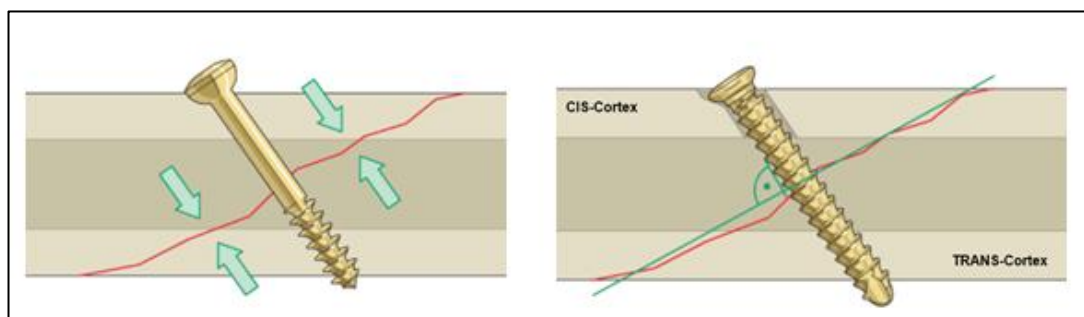


Figure 29: Left: True lag screw used; Right: Fully threaded screw used as lag screw.
Perpendicular application of the screws can be noticed [25]

1.3.1 Surgical Approaches

The surgery for reducing forearm shaft fractures is quite complex. Regarding the fractures of the diaphysis of the radius two approaches are generally used to reach the bone and be able to implant plate and screws.

I. Dorsolateral (Thompson) Approach

This approach offers good exposure of the middle and distal third of the radius shaft. The two landmarks of such approach are the lateral epicondyle of the humerus and the styloid process of the radius or the Lister's tubercle as shown in Figure 30.

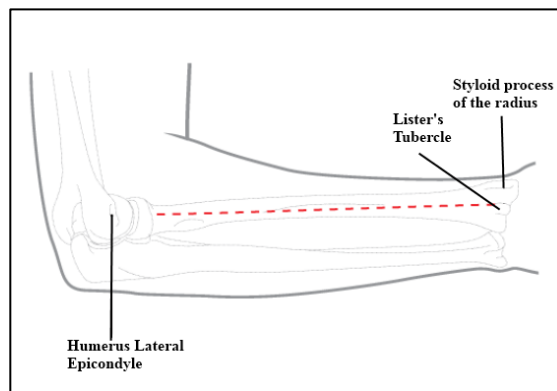


Figure 30: Dorsolateral approach to the radius. Landmarks and incision [25]

The access to the radial shaft is placed between the extensor carpi radialis brevis and the extensor digitorum muscles which have to be split along the septum. It might also be necessary to mobilize the abductor pollicis longus in order to be able to place the plate when distal shaft radius fractures are present. Some fracture configurations could need the mobilization of the pronator teres as well.

In performing the Thompson approach the radial nerve is vulnerable and particular attention is made in not damaging it. [20] [25] The plate positioned through the described approach is shown in Figure 31.

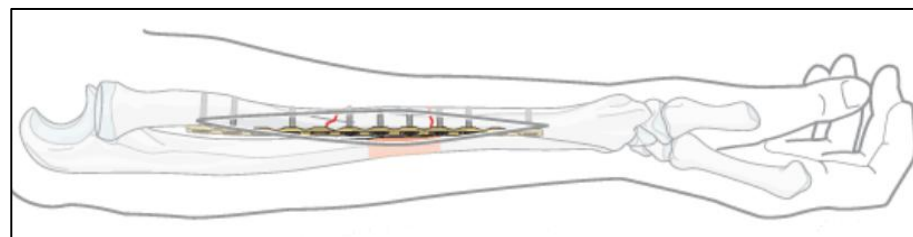


Figure 31: Dorsolateral plate [25]

II. Volar (Henry) Approach

This approach offers good exposure of the whole length of the radius. The two landmarks are the biceps tendon which crosses the front of the elbow joint and the styloid process of the radius as can be seen in Figure 32. The length of the incision depends on the extent of exposure needed

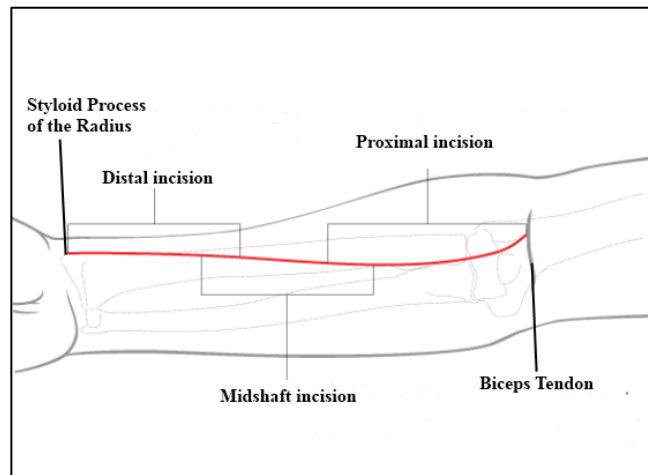


Figure 32: Volar approach to the radius. Landmarks and incision [25]

This approach requires attention in regards to the radial artery, which lies deep to the brachioradialis in the middle part of the forearm, and to the radial nerve which is placed laterally to it. The plate placement is allowed if the supinator muscle is incised and gently elevated from the surface of the bone (placement on proximal third), the pronator teres is partially detached from the radius surface (placement on the middle third) and the flexor pollicis longus and pronator quadratus are elevated (placement on the distal third). [20] [25] The plate placed following the volar approach is shown in Figure 33.

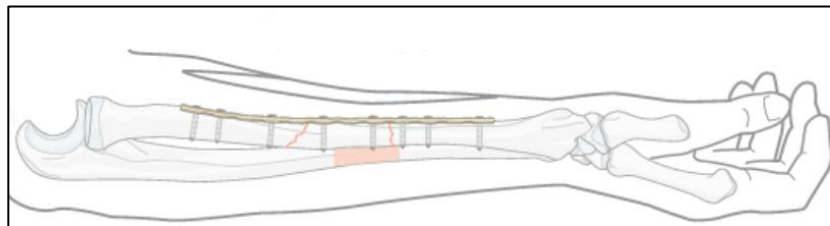


Figure 33: Volar plate [25]

1.4 Screw removal

The removal of the implanted plates after fracture healing is not mandatory and rarely indicated. This suggestion is made because there is a risk of complications, such as neurovascular injuries and re-fractures during and after the removal procedure. However, in some situations the removal is indicated. In these cases it is suggested to perform it at least 2 years after the internal fixation has taken place. [20] When plates and screws are removed from the bone, screw holes are present and defects remain visible for many months since the growth of fibrous tissue and re-ossification of the site requires time. [55] Holes left after screw removal are filled initially by fibrous tissue or fibrocartilage which are then replaced with woven bone (isotropic material formed by an irregular pattern of collagen with increased cellularity and an irregular pattern of mineralization) and successively with lamellar bone (anisotropic material). [56]

Various studies have been undertaken in order to study the time needed to achieve a complete filling of the holes left by the screws with newly formed bone. Many studies have taken animals as models for the tests. Results of these studies are not completely comparable with humans.

Burstein et al., 1972 performed tests on rabbits. Self-tapping screws were inserted and then removed from the femur of the animal leaving a tapped hole. After four weeks the amount of formed bone was evaluated. It appeared that most of the specimens presented a great portion of the hole with new bony tissue but the hole was not completely re-filled. [55]

Rosson et al., 1991 performed, instead, tests on humans. He showed that bone mass was close to normal, in correspondence of the screw defects after approximately 18 weeks in humans. The healing process was much slower than in animals as can be noticed comparing these results with the findings of Burstein et al., 1972. The fact that bone mass recovers in 4-5 months after hardware removal, however, does not prove that the bone structure recovers at the same time the mechanical and strength properties. [57]

Other authors stated instead that the exact duration of bone strength reduction due to screw holes is approximately 1 to 2 months. [56]

An interesting finding by Burestein et al., 1972 was the fact that the bone formed to fill the hole appeared at first in the outermost portion of the cortical defect. Slowly it became thicker until it managed to completely fill the defect. From an engineering point of view this is actually the most efficient and rapid way to remove the stress concentrating effect of the hole. [55]

From a mechanical point of view the presence of a change of section (hole, groove, etc) in any sort of structural member leads to two main consequences:

- i. The cross section in correspondence of the hole is smaller. This causes, for example during tension or bending, the generation of a greater stress if compared to the situation when no hole is present.

- **Tension:** the stress (σ) is given by the ratio between the applied force (F) and the cross section (A) as seen in (1).

If the cross section decreases there is an increase of the generated stress.

$$\sigma = \frac{F}{A} \quad [\text{MPa}] \quad (1)$$

- **Bending:** Since the stress (σ) depends as well on the second moment of inertia (I), a decrease of this last parameter (given for example by a reduction of area) leads to a higher stress level. y represents instead the distance between the neutral axis and the point where the stress wants to be calculated. The stress equation is reported below.

$$\sigma = \frac{M}{I}y \quad [\text{MPa}] \quad (2)$$

During tension or bending, an increase of the diameter of the hole causes the generation of higher stresses

- ii. The presence of a hole or of a change of section also results in a modification of the simple stress distribution, localized high stresses in fact occur near the section variation. This localization of high stresses is known as stress concentration and can be described by the stress concentration factor (k_t) of equation (3) where σ_{\max} is the maximum stress actually present and σ_{nom} is the stress calculated for example through (1) and (2) without considering any stress concentration effect.

$$k_t = \frac{\sigma_{\max}}{\sigma_{\text{nom}}} \quad [-] \quad (3)$$

The result in terms of stress distribution for a bar with a hole in tension is presented as example in Figure 34. [58]

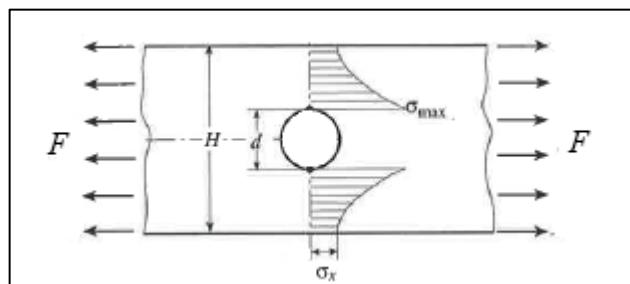


Figure 34: Stress concentration in a bar with hole [59]

The stress concentration factors k_t which arise in correspondence of holes of different dimensions are displayed in Figure 35.

It can be noticed that with small d/H ratios the corresponding stress concentration factor is 3 meaning that the σ_{\max} present is three times the stress calculated without taking into account the stress concentration caused by holes.

K_t (and consequently σ_{\max}) decreases when the ratio d/H gets bigger, for example when the hole size increases.

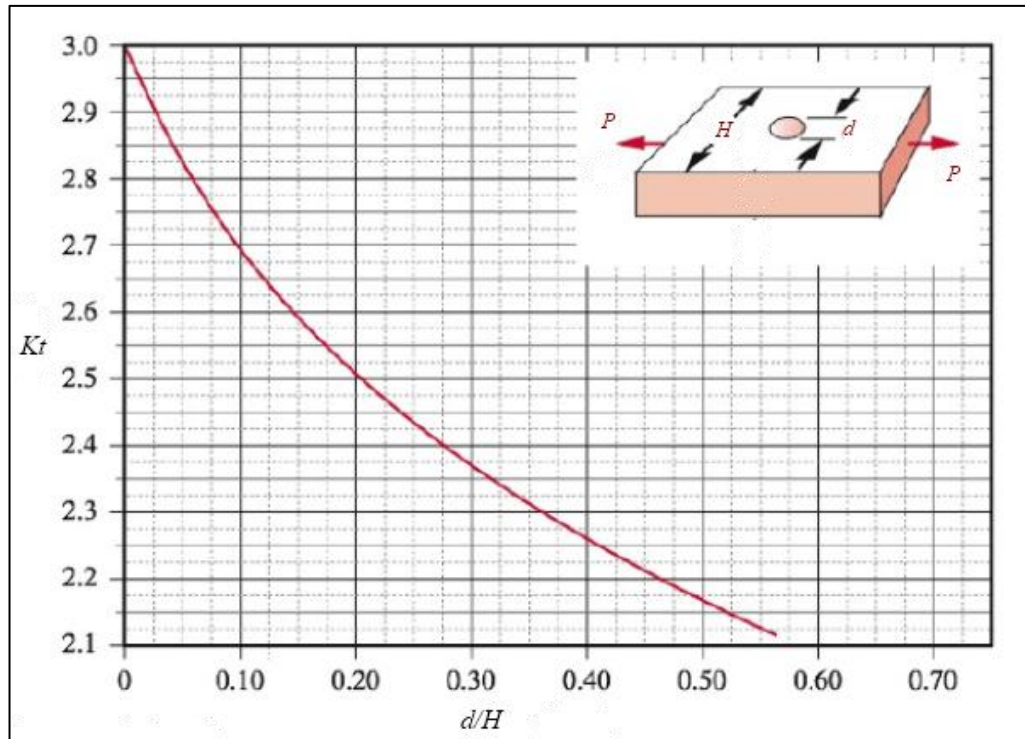


Figure 35: Stress concentration factors for the bar with hole in tension [60]

The principal aspect which is evident from the above presented discussion is that the presence of a hole can influence the maximum stresses in two opposite ways. The presence of bigger holes leads to higher nominal stress (see formula (1)) but lower stress concentration (see Figure 35).

Several scientific studies had the goal of evaluating the influence of the hole in the risk of re-fracture of long bones.

Rosson et al., 1991, for example, experimentally evaluated the influence of screw holes in reducing the strength of the bone by comparing the energy to failure absorbed by the structure with and without defects when a three point bending test was performed. Holes drilled were of 1.5 mm and 2 mm.

The results regarding the 1.5mm hole actually showed that the presence of such holes reduced the maximum applicable bending moment to 70% of the one applied when the intact bone was tested and the adsorbed energy to 53% of the one present in normal conditions. The 2 mm holes showed a 66% bending moment reduction and a 49% adsorbed energy reduction compared to the situation when no hole is produced on the bone.

Such results show the great effect of residual screw holes on the strength of the bone and on its capacity to adsorb energy. [61]

Johnson et al., 1997 tested in a three point bending test to failure configuration various cadaver fibula bones with and without a 3.5mm single hole drilled in the diaphyseal region. The results showed that the bones which presented the hole experienced failure with the application of 59.63% of the load needed to break the intact bones. [56]

1.5 Re-fractures

Re-fractures in forearm bones after plate removal vary in literature from 1 to 35%. [43] The causes of such complications can be multiple. Re-fractures due to inadequate technique, delayed union or non-union and premature plate removal have been mostly reported. [23] The interest of this study regards the analysis of the re-fracture patterns of the radius bone shaft due to the presence of holes derived from the removal of the previously implanted plates and screws.

Chapman et al., 1989 analyzed the healing of forearm shaft fractures after treatment with compression plates of 63 radius bones and 66 ulnas. The surgical approaches chosen were the Henry approach when the fractures involved the distal one third of the radius, the Thompson approach when the middle one third had to be exposed and the Henry or Thompson approach when the proximal portion of the shaft had to be treated.

The removal of plates was rarely done before 12 months from the implant and was always performed after achievement of union between the bone fragments.

In total 31 3.5mm AO compression plates, 2 4.5 mm AO dynamic compression plates and 1 semi-tubular plate were removed. Both bones which had the 4.5 AO dynamic compression plate re-fractured through a screw hole while no re-fracture was noticed on patients which had the other plates removed. [31]

193 fractures of the radius treated with compression plates were analyzed in the work of Anderson et al., 1975. The dimension of the used screws was not reported. When the fracture involved the distal half of the radius the anterior (Henry) approach was used, when it was on the proximal half the dorsal (Thompson) approach was preferred. For fractures involving the middle third of the radius both approaches could be used.

The chosen plates were 4-hole plates for non-comminuted transverse fractures, 5-hole and 6-hole plates for comminuted fractures or when there was obliquity of the plane of fracture.

Less than 10% of the plates were removed already after a few months and 8 re-fractures occurred in the first few weeks after hardware removal. Of the total number of re-fractures 3 were due to the presence of the screw hole and occurred in correspondence of the most distal one. [37]

Hidaka et al., 1984 analyzed the treatment of 32 fractures of forearm shaft bones. 14 fractures involved the radius and 18 fractures the ulna. The cases were treated implanting 26 DCP with 5, 6 or 7 screw holes (no screw dimension mentioned), 5 semi-tubular plates and one AO non-compression plate designed for forearm bone. The plates were removed after complete healing had been clinically confirmed and was elective or was due to slight discomfort of the patient.

Re-fractures occurred in 7 cases. Three re-fractures happened through the original fracture site, three involved the original fracture site and the nearest screw hole and one re-fracture was through a screw hole. [41]

Patients who had fractures of radius and ulna (88 fractures in total) were treated with plate fixation in the work presented by Rumball et al., 1990. The used plates were semi-tubular plates, narrow 4.5 mm DCP and small 3.5 mm DCP. Plates were removed after an average of 15.3 months. Four re-fractures occurred after plate removal. Two involved only the old fracture site, one involved the hole left by the removal of the screw and one involved both the fracture site and the nearest hole.

The two holes which were involved in re-fracture had a 4.5mm screw implanted. [43]

Rosson et al., 1991 presented the results of the treatment of 73 fractures of radius and ulna using plates. In particular 36 one-third tubular plates and 29 DCP all with 3.5 mm screws were implanted on the patient's bone. An interfragmentary screw was used outside the plate in 5 cases.

Re-fracture was present in four cases; three occurred in correspondence of the original fracture site and one in correspondence of the defect produced by the removal of the countersunk interfragmentary screw after 10 months. [42]

Hertel et al., 1996 analyzed the outcomes of 132 fractures of radius and ulna occurred during a ten year period. Every fracture was stabilized with 3.5mm dynamic compression plates which were removed at the surgeon's discretion (70% of the removals were performed at a mean of 33 months after the first operation). Three re-fractures were noticed and only one occurred through the screw hole but it was a iatrogenic fracture (probably induced by medical treatment and therefore it was probably avoidable). [30]

The above presented results regarding re-fracture through the screw hole are summarized in Table 2.

| Source | Total plates removed | Number of re-fractures through screw holes (%) | Dimension of screws involved in re-fracture |
|----------------------------|----------------------|--|---|
| Chapmann et al., 1989 [31] | 34 | 2 (5.88%) | 4.5 mm |
| Anderson et al., 1975 [37] | circa 19 | 3 (15%) | n/a |
| Hidaka et al., 1984 [41] | 32 | 1 (3.125%) fracture only through screw hole 3 (9.375%) fracture through screw hole and original fracture site | n/a |
| Rumball et al., 1990 [43] | 88 | 1 (1.13%) fracture only through screw hole 1 (1.13%) fracture through screw hole and original fracture site | 4.5 mm |
| Rosson et al., 1991 [42] | 73 | 1 (1.36%) | 3.5 mm + counterink |
| Hertel et al., 1996 [30] | 32 | 1 (0.75%) | 3.5 mm |

Table 2: Summary of the analyzed literature regarding re-fractures through the screw hole

2. Experimental Testing

The experimental test had the aim of evaluating the eventual influence that the holes, left in consequence of screw removal, have on the failure of the radius bone during mechanical loading.

As reported in the previous section there are various clinical evidences that confirm the actual possible re-fracture of the bone in the time between implant removal and screw hole filling by newly formed bone.

The objective of this section was therefore to quantitatively characterize, through an experimental test, the difference in terms of possible re-fracture between bone with and without holes and to compare various situations in regards to possible implanted screws and plates.

The idea behind the experimental test was to simulate implant and removal of plate and screws in a radius bone model and analyze how the system behaved during mechanical testing in comparison to the untreated bone (without holes).

Various points had to be evaluated in the definition of the actual experimental tests, setups and comparisons to be made. Every decision was made considering clinical, anatomical, mechanical and biomechanical aspects.

2.1 Material and Methods

2.1.1 Clinical Decisions

The definition regarding which material would be used, which comparisons would be made and which setup would be adopted for the experimental test performance needed at first some clinical decisions and considerations to be made. These decisions would have an influence on all the following steps.

As first step the specific type of fracture for which fixation would be simulated, the type of surgical approach, the plate length and the total number of screws to implant were defined according to clinical practice, literature data, Stryker Marketing inputs and Dr. Adamany's and Dr. Araghi's feedback.

- **FRACTURE TYPE AND LOCATION**

The type of fracture for which plate and screw implant and removal would be performed was decided according to literature data (see Chapter 1). The choice criterion was, therefore, the most frequent radius fracture types reported in scientific papers. The percentage of incidence of each major fracture group found in scientific works, analyzed in Chapter 1.2, is summarized in Table 3.

The division of fractures was made according to the AO/OTA classification: type A fractures represents simple fractures (transverse-oblique-spiral), type B comprehends all wedged fractures and type C includes more complex fractures such as comminuted, bifocal fractures etc. [20]

| Reference | Type A fractures (%) | Type B fractures (%) | Type C fractures (%) |
|----------------------------|----------------------|----------------------|----------------------|
| Bucholz et al., 2009 [23] | 86.4% | 11.9% | 1.7% |
| Wei et al., 1999 [32] | 34.75% | 13% | 54% |
| Chapmann et al., 1989 [31] | 47.1% | 23% | 30.17% |
| Lindvall et al., 2006 [36] | 39.6% | 47.1% | 13.2% |
| Average | 51.96% | 23.75% | 24.76% |

Table 3: Occurrence of the different fracture types

As evident from the presented table type A fractures (*simple fractures*) are the most common in the radius (Figure 36) and in general in forearm shaft bones.

A minor incidence was in general noticed for type B and type C fractures.

The specific fracture chosen, belonging to type A, was the *transverse fracture*.

The exact location of the fracture was decided to be the middle portion of the shaft since it is the most frequently fractured area as shown in Figure 21 in Chapter 1.



Figure 36: Transverse (top) and oblique (bottom) radius shaft fractures [8]

- **SURGICAL APPROACH**

The common surgical approaches for radius fracture fixation have been described in Chapter 1.3.1. Both approaches are possible and are commonly used for the fixation of diaphyseal fractures of the radius and are characterized by positive and negative aspects. For example the Henry approach assures the presence of better soft tissue coverage of the implanted plate and its easier placement since the volar surface of the bone is flat. This approach has, although, the disadvantage of not permitting the implant of the plate on the most frequently tensioned side of the bone (dorsal surface) which is possible via the Thompson approach. The negative aspect of the dorsal approach is, instead, the big risk of damaging the posterior interosseous nerve during plate insertion and removal. [62] Eglseder et al., 2003 stated that the anterior plating (Henry approach) is usually preferred since it is easier to perform and has a reduced risk of damaging the surrounding structures (neves and tendons). [40] However, the choice of one specific approach is taken, in most of the cases, according to the surgeon's preference. [25]

The surgical approach chosen for this work was the *Henry approach* especially for the ease in plate implant due to the presence of a flat and defined surface.

- **PLATE LENGTH AND SCREW NUMBER**

The choice regarding the length of the plate and the number of screws for simple transverse fractures was made considering the data presented in Chapter 1 which are summarized in the following table.

| Reference | Plate length suggested | Number of screws suggested |
|--------------------------------|------------------------|---|
| Rüedi et al., 2000 [20] | 7-hole / 8-hole | 6 screws |
| Mehdi Nassab et al., 2012 [53] | 7- hole plate | 4 screws are suggested 6 screws are common |
| Lindvall et al., 2006 [36] | 7-hole plate | 4 screws are suggested 6 screws are common |
| Sanders et al., 2002 [52] | maximized | 4 screws are suggested 6 screws are common |
| Roberts et al., 2007 [63] | 8-hole plate | 6 screws |

Table 4: Plates and screws suggested in literature

As evident, most of the presented works suggest using, for diaphyseal simple fractures of the radius, 7-hole plates.

There is less agreement regarding the number of screws since various authors have proved the non-difference in terms of strength, healing time and healing capacity between the usage of 6 screws and the usage of 4 screws. Since fewer screws allow a smaller damaging of the bone it was suggested by various authors to adopt this last configuration.

Anyway, as stated in Chapter 1, the use of 6 screws appears the most common between orthopedic surgeons. For this reason the chosen configuration for this test campaign was a *7-hole plate* with *6 screws*, leaving the empty hole in correspondence of the imaginary fracture site.

- **PLATE TYPE**

As already mentioned in Chapter 1.3 various solutions are possible regarding the type of plates to use in case of radius shaft fractures. The systems which were adopted for the tests are here reported and they were mainly chosen because largely used by surgeons, because specifically suggested for radius forearm shaft fractures by the relative operative techniques and because they allow versatility in terms of plating technique.

Stryker offers the *VariAx Straight Narrow plating system* which comprehends locking compression plates which enable surgeons to fix a variety of small fragment midshaft fractures. These plates allow the usage of locking screws (which can be placed with a 15° angulation in each direction) together with non-locking screws, giving flexibility to the surgeon in terms of plating technique. These plates can therefore be used as compression plates, bridging plates or neutralization plates. [49] The Stryker VariAx, 7 hole, straight narrow plate used (Ref#: 629527) is shown in Figure 37.



Figure 37: Stryker VariAx 7 holes straight narrow plate

A second possibility for the fixation of forearm shaft fractures is given by *DePuy Synthes 3.5 mm LCP plates*. These plates have the characteristic of presenting combi-holes which allow placement of standard cortex screws on one side of them and locking screws on the opposite side. LCP plates can be used in compression configuration (with conventional or cortex screws), in locking configuration and with combined cortex and locking screws. [64] The DePuy Synthes 3.5 mm LCP 7 holes plate (Ref#:233.571) is shown in Figure 38:



Figure 38: DePuy Synthes LCP 3.5mm plate

- **SCREW TYPE AND SCREW DIMENSIONS**

The decision regarding which type of screws would be used depended on the plating technique chosen by the surgeon. For radius midshaft transverse fractures compression is usually required. [25] The above chosen plates allow obtaining compression in two ways: through the use of only bone screws (standard configuration) and through the combined use of bone and locking screws (hybrid configuration). Therefore, the chosen type of screws for the present work comprehended both locking and compression screws. Their diameter was chosen after literature research (Chapter 1) and after the evaluation of what possibilities were given by the chosen plating systems (VariAx straight narrow plates and DePuy Synthes LCP plates).

Literature research showed that 3.5 mm screws are nowadays the most widely used in forearm clinical applications. The Stryker VariAx Straight Narrow plating system allows the usage of the 3.5 mm screws and of 2.7 mm screws as well [49] while the DePuy Synthes LCP 3.5 mm plates permit the use of only 3.5 mm screws. [64]

It was also noticed that for a long period 4.5 mm screws were used, even if it seemed they could lead to higher re-fracture risk after removal.

The length of the screws was not an important parameter for this test since its aim was the evaluation of the influence on the fracture risk of the radius of holes of different dimensions left in consequence of screw removal. The length of the screws was then chosen according to the availability in stock. All the screws used for this work are listed in the following table and are shown in Figure 39 and Figure 40.

| Screw Ø [mm] | Length [mm] | Screw type | Producer | Ref # | Reason of choice |
|--------------|-------------|----------------|---------------|---------|--|
| 3.5 mm | 32 mm | Bone screws | Stryker | 614832 | -Most frequently Ø used in clinical applications. -Standard and hybrid configuration possible |
| 3.5 mm | 32 mm | Locking screws | Stryker | 614632 | |
| 3.5 mm | 32 mm | Cortex screws | DePuy Synthes | 204.832 | -Most frequently Ø used in clinical applications. -Standard and hybrid configuration possible |
| 3.5 mm | 32 mm | Locking screws | DePuy Synthes | 212.111 | |
| 2.7 mm | 32 mm | Bone screws | Stryker | 614732 | -Screw dimension offered by the VariAx plating system for forearm bones -Standard and hybrid configuration possible |
| 2.7 mm | 32 mm | Locking screws | Stryker | 614532 | |
| 4.5 mm | 32 mm | Bone screws | DePuy Synthes | 414.830 | Screws used in the past which showed clinically higher re-fracture risk |

Table 5: Screw adopted in the present work

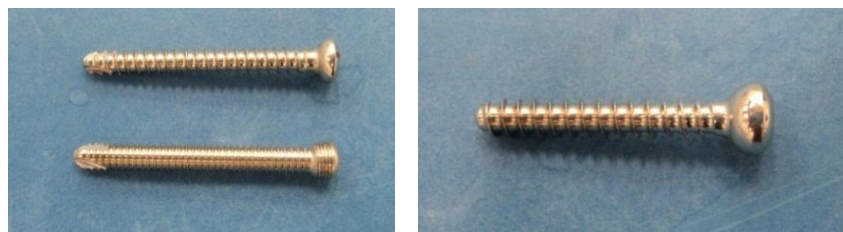


Figure 39: Left Top: DePuy Synthes 3.5mm cortex screw; Left bottom: DePuy Synthes 3.5mm locking screw; Right: DePuy Synthes 4.5mm cortex screw



Figure 40: Left: Stryker locking an bone screws 3.5mm; Right Stryker bone and locking screws 2.7 mm

2.1.2 Test Definition

The ideation, design and production of the test setup and of the samples used for the experimental test performance comprehended all the clinical considerations discussed in section 2.1.1 as well as various mechanical and biomechanical aspects which are presented below.

The first step in the definition and design of the test setup regarded the evaluation of the loads and loading patterns which lead to the chosen fracture type (radius diaphyseal transverse fracture).

This aspect was thought to be of major importance in the definition and in the justification from an injury point of view of the loading conditions to apply. An understanding of how bones respond to loads can help evaluating the forces and force patterns that caused the damage.

The bone, as most of the materials, is weakest in tension and strongest in compression. Therefore, when one or more forces create tensile stresses in one region, failure will most likely happen there.

The application of a pure bending moment on a long bone produces the elongation of one surface of the bone itself and the compression of the opposite portion. The failure initiates with the formation of a crack (when the failure stress is reached) on the surface characterized by tension, which then propagates until total failure of the structure occurs. The fracture generated by pure bending moments usually appears as a transverse fracture. This kind of fracture is normally seen on bones which are not bearing weight and are struck by a direct blow. Transverse fractures can also happen in presence of simple traction forces. [23] [65] [66]



Figure 41: Transverse fracture on a long bone produced by a bending moment [67]

Since it is most likely that a forearm bone fractures in consequence of the application of a bending moment rather than of a tensile force (since muscle tension tends to compress the bones) the application of one or more bending forces appeared to be a possible and justified solution for the performance of the experimental tests.

From a mechanical point of view the failure of a structure in presence of a bending moment can be described by equation (2) initially reported in Chapter 1 and presented again below.

In reference to the real bone structure, the application of the following equation could not give the exact stress value reached since the geometry of the bone is usually simplified in order to be able to use the formula. However, the result of the calculation can give an idea about the stress level reached when applying a certain force.

$$\sigma = \frac{M}{I} y \quad [\text{MPa}] \quad (2)$$

When σ (stress induced by the applied moment) reaches the stress limit of the material, usually σ_{rupture} for brittle materials (ex. cortical bone) and σ_{yielding} for ductile materials, the structure will fail (breakage or yielding).

The second aspect which was considered in defining the type of test performed comprehended the analysis of the forces that act on the radius bone during normal activities.

As described in Chapter 1 the muscles which find attachment on the radius are various and each one of them has a specific function to carry out.

Since the arm and forearm are the compartments which possess the main function of rotating the hand in space they must have a wide range of motion in order to precisely reach various positions with sufficient accuracy. The upper extremity complex permits to have an elbow flexion between 0° and 142° , 80° of pronation and 90° of supination capability. [68]

This range of motion, especially of the prono-supination, is permitted by the rotation of the forearm about a longitudinal axis passing approximately through the head of the radius and the lower end of the ulna. During the movement of pronation, the radius, carrying the hand with it, turns antero-medially across the ulna with the result that its lower part comes to lie medially to the ulna and the palm faces posteriorly. Oppositely during supination, the radius goes back to its original position (parallel and lateral to the ulna) so that the palm faces anteriorly. [6] [69] The forearm bones during pronation and supination are shown in Figure 42.

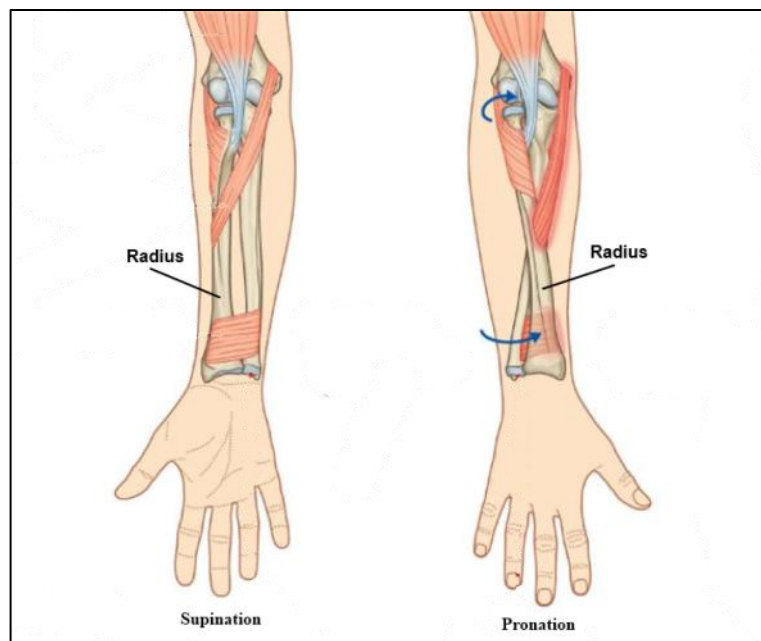


Figure 42: Forearm bones during pronation and supination [11]

As evident from the previous figure the orientation of the forearm bones can vary considerably. In fact, in supinated position the volar surface of the bone faces anteriorly while in pronated position it faces posteriorly and the radius crosses the ulna. Therefore similar actions performed with the forearm in pronated or supinated position will stress the bone structure in completely different ways, also because the muscle attachments are fixed and do not change in dependence to the rate of rotation reached.

A literature research was performed with the aim of evaluating if some scientific works giving an overview about the main loads acting on the radius shaft, existed. The first outcome of the research was the wide range of results reported for the reason that the movements that can be performed and the orientations that can be assumed by the radius are multiple. In addition, every action requires the activation of different muscles and therefore different force and stress patterns on the radius and ulna.

For example, Ekenstam et al., 1984 evaluated the compression forces that acted on the radius and ulna in correspondence of various orientations of the forearm during a test on cadaveric limbs when diverse axial loads were applied on four tendons of the wrist. The result showed that it did not matter whether the forearm was in neutral, supinated or pronated position. The radius in fact always bore the biggest part of the load (63 – 92 %) in comparison to the ulna. [70]

Similar test was performed by Palmer et al., 1984. The results of this work were in accordance with the previously reported ones. The radius, in fact, showed to carry approximately 80% of the axial load of the forearm, even when in different positions. [71]

The two summarized works showed that when axial forces are applied to the forearm the radius bears the biggest portion of the loads. However, the presented tests were performed to simulate just one type of situation, the loading caused by the wrist muscles, in correspondence of different forearm orientations. This was not considered as a situation of main interest for the purpose of this work since it did not analyze a defined and specified action. It only justified the choice of evaluating the radius bone behavior after screw removal since it commonly carries more loads.

An internal test which used the software Anybody Modeling System (AMS) V. 4.1 was analyzed. The aim of the test was to evaluate the forces and moments acting on the forearm bones during common daily activities. In particular the lifting of a box of 2, 5, 10 Kg with both hands and of a 1, 2, 5 Kg weight with one hand were simulated. The results are presented in the following figures for the 5 Kg actions, together with the coordinate system used to define forces and moments. [72]

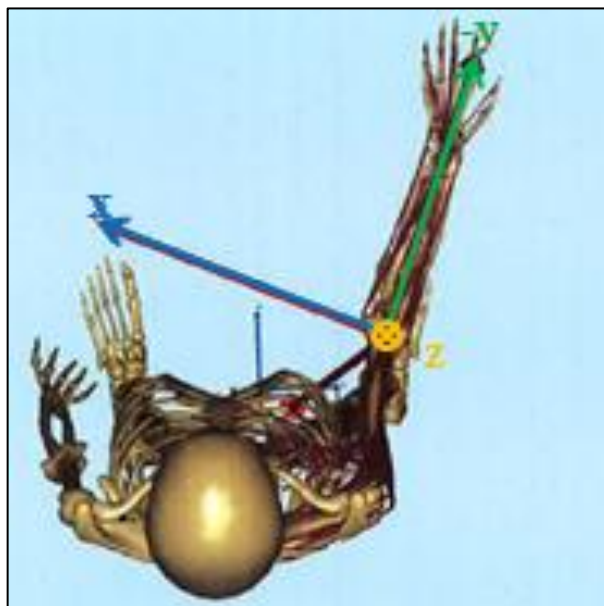


Figure 43: Coordinate system for the AnyBody study [72]

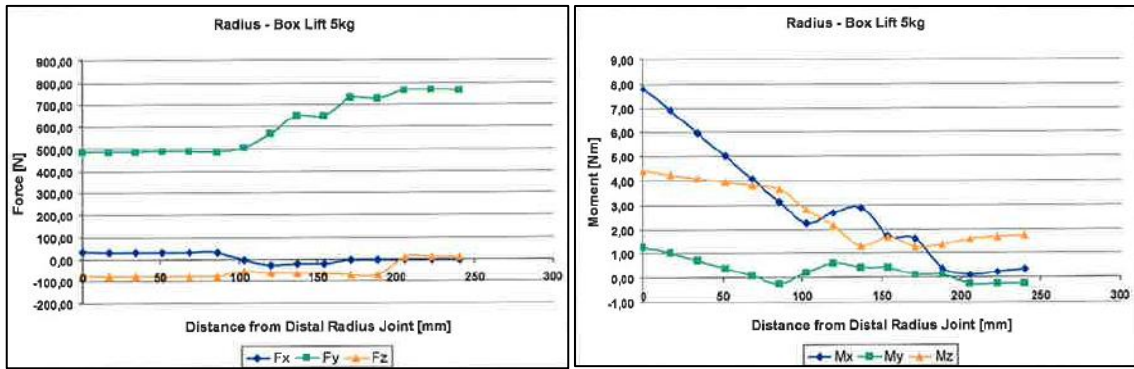


Figure 44: 5 Kg box lifting with both hands. Left: Internal forces; Right: Internal moments [72]

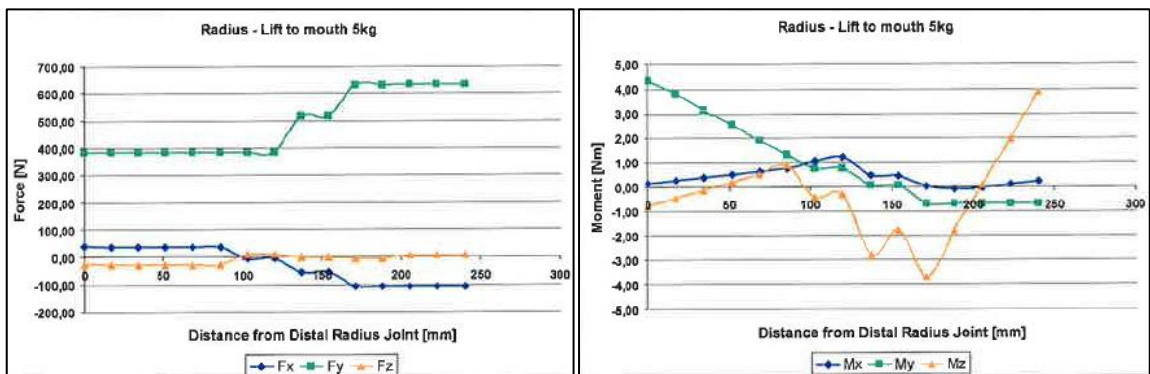


Figure 45: 5 Kg weight lifting with one hand. Left: Internal forces; Right: Internal moments [72]

The analysis of Figure 44 and Figure 45 showed that both actions analyzed led to evident compression of the radius (F_y) in a stepwise trend. This happens because the attachments of the muscles, as described in detail in Chapter 1, are located at different distances from the distal radius joint. Therefore, each step occurs at the insertion point of a muscle where a new compressive force sums to the one present more distally. The region subject to maximum compression is the most proximal part of the radius, where the axial forces given by each muscle are summed. The two analyzed movements showed a similar force pattern since muscles always work compressing the bones and the attachment sites are in both cases the same. Shear forces (F_x and F_z) are not so influent if compared to the axial loads.

On the opposite, the moments generated during the box lifting and during the one hand weight lifting do not show any similarity between themselves.

In the box lifting M_x and M_z assume a higher average value if compared with M_y (torque) while during the action of weight lifting with one hand M_y and M_z assume in general greater absolute values in comparison to M_x .

The problem in such results was the difficulty in understanding what stress was generated by each moment since it is not clear from the related report if the associated coordinate system moves together with the bone movement or if it is fixed in the elbow joint.

Secondarily, the complexity of the moment trends on the bone and their difficult reproduction in an experimental test are evident.

The already mentioned big difference present between moment trends, when different activities are performed, would require the analysis of a great number of situations for finding the worst case to reproduce accurately in an experimental test.

Moments generated by the execution of daily activities were also studied by Winemaker et al., 1998 who instrumented external fixators with strain gauges in order to quantify bending and torsional forces. The patients which had the system mounted were four and had a metaphyseal fracture of the distal radius. The results of the test in terms of maximum moments recorded are given in Figure 46.

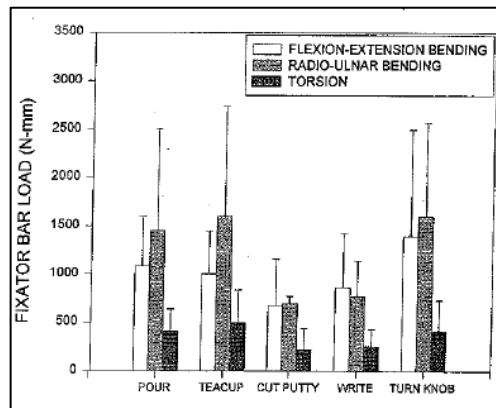


Figure 46: Maximum flexion and torsion on the forearm external fixator [73]

Flexion-extension bending refers to an antero-posterior moment on the radius while radio-ulnar bending to a medio-lateral moment on the bone itself.

The results of this work show that during normal life activities medio-lateral and antero-posterior flexions are the most present on the external fixator and therefore on the radius bone.

However, it must be kept in mind that the numerical values obtained were measured on the bar of the external fixator. Therefore, the entity and relationship between moments actually present on the bones might be different since there could be various factors which alter the measurement. [73]

The most evident aspect from the analyzed scientific works is that it did not appear possible to find a consistent number of articles which considered and compared the same situations or defined a worst case in terms of forearm loading. As mentioned previously, in fact, the possible movements of the upper extremities is very wide and the choice of one specific activity on which to analyze and compare all the present forces, moments and stresses was never performed.

It was therefore decided to analyze the standard situation described by the biomechanical model of the flexed elbow with the forearm in supinated position presented in various books (for example Frankel et al., 1980 [69]) since it represented a well-established study case (Figure 47).

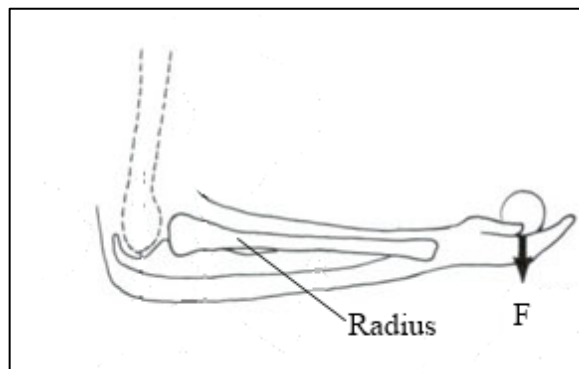


Figure 47: Elbow and forearm biomechanical model [74]

Muscles were intentionally not inserted in Figure 47 since the idea was to also consider electromyography (EMG) data which would help choosing the most active and most important muscles attached on the radius when the elbow is in 90° flexion with the forearm in supinated position.

Frenkel et al., 1980 and Berme, 1980 gave an idea of the most activated muscles of the forearm during elbow flexion. Regarding only the muscles inserted on the radius the biceps brachii and the brachioradialis were considered as primary flexors while the pronator teres was described as accessory flexor. [69] [75]

Naito et al., 1998 performed electromyographic measurements during a forearm pronation - supination - pronation movement against increasing torques while the elbow was flexed at different angulations.

The results showed the same pattern of activation of the muscles. The differences were evident in terms of activation entity: the higher torque caused, in fact, higher muscle contraction. The results of the measurements with the elbow flexed at 90° are shown in Figure 48. The highlighted muscles are the muscles which insert on the radius bone (BL and BS represent the long and short heads of the biceps brachii; BR represents the brachioradialis) while B (brachialis muscle) and TL (lateral head of triceps brachii) find attachment on the ulna.

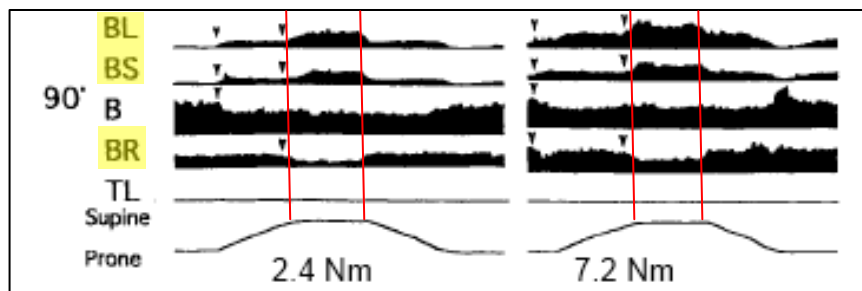


Figure 48: EMG measurements for pronation-supination-pronation of the forearm in 90° flexion against 2.4 Nm and 7.2 Nm torque [76]

The result of the study showed an increase of the activation of the biceps brachii muscle and a decrease of the brachioradialis when the forearm is in supinated position. Despite the mentioned decrease, the brachioradialis muscle is still significantly active during supination. [76]

The analyzed EMG results are summarized in the following table.

| Source | Main flexor muscles | Accessory flexor muscles |
|---------------------------|---------------------------------|--------------------------|
| Frenkel et al., 1980 [69] | Biceps brachii, brachioradialis | Pronator teres |
| Berme, 1980 [75] | Biceps brachii, brachioradialis | - |
| Naito et al., 1998 [76] | Biceps brachii, brachioradialis | - |

Table 6: Main activated muscles during elbow flexion with supinated forearm

The analysis of the above presented EMG data suggested the choice of the biceps brachii, brachioradialis and pronator teres muscles to be inserted in the previously presented biomechanical model.

The resulting model, comprehensive of the selected muscles, is shown in Figure 49.

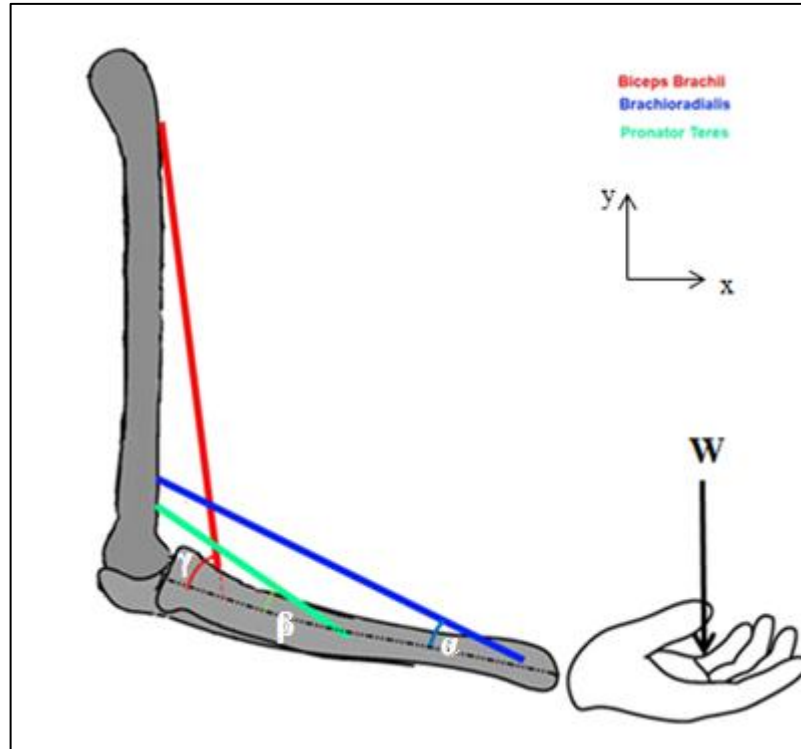


Figure 49: Forearm biomechanical model with the three considered muscles

The work of Amis et al., 1980 gave the values of the normalized components of the force exerted by each forearm muscle (F_x , F_y , F_z) during different positions in terms of degree of elbow flexion. [77]. The knowledge of F_x and F_y allowed the calculation of the angle between each muscle insertion and axis of the bone through the following formula:

$$\text{angle} = \tan^{-1} \left(\frac{F_y}{F_x} \right) \quad (4)$$

The values of the two normalized components of the force and of the angles calculated between each muscle and the x axis (longitudinal axis of the radius) are listed in Table 7 for the elbow in 90° flexion.

| Muscle | F_x | F_y | angle[°] |
|-----------------|--------|-------|------------------------|
| Brachioradialis | -0.916 | 0.389 | $\alpha = 23,01^\circ$ |
| Pronator Teres | 0.956 | 0.071 | $\beta = 4.23^\circ$ |
| Biceps Brachii | -0.168 | 0.985 | $\gamma = 80.32^\circ$ |

Table 7: F_x and F_y relationships for the muscles inserted on the radius

The values presented in Table 7 show how the force is divided between horizontal and vertical components in the x –y plane. It is evident that the biggest part of the force exerted by the biceps brachii is vertical while the biggest part of the force exerted by the brachioradialis and by the pronator teres is horizontal.

The studied situation (Figure 49) can be developed as shown in the following figure. The grey arrows represent the exchanged forces and moments between radius and humerus in correspondence of the elbow joint.

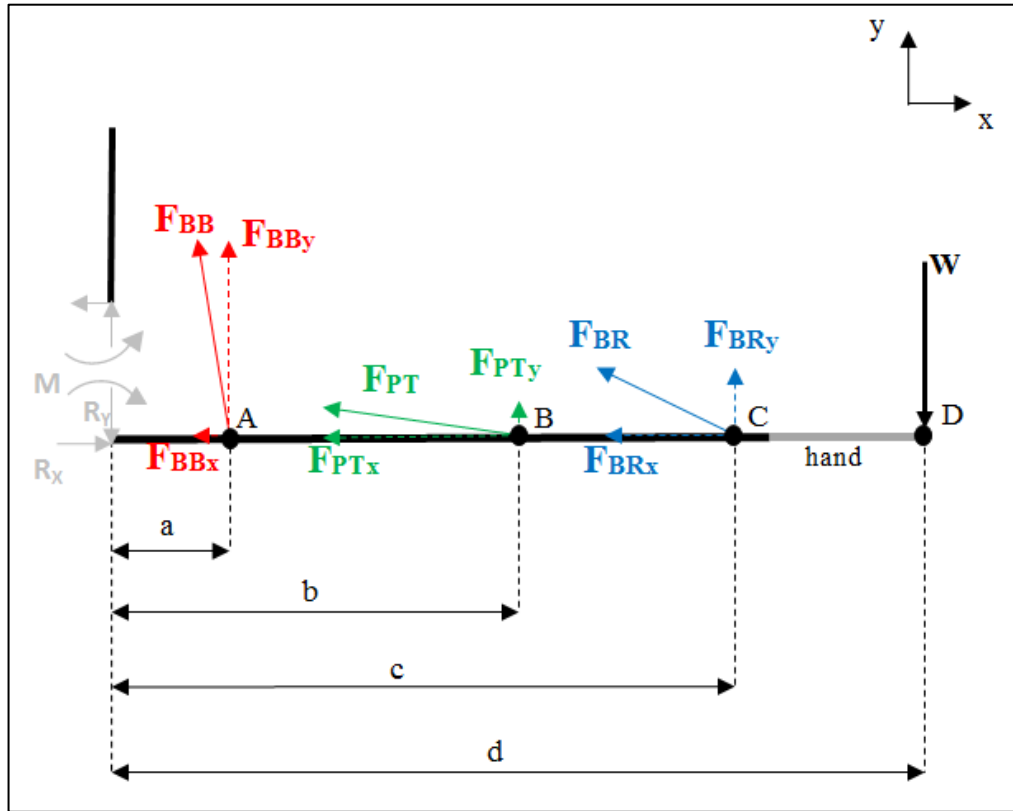


Figure 50: Biomechanical model of the forearm.

F_{BB} : biceps brachii force; F_{PT} : pronator teres force; F_{BR} : brachioradialis force

The distances between the points of application of each force and the elbow joint have been taken from various sources and are listed below:

| Dimension | Distance between | Distance | Source |
|-----------|-------------------------|----------|---------------------------------|
| a | Elbow – biceps brachii | 50 mm | Frankel et al., 1980 [69] |
| b | Elbow – pronator teres | 125 mm | Anatomical tables |
| c | Elbow – brachioradialis | 230 mm | Measurement on CAD radius model |
| d | Elbow – hand center | 350 mm | Stanley et al., 2012 [68] |

Table 8: Distance between the elbow joint and the insertion of the considered muscles

Calculating the equilibrium equations the following system was obtained:

$$\begin{cases} R_y = F_{BB_y} + F_{PT_y} + F_{BR_y} - W & [N] \\ R_x = F_{BB_x} + F_{PT_x} + F_{BR_x} & [N] \\ M = F_{BB_y} * a + F_{PT_y} * b + F_{BR_y} * c - W * a & [Nmm] \end{cases} \quad (5)$$

The axial and compression trends that appear on the radius are presented in the following figure. Since the force values are not known the trends are just indicative. The relationship between each zone was in fact made qualitatively but keeping in account the muscles that are generally more active and the prevalence of F_x or F_y for each muscle.

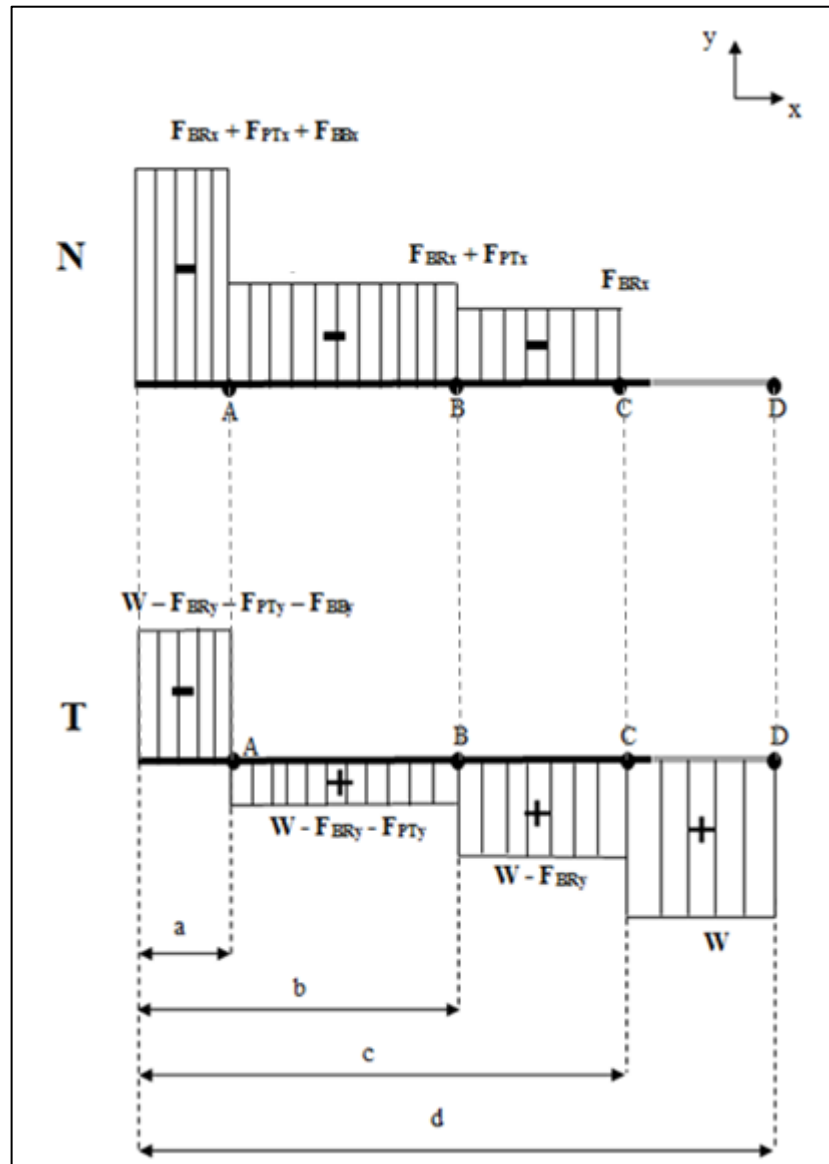


Figure 51: Qualitative Axial (N) and shear (T) trends resulted from the biomechanical model

The moment trend can also assume various different shapes since it depends as well on the entity of the forces exerted by the muscles, on the carried load W and on the angle of flexion of the elbow.

A possible moment trend on the radius is presented in Figure 52. The slopes were qualitatively drawn keeping in consideration, as done for axial and shear forces, the angle between the insertion of the muscle and the bone axis and the more active muscles during elbow flexion.

Therefore, in the areas characterized by a slow change of the slope (for example B-C) there is a low vertical force applied (or a very small lever arm). In B, in fact, the pronator teres, which showed a small angle with the x axis and therefore a small vertical force component, finds attachment.

In the areas where the slope gradient is high (for example C-D) there is a high force applied (or a large lever arm). The biceps brachii, which is inserted in C, is the strongest elbow flexor and can develop forces which can reach 7 times the weight W in the hand. The other muscles exert maximum 2 or 3 times the force applied on the hand [68]

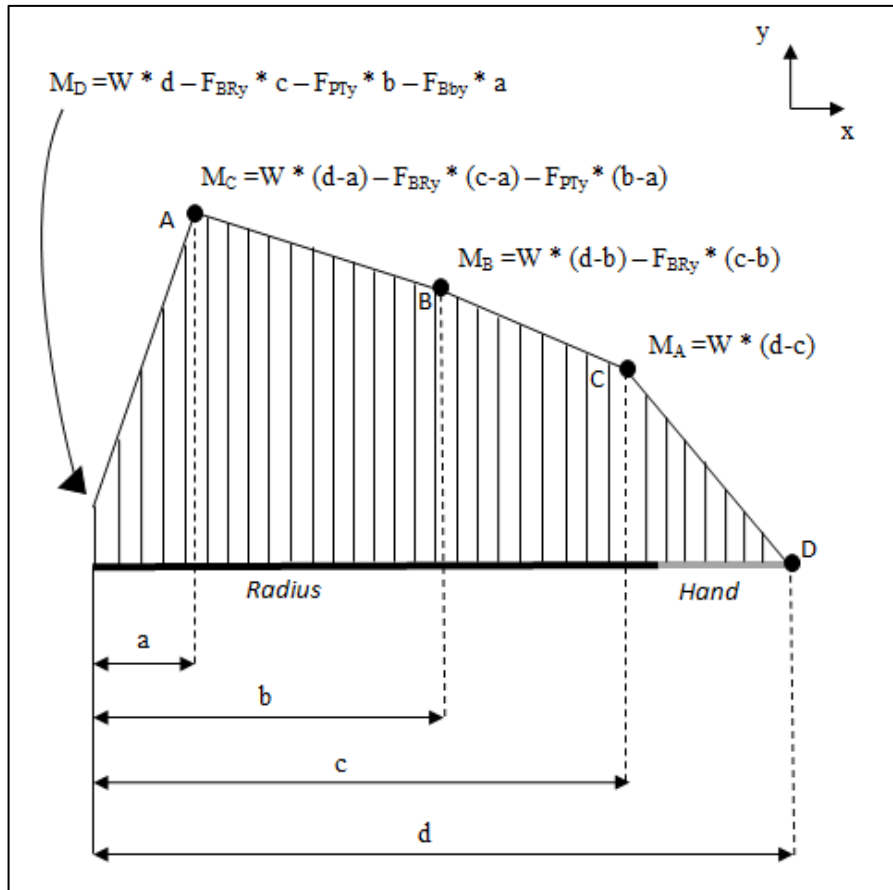


Figure 52: Qualitative moment trend resulted from the biomechanical model

Considering the forearm positioned as described in the model of Figure 49, which represents the forearm in supinated position and with the elbow flexed at 90° , and the moment distribution of Figure 52, the volar surface of the radius appears to be the surface which is subject to tension and therefore at more risk of failure.

However, even high compressive and shear forces are present as can be noticed from Figure 51.

In standard mechanical verification and testing shear forces can be excluded since they appear less dangerous compared to bending and tension.

With reference to the presented data the possibilities in terms of testing reduce to a compression test in axial direction or a bending test.

- **COMPRESSION TEST**

The main positive aspect regarding the compression test regards the fact that the radius bone, like most of the bone structures, is normally compressed by the action of the muscles. This test would, therefore, simulate a real condition which is always present in physiological situations.

The negative aspect regards the actual outcome of the test. In fact, since the radius is characterized by a curvature in the central portion, compressing the bone by applying a force at one end of the bone would generate a growing moment with its maximum in correspondence of the maximal lever arm as shown in the following figure.

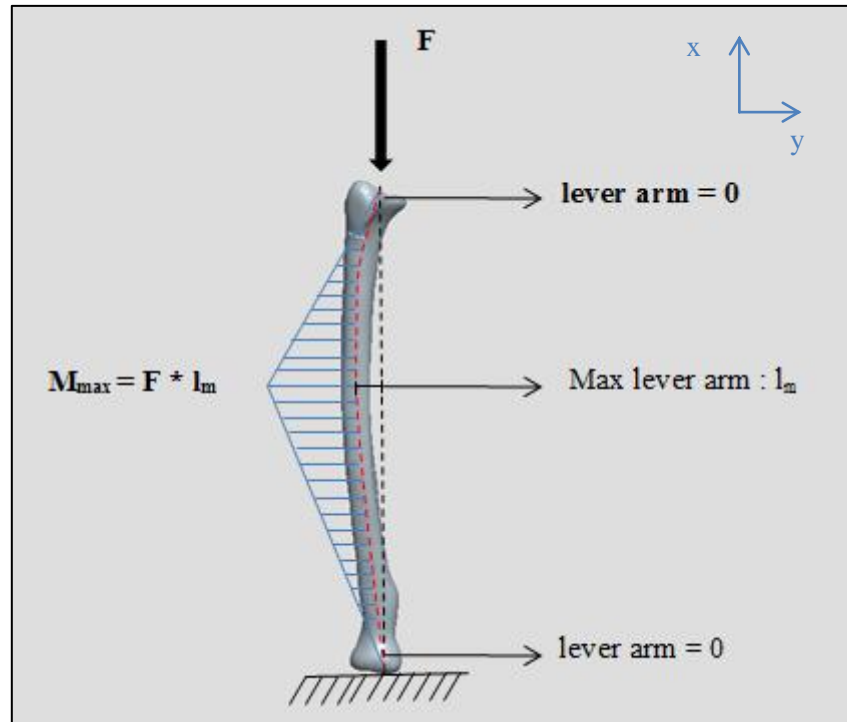


Figure 53: Compression test analytical analysis

The presence of one peak would probably cause the failure of the structure in the proximity of that point, not allowing seeing eventual weaknesses in other parts of the structure caused for example by the presence of a hole in a critical point, by the presence of a smaller cross section, etc. The correct compression test should simulate the trend of Figure 51 but the needed test setup would be much more complicated.

- **BENDING TEST**

The most common bending tests are 3-point bending test, cantilever bending test and 4-point bending test.

The cantilever bending test does not replicate at all the loading situation presented in Figure 52.

The 3-point bending test would produce an output comparable to the one showed in Figure 53 and therefore it was not taken into account as a possible test.

A 4-point bending test occurs when two couples of opposite forces, acting on a structure produce two equal moments. The resultant bending moment magnitude between the two central forces is constant. The structure being tested should fracture at its weakest point since this test does not influence the samples by locating a maximum bending moment in a specific position. [78]

The 4-point bending test is schematically presented in Figure 54.

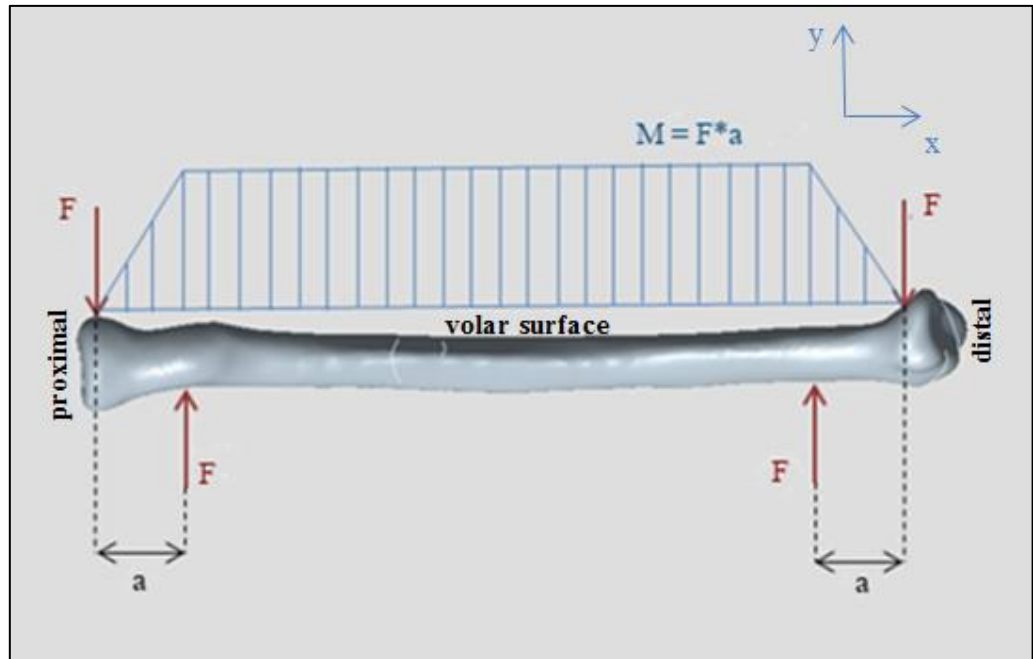


Figure 54: 4-point bending test

Comparing the moment trends of Figure 52 and Figure 54 it is possible to consider the 4 point bending test as a worst case of the biomechanical model. The trends are in fact not completely different in shape and a higher moment on almost all the structure is present (see Figure 55)

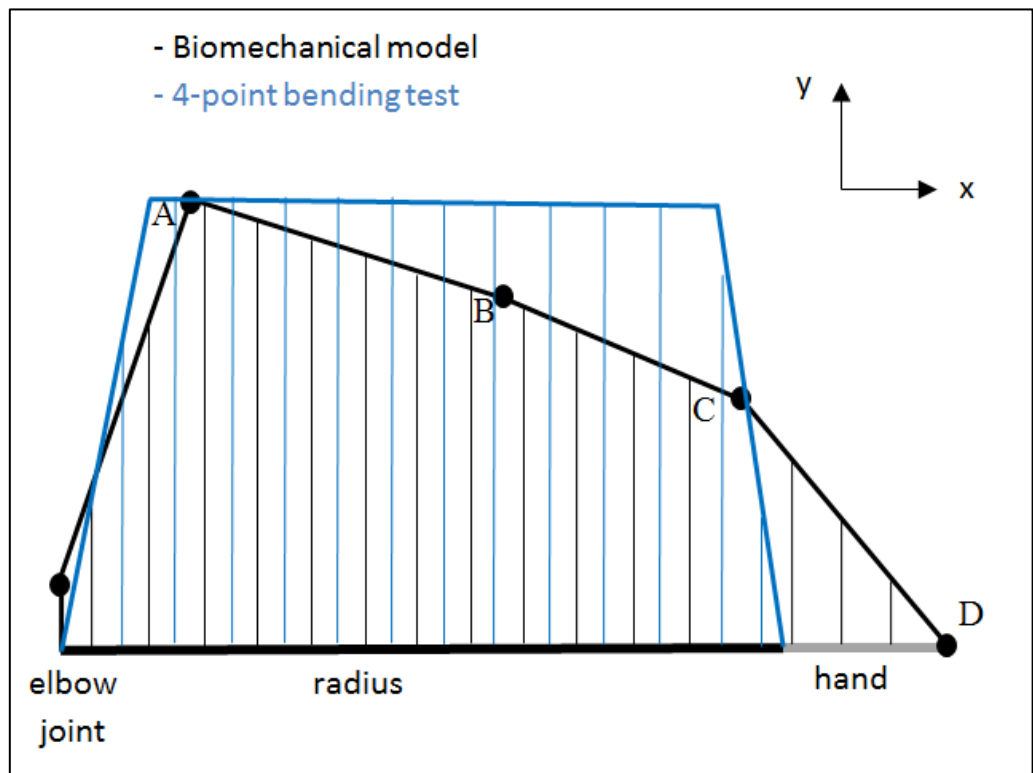


Figure 55: 4-point bending test and biomechanical model moment comparison

The type of test performed on the radius bone was finally decided to be a *4-point bending test*. The moment would be applied in the *antero-posterior plane* and directed from *antero-to-posterior*. This would cause a tensioning of the volar surface of the radius. The choice of the plane and direction of bending was taken due to the biomechanical model output in terms of bending moment (Figure 52) and after the consideration of the following mechanical aspects.

- I. The tests performed would have the aim of evaluating the influence in the fracture of the bone of the holes left after the removal of screws. The presence of a hole, as already stated in the previous chapter, acts as a stress riser because of the reduction of the cross section (and of the second moment of inertia) and because of the uprising of a stress concentration in proximity of the hole.

The application of a moment in different planes in reference to the direction of the axis of the hole gives different results in terms of generated stresses and therefore in terms of risk of failure of the structure since the second moment of inertia is not always the same but it depends on the reference axis for its calculation. Two main planes of bending are possible on the radius: bending in the antero-posterior plane (AP) and bending in the medio-lateral (ML) plane. All other bending are intermediate situations.

Considering the bone as a cylindrical tube and assuming the screws were implanted following the Henry surgical approach, as shown in the 3D simplified model in Figure 56, the two chosen possible planes produce the situations described in Table 9.

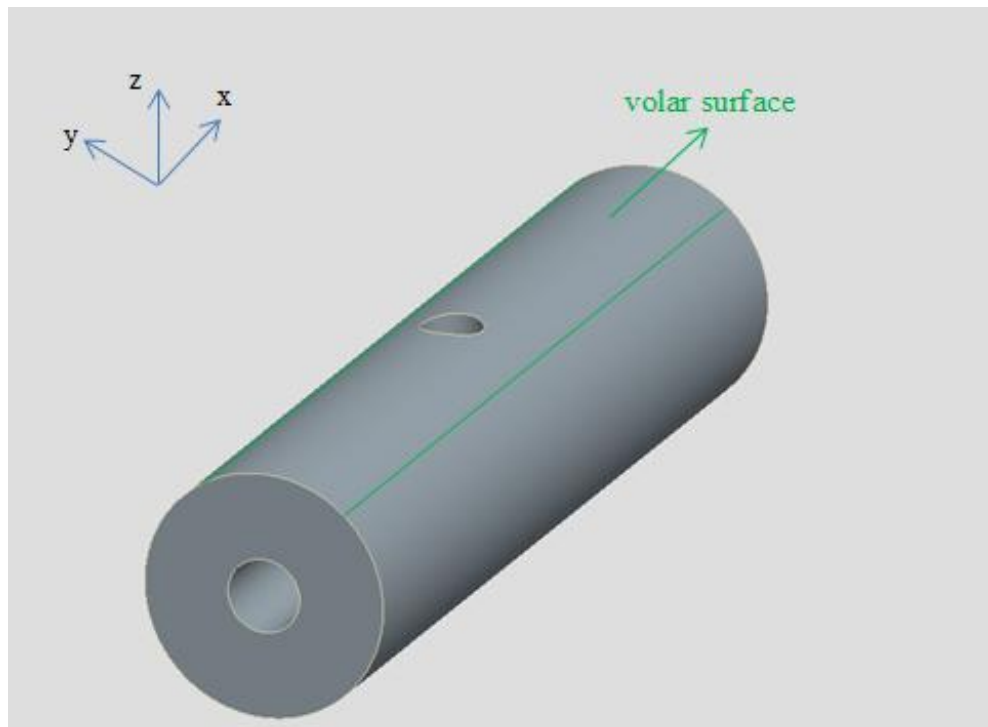


Figure 56: Simplified model of the bone and hole

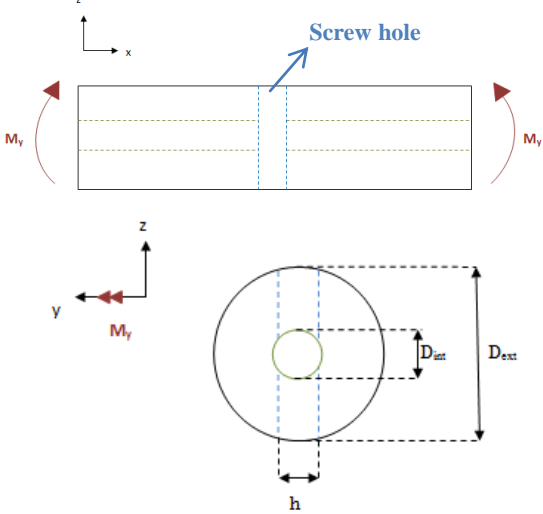
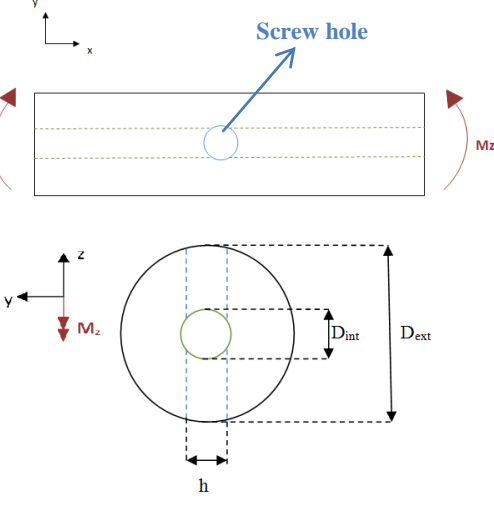
| Bending in the AP plane | Bending in the ML plane |
|--|--|
|  |  |
| $I_{yAP} = I_{y \text{ tube}} - I_{y \text{ rect}}$ $= \frac{\pi (D_{\text{ext}}^4 - D_{\text{int}}^4)}{64} - \frac{D_{\text{ext}}^3 * h}{12}$ | $I_{yML} = I_{y \text{ tube}} - I_{y \text{ rect}}$ $= \frac{\pi (D_{\text{ext}}^4 - D_{\text{int}}^4)}{64} - \frac{D_{\text{ext}} * h^3}{12}$ |
| $I_{yAP} < I_{yML}$ | |
| $\sigma_{AP} = \frac{M_y * \frac{D_{\text{ext}}}{2}}{I_{yAP}}$ | $\sigma_{ML} = \frac{M_y * \frac{D_{\text{ext}}}{2}}{I_{yML}}$ |
| $\sigma_{yAP} > \sigma_{yML}$ | |

Table 9: Stress calculation for AP and ML bending

The calculations in Table 9 demonstrate that the worst case bending is the one performed in the same plane of the axis of the screw.

➔ The bending in the antero-posterior plane is the worst case in terms of generated stresses, when the screws are implanted following the Henry approach.

- II. Once the worst bending plane was found the direction of application of the moment had to be chosen. In fact, since the radius is not really a straight tube, the application of an antero-to-posterior (blue) or of a postero-to-anterior (red) moment generates different outputs. This aspect is due to the curvature of the radius which can be simplified as a curved beam (Figure 57).

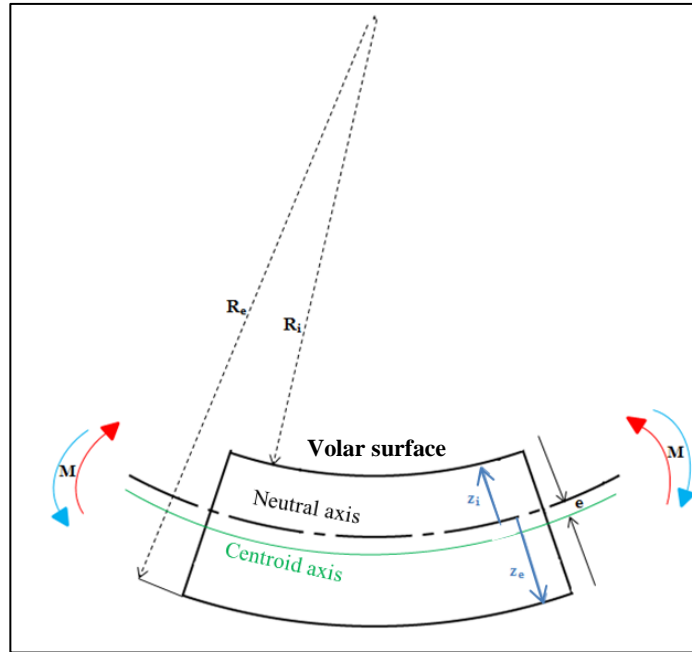


Figure 57: Curved beam theory (modified from [59])

The inner surface represents the anterior surface of the radius.

R_e and R_i are respectively the external and internal radiuses of the beam referred to the center of curvature; e is the distance between the centroid of the cross section the position of the neutral axis; z_i and z_e are the distances between the inner and outer surfaces of the beam and the neutral axis; A is the area of the cross section.

The curved beam theory states that since the neutral axis of the beam does not pass through the centroid of the cross section (it is shifted towards the center of curvature of the beam) the generated stress distribution during bending becomes non-linear.

The stress distribution is, in fact, hyperbolic and is characterized by the following two extreme values on the inner and outer surface of the beam (σ_i and σ_o):

$$\sigma_i = \frac{M z_i}{e A R_i} \quad (6)$$

$$\sigma_o = -\frac{M z_o}{e A R_o}$$

The sign convention considers a positive moment as the one tending to straighten the beam (blue moment in Figure 57).

The maximum stress (σ_i) is always achieved on the closest surface to the center of rotation (inner surface). When a positive moment is applied it is a tension stress, when a negative moment is applied it is a compression stress. On the outer surface the opposite stress is present and it has a lower absolute value. [79] [80] The complete demonstration of the stresses in bended beams in presented in Attachment 1.

The actual stress trend on a curved beam is shown in the following image:

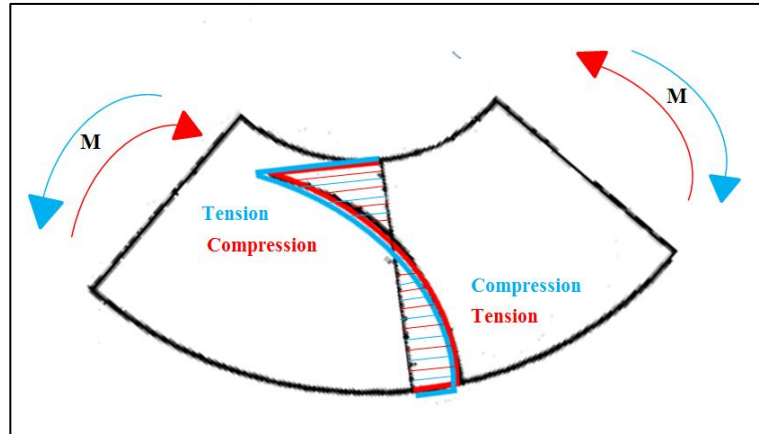


Figure 58: Moment distribution in a curved beam with positive (blue) and negative (red) moments (modified from [59])

- The worst case, considering the radius as a bended beam is, an anterior-to-posterior bending since it tends to straighten the structure and generates a peak of tension stress in correspondence of the anterior surface of the bone (surface where the plate is implanted following the Henry approach). The opposite moment generates a peak stress of compression in correspondence of the same surface (a compression is usually less dangerous in terms of static resistance if compared with tension).

The choice of performing a 4-point bending test with tensioning of the volar surface was also taken in other scientific works.

For example, Gardner et al., 2005 tested some plates applied on the radius by tensioning the volar surface in a 4-point bending configuration. [81] No justification was made regarding the reason why this loading pattern was chosen.

Eglseder et al., 2003, also tested various plates implanted on the volar surface of the radius. The moments applied were from antero-to-posterior since, it was stated, it was the configuration that simulated better the bending stress caused by muscle forces on the forearm. [40] No more detailed explanation was given. The setup used in this last work is presented in the following figure.

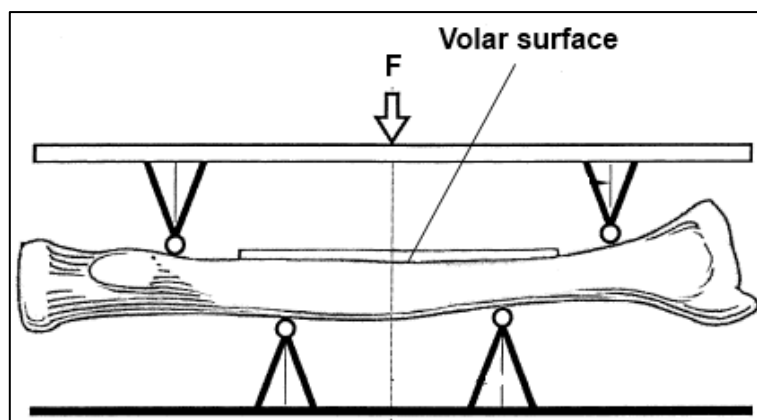


Figure 59: Test setup used by Eglseder et al., 2003 [40]

2.2 Experimental test 1

2.2.1 Sample definition

The successive phase was the actual CAD design of the samples to test and of the test setup considering all the above discussed aspects. As described in the previous pages the designated test would be a 4-point bending test with tensioning of the volar surface of the bone on which holes left by screw removal are present.

The design of the samples was done using the CAD software PTC Creo /Pro.

As first step a radius 3D bone model was requested from the Stryker SOMA bone database. The radius was scanned from a single patient and had dimensions similar to the average bone of the database. Additionally, the bone marrow canal + trabecular bone model was also requested.

The received models were obtained through CT scan of the forearm of a 39 years old Caucasian man, 189 cm tall and 75 Kg in weight. The radius was the left bone and it was never subject to fractures. The max length of the radius was 233.7 mm.

The following figures show the mentioned CAD radius bone models.

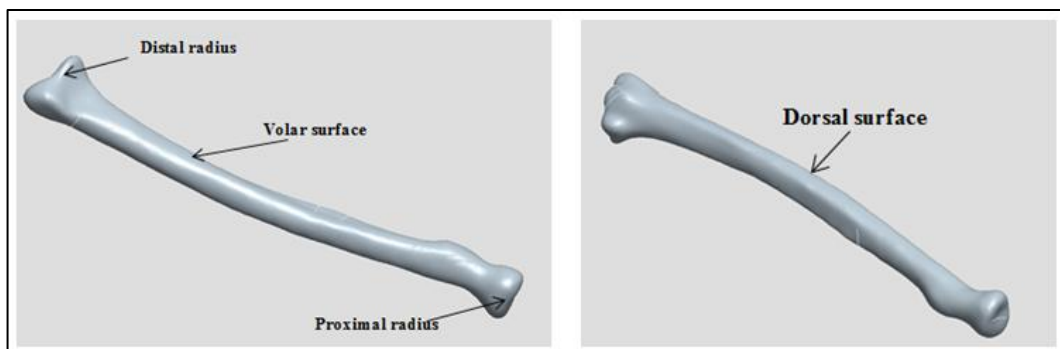
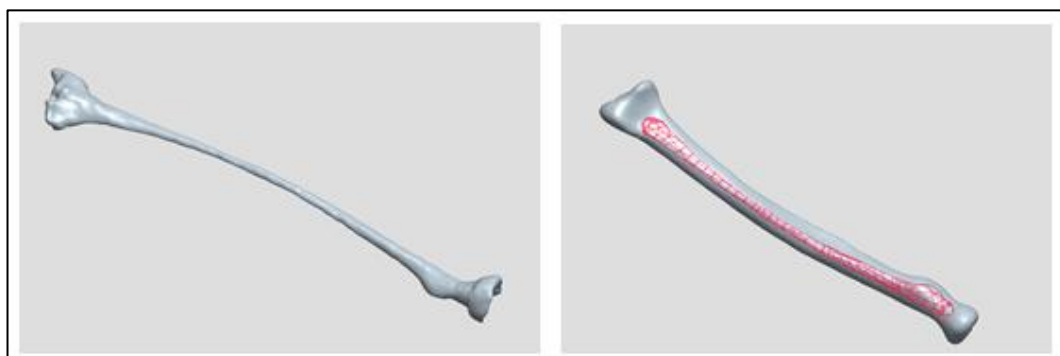


Figure 60: Radius bone model



*Figure 61: Left: Bone marrow canal + spongy bone;
Right: Subtraction of the bone marrow from the cortical bone model*

Figure 61 right showed that the subtraction involved only part of the bone marrow + spongy bone since the distal and proximal regions of the radius were not of interest for the test and would be needed as parts of the supports of the samples

The 3D models of the chosen plates (VariAx 7 holes Straight Narrow plate and DePuy Synthes LCP 7 holes plate) were also obtained and were assembled on the radius. They were placed on the volar surface of the bone according to the Henry approach and, as explained in the previous sections, they were mounted in the central portion of the shaft. Attention was paid in virtually placing the center of both plates in the same point and in aligning the front and top planes of both plates. This was done to have the exact same placement and orientation of plates and holes. The only parameters that vary are the parameters regarding the screws (diameter) and the actual plate design (distance between screws).

The radius bone with both plates implanted is shown in Figure 62.

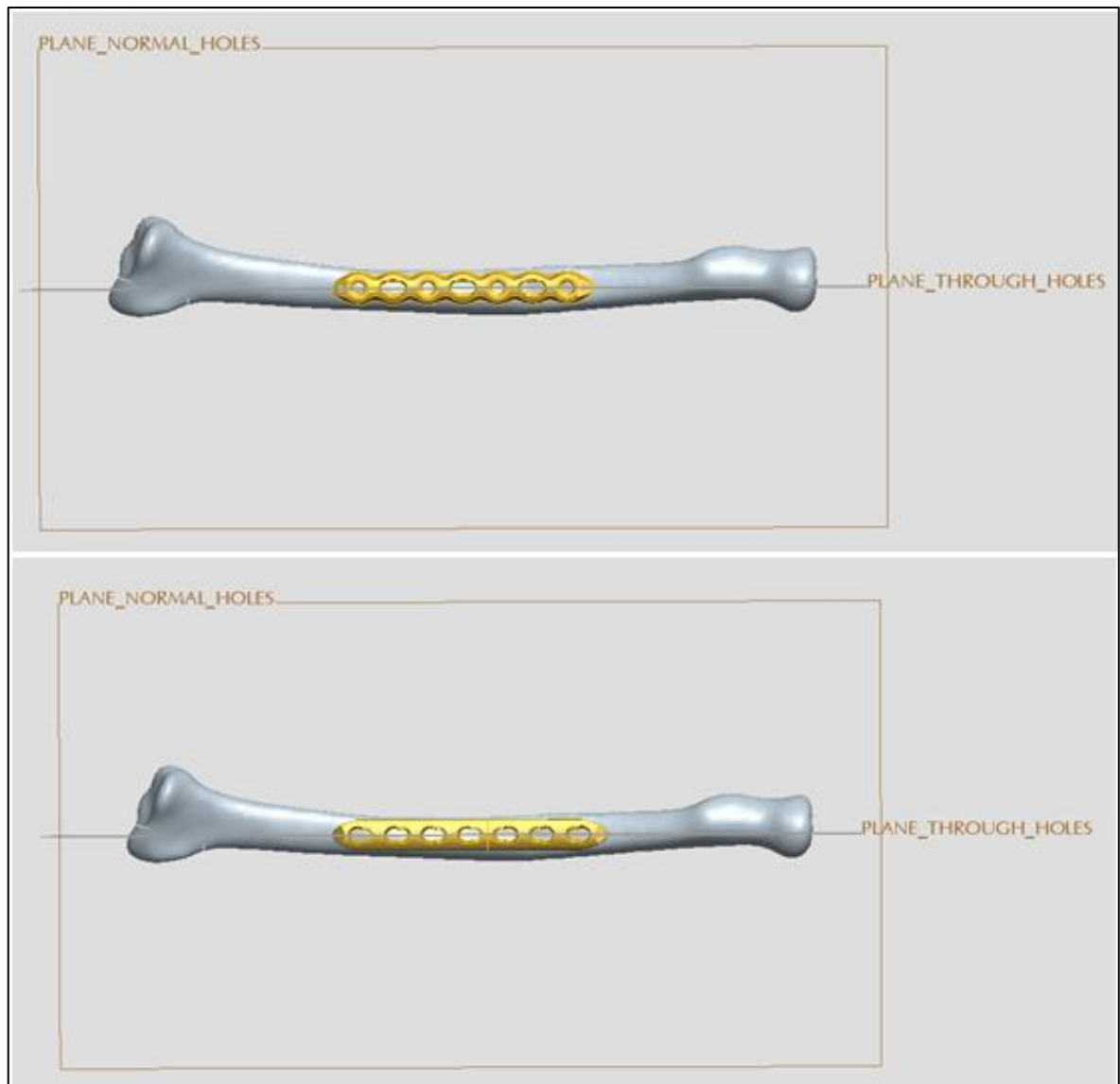


Figure 62: Plates positioned on the radius bone model.
Top: VariAx 7 hole Straight Narrow plate; Bottom: DePuy Synthes LCP 7 hole plate

The radius with the positioned plate and screws was created in order to get a clinical approval regarding the placement by Dr. Araghi and Dr. Adamany.

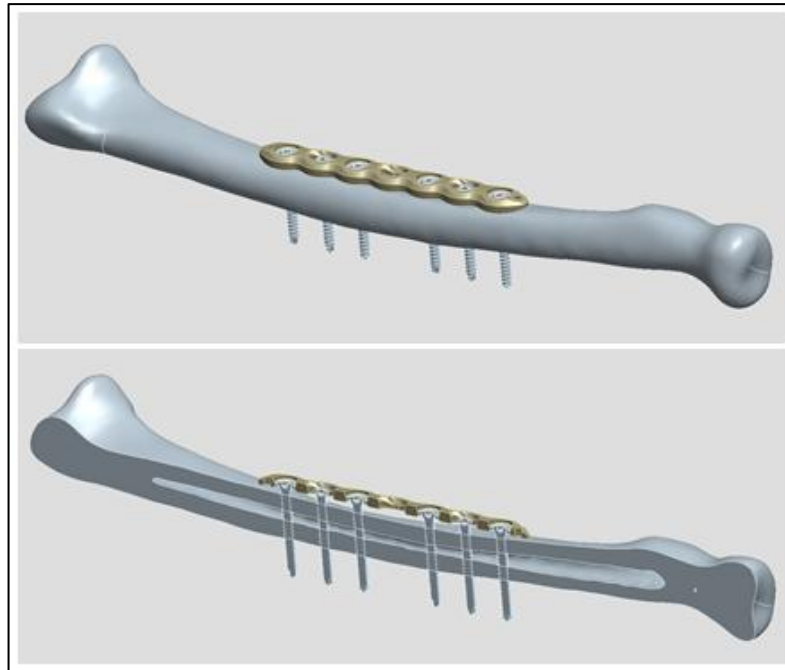


Figure 63: Top: Radius bone with VariAx 7 hole plate and 3.5 mm screws; Bottom: Cross section through the axis of the screws

A plane passing through the axes of the holes of the plates and a plane normal to it were created (plane_through_holes; plane_normal_holes) as can be also seen in Figure 62.

This allowed an easier design of the four areas of force application (couplings) assuring that the moments applied were in the same plane as the axes of the screws as required by the mechanical considerations discussed in section 2.1.2. The four couplings (2 for loading and 2 for support) designed to permit the tensioning of the volar surface during the test are shown in Figure 64.

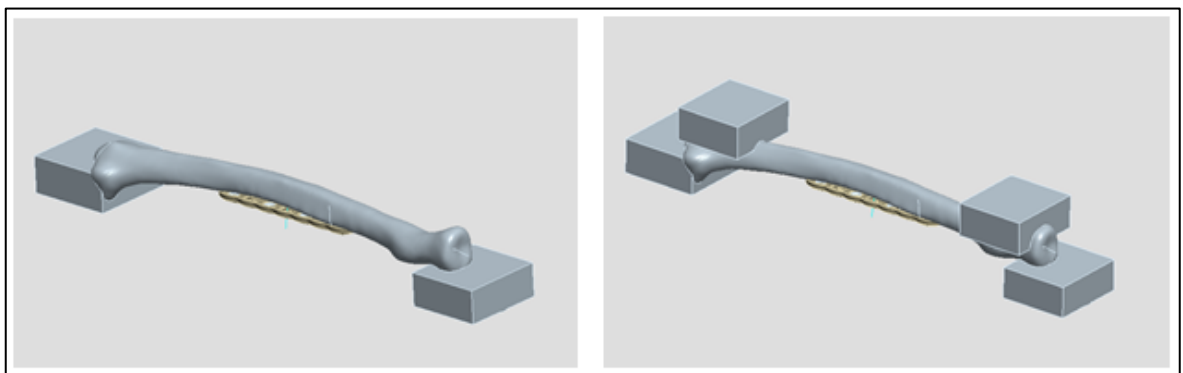


Figure 64: Inferior and superior couplings for force application

The most important parameter of a 4 point bending test is the distance between upper and lower couplings (defined as ‘a’ in the following image). This dimension must be the same for the left part and for the right part of the sample in order to be sure to obtain a constant moment in the central portion of the sample.

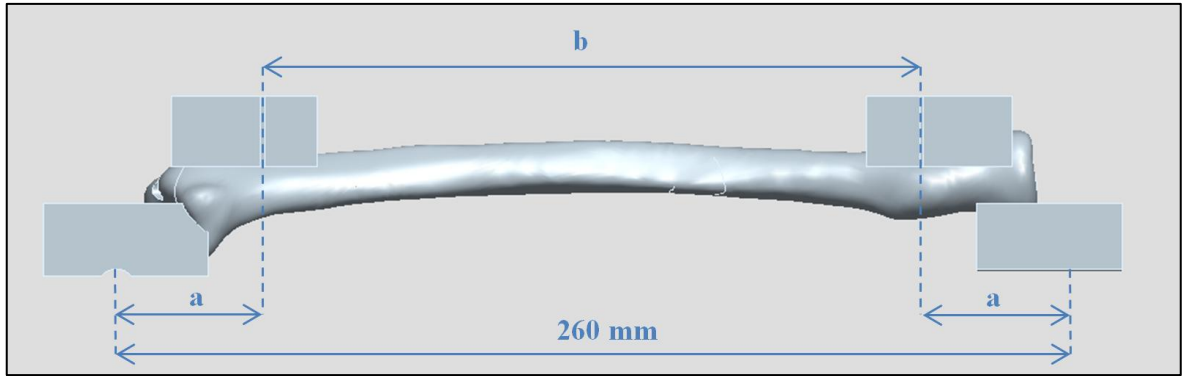


Figure 65: Frontal view of the samples

The choice of the distance between upper and lower forces ('a' in Figure 65) was taken together with the choice of the material with which the samples would be produced.

The target was to have a material which allowed the application of enough force to be able to detect eventual differences in terms of energy to failure between different samples and at the same time required the use of load cells available in the laboratory equipment.

A second requirement regarded the need to have a rapid and economically feasible production of the samples since the initial idea was to test a large number of different specimens belonging to different groups.

The chosen production technique was selective laser sintering (SLS). This technology allows the production of highly stressable prototypes by melting plastic powder, layer by layer, in a short time. Various different materials can be used depending on the application. Unfilled polyamide (PA), glass filled PA, carbon filled PA, alumide, and polystyrene are some examples of possible materials. [82]

The chosen material was PA GF (glass filled polyamide) mainly because it was suggested by internal testing and by previous works. Its data sheet is given in Attachment 2.

The decision regarding the dimension of the lever arm (a) was made following the below presented procedure.

The stress reached in the bone with no screw holes and subject to bending is given by the already mentioned formula:

$$\sigma = \frac{M y}{I} \quad [\text{MPa}] \quad (2)$$

M is the applied moment, y is the distance between the neutral axis and the maximum stressed fibers and I is the second moment of inertia of the cross section.

Simplifying once again the bone as a hollow cylinder and knowing that the moment is given by the multiplication between the applied force and the lever arm the equation can be developed as:

$$\sigma = \frac{M y}{I} = \frac{F * a * \frac{D_{\text{ext}}}{2}}{\frac{\pi (D_{\text{ext}}^4 - D_{\text{int}}^4)}{64}} \quad [\text{MPa}]$$

The moment which produces sample failure can be found inserting in the previous equation the flexural strength of the PA GF (51 MPa) given in the material data sheet and the geometrical parameters of the bone ($D_{ext} = 14 \text{ mm}$; $D_{int} = 3 \text{ mm}$). Obviously, since the bone is not a perfect cylinder, the presented formulas are an approximation of the real value.

$$M = F * a = \frac{\sigma \pi (D_{ext}^4 - D_{int}^4)}{\frac{64}{D_{ext}} \cdot \frac{1}{2}} = 13697 \quad [\text{Nmm}]$$

The total force ($2 * F$ in Figure 68) was chosen to be circa 700 N since the initial idea was to use the 1kN load cell in a range which allowed having high measurement precision and also with a good safety factor in reference to the load cell.

The lever arm ($a = M/F$) was found to be 39 mm and was, for simplicity, approximated to 40 mm in the 3D model. Since the distance between the lower supports was designed to be 260 mm the distance between the upper rollers (b in Figure 65) had to be 180 mm.

The 4-point bending test was carried out using a jig designed for that purpose which is shown in the following image:

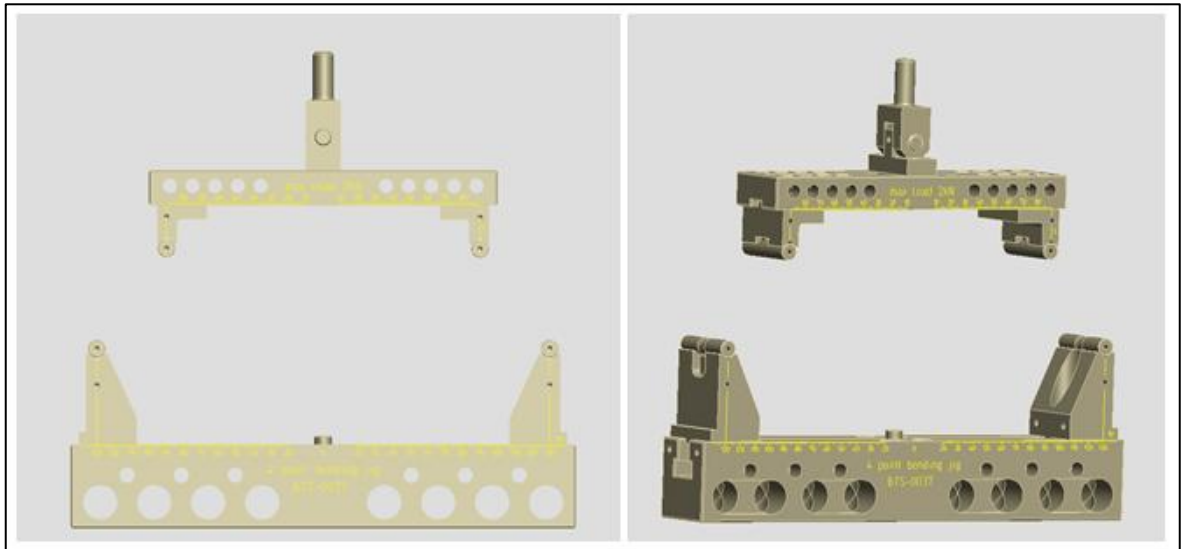


Figure 66: 4-point bending jig

The samples to be tested in a 4-point bending configuration were then refined by adding some further details in order to allow an easier and more precise coupling with the above presented jig as can be seen in the following figure.

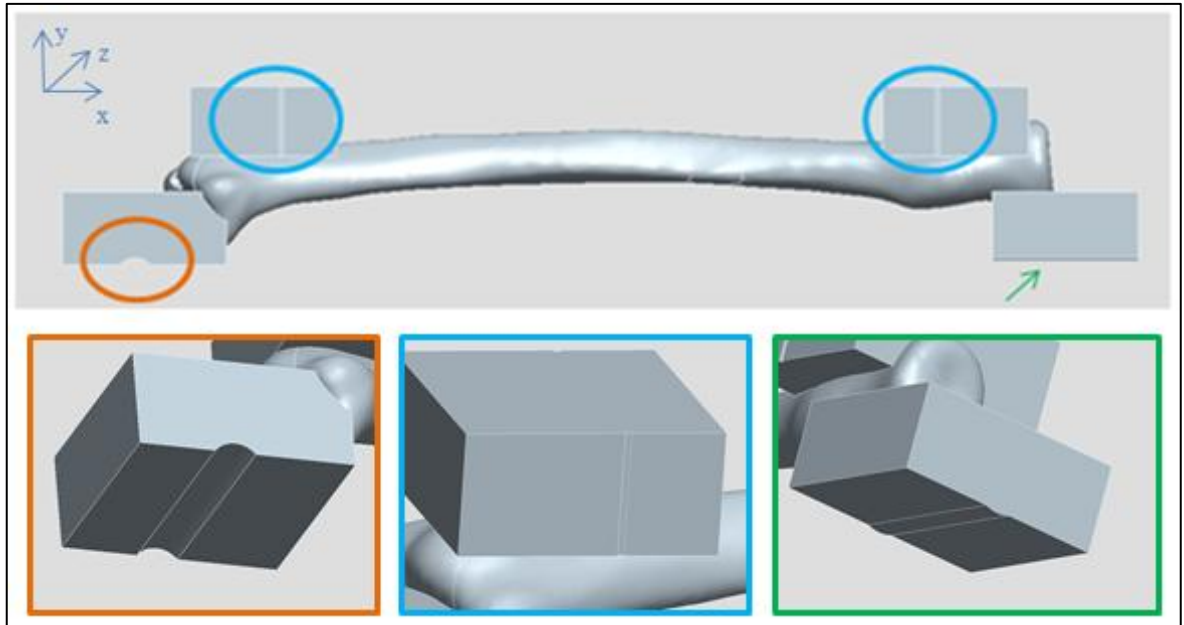


Figure 67: Details of the tested samples

Details 1 and 3 allow a unique and fixed alignment of the sample respectively in the x-y plane and y-z while 2 permits a visual verification of the correct distance between the upper rollers. The complete test setup (sample + jig) is shown in the following image:

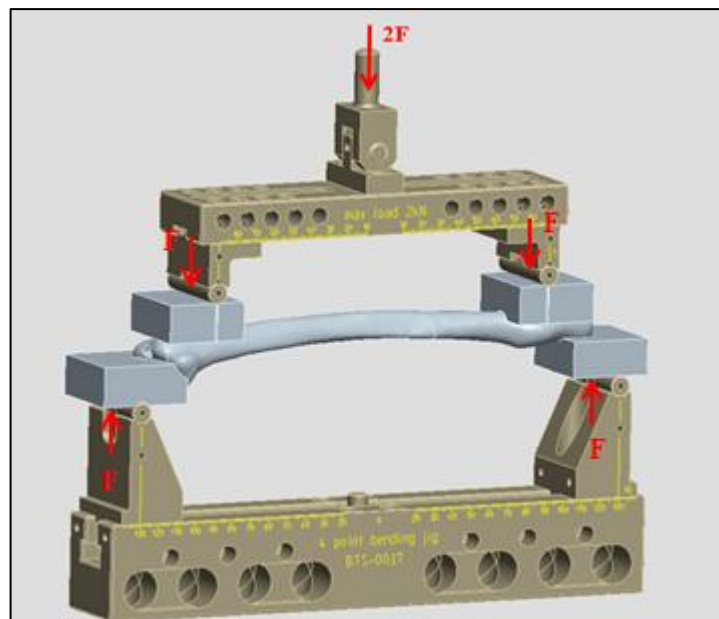


Figure 68: Final test setup

As last step 1mm pre-holes were drawn on the 3D model in correspondence of the position of each screw so that the SLS process left the small holes in every sample (Figure 69). This allowed implanting the plates and screws in the correct position for every tested group and with the certainty of obtaining a precise result for each sample of every group.

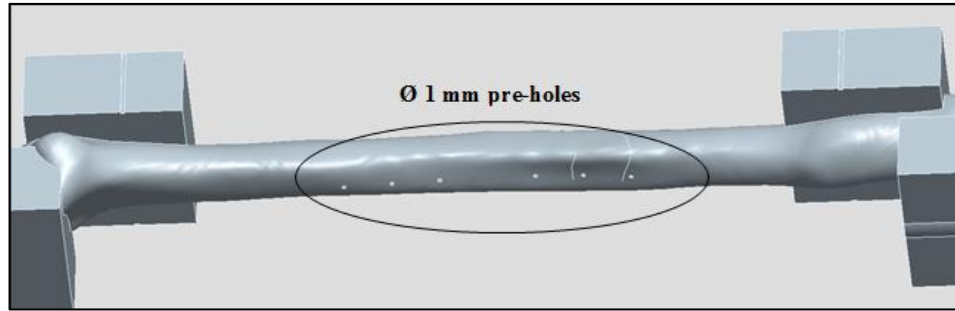


Figure 69: Ø 1 mm pre- holes for the HybSYK 3.5 mm and 2.7 mm samples

Finally, a pre-test was decided to be performed in order to check if the test setup, the material and the samples behaved as expected. The pre-test was performed on 5 samples:

- 3 samples with no holes
- 1 sample with a central 2.7mm hole
- 1 sample with a distal 2.7mm hole

The samples were mounted on the above described 4 point bending jig and they were loaded in the same way as the specimens for the final tests would be (Chapter 2.2.2 - Table 11).

The results of the pre-test are shown in the following figure.

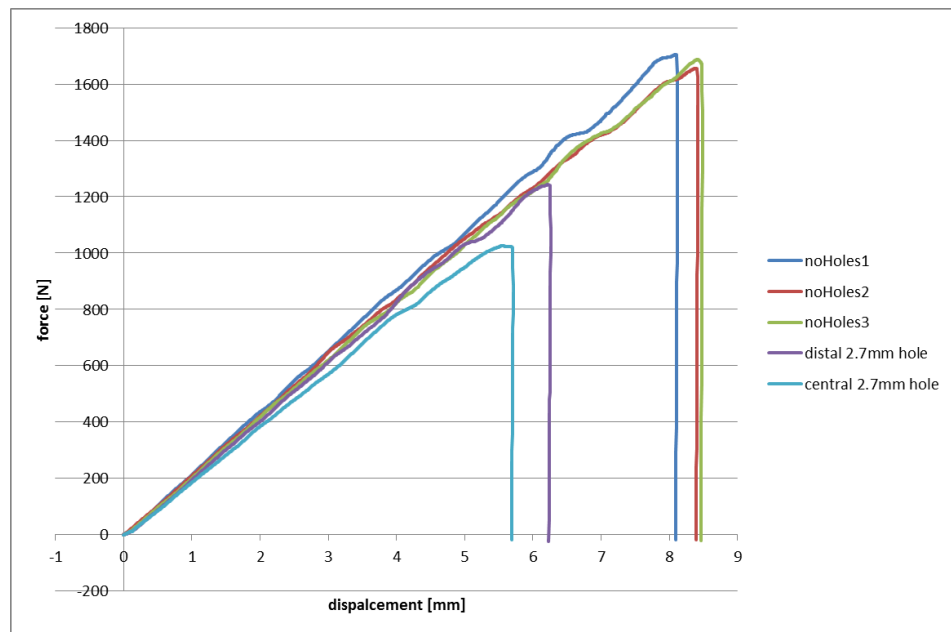


Figure 70: Pre-test results

The results of the pre-test showed a satisfactory behavior. In fact the three samples with no holes behaved approximately in the same manner. Stiffness, force to failure, displacement to failure and energy to failure appeared very similar as evident from Figure 70.

The two samples which presented one hole showed instead a slight decrease of the stiffness and a markedly reduced energy to failure, both due to the presence of the hole.

The only unexpected result consisted in the actual values of the force to failure. In fact the samples with no holes were designed to fail approximately at 700 N. It appeared that the material was stronger than defined in the PA GF data sheet. The solution to this problem would have been the use of a bigger load cell during the actual test performance.

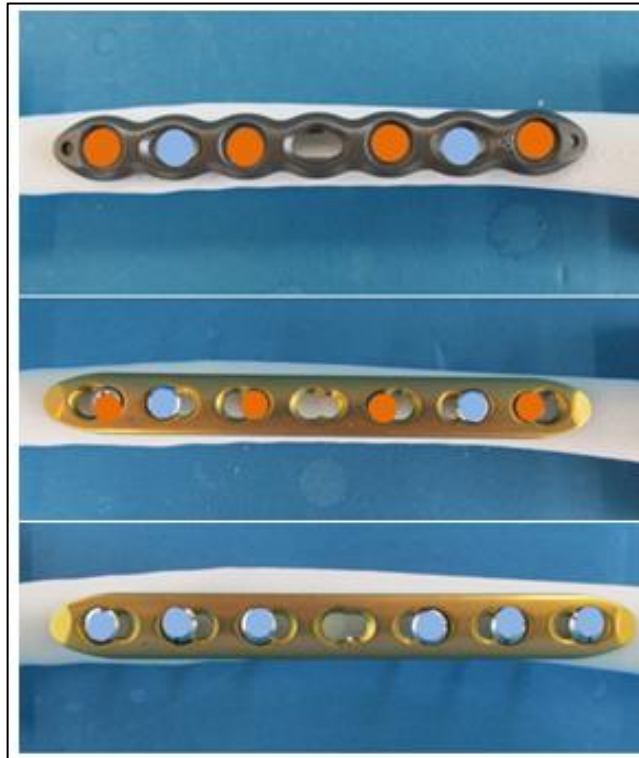
2.2.2 Test Execution

The 4-point bending test was performed on the samples designed in Chapter 2.2.1. Since the aim of the test was to compare various situations in terms of risk of re-fracture the following groups had been chosen for testing and confrontation.

| | Name | Plate used (Ref#) | Screws used (Ref#) | Screw configuration | Comments |
|---|--------------|---|---|------------------------|---|
| 1 | NoHoles | No plate | No screws | - | Reference samples |
| 2 | SingSYK3.5mm | No plate | 1 Stryker VariAx bone screw 3.5mm (614832) | - | Effect of the different Ø and geometry of one single screws in the fracture of the radius |
| 3 | SingSYK2.7mm | No plate | 1 Stryker VariAx bone screw 2.7mm (614732) | - | |
| 4 | SingLCP3.5mm | No plate | 1 Synthes LCP cortex screw 3.5 mm (204.832) | - | |
| 5 | SingLCP4.5mm | No plate | 1 Synthes LCP cortex screw 4.5 mm (414.830) | - | |
| 6 | HybSYK3.5mm | Stryker VariAx Straight narrow plate (629527) | 3 Stryker VariAx bone screws 3.5mm (614832) 3 Stryker VariAx locking screws 3.5mm (614632) | Hybrid configuration | Comparisons between different configurations in the re-fracture risk of the radius |
| 7 | HybSYK2.7mm | Stryker VariAx Straight narrow plate (629527) | 3 Stryker VariAx bone screws 2.7mm (614732) 3 Stryker VariAx locking screws 2.7mm (614532) | Hybrid configuration | |
| 8 | HybLCP3.5 mm | Synthes LCP 3.5 mm plate (233.571) | 3 Synthes LCP cortex screws 3.5mm (204.832) 3 Synthes LCP cortex screws 3.5mm (212.111) | Hybrid configuration | |
| 9 | StdLCP3.5 mm | Synthes LCP 3.5 mm plate (233.571) | 6 Synthes LCP cortex screws 3.5mm (204.832) | Standard configuration | |

Table 10: Test1 experimental groups

The following images show the differences between the tested configurations (multiple holes) in terms of implanted screws:



**Figure 71: Top: Screw order in Hybrid configuration;
Bottom: Screw order in Standard configuration
● : Locking screws; ● : Bone/Cortex screws**

The implant of the plate and screws was performed after pre-drilling the holes following the Stryker and DePuy Synthes operative techniques regarding the drill size:

- Stryker 3.5 mm screws → 2.6 mm drill [49]
- Stryker 2.7 mm screws → 2 mm drill [49]
- DePuy Synthes 3.5 mm screws → 2.8 mm drill [64]
- DePuy Synthes 4.5 mm screws → 3.2 mm drill [83]

The instructions of the operative techniques regarding how to implant the plates and screws were not followed in detail since they suggested how a fracture can be correctly reduced. In this study there was no actual fracture to fixate since the interest was in analyzing the effect of holes on an already healed bone model. The order of insertion of the screws, the torque of tightening of the screws and other aspects reported in the operative technique were therefore not relevant. The following images showed different phases of the sample preparation and all the tested groups with holes.

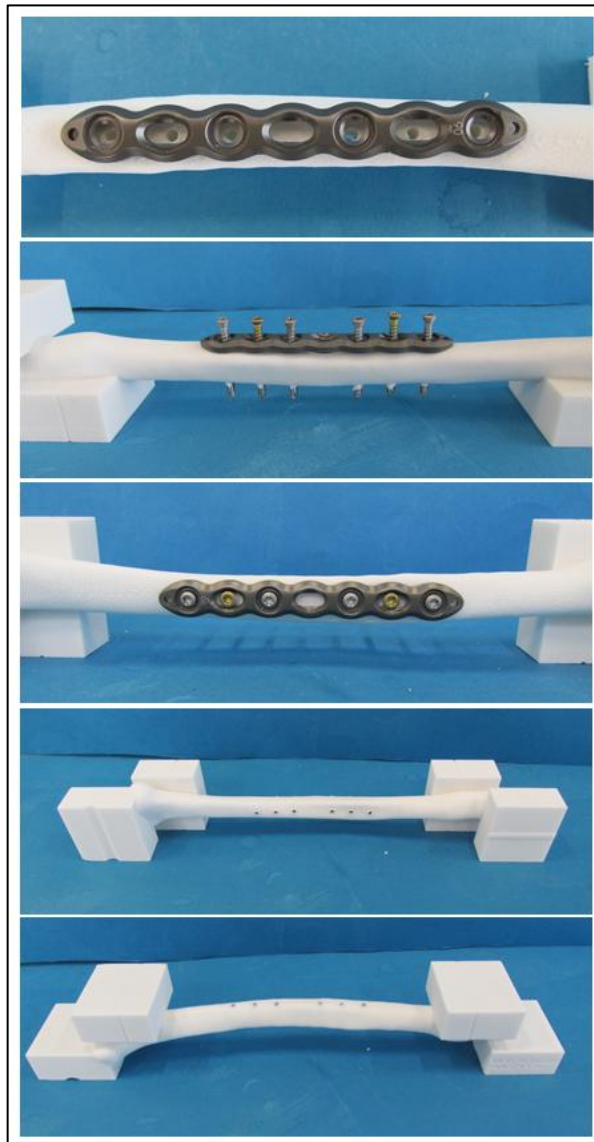


Figure 72: Different phases of the preparation of the HybSYK3.5mm samples

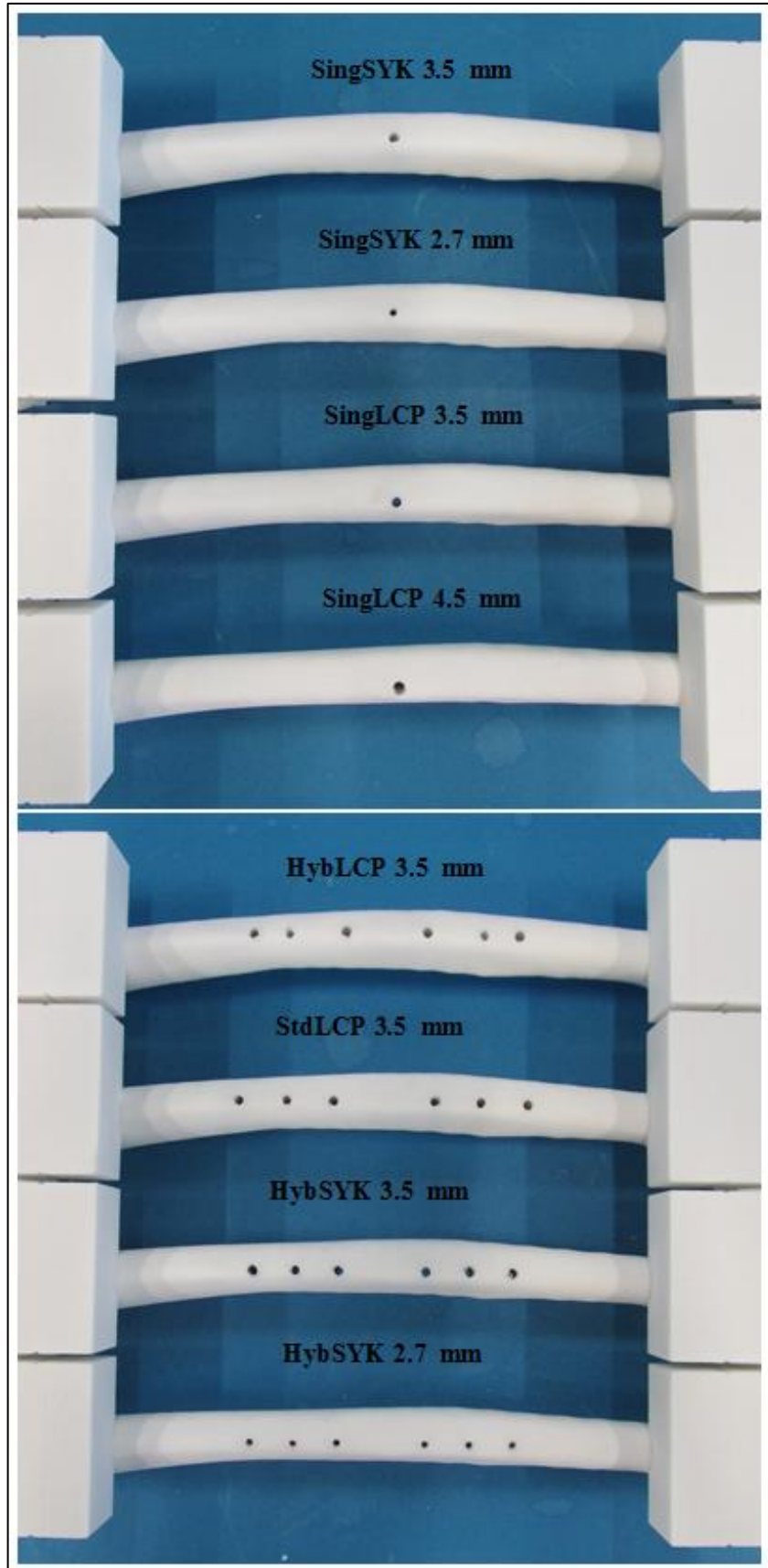


Figure 73: Tested groups with holes

Once the samples were prepared the mechanical test could be performed using the Test 108 static machine with a 5kN load cell (PM#: 2866) since during the pre-test the force to failure appeared higher than the limit of the load cell which was programmed to be used (1 kN). The setup placed on the testing machine is shown in the following image.

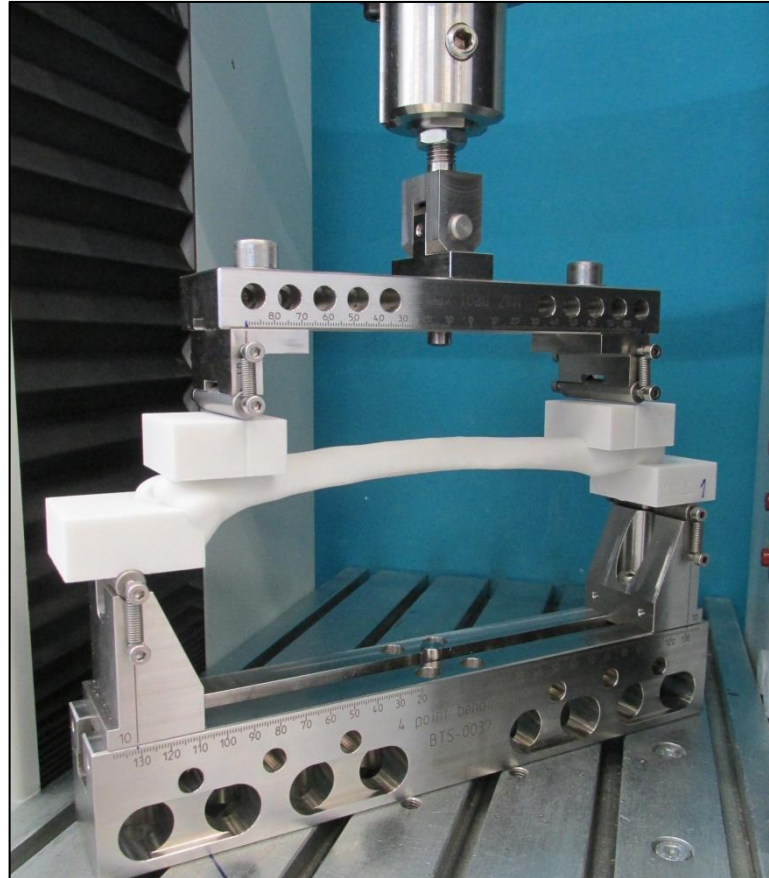


Figure 74: Sample and setup mounted on the TesT108 machine

The main parameters set on the machine are listed in the following table:

| # | Parameter | Value | Comments |
|---|---------------|-----------------|---|
| 1 | Feed-rate | 0.2 mm/s | Common parameter in internal tests |
| 2 | Pre-load | 20 N | Enough to eliminate the “toe-region” from the force-displacement output |
| 3 | Stop criteria | Sample breakage | - |
| | | Force = 4900 N | Max force measurable by the machine |

Table 11: Parameters set on the Tes108 machine

The machine gives, in correspondence of each measurement, a force vs displacement output as shown in the following image.

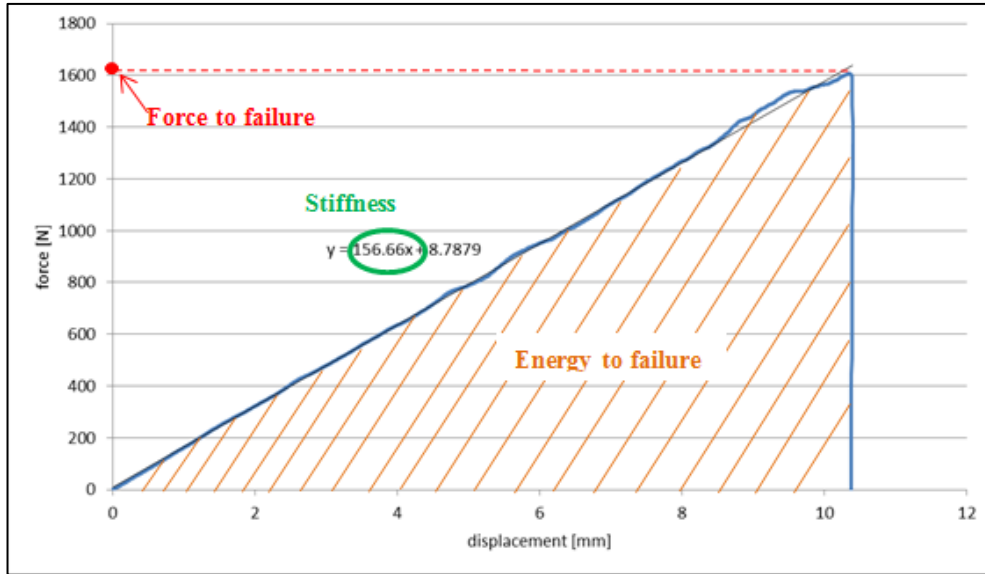


Figure 75: Example of the output of the machine on a sample with no holes

The parameters on which comparisons and evaluations were thought to be made were the following:

- **Force to failure [N]** : maximum force needed to break the tested samples
- **Stiffness [N/mm]**: slope of the force – displacement curve. This parameter allowed to control if there were material variations within the same tested groups. In fact, samples characterized by same geometry, same number and disposition of holes and same material had to show the same stiffness.
- **Energy to failure [Nmm]**: measurement of the area under the force – displacement curve. This parameter was calculated through the creation of an Excel function which is explained below.

With reference to Figure 76, defining x_i one generic displacement, x_{i+1} the successive one and the respective forces F_i and F_{i+1} it was possible to calculate the infinitesimal energy (area under the portion of curve described by the mentioned points) as the sum of the area of a rectangle + the area of a triangle.

$$\text{Area}_{\text{inf}} = (x_{i+1} - x_i) F_i + \frac{(x_{i+1} - x_i)(F_{i+1} - F_i)}{2} \quad (7)$$

The total area under the whole force – displacement curve was therefore calculated as the sum of all the infinitesimal areas between 0 and n (number of measured points):

$$A_{\text{tot}} = \sum \text{Area}_{\text{inf}} = \sum_{i=0}^n (x_{i+1} - x_i) F_i + \frac{(x_{i+1} - x_i)(F_{i+1} - F_i)}{2} \quad (8)$$

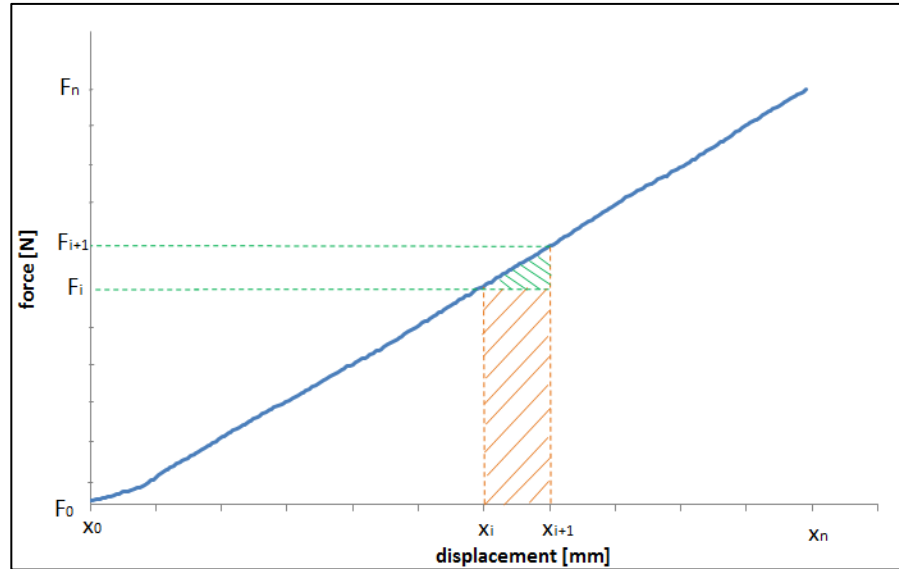


Figure 76: Calculation of the infinitesimal area

The precision of the calculation can be increased by increasing the sampling rate on the machine since forces and relative displacements are evaluated in more frequent time instants and the eventual curvatures of the trend are better approximated.

The tests performed were characterized by a sampling rate of 5 ms. With this setting the outputs showed a displacement evaluation every ca. 0.001 mm and a correspondent force measurement every ca. 0.2 N of force, which was considered enough for the purpose of this study.

The calculation of the energy to failure of each sample would have been used to evaluate a “safety coefficient” defined as:

$$\alpha = \frac{E_{\text{holes}}}{E_{\text{noHoles}}} \quad [-] \quad (9)$$

E_{holes} : energy to failure for the samples with one or multiple holes;

E_{noHoles} : energy to failure for the samples with no holes (reference samples)

The safety coefficient (α) should always be comprehended between 0 and 1.

Comparing the safety coefficient of the different groups would allow the evaluation of what situation is the most secure for the patient in terms of re-fracture risk (values of α close to 1 indicate a safer situation compared to values of α close to 0).

2.2.3 Results

The tests were performed on the samples belonging to the groups listed in Table 10. The results are presented in Attachment 3 and are discussed below.

The first evident aspect from the reported results was that not all the samples could be tested until failure. Almost all groups presented some specimens which could not be brought to failure because the maximum possible applicable displacement was reached and the tests had to be stopped. The worst cases were represented by the HybLCP3.5mm and by the SingLCP4.5mm groups where only one sample out of six was managed to be brought to failure.

All the samples which did not break showed a very flexible behavior and reached very high values of displacement. In these cases it was obviously not possible to calculate the energy to failure or the force to failure. The only parameter which could be used in order to compare samples and groups was the stiffness.

The stiffness analysis gave as well uncommon results. It was in fact expected that samples belonging to the same group would be characterized by the same (or similar) stiffness. This was not verified, as can be noticed for example in Figure 77, since in the same group stiffness ranging from 73.63 N/mm up to 153.23 N/mm was measured (108% max increase).

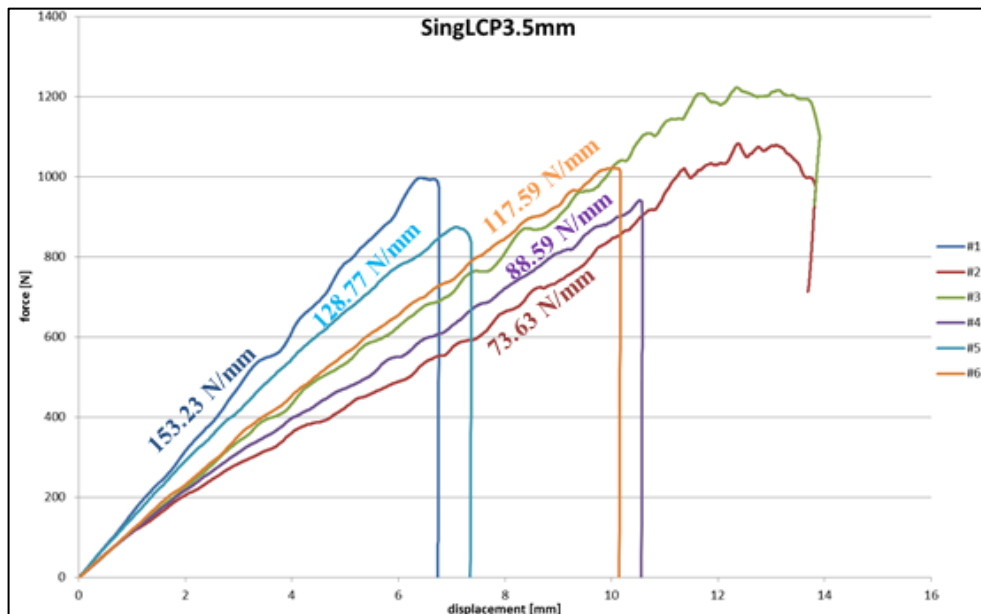


Figure 77: Stiffness evaluation for the SingLCP 3.5mm samples

At the same time, samples with holes were expected to be slightly less stiff when compared with samples with no holes since the defect left by screw removal should have weakened the structure. This was not always verified as can be seen from the comparison of the stiffness of the totality of the samples tested (Figure 78).

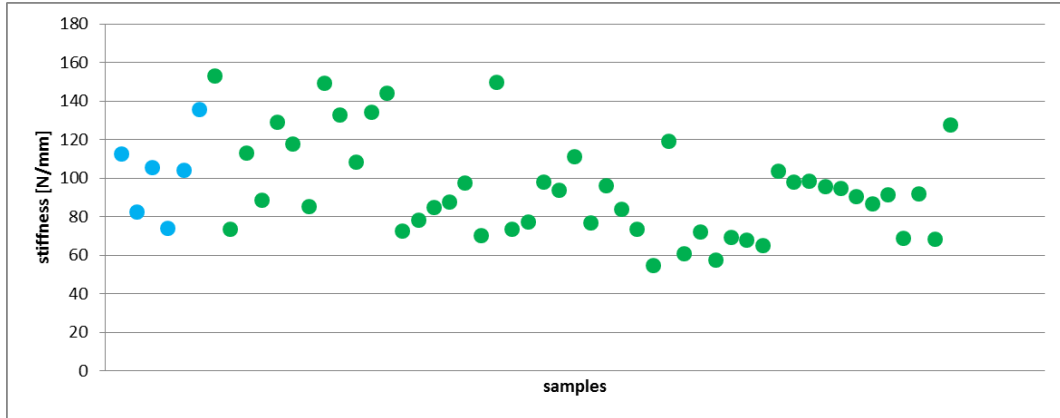


Figure 78: Stiffness distribution for the tested samples. Six consecutive points represent a group.
 ● : samples with no holes ● : samples with holes

The reported results were surely not due to an error in the mounting and dismounting of the screws and plates since, as evident from Figure 78 and Figure 79, a wide distribution of stiffness values also appeared for the samples with no holes which were tested shortly after they were received from the production company without any plate implant or screw insertion. Since stiffness depends on the shape of the samples and on the material itself and since the shape does not change between specimens belonging to the same group, the different stiffness measured must be due to a production or material issue.

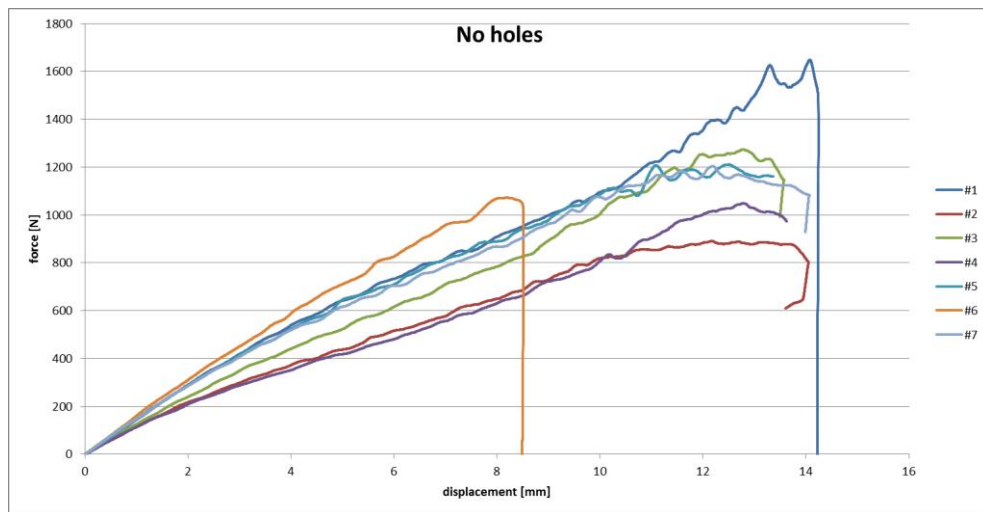


Figure 79: Force – displacement results for the NoHoles samples

Another evident outcome of the test (Figure 80) was that no force to failure or max force measured was close to the expected 700 N (design parameter), meaning that the ultimate properties of the material were extremely different from the ones presented in the data sheet. It was surprising that also the samples which had holes (green points) failed in correspondence of higher forces than 700 N. This fact confirmed the results of the pre-test which suggested the use of a bigger load cell compared to the one initially decided.

The material appeared stronger than expected and almost every sample, even belonging to the same group, showed independent behavior also in terms of force as evident from the wide distribution of Figure 80.

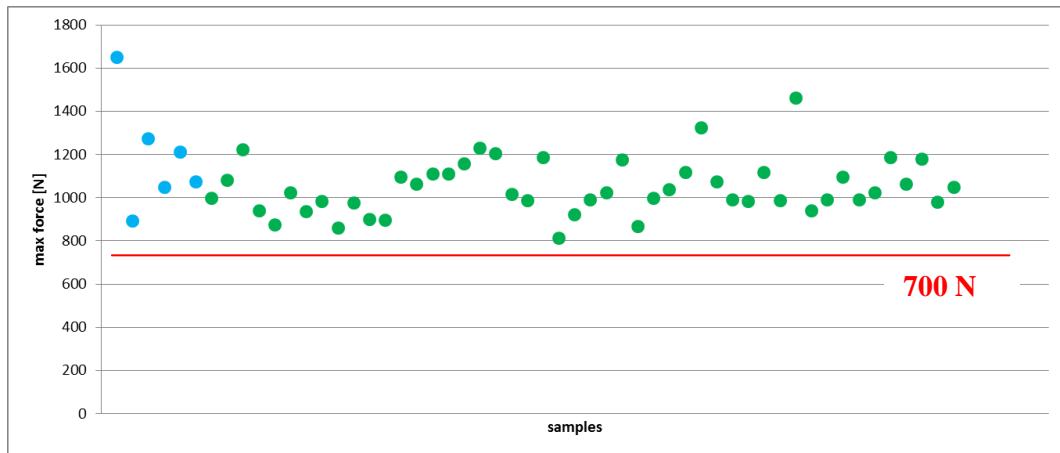


Figure 80: Max force measured for all the tested samples. Six consecutive points represent a group.
 ● : samples with no holes; ● : samples with holes

Regarding the displacement in correspondence of which sample failure occurred there was also a wide distribution of values even for the samples belonging to the same group. As example the case of the SingSYK3.5mm group is reported in the following image. The displacement at failure occurred in a range of values varying from 6.90 mm to 10.18 mm which is too wide to be considered acceptable (47% max increase).

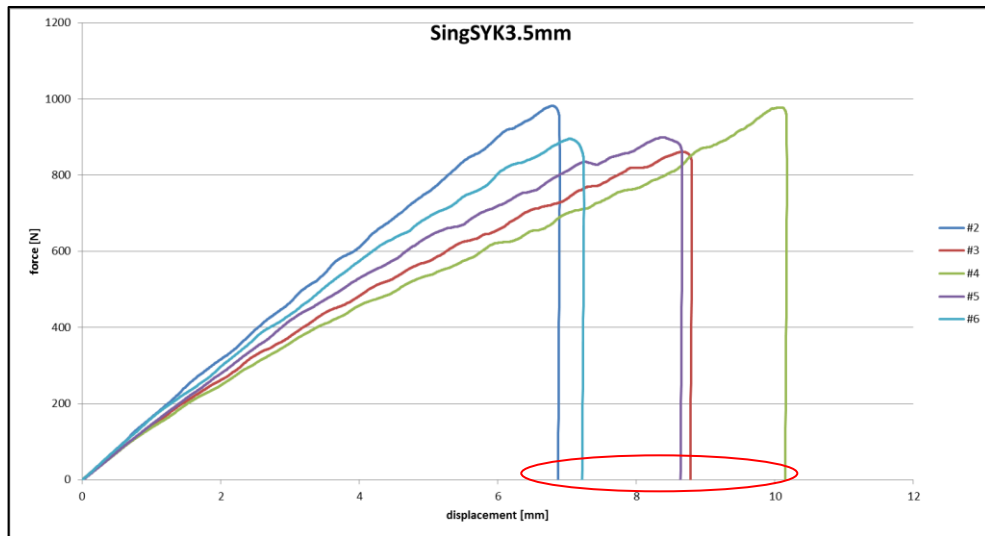


Figure 81: Force-displacement trend for the SingSYK3.5mm group

The major outcome of this test was that the material properties were not comparable with the given ones in the PA GF data sheet and that even samples which should have been considered the same because belonging to the same group showed completely different behavior in terms of stiffness, force and displacement to failure, etc.

It was evident that the chosen production technique and material did not allow obtaining similar samples on which performing comparisons. No comparison between the tested groups could be made and no conclusions in terms of failure risk given by different hole dimension or hole pattern could be stated from the tests performed on PA GF samples.

2.3 Experimental test 2

2.3.1 Sample definition

In consequence of the unexpected results obtained from the experimental test 1 (Chapter 2.2) some modifications, especially in terms of material with which the samples were produced, had to be taken.

The main request regarding the chosen material and production techniques had to be the assurance that samples, all with a very similar mechanical behavior, would be supplied and used during this second experimental test. Only in this case the effective influence of the holes left in correspondence of screw removal could be seen since the only difference between groups would be the dimension, shape and position of the defects.

The chosen samples for testing were 4th generation composite radius bones from the company Sawbones®. This decision was taken since the mentioned samples have similar properties to real bone and are most commonly used when the actual strength properties of real bone are required and when mechanical testing is needed to be performed. [84] The Sawbones® radius models are composed by an outer material (short fiber epoxy) which simulates the cortical bone and an inner material (solid rigid polyurethane foam) which simulates the trabecular bone. A constant 5 mm hole is present throughout the length of the bone representing the inner bone marrow canal. The average properties of the materials of the adopted models are listed in the following tables.

| Material | Density [g/cm ³] | Longitudinal Tensile | | Longitudinal Compressive | | Transverse Tensile | | Flexural | | Poisson ratio [-] |
|--------------------------|------------------------------|----------------------|---------------|--------------------------|---------------|--------------------|---------------|----------------|---------------|-------------------|
| | | Strength [MPa] | Modulus [GPa] | Strength [MPa] | Modulus [GPa] | Strength [MPa] | Modulus [GPa] | Strength [MPa] | Modulus [MPa] | |
| Short fiber filled epoxy | 1.64 | 106 | 16 | 157 | 16.7 | 93 | 10 | 148 | 13700 | 0.26 |
| Solid rigid PU foam | 0.24 | 3.7 | 0.173 | 4.9 | 0.123 | 2.8 | 0.033 | - | - | 0.3 |

*Table 12: Average properties of the materials in the 4th generation bone models.
All data were provided by Sawbones® company*

One of the samples used for testing is shown in the following image:



Figure 82: 4th generation composite radius bones

2.3.2 Test Execution

The experimental test was performed on fewer groups than the ones initially programmed (listed in Table 10). This was mainly due to the long time needed and to the high costs for producing and delivering a great number of samples. The groups which were decided to be tested are listed in the following table:

| | Name | Plate used (Ref#) | Screws used (Ref#) | Screw configuration | Comments |
|---|-------------|---------------------------------------|---|---------------------|--|
| 1 | No Holes | No plate | | - | Reference samples |
| 2 | HybSYK2.7mm | VariAx straight narrow plate (629527) | 3 VariAx bone screws 2.7 mm (614732) 3 VariAx locking screws 2.7 mm (614532) | Hybrid | Comparison between the influence of different screw dimensions, offered by the Stryker VariAx narrow plating system, in the re-fracture risk of the radius |
| 3 | HybSYK3.5mm | VariAx straight narrow plate (629527) | 3 VariAx bone screws 3.5 mm (614832) 3 VariAx locking screws 3.5 mm (614632) | Hybrid | |

Figure 83: Test2 experimental groups

The plate was mounted on each sample in the most similar and reproducible way possible. It was assured in fact that its center was in correspondence of the center of the radius bone (124 mm from the proximal surface) and that its lower surface fitted precisely on the volar surface of the bone. Obviously the positioning of the plates and holes on each sample is less precise compared to the one of the experimental test1 since it was not possible to have a CAD file on which pre-holes could be placed.

The implant of the screws was performed on the samples belonging to the groups with holes after a pre-drilling, done following the Stryker operative technique in regards to the drill size, had taken place:

- Stryker 3.5 mm screws → 2.6 mm drill [49]
- Stryker 2.7 mm screws → 2 mm drill [49]

The image of a sample ready for being tested and some pictures of the various phases of plate and screw implant and removal are shown below.



Figure 84: Sample belonging to the HybSYK3.5mm group ready for testing

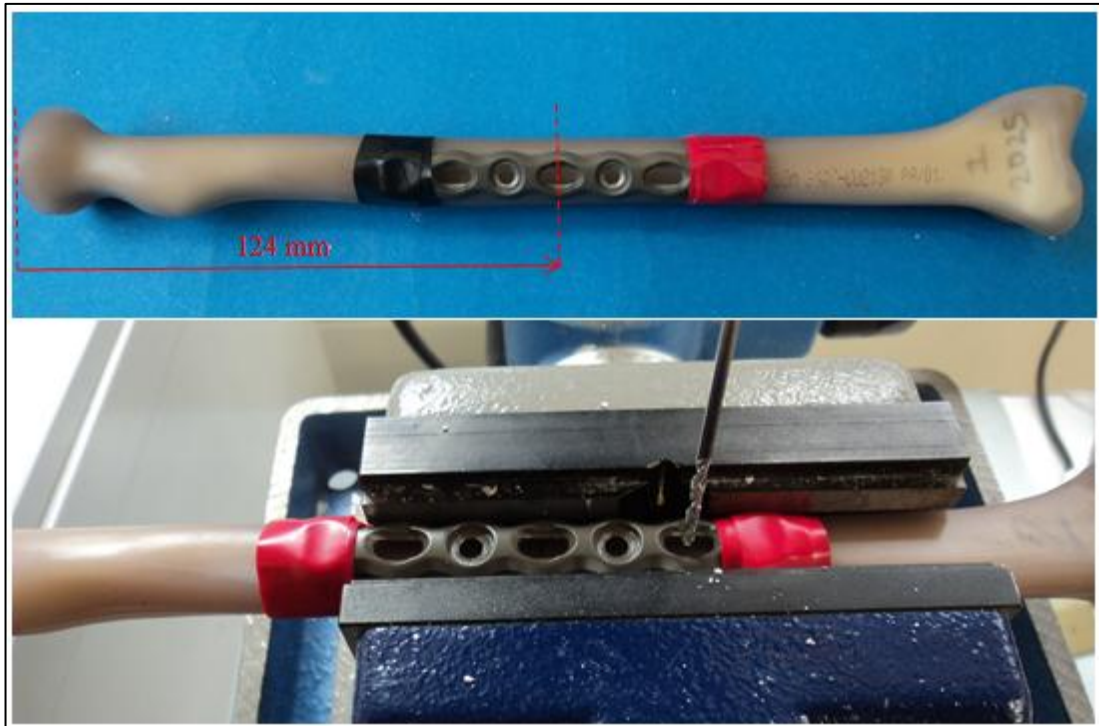


Figure 85: Top: Plate positioning; Bottom: Pre-hole drilling for a 3.5 mm screw (drill $\varnothing = 2.6$ mm)

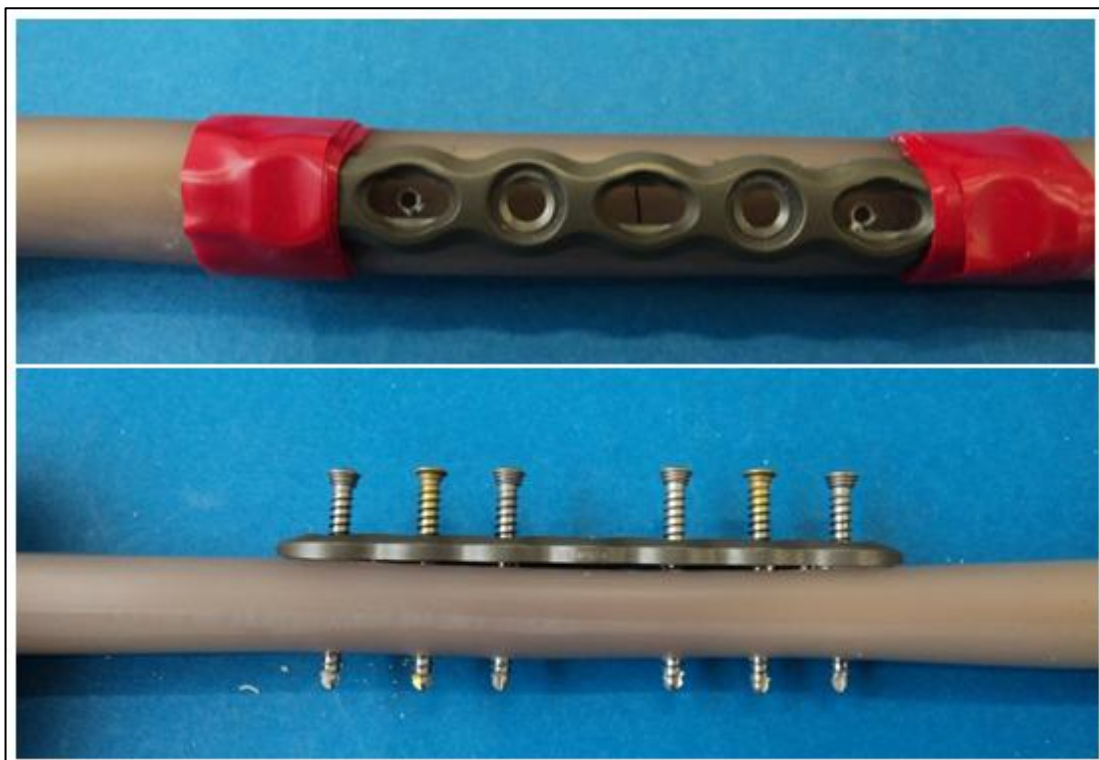


Figure 86: Top: Central pre – holes; Bottom: All screws inserted (yellow screws are compression screws; grey screws are locking screws)

Before placing the samples on the 4-point bending test jig the metallic rollers were changed with rollers made of carbon fibers (Figure 87). This was done because it was noticed from some pre-tests that the metallic rollers significantly damaged the surface of the bone when applying an increasing load since they were stiffer if compared to the short fiber epoxy which simulates the cortical bone.

The lever arm of the 4-point bending test was chosen to be $l_a = 20 \text{ mm}$ since it was not possible to have a larger one due to the presence of the proximal tuberosity and to the curvature of the distal end of the bone which would not have allowed a flat and stable placement of the radius. This choice was approved after applying formula (2) presented in Chapter 1.4 which showed that the approximate force to failure for the sample with no holes and with a 20 mm lever arm would be 3800 N. The m load cell of the Test 108 static machine (5kN – PM # 2866) would therefore have been enough for performing the test.

Particular attention was paid in placing each bone in the same position in order to perform every time the exact same measurement. To do this the radius was aligned on its flat volar surface on the lower rollers and a distance of 20 mm from a left vertical reference was measured each time as shown in Figure 87.

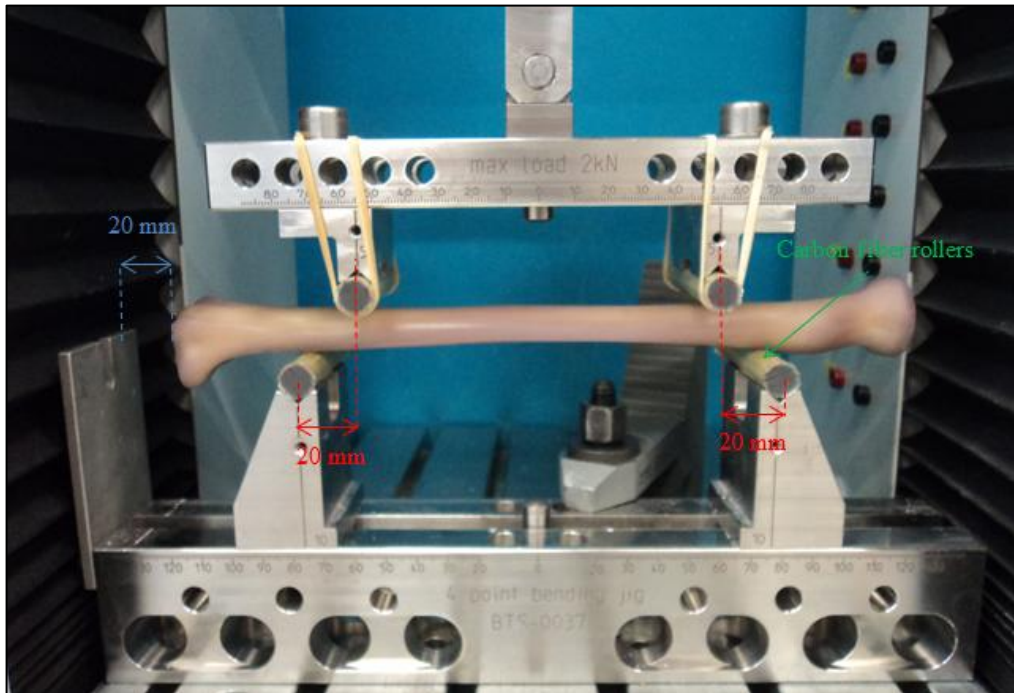


Figure 87: Sample mounted on the 4-point bending jig

The main parameters set on the machine are listed in the following table:

| # | Parameter | Value | Comments |
|---|---------------|-----------------|---|
| 1 | Feed-rate | 0.2 mm/s | Common parameter in internal tests |
| 2 | Pre-load | 20 N | Enough to eliminate the “toe-region” from the force-displacement output |
| 3 | Stop criteria | Sample breakage | - |
| | | Force = 4900 N | Max force measurable by the machine |

Table 13: Parameters set on the Tes108 machine

All phases of sample preparation and testing were done trying to make sure most of the considerations made in the test definition (Chapter 2.1.2) were fulfilled since all the decisions were taken with a specific reason as explained in the previous sections.

The machine gave, in correspondence of each measurement, a force vs. displacement output and the evaluated parameters were the same as the ones evaluated during the performance of experimental test 1 (described in detail in Chapter 2.2.2): force to failure [N], stiffness [N/mm], energy to failure [Nmm]. In addition the displacement to failure [mm] parameter was also analyzed since in the previous test a very wide variance of this value was also noticed.

The comparisons between different groups were performed through a statistical analysis following the Stryker statistical guidelines [85]

The chosen statistical test was the Mann-Whitney-U Test which is particularly indicated for the comparison of any variable of interest between two independent groups.

The confidence level was set to 95% (not risk level based test) and therefore the α -value is 0.05. The calculation of the significance level (p-value) of the statistics was performed through the Monte Carlo method since it allows obtaining accurate results when the data set is small, the tables are sparse or unbalanced or the data are not normally distributed [85]. This method creates a distribution of values similar to the one found during the tests and it then takes several samples from it (10000 for default) and the significance value is calculated. [86]

The following hypotheses were therefore created:

- Null Hypothesis: the two test groups belong to the same population in reference to the analyzed variable (no significant difference between groups). This hypothesis is accepted whether $p\text{-value} > 0.05$;
- Alternative Hypothesis: the two test groups do not belong to the same population in reference to the analyzed variable (significant difference between groups). This hypothesis is accepted whether $p\text{-value} < 0.05$. [85]

2.3.3 Results

The results for all the tested samples are presented in Table 14.

The first important aspect to be highlighted, differently from experimental test 1, is the fact that all the samples tested were managed to be brought to failure. Groups HybSYK2.7mm and HybSYK3.5mm always failed in correspondence of one of the most proximal holes left by screw removal. The rupture did not always occur through the same hole. However the fifth hole (from distal) appeared the most frequent point of failure. The samples with no holes showed in most cases a failure in between the central and proximal thirds of the radius bone.

The different force to failure, displacement to failure and therefore energy to failure between groups with and without holes appears very evident from the presented results.

It can also be noticed that the results for the groups HybSYK2.7mm and HybSYK3.5mm are similar, meaning that an apparent difference is not present when applying and removing plates with different screw dimension.

| Group | Sample # | Max Force [N] | Max displacement [mm] | Stiffness [N/mm] | Energy to failure [Nmm] | Failure point |
|-------------|-----------------|----------------|-----------------------|------------------|-------------------------|----------------|
| No Holes | 1 | 4245.97 | 6.69 | 871.49 | 16436.00 | proximal third |
| | 2 | 3950.89 | 5.76 | 878.45 | 12704.21 | pr/cen third |
| | 3 | 3789.85 | 6.30 | 804.01 | 13657.17 | pr/cen third |
| | 4 | 3811.04 | 5.08 | 921.68 | 10577.51 | pr/cen third |
| | 5 | 4011.16 | 4.98 | 949.31 | 10677.42 | pr/cen third |
| | 6 | 4041.28 | 6.47 | 871.54 | 15075.45 | pr/cen third |
| | Mean | 3975.03 | 5.88 | 882.74 | 13178.96 | |
| | St. dev. | 167.85 | 0.73 | 49.83 | 2353.03 | |
| HybSYK2.7mm | 1 | 2245.38 | 2.91 | 842.67 | 3332.22 | hole 5 |
| | 2 | 2530.37 | 3.74 | 752.65 | 4967.00 | hole 5 |
| | 3 | 2301.32 | 2.99 | 830.70 | 3501.72 | hole 6 |
| | 4 | 2254.65 | 3.25 | 755.54 | 3758.40 | hole 5 |
| | 5 | 2138.91 | 2.89 | 794.56 | 3128.2 | hole 4 |
| | 6 | 2181.83 | 2.94 | 799.35 | 3284.79 | hole 6 |
| | Median | 2275.41 | 3.12 | 795.91 | 3662.06 | |
| | St. dev. | 137.40 | 0.33 | 37.18 | 674.39 | |
| HybSYK3.5mm | 1 | 2284.43 | 3.11 | 792.48 | 3627.80 | hole 5 |
| | 2 | 2334.35 | 3.29 | 791.13 | 3984.95 | hole 6 |
| | 3 | 2250.14 | 2.97 | 809.62 | 3396.43 | hole 4 |
| | 4 | 2241.87 | 3.23 | 763.69 | 3785.59 | hole 5 |
| | 5 | 2106.63 | 2.7 | 839.01 | 2858.29 | hole 5 |
| | 6 | 2027.84 | 2.8 | 771.58 | 2858.39 | hole 5 |
| | Median | 2207.54 | 3.01 | 794.58 | 3418.57 | |
| | St. dev. | 116.16 | 0.24 | 27.20 | 474.86 | |

Table 14: Results of the experimental test 2.

(pr / cen third: zone in between the proximal and central third of the radius)

The calculation of the safety coefficient α gave the following results which do not highlight a big difference between the two groups with holes.

| Group | Safety coefficient |
|-------------|--------------------|
| HybSYK2.7mm | 0.278 |
| HybSYK3.5mm | 0.259 |

Table 15: Safety factor for the tested groups

The previously described results are summarized with the chart presented in Figure 88 where the force-displacement output is plotted for every sample tested.

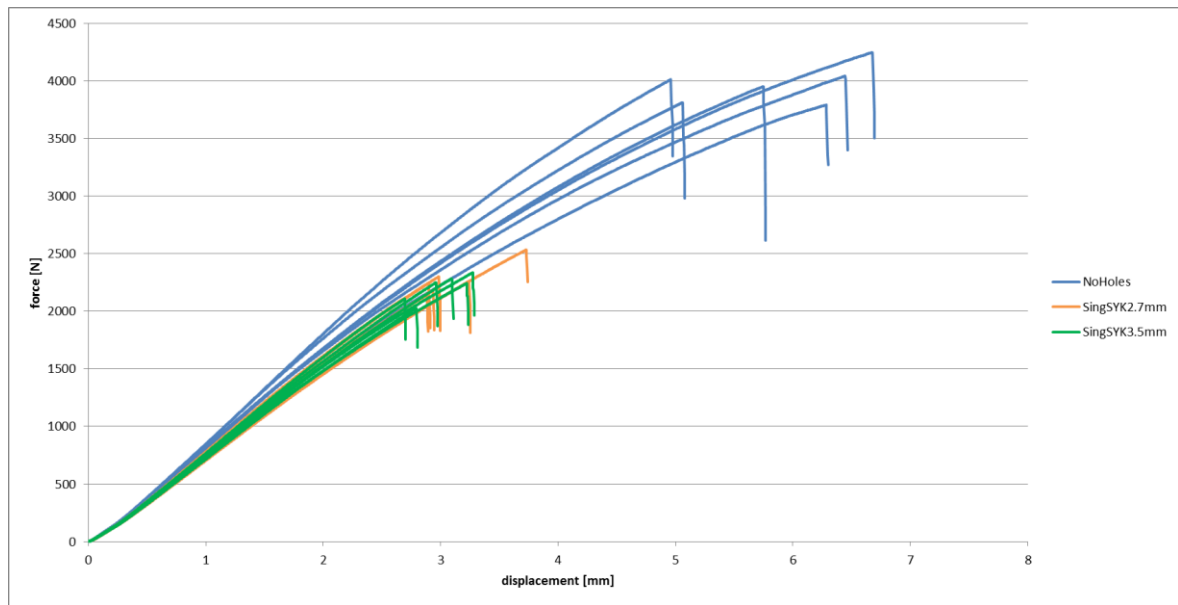


Figure 88: Force – displacement chart for the experimental tests 2

The maximum percentage differences found within the same group and for each evaluated parameter are presented in Table 16.

| | MAXIMUM PERCENTAGE DIFFERENCE | | | |
|-------------|-------------------------------|--------------------------|---------------------|----------------------------|
| | on max Force | on max displacement [mm] | on stiffness [N/mm] | on energy to failure [Nmm] |
| NoHoles | 10% | 25% | 15% | 35% |
| HybSYK2.7mm | 15% | 22% | 10% | 37% |
| HybSYK3.5mm | 13% | 17% | 9% | 28% |

Table 16: Maximum percentage difference for every parameter of every group

The results of the statistical analysis are presented below. In particular the boxplot of each variable analyzed and the results of the statistical comparisons are presented. Every value cited can be found in the tables of Attachment 5.

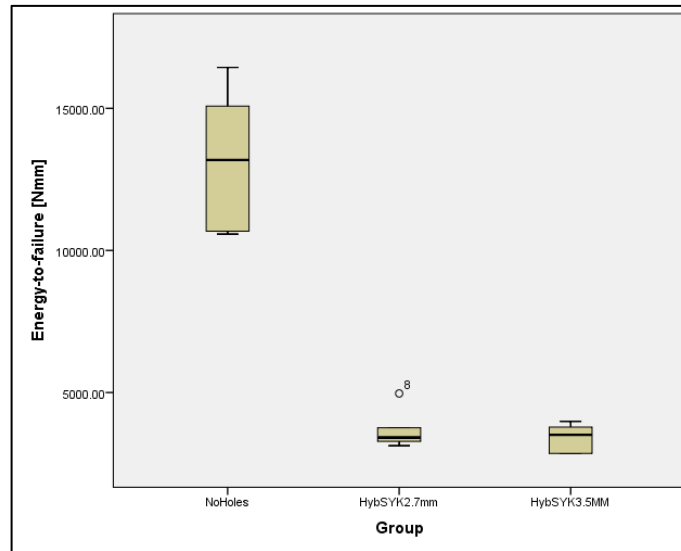


Figure 89: Energy to failure comparison between the three tested groups

***8: data number eight represents an outlier (an observation very different from the others)**

In terms of energy to failure the statistical comparison showed *significant difference* between:

- NoHoles and HybSYK2.7mm (p-value=0.002 < α -value=0.05);
- NoHoles and HybSYK3.5mm (p-value=0.003 < α -value=0.05).

In both cases the energy to failure of the sample with no holes was greater than the energy to failure of the samples with holes.

The statistical comparison showed *no significant difference* between:

- HybSYK2.7mm and HybSYK3.5mm (p-value=0.937 > α -value=0.05).

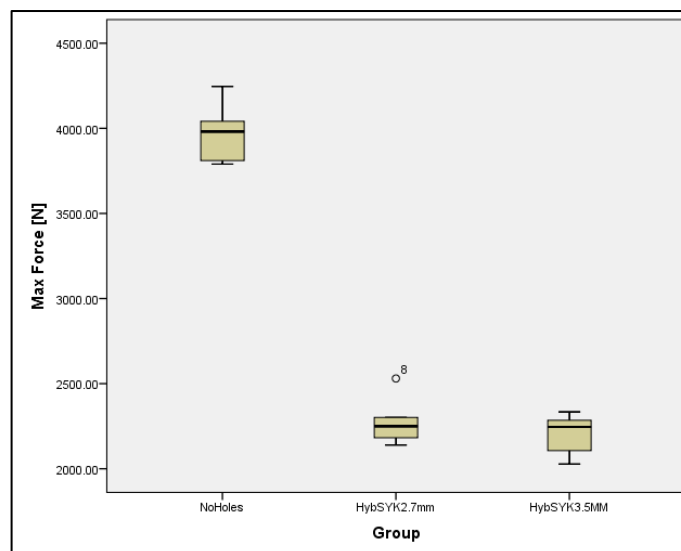


Figure 90: Max force comparison between the three tested groups

***8: data number eight represents an outlier (an observation very different from the others)**

In terms of force to failure the statistical comparison showed *significant difference* between:

- NoHoles and HybSYK2.7mm (p-value=0.002 < α -value=0.05);
- NoHoles and HybSYK3.5mm (p-value=0.002 < α -value=0.05).

In both cases the force to failure of the sample with no holes was greater than the force to failure of the samples with holes.

The statistical comparison showed *no significant difference* between:

- HybSYK2.7mm and HybSYK3.5mm (p-value=0.586 > α -value=0.05).

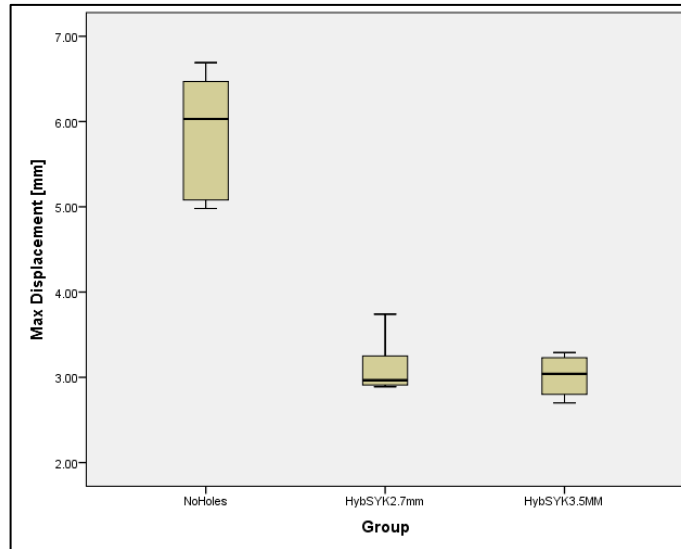


Figure 91: Displacement to failure comparison between the three tested groups

In terms of displacement to failure the statistical comparison showed *significant difference* between:

- NoHoles and HybSYK2.7mm (p-value=0.002 < α -value=0.05);
- NoHoles and HybSYK3.5mm (p-value=0.003 < α -value=0.05).

In both cases the displacement to failure of the sample with no holes was greater than the displacement to failure of the samples with holes.

The statistical comparison showed *no significant difference* between:

- HybSYK2.7mm and HybSYK3.5mm (p-value=0.823 > α -value=0.05).

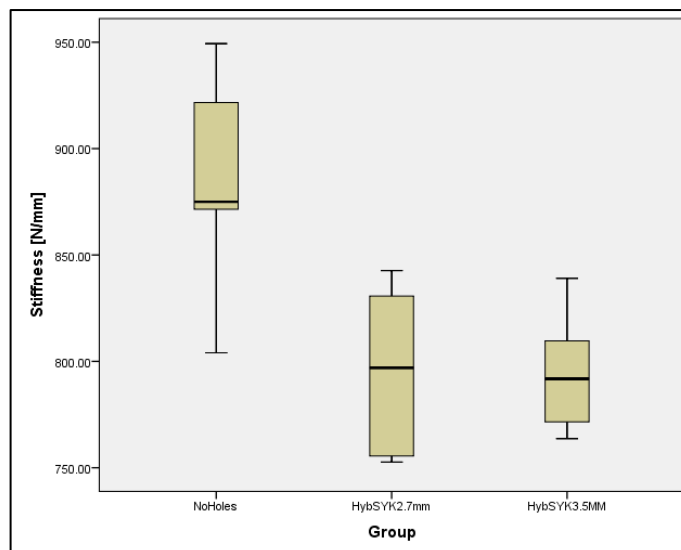


Figure 92: Stiffness comparison between the three tested groups

In terms of stiffness the statistical comparison showed *significant difference* between:

- NoHoles and HybSYK2.7mm ($p\text{-value}=0.008 < \alpha\text{-value}=0.05$);
- NoHoles and HybSYK3.5mm ($p\text{-value}=0.008 < \alpha\text{-value}=0.05$).

In both cases the sample with no holes appeared stiffer than the samples with holes.

The statistical comparison showed *no significant difference* between:

- HybSYK2.7mm and HybSYK3.5mm ($p\text{-value}=0.941 > \alpha\text{-value}=0.05$).

Some pictures of the failed samples are presented below:

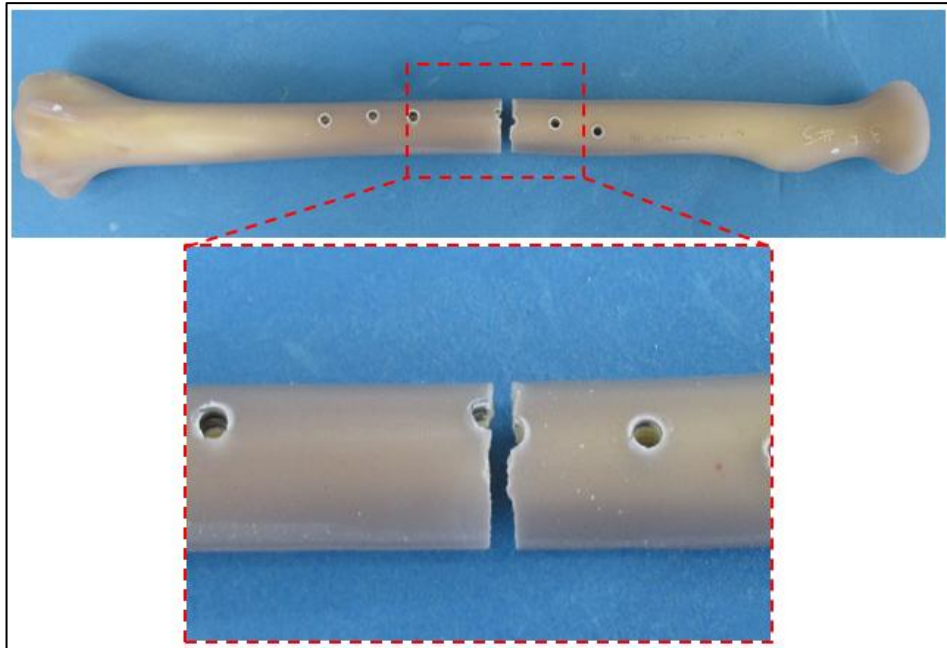


Figure 93: Failed sample #5 from group HybSYK3.5mm in correspondence of the fourth hole

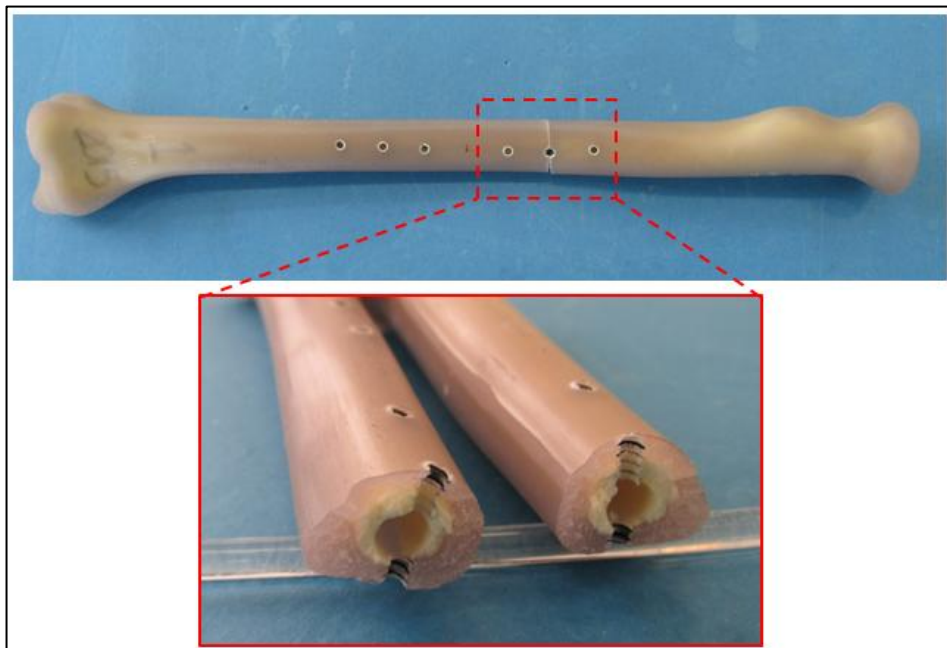


Figure 94: Failed sample #1 from group HybSYK2.7mm in correspondence of the fifth hole

3. Computational Test

The computational approach uses the finite element method (FEM) to approximate the solution of a problem through its mathematical modeling. These types of tools are nowadays used in multiple fields such as structural mechanics, fluid dynamics, acoustic study, etc. [84]

One of the biggest advantages given by FEM is the possibility of studying elements of complex geometry or material which could not be studied with analytical standard calculations. Secondly, they allow building and changing the parameters of “virtual prototypes”, such as materials, dimensions, etc., without the need of having an actual physical sample for evaluating its behavior during mechanical testing.

The major disadvantage of FE methods is the possibility of obtaining wrong results if the model is not built or evaluated correctly. For example, the imposition of incorrect boundary or loading conditions can lead to stress distributions, deformations, etc. which do not simulate what happens in reality. Complex models can also need very long times before giving a solution since the number of calculations and iterations needed could be very high. [85]

Regarding the present work, the creation of a computational model had the aim of giving an instrument for the evaluation of the risk of re-fracture of the radius, when different clinical situations were simulated, without the need of building the samples, implanting and removing the screws and testing the resulting specimens.

The building of the geometries was performed with the CAD software PTC Creo /Pro while the finite element analysis was carried out with the software Ansys Workbench 14.5.

3.1 Materials and Methods

The *geometrical model* used for the finite element analysis was the same created for the production of the samples used during the experimental test 1. This choice was taken despite the results obtained. In fact, the issue regarded mainly the “real” material and not the actual shape of the samples which was still considered appropriate for the study purpose. For having a simpler and faster model to create and simulate it was decided to consider the holes left by the screws as cylinders without the need of virtually assembling and cutting out from the radius model the 3D models of the screws. The radius geometry was divided in various regions, as evident from Figure 95, in order to allow an independent meshing of each one of them. The zones of greater interest for the study (highly stressed areas) could have been refined more than the zones of limited interest (areas of small stress). This allowed limiting the number of elements of the whole model and therefore the simulation time.

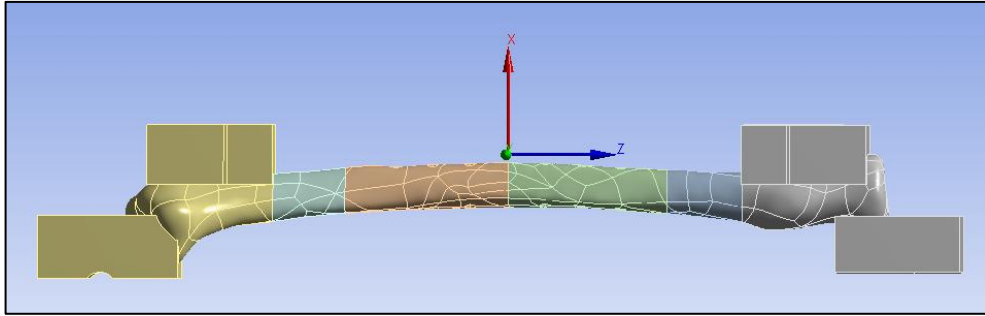


Figure 95: Model for the computational test divided in multiple regions

The *boundary conditions* were defined in the model in order to simulate the supports for the sample used during the experimental test 1 and the pre-test without the need of actually modeling them. They were defined as displacement conditions on the lower blocks as can be seen in Figure 96 and Table 17.

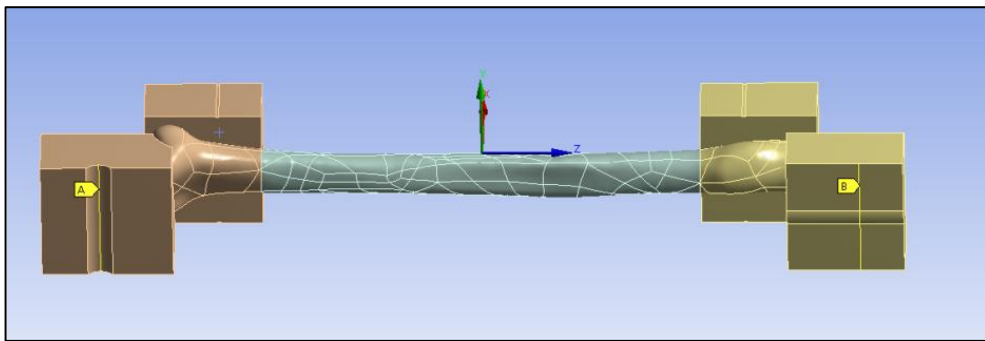


Figure 96: Boundary conditions defined on the supporting blocks

| Boundary Condition | Type | X component [mm] | Y component [mm] | Z component [mm] |
|--------------------|--------------|------------------|------------------|------------------|
| A | Displacement | 0 | 0 | 0 |
| B | Displacement | 0 | 0 | Free |

Table 17: Boundary conditions values

The *loading conditions* applied to the model assumed a different value for validation and for convergence analysis. The reason of this choice is described in more detail in the following sections together with the definition of the *material properties* to be assigned to the computational groups.

The *mesh* was defined on all the parts in which the radius 3D model was divided. It was decided that the type of elements forming the mesh should be all “3D quadratic tetrahedral elements” (tetrahedral elements with 10 nodes - Tet10). The following image shows the type of elements that were present in the model (only Tet10) and their quality. Higher values of element metrics indicate, in fact, better quality.

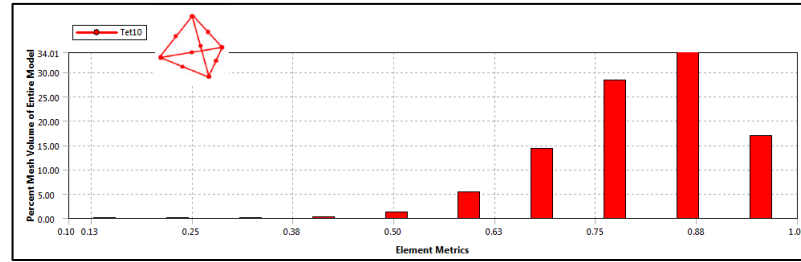


Figure 97: Mesh quality evaluation histogram

The choice of using quadratic tetrahedral elements was made since they appear to be the most efficient and common elements for performing FE analysis. These elements can simulate the stiffness of the structure with small uncertainty allowing a good approximation of the stress concentration that appears near holes and notches. [86]

A convergence analysis and a validation were performed on the model in order to respectively decide the grade of mesh refinement and ensure that the model reproduced correctly the experimental test. A detailed description of these phases is presented in Chapter 3.1.1 and 3.1.2.

Once the convergence analysis was performed and once the model was validated it was possible to perform the final simulations.

The models for which simulations were decided to be performed are described in Table 18.

As already mentioned previously, the holes eventually present in the model were for simplicity simulated as cylinders.

| | Model Name | Plate used | Screw Ø and configuration | Evaluations made |
|---|-------------|--|---------------------------|--|
| 1 | No Holes | - | - | Reference samples |
| 2 | Sing3.5mm | - | 3.5mm -Central hole | Influence of the Ø of the screws on the failure of the radius bone |
| 3 | Sing2.7mm | - | 2.7mm -Central hole | |
| 4 | Sing4.5mm | - | 4.5mm -Central hole | |
| 5 | HybSYK3.5mm | Stryker VariAx 7 holes | 3.5 mm -Hybrid | Influence of the different approaches (screw Ø and screw distance) on the failure of the radius bone |
| 6 | HybSYK2.7mm | Stryker VariAx 7 holes | 2.7mm- Hybrid | |
| 7 | HybLCP3.5mm | DePuy Synthes LCP 7 holes – small fragment plate | 3.5mm -Hybrid | |
| 8 | StdLCP3.5mm | DePuy Synthes LCP 7 holes - small fragment plate | 3.5mm - Standard | |
| 9 | HybLCP4.5mm | DePuy Synthes LCP 7 holes – large fragment plate | 4.5mm - Hybrid | Verification of the literature outputs regarding the higher risk of using 4.5 mm plates |

Table 18: Groups for the computational comparison

The material assigned to the samples was cortical bone since the radius bone model was obtained from CT scans of a human bone with a successive CAD cut-out of the bone marrow and of the trabecular bone. The choice of performing this last operation was taken since the radius bone diaphysis is formed for the largest part by cortical bone (approximately 95%) [87]

The cortical bone was considered to be an isotropic linear elastic material with brittle failure in correspondence of σ_{\max} [88]. This is surely an approximation of the real properties of the cortical bone and this choice was taken for multiple reasons.

For example one requirement was the capability of performing various simulations in a reasonable amount of time and the imposition of ductile and/or viscoelastic materials would have led to higher computational time for reaching a convergent solution.

A second aspect which led to the imposition of only elastic properties to the cortical bone material regarded the fact that considering the bone as a ductile material (as suggested by various sources) the yielding stress would have been considered as the failure stress of the radius bone structure. This because once the yielding point is reached and exceeded a plastic deformation is present on the sample and the original shape can't be restored. Since the yielding point is normally the ending of the elastic region (Figure 98) it can then be decided to only assign the elastic properties to the cortical bone material used in the computational simulations.

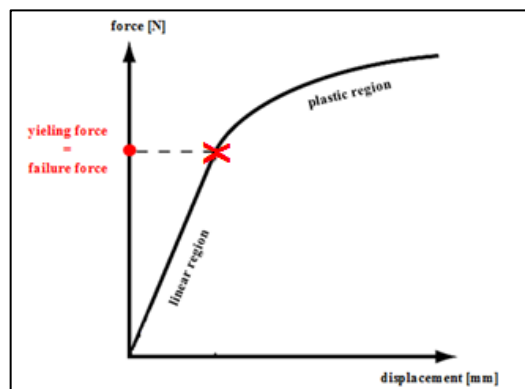


Figure 98: Force-displacement trend for cortical bone

Additionally, if the stress-strain curves of cortical and trabecular bone models are analyzed (Figure 99) it can be noticed that the properties of the two main tissues forming the bone are very different. In fact trabecular bone shows a wide plastic region and a small elastic portion while the cortical bone displays almost only an elastic region and a very limited plastic area.

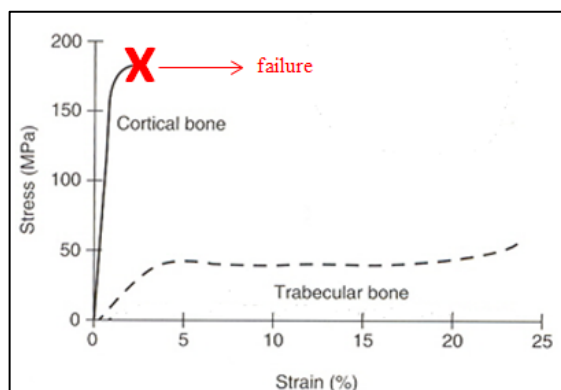


Figure 99: Stress – strain curves for cortical and trabecular bone [89]

For the above presented reasons the approximation made in considering the cortical bone as an elastic and brittle material seems to be relatively acceptable.

As a further justification of the choice made in assigning to the cortical bone material a brittle behavior Narayan et al., 2009 stated that cortical bone can be considered a relatively brittle material for transverse loading (situation that occurs in the present work) while a relatively ductile material when longitudinal loading is applied. [90]

The outputs in terms of force – displacement trends were not expected to be exactly the ones that would occur during the testing of real bone since some material approximations were made, but the eventual different influence of the different holes and hole pattern was expected to be noticed and to be correct since it mainly represents a geometrical rather than a material influence.

The cortical bone properties assigned to the FE model are listed in Table 19:

| | Property | Value | Source |
|---|--|-----------------------|---|
| 1 | Density (ρ) | 1.7 g/cm ³ | Bureau et al. [88]; Stryker [87] |
| 2 | Young's modulus (E) | 18.9 GPa | Stryker [87] |
| 3 | Tensile ultimate strength (σ_{max}) | 110 MPa | Bureau et al. [88]; Stryker [87]; Chen et al., [89]; Keaveny et al., [90]; University of Cambridge [91] |
| 4 | Poisson's ratio (ν) | 0.4 | Keaveny et al., [90] |

Table 19: Properties of cortical bone assigned to the FE model. The proposed values are the average between the ones found in the cited articles

The aim of the computational analysis, just like the experimental test, was the evaluation of the energy to failure of each model in order to permit the calculation of the safety factor $\alpha = E_{holes} / E_{noHoles}$ (already defined for the experimental test in Chapter 2) and the comparison of the different risk of re-fracture given by the removal of different screws and/or screw patterns.

The energy to failure was evaluated from the force – displacement trend where the force was virtually measured as reaction force on the support couplings (Figure 101) while displacement was the parameter set as loading condition on the upper blocks (Figure 100).

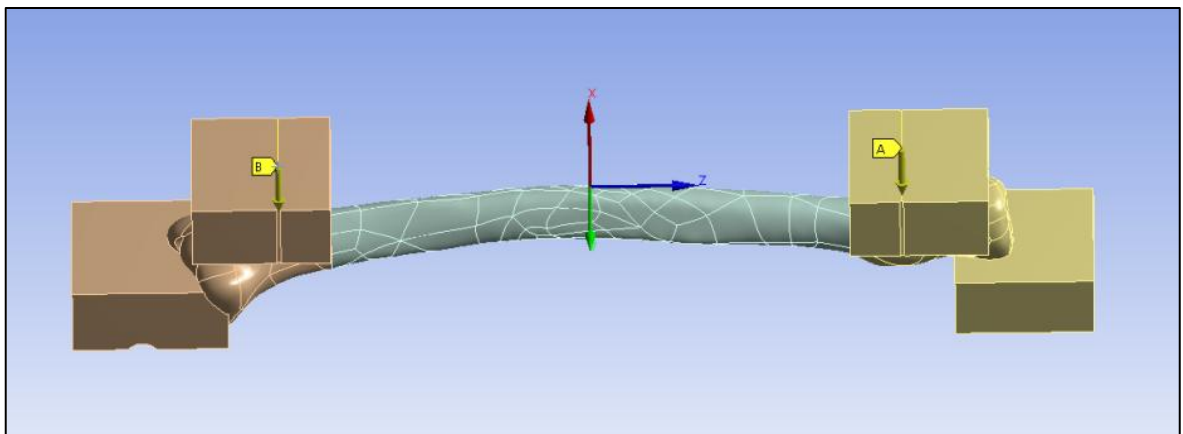


Figure 100: Loading conditions defined on the upper couplings

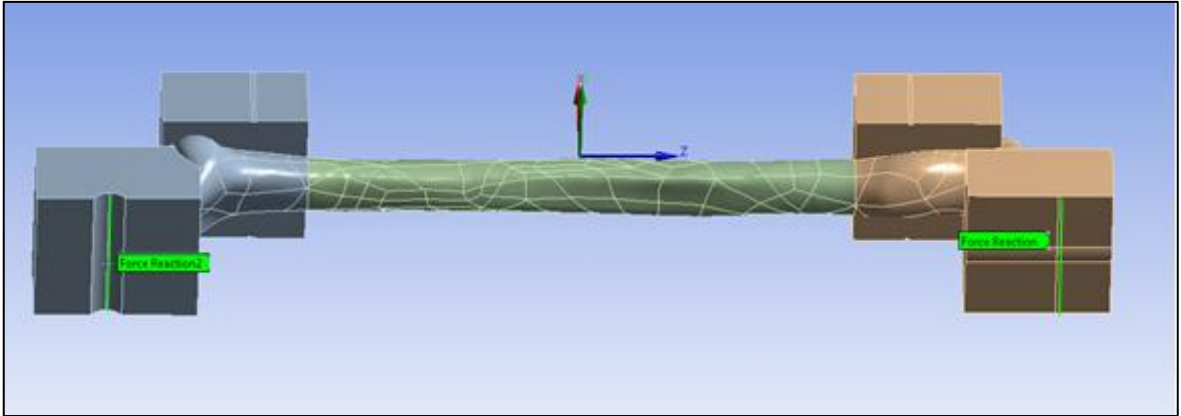


Figure 101: Edges of evaluation of the reaction force

The criterion used to define the force and displacement to failure, and therefore the force-displacement curve, was based on a maximum principal stress criterion. This was done because the cortical bone was considered a brittle material and it could therefore be assumed that when the principal tensile stress reached σ_{\max} failure would occur. [58] This approach usually gives good results for brittle materials but should not be used in presence of ductile materials for which the equivalent Von Mises stress analysis gives better results. [79]

The force and displacement to failure of each model were evaluated when the maximum principal stress in the structure reached $\sigma_{\max} = 110$ MPa. The force-displacement trend could then be plotted and the energy to failure of the each computational group calculated.

Finally the evaluation of the safety coefficient α could be performed for every group.

3.1.1 Convergence Analysis

The convergence analysis was carried out by initially calculating the solution of the model with a coarse mesh (element dimension = 2 mm) and evaluating the following parameters:

- maximum principal stress [MPa];
- equivalent von Mises stress [MPa]: within the same model it was always evaluated in the same point;
- principal stress [MPa]: within the same model it was always evaluated in the same point;
- maximum displacement [mm]

The mesh was successively gradually refined in correspondence of the parts of most interest (generally the radius shaft area) and the solution was again computed.

The decision on the final mesh to be adopted was taken when the percentage difference for each evaluated parameter between one mesh and the successive one (finer mesh) was $< 5\%$.

The zone of application of the loading conditions was shown in Figure 100 while their value within the convergence analysis phase is listed in Table 20.

| Loading Condition | Type | X component [mm] | Y component [mm] | Z component [mm] |
|-------------------|--------------|------------------|------------------|------------------|
| A | Displacement | -8.5 | Free | Free |
| B | Displacement | -8.5 | Free | Free |

Table 20: Loading conditions for the convergence analysis

The value of the x-displacement does not represent any real situation. In fact it is not the displacement which brings to failure the actual physical model. It was defined only with the purpose of finding the correct mesh refinement.

The models used for the convergence analysis are described in Table 21 and shown in Figure 102.

| Model Name | Description | Reason for choice |
|--------------|--|--|
| NoHoles | No holes on the shaft | General mesh dimension definition |
| SingSYK2.7mm | One central $\varnothing 2.7$ mm hole | Eventual influence of the presence of a hole in reaching convergence |
| HybSYK3.5mm | Holes left by the removal of the VariAx plate with six 3.5 mm screws | Eventual influence of the presence of multiple holes in reaching convergence |

Table 21: Models chosen for convergence analysis

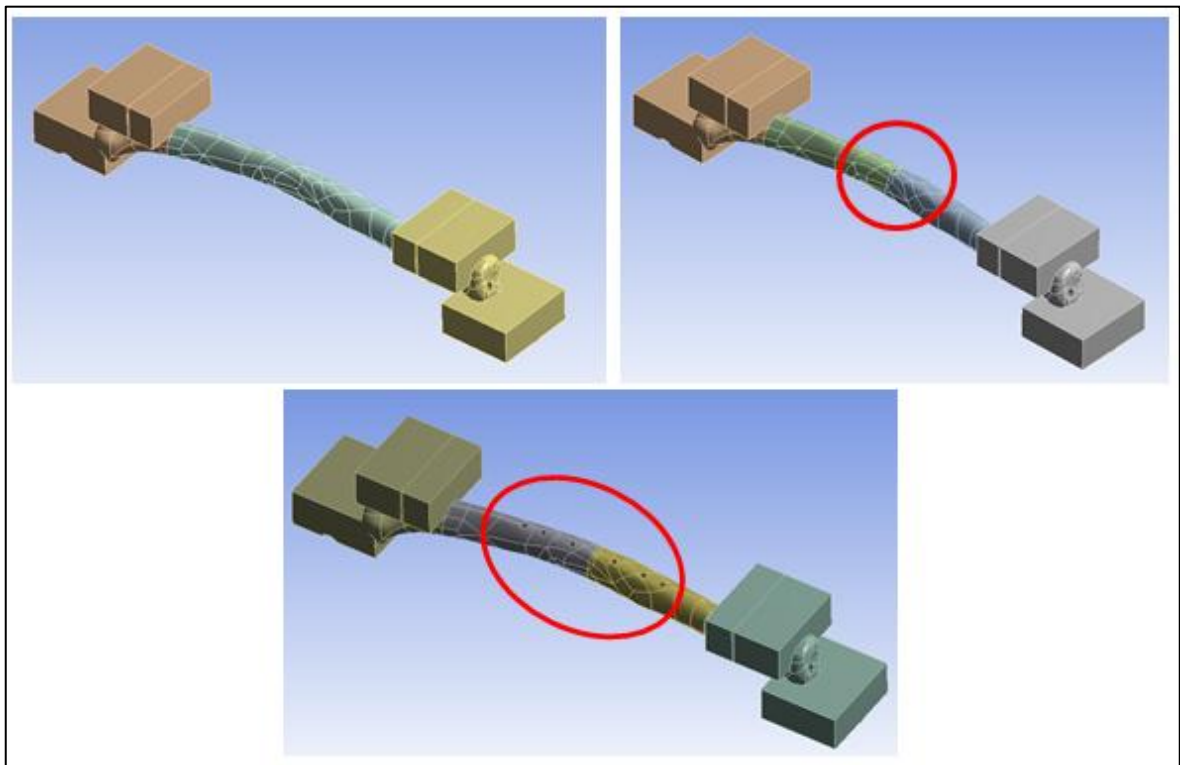


Figure 102: Models used for convergence analysis.

Top left: NoHoles; TopRight: SingSYK2.7mm; Bottom: HybSYK3.5mm

The material properties chosen to be assigned to the model for performing the convergence analysis were the ones defined for PA GF by the data sheet in Attachment 2. These properties were assigned to the model even if, as explained in Chapter 2, it was evident from the experimental pre-test that the actual samples were not characterized by them. This was done because there was no time to re-perform the convergence analysis once the material issue was clear and the results in terms of element dimension would anyway not have changed when using a different elastic and brittle material for this purpose.

The following tables show the results of the convergence analysis for each one of the chosen models.

| Model | Mesh | Element dimension [mm] (central part of the shaft) | 1/ element dimension | Max principal stress [MPa] | Principal stress in A [MPa] | Equivalent VM stress in B [MPa] | Min displacement [mm] |
|---|------|---|-------------------------|-------------------------------|--------------------------------|------------------------------------|--------------------------|
| noHoles | A | 2 | 0.5 | 63.25 | 59.86 | 68.6 | -19.12 |
| | B | 1 | 1 | 64.31 | 60.32 | 68.16 | -19.10 |
| | C | 0.8 | 1.25 | 64.76 | 60.47 | 68.14 | -19.10 |
| | D | 0.6 | 1.667 | 64.74 | 60.33 | 68.23 | -19.10 |
| Point A was set approximately in the middle of the volar surface (zone with the highest principal stresses applied) Point B was set approximately in the middle of the dorsal surface | | | | | | | |
| SingSYK2.7mm | A | 2 | 0.5 | 147.21 | 138.43 | 124.61 | -19.19 |
| | B | 1 | 1 | 136.86 | 130.25 | 122.74 | -19.18 |
| | C | 0.667 | 1.5 | 144.89 | 132.17 | 131.53 | -19.19 |
| | D | 0.5 | 2 | 154.78 | 134.52 | 131.28 | -19.20 |
| | E | 0.4 | 2.5 | 152.48 | 138.18 | 135.84 | -19.20 |
| Point A and point B were set on one edge of the hole on the volar surface side | | | | | | | |
| HybSYK3.5mm | A | 2 | 0.5 | 172.70 | 44.37 | 138.11 | -19.41 |
| | B | 1 | 1 | 173.70 | 48.28 | 164.67 | -19.42 |
| | C | 0.667 | 1.5 | 167.65 | 49.00 | 185.31 | -19.44 |
| | D | 0.5 | 2 | 166.73 | 46.75 | 188.38 | -19.44 |
| | E | 0.4 | 2.5 | 167.72 | 47.10 | 179.9 | -19.43 |
| Point A was set in the center of the volar surface (zone with the highest principal stresses applied) Point B was set on the edge of the second hole (from distal) on the dorsal surface | | | | | | | |

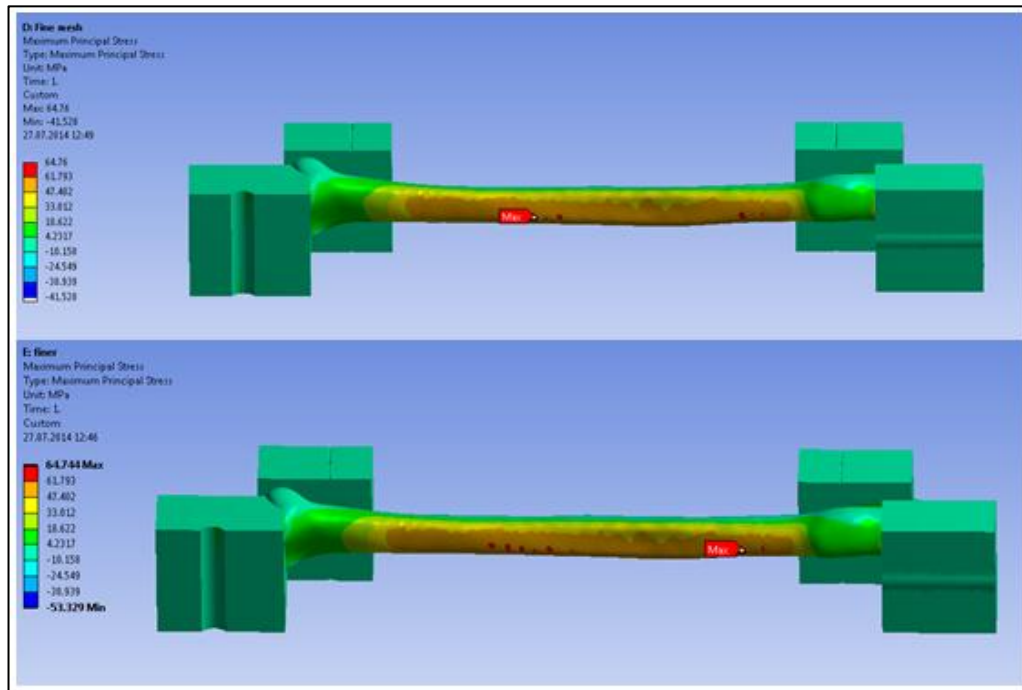
Table 22: Results regarding the evaluated parameters during the convergence analysis of each model

| Model | Comparison | % difference on max principal stress | % difference on principal stress in A | % difference on equivalent VM stress in B | % difference on min displacement |
|--------------|------------|--------------------------------------|---------------------------------------|---|----------------------------------|
| noHoles | A-B | 1.68 | 0.79 | -0.64 | -0.078 |
| | B-C | 0.70 | 0.24 | -0.018 | 0 |
| | C-D | -0.025 | -0.23 | 0.13 | 0 |
| SingSYK2.7mm | A-B | -7.03 | -5.91 | -1.50 | -0.036 |
| | B-C | 5.87 | 1.47 | 7.16 | 0.021 |
| | C-D | 6.82 | 1.77 | -0.19 | 0.063 |
| | D-E | -1.52 | 2.72 | 3.47 | -0.010 |
| HybSYK3.5mm | A-B | 0.58 | 8.90 | 19.23 | 0.031 |
| | B-C | -3.48 | 1.49 | 12.53 | 0.077 |
| | C-D | -0.54 | -4.59 | 1.65 | 0.026 |
| | D-E | 0.59 | 0.75 | -4.50 | -0.046 |

Table 23: Results of the convergence analysis in terms of percentage difference between one mesh and the successive one (finer mesh)

The ‘noHoles’ model already showed convergence when the coarser mesh was set (mesh A) since the percentage difference for all the evaluated parameters was always <5% (Table 23). It was decided to further refine the mesh since the area subject to high and similar stress was very large and the position of the exact point of max principal stress could have not been very precise when a coarse mesh was set.

It was in fact noticed that the point subject to the highest stress (point where most likely failure would occur) shifted when mesh D was used, as can be seen in the following image.



**Figure 103: Top: Maximum principal stress with mesh C applied;
Bottom: Maximum principal stress with mesh D applied**

The position of the max principal stress in correspondence of mesh D (proximal part of the shaft) found various confirmations within the experimental tests performed. In fact, in most of the cases a failure was noticed to occur in that area of the radius meaning that the proximal region is a particularly weak point of the intact bone in regards to a loading pattern that leads to a constant bending moment on the bone itself (Figure 104).

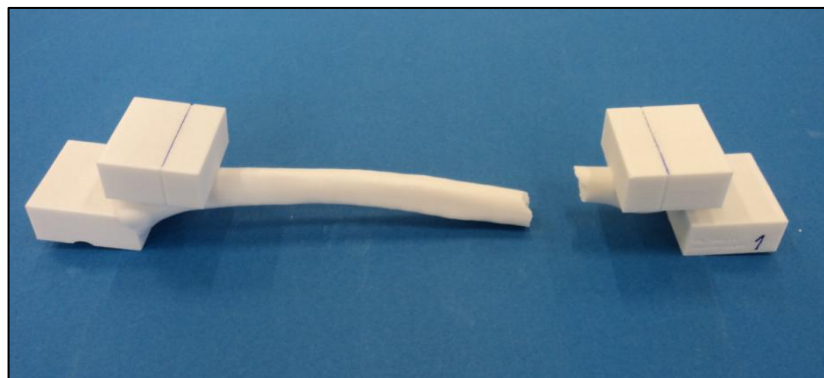


Figure 104: Proximal failure of one noHoles sample testes during experimental test 1

Mesh D (element dimension in correspondence of the radius shaft = 0.6 mm) was chosen for performing the final simulations of the 4 point bending test on samples with no holes.

The model SingSYK2.7mm showed convergence in correspondence of mesh D (element dimension 0.5 mm) since the percentage difference calculated in regards to the finer mesh was for every considered parameter below 5% while the model HybSYK3.5mm showed convergence with the imposition of mesh C (element dimension 0.667 mm).

Therefore element dimension = 0.5 mm was chosen for all the simulations which were characterized by one single hole and element dimension = 0.667 mm was adopted in case of models with multiple holes.

From the results presented in Table 22 and Table 23 it is possible to notice that displacement is the parameter that always converges more rapidly. This is due to the fact that stress is a derived parameter while displacement is a primary variable within the mathematical approach used by finite elements software. [94]

It is also evident that the minimum vertical displacement is always present in the central part of the specimen as shown in the following example for the model noHoles.

The models which present holes on the shaft show slightly smaller minimum displacement in correspondence of the same loading conditions, boundary conditions and material.

This aspect already shows a probable weakening of the structure when holes are produced into it.

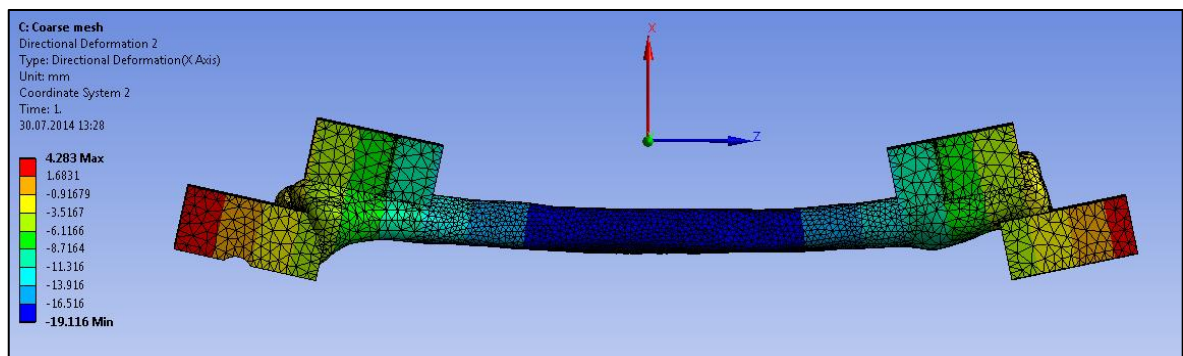


Figure 105: Vertical displacement on the noHoles model

3.1.2 Validation

For verifying the correctness of the FE model it was necessary to compare the results of the simulation with the results obtained from experimentally tested samples. The validation was performed using the two computational models noHoles and SingSYK2.7mm (see Table 10 for description of the models).

The forces or displacements measured during the experimental tests had to be applied to the computational model in order to allow a comparison of the outputs and evaluate the eventual correctness of the results. Since the results of the experimental test1 showed an extremely large deviation, two specific situations belonging to the pre-tests were chosen for comparison (noHoles 1 and central 2.7mm hole, whose results are presented in Figure 70 in Chapter 2). As done during the convergence phase, the applied loading conditions were defined as displacement conditions and set on the upper couplings, in the areas of load application during the experimental test (Figure 100). The displacements applied to the two models are listed in the following table. Their values were taken from the laboratory testing machine output.

| Loading Condition | Type | X component [mm] | Y component [mm] | Z component [mm] |
|-------------------|--------------|------------------|------------------|------------------|
| A | Displacement | -8.12 | Free | Free |
| B | Displacement | -8.12 | Free | Free |
| A | Displacement | -6.26 | Free | Free |
| B | Displacement | -6.26 | Free | Free |

Table 24: Loading conditions values for convergence and validation

The material to assign to the computational model had to be exactly the same as the one with which the samples used for the pre-tests were made of. It was clear that the material properties defined in the PA GF data sheet were different from the actual properties of the real material. The definition of the material to assign to the model was therefore performed by adjusting and changing in various steps the material elastic parameters until the comparison between experimental and computational showed good results.

The specific properties assigned to the two models used for the comparison with the experimental results of the pre-tests are listed in Table 25.

| | |
|------------------------------|----------------|
| Behavior | Linear elastic |
| Tensile modulus [MPa] | 6090 |
| Poisson's ratio | 0.4 |

Table 25: Material properties of the samples used for pre-tests

The validation was performed comparing the force applied vs roller displacement outputs resulted from the experimental and from the computational tests.

The computational force was evaluated as reaction force on the edges where the boundary conditions were applied (Figure 101). The total force to be compared with the experimental data was the sum of the two (left and right) reaction forces.

In order to consider the FE models validated the percentage difference between the experimental and computational forces present in correspondence of the same displacements had to be <10%.

This had to be verified in correspondence of all the 10 force – displacement couples which represented the output of the computational analysis.

The results of the validation are presented in the following charts.

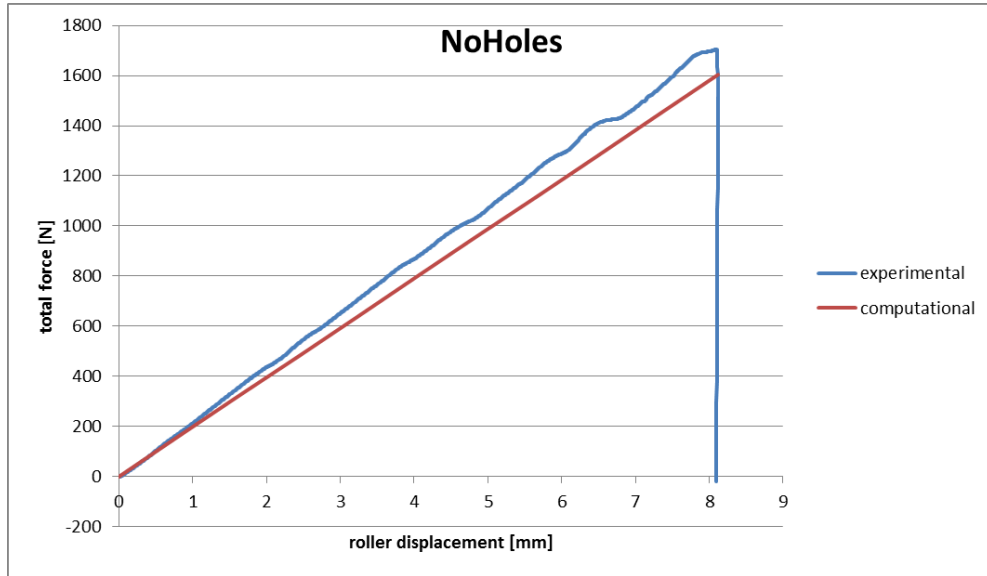


Figure 106: Computational-experimental comparison for the sample noHoles

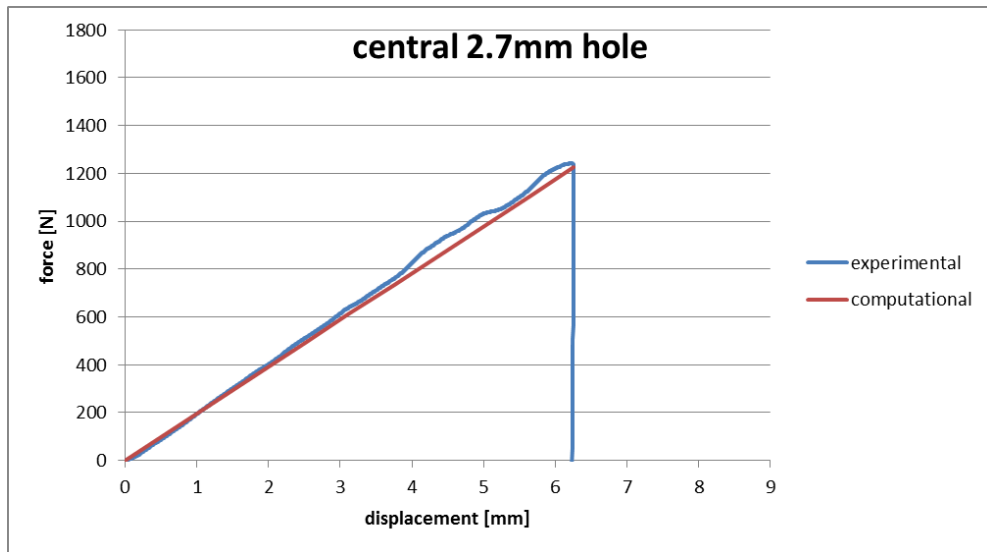


Figure 107: Computational-experimental comparison for the sample with central 2.7mm hole

The percentage difference between experimental and computational forces in correspondence of ten displacements was always lower than 10% for both models evaluated. Complete results are presented in Attachment 4.

As already mentioned, the main output of this phase was the verification that when on the computational model the displacement measured during the experimental test is applied and the correct material properties are set, the resultant forces (experimental-computational) are the same.

The results of the validation phase confirm that all the computational models which will be used for the following evaluations can be considered as correct representatives of the experimental situation, when the right material properties are inserted, since they behave in a similar way as they would in an experimental test.

A second phase of the validation of the model was made qualitatively (by eye) analyzing the deformation mode of the two samples (experimental vs computational) which appeared very similar as can be seen from the below described aspects (also visible in Figure 108).

1- Both experimental and computational models show the presence of only a rotation of the left coupling around the supporting roller.

2- In both cases, the right block of the samples undergoes only a z-displacement of the zone of contact with the supporting roller

The outcome of these two visual evidences is the verification that both samples slide on the right roller allowing the application of only vertical forces (no shear force and no axial forces on the radius shaft) with a fixed lever arm in both experimental and computational models.

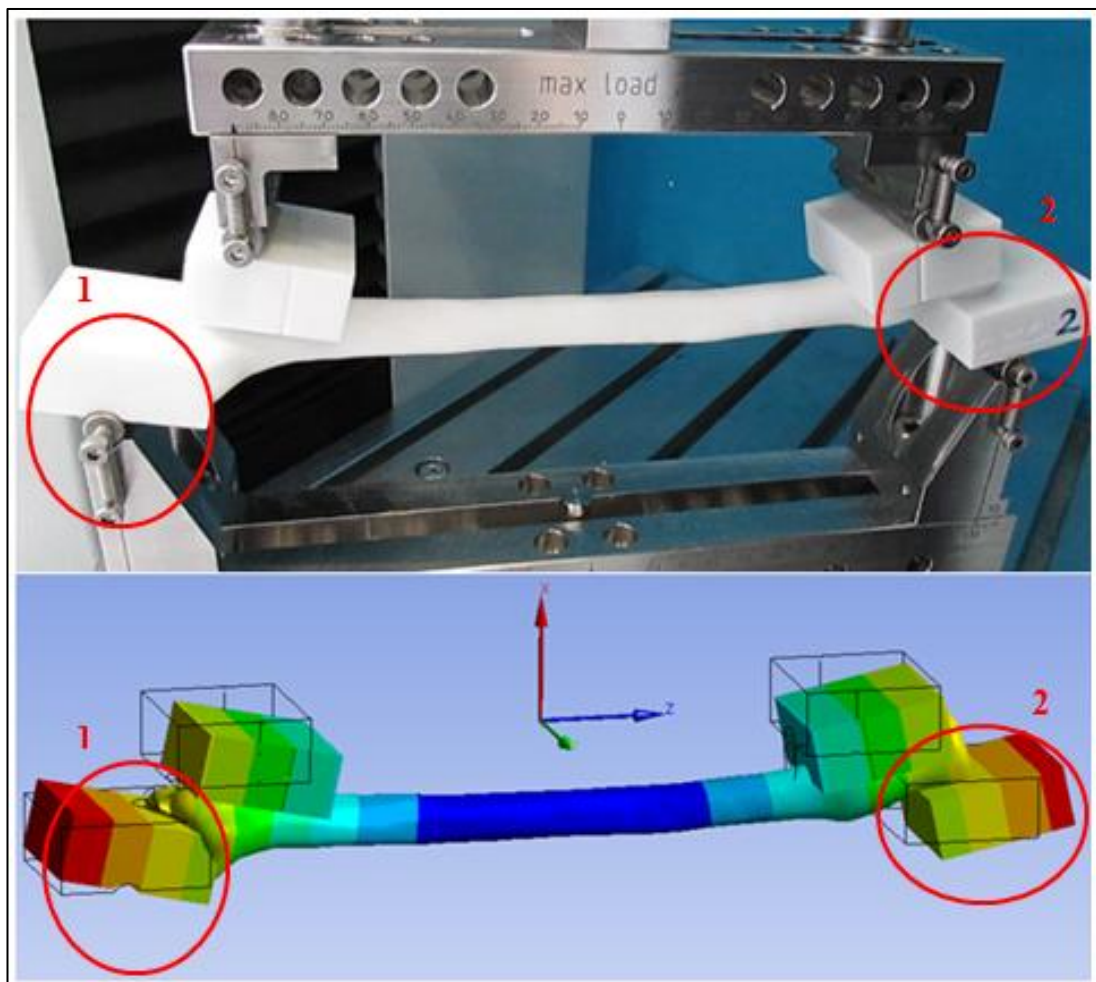


Figure 108: Comparison between the deformed experimental and computational samples

3.2 Computational Results

The results in terms of energy to failure, force to failure and roller displacement to failure of the computational simulations are presented Figure 109, Figure 110 and in Table 26.

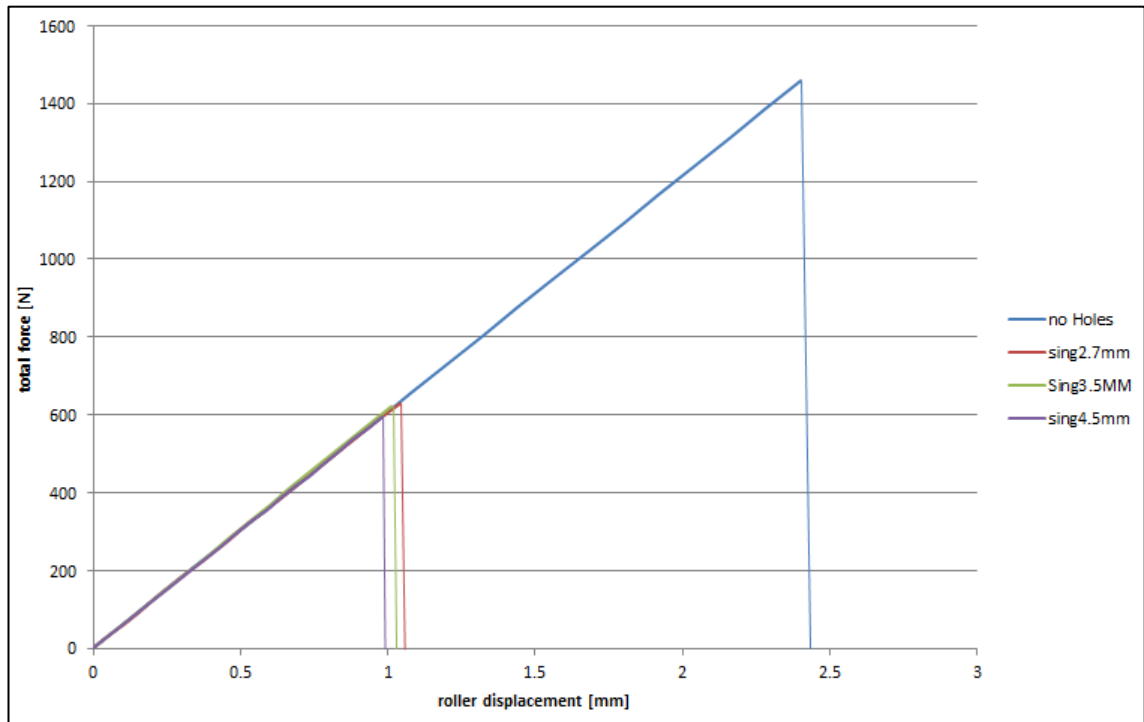


Figure 109 Force – displacement comparison between single hole and noHole groups

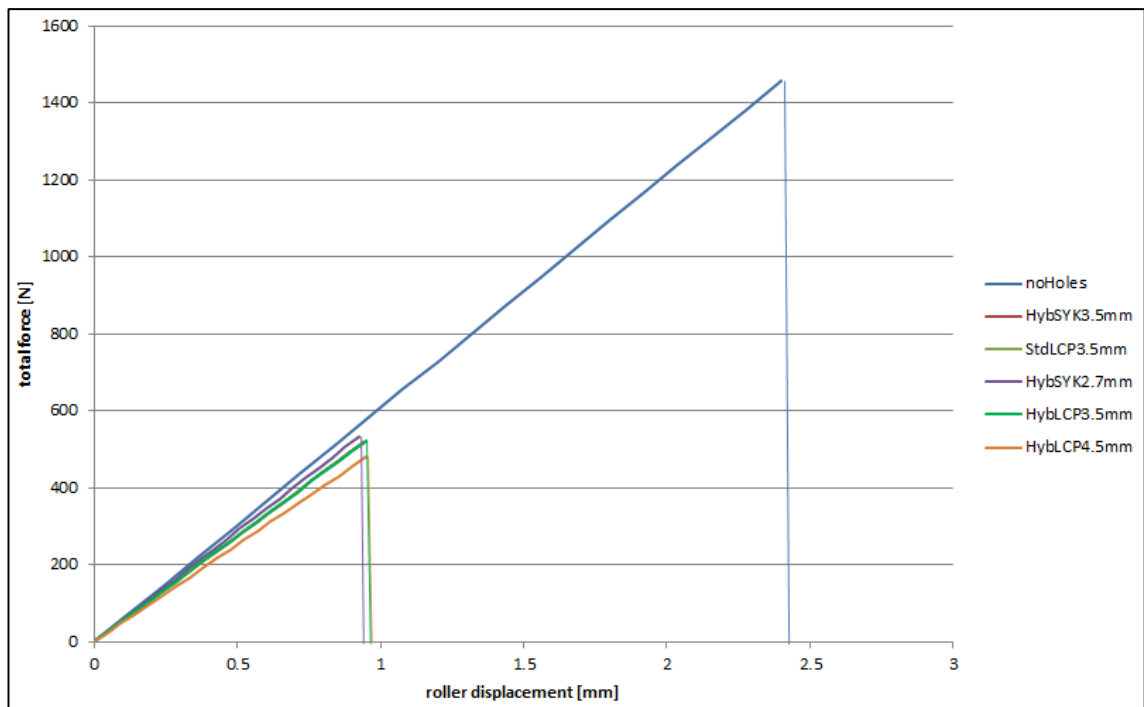


Figure 110: Force – displacement comparison between multiple holes and noHole groups

| | Model | Force to failure [N] | Displacement to failure [mm] | Stiffness [N/mm] | Energy to failure [Nmm] |
|---|-------------|----------------------|------------------------------|------------------|-------------------------|
| 1 | NoHoles | 1458.02 | 2.4 | 607.51 | 1924.58 |
| 2 | Sing3.5mm | 621.39 | 1.01 | 615.23 | 314.58 |
| 3 | Sing2.7mm | 630.79 | 1.04 | 606.53 | 328.01 |
| 4 | Sing4.5mm | 594.53 | 0.98 | 606.66 | 292.05 |
| 5 | HybSYK3.5mm | 517.48 | 0.94 | 550.51 | 243.82 |
| 6 | HybSYK2.7mm | 533.04 | 0.925 | 576.26 | 271.80 |
| 7 | HybLCP3.5mm | 522.55 | 0.95 | 550.05 | 248.83 |
| 8 | StdLCP3.5mm | 522.22 | 0.95 | 549.70 | 248.68 |
| 9 | HybLCP4.5mm | 479.98 | 0.95 | 505.24 | 228.62 |

Table 26: Computational simulation results

The safety coefficients α , which were decided to be the parameters of comparison between groups, are presented in Table 27.

| | Configuration | Model | Safety coefficient α [-] |
|---|----------------|-------------|---------------------------------|
| 1 | Single hole | Sing3.5mm | 0.164 |
| 2 | | Sing2.7mm | 0.171 |
| 3 | | Sing4.5mm | 0.152 |
| 4 | Multiple holes | HybSYK3.5mm | 0.128 |
| 5 | | HybSYK2.7mm | 0.142 |
| 6 | | HybLCP3.5mm | 0.129 |
| 7 | | StdLCP3.5mm | 0.129 |
| 8 | | HybSYK4.5m | 0.119 |

Table 27: Results in terms of safety coefficient for the tested models

For each configuration the maximum (green) and the minimum (red) are highlighted

All the images regarding the maximum principal stress distribution obtained after the performance of the simulations on the various models are presented in Attachment 6.

4. Discussion and Conclusions

4.1 Discussion

4.1.1 Experimental Test

The most evident result after the performance of the experimental test was the great reduction of the energy needed to bring to failure the radius bone with holes left in correspondence of screw removal in comparison to the intact bone. The energy reduction was of 72% with the 2.7 mm holes and 74 % when the 3.5 mm holes were present while the decrement in regards to the maximum applied load was 42% and 44% respectively for the groups HybSYK2.7mm and HybSYK3.5mm. The results regarding the reduced force to failure have some similarities with the findings of Johnson et al., 1997. In this work fibula bones were tested in a three point bending configuration after a 3.5 mm hole was drilled on the shaft. The results showed a mean load reduction of 40%. [56] The data dispersion is evidently quite important (Table 28) and only five pairs of bones were tested. More data would probably be needed to confirm the results.

| Load application at failure | | | |
|-----------------------------|-------------------------|--------------------------|------|
| Cadaver | Intact Fibula (Newtons) | Drilled Fibula (Newtons) | |
| 1 | 250.32 | 71.33 | -71% |
| 2 | 800.14 | 600.61 | -25% |
| 3 | 365.16 | 195.66 | -46% |
| 4 | 207.01 | 66.49 | -68% |
| 5 | 181.69 | 141.89 | -22% |

Table 28: Load-to-failure for intact fibula and with one single 3.5mm hole fibula [56]

However, these findings present some important differences if compared to the results of other scientific articles (for example Rosson et al., 1991) in which a reduction of the energy to failure of circa 50% in consequence of the removal of previously implanted screws was noticed. [61]

Both works were cited since they evidently show the influence on the strength of a bone structure of holes left after screw removal and since no reference was found describing the results of a more similar test to the one performed in the present work. The comparison between the results of this work and of the two mentioned articles must be mainly a qualitative comparison since the differences, in terms of samples, loading conditions, etc., are multiple.

Johnson et al., 1997, for example, tested fibula bones in a three point bending configuration after one 3.5 mm hole was drilled on the shaft.

Rosson et al., 1991 tested instead tibiae from rabbits in which 1.5 mm and 2 mm screws were inserted and removed. The mechanical test performed was a 3 point bending test and the load formed a 45° angle with the axis of the screw. [61]

The statistical analysis performed on the results of the experimental test 2 results showed that the energy to failure, the force to failure and the displacement to failure of the groups HybSYK2.7mm and HybSYK3.5mm do not show any statistical significant difference. These results indicate that in regards to a bending test the presence of 2.7 mm or 3.5 mm holes induces a similar risk of re-fracture.

However the analysis of the mean values (and of the sum of ranks given by the statistical analysis in Attachment 5) shows a slight better situation when 2.7 mm screws are implanted and removed.

The calculation of the safety factor α showed in fact a greater value for the HybSYK2.7mm group rather than for the HybSYK3.5mm group.

This small advantage will be confirmed by the computational test whose results will be discussed in the following section.

Analyzing Table 14 it can be noticed that, in particular for the samples with holes, the failure location was not always the same but was in each case located in correspondence of the most proximal defects. In fact for the group HybSYK2.7mm three failures occurred through the 5th hole from distal, two through the 6th and one through the 4th while for the group HybSYK3.5mm four failures occurred through the 5th hole, one through the 4th and one through the 6th. This was probably due to a non-perfect precision in mounting plate and screws. Small differences in terms of positioning of the hardware can lead to a change in the location of the weakest cross section of the bone and therefore of the failure point during mechanical loading.

A further aspect which is worth mentioning regards the maximum percentage differences observed for every measured parameter within each tested group in the experimental test 2. Table 16 shows values up to 37%, which could appear as a very important difference.

It must be considered that between different samples, belonging to the same group, there can be differences due to material non-uniformity and to a non-perfectly reproducible production process. In addition some errors could have been inserted during the plate and screw mounting and during the testing phase. The percentage differences calculated are therefore in line with the usual values expected when performing mechanical tests on parts.

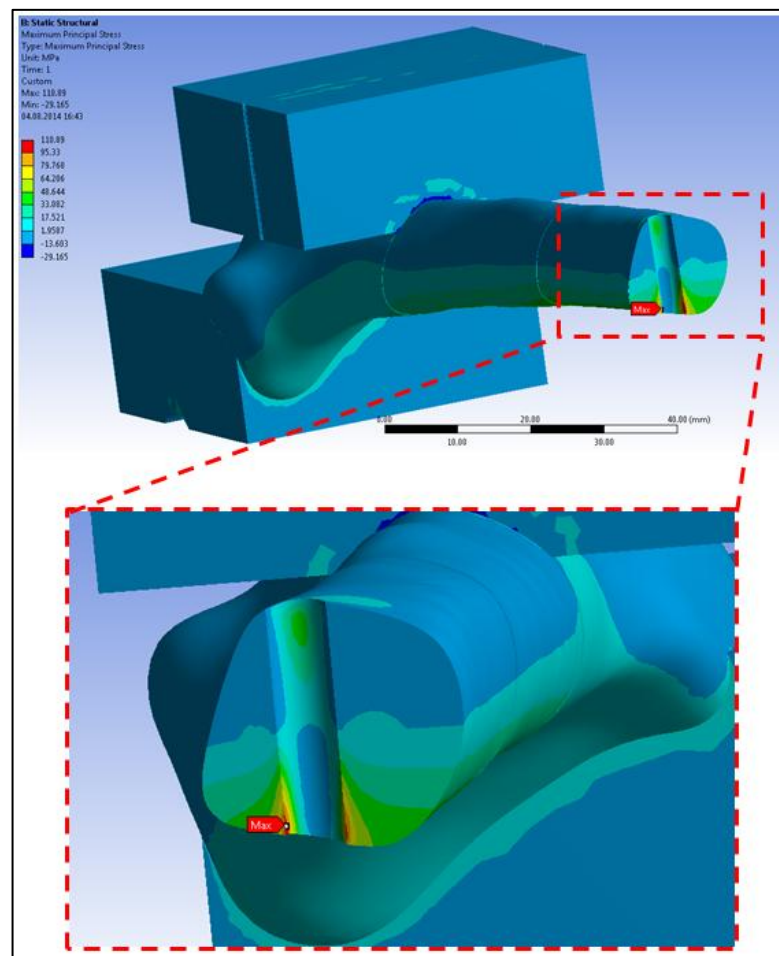
4.1.2 Computational Test

As described in Chapter 3 the computational analysis was performed on radius models with no holes, single holes and multiple holes.

The first consideration after the computational test performance on samples with *single holes* regarded the evident influence that their presence had on the strength of the radius when subject to a 4-point bending test (Figure 109 and Table 26). The results showed, in fact, a reduction of the energy needed to bring the bone to failure of approximately 82% when a 2.7 mm hole is present, 83% with a 3.5 mm hole and 84% with a 4.5 mm hole. Very evident results can also be observed for the other evaluated parameters (mainly displacement to failure and force to failure).

Results appear worse compared to the ones obtained by Johnson et al., 1997 and by Rosson et al., 1991 (Table 28) but As already explained in Chapter 4.1.1 they analyzed a not completely comparable situation in regards to the one studied in the present work.

As reported in Chapter 3 it was assumed that failure occurred in the point that first reached $\sigma_{\max} = 110$ MPa. This stress level appeared to be for all the samples with holes in the inner wall of the hole itself (Figure 111) and not on the most distant surface from the neutral axis as happens in other cases (for example noHoles model).



**Figure 111: Location of the maximum stress for the samples with one single hole.
In this example the 3.5 mm hole is shown**

This aspect was expected since Pilkey et al., 2008 had reported that when a tube or bar of circular cross section with one hole is subject to bending the maximum stress does not occur on the surface of the shaft but at small distance inside the hole [58] This cited work helped giving a confirmation on the reliability of the computational model which, at least in correspondence of the holes, behaved exactly as expected in theory.

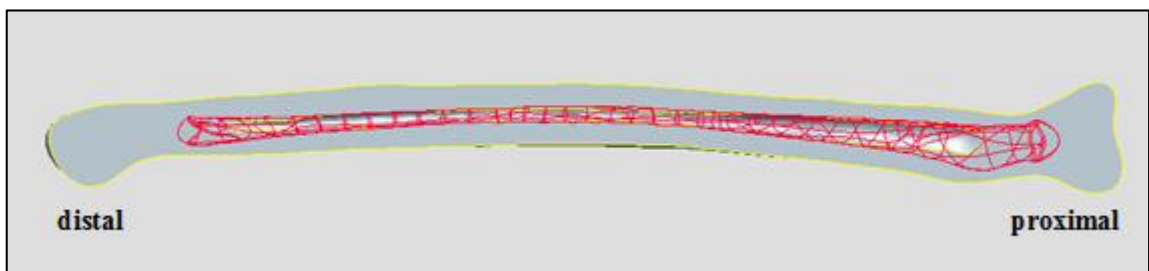
A further consideration after analyzing the outputs of the computational data permitted to state that the presence of single holes of diverse diameter (in particular 2.7 mm, 3.5 mm and 4.5 mm) does not seem to vary significantly the behavior of the bone model. This could be stated since the energy to failure of the samples with holes does not differ significantly between the different groups, as can be verified in Table 26.

This aspect is due to the fact that a hole influences the resistance of the structure in two ways, as already briefly introduced in Chapter 1.4.

- i. The hole introduces a reduction of the cross section and therefore of the second moment of inertia. The bigger the hole diameter is, the smaller the cross section and second moment of inertia will be. Therefore for equation (2) larger holes will cause the generation of higher stresses, especially on the most tensioned areas of the bone (the furthest from the neutral axis).

$$\sigma = \frac{M}{I}y \quad [\text{MPa}] \quad (2)$$

The different stresses due to the reduced moment of inertia in correspondence of holes of different dimensions can be analytically calculated applying the above equation. The main source of errors in this calculation (which should be minimized) can be caused by an excessive simplification of the bone geometry, which is often considered as a hollow cylinder. In reality its shape is much more complex since there is, for example, a curvature and a non-constant bone marrow canal + trabecular bone shape as can be seen in the following image.



**Figure 112: Longitudinal cross section of the radius bone.
The bone marrow canal + trabecular bone are highlighted in red**

The calculation of the maximum stress in the real bone structure is presented below and it was done considering the exact shape of the cross section in correspondence of which failure occurred. The precise second moment of inertia (evaluated through the CAD software in correspondence of the cross section of interest, as shown in Figure 113), an estimated value of y (distance between the center of gravity and the point of max stress as shown in Figure 114) were used when applying equation (2).

Some approximations were anyway introduced in these calculations as well and mainly regarded y , which in formula (2) represents the distance between the neutral axis of the cross section and the

point in which the stress calculation is desired. The neutral axis position was not evaluable with the CAD software used; therefore the center of gravity was chosen to be used as it was a point (probably quite close to the neutral axis) which the software could calculate precisely.

A second source of imprecision was given by the point named “max_stress” which is not perfectly placed since, as explained previously and as evident from Figure 111, the highest stress is not found on the surface of the sample. This point was chosen because it was the nearest selectable point to the area subject to maximum stress and since the actual location of σ_{\max} was not measurable through the CAD software.

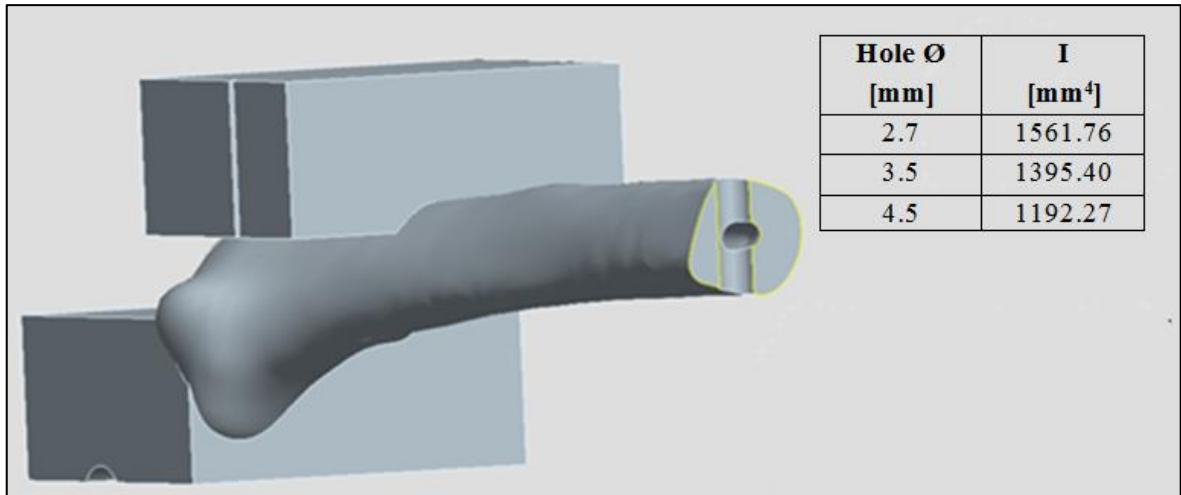


Figure 113: Cross section for calculating the second moment of inertia and values of I for different hole \emptyset

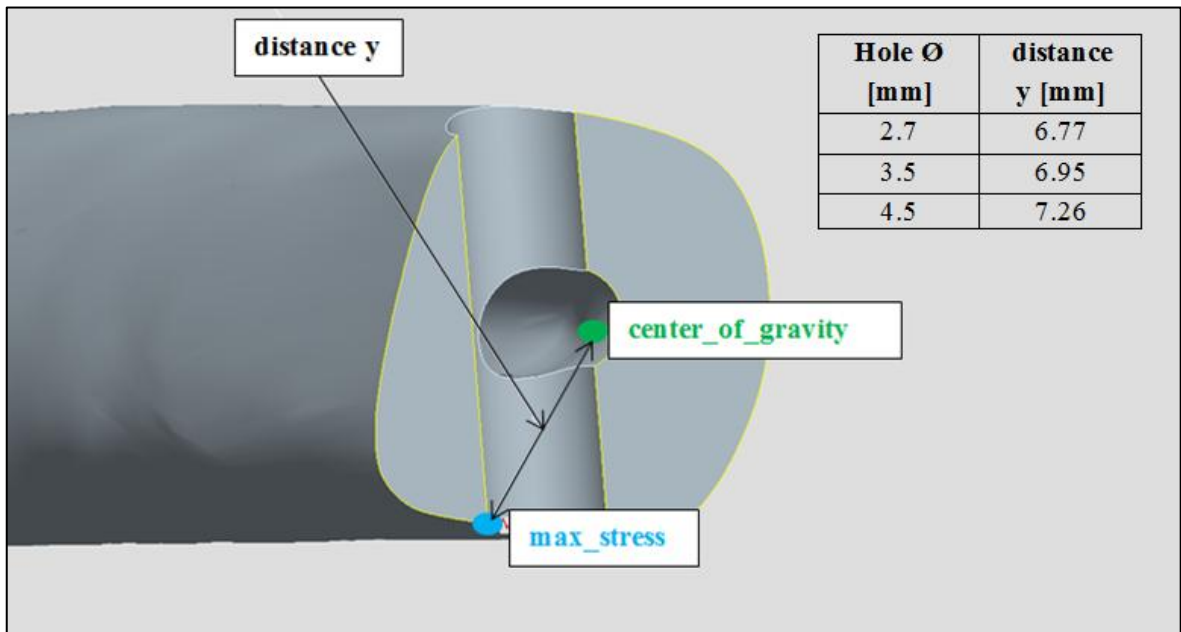


Figure 114: Distance between the center of gravity and the area of maximum tension stress for the models with one single hole

Knowing from the computational simulations the force-to-failure applied to the sample and the lever arm of the force itself, it was possible to calculate the analytical stress reached in correspondence of the point defined as “max_stress” in the previous image.

Regarding the stress calculations for the group noHoles, they were performed considering the moment of inertia of the cross section in correspondence of which failure occurred (circa 20 mm from the proximal upper block as shown in Figure 115). The distance y was measured between the center of gravity of the mentioned cross section and the volar surface of the radius bone. Results are presented in Table 29.

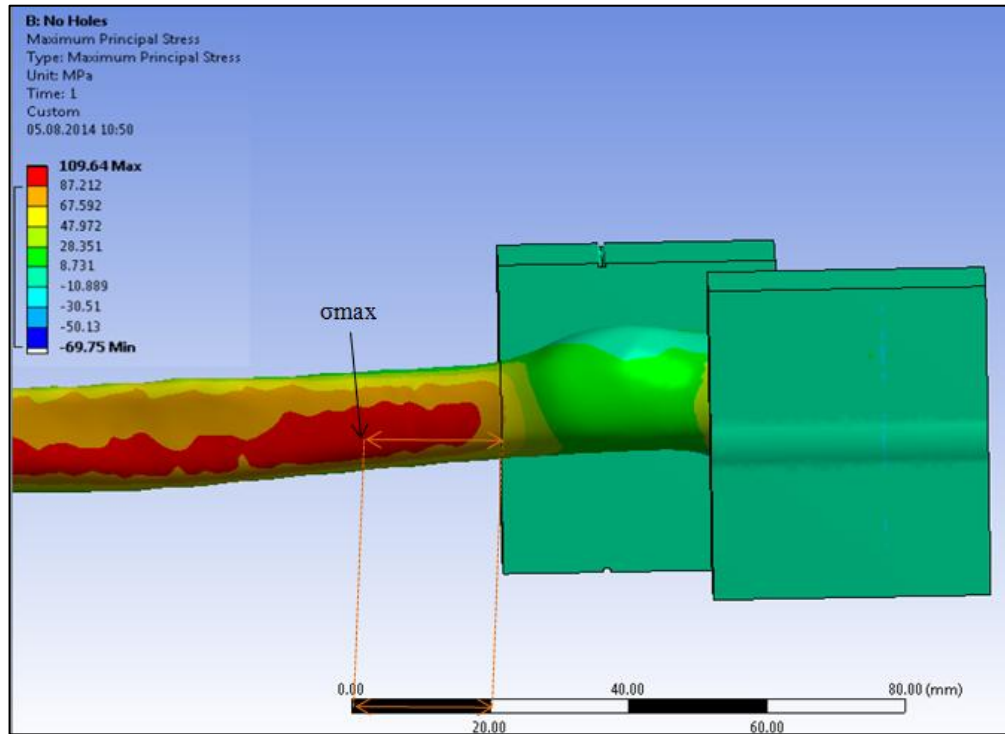


Figure 115: Measurement of the position of the section subject to max stress

| sample | I [mm ⁴] | y [mm] | max force [N] | σ_{nom} [MPa] |
|-----------|----------------------|--------|---------------|-----------------------------|
| noHoles | 2005.01 | 6.97 | 1458.06 | 101.22 |
| Sing2.7mm | 1561.76 | 6.77 | 636.86 | 55.21 |
| Sing3.5mm | 1395.40 | 6.95 | 621.39 | 61.89 |
| Sing4.5mm | 1192.27 | 7.26 | 594.53 | 72.40 |

Table 29: Analytical σ calculation for the computational no holes and single hole groups

The calculation of the stress at failure for the sample with no holes gave the value of 101.22 MPa which is smaller than the circa 110 MPa given by the computational model output and which represents the failure stress of the material. The percentage difference between the two stresses is ca. 7% and it was considered irrelevant since some of the previously described approximations in the calculations performed were inevitably inserted. The results of the computational simulation and of the analytical calculation were therefore considered equivalent.

The situation for the samples with holes appeared quite different since an apparent failure in correspondence of a much lower stress than the cortical bone $\sigma_{\text{max}} = 110$ MPa was calculated.

- This fact introduces the second influence given by a hole in regards to the static resistance of a structure. The presence of a geometrical discontinuity originates a stress concentration, in this case near the hole. In order to graphically see the mentioned stress rising (Figure 117) the stress distribution on a path defined in correspondence of the hole (Figure 116) was plotted. The point where the stress concentration is present is the most probable location of failure of the structure since σ_{\max} is reached earlier than in other areas. As stated previously an even greater stress is present in the inner surface of the hole must be highlighted.

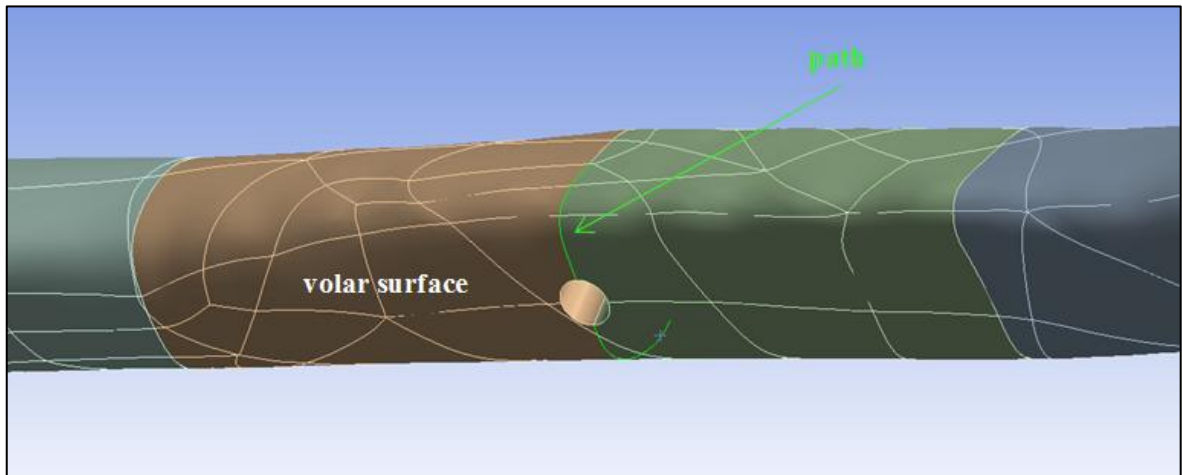


Figure 116: Path definition on the volar surface of the radius

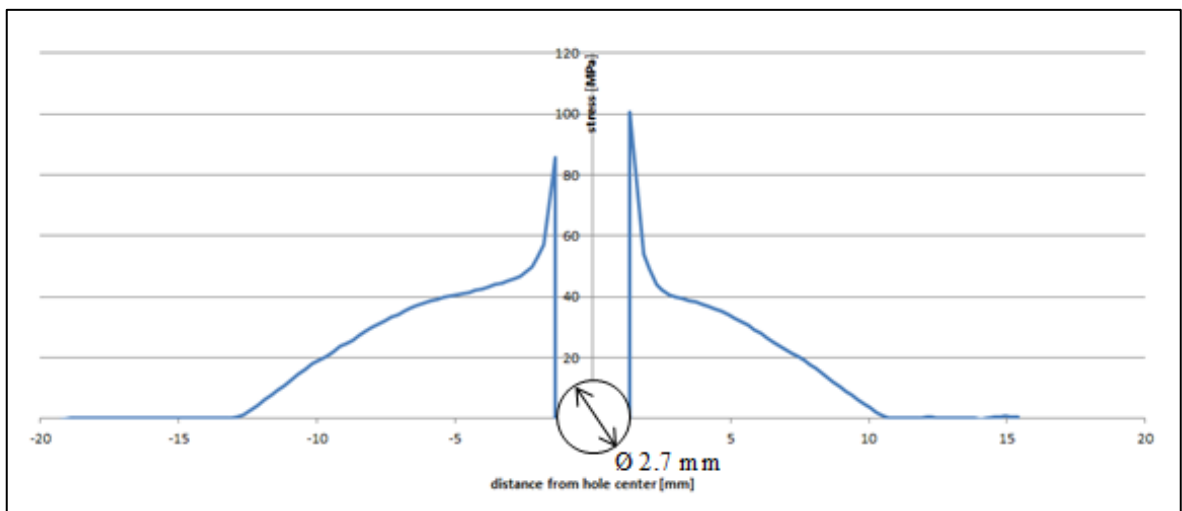


Figure 117: Stress on the path defined in proximity of the 2.7mm hole

This aspect, which was already briefly introduced in Chapter 1.4, is not considered during the standard analytical stress calculations (results listed in Table 29). Therefore in case holes, notches, etc are present the stress evaluation should use as well other instruments (charts or finite element analysis) in order to correctly estimate the real stress level reached in the structure.

The stress concentration originated on the radius bone by the presence of a hole can be described through the stress concentration factor k_t (formula (3)).

$$k_t = \frac{\sigma_{\max}}{\sigma_{\text{nom}}} \quad [-] \quad (3)$$

- σ_{\max} [MPa] represents the maximum stress actually reached in the structure. In this case it is equal to 110 MPa since the loading to failure is analyzed.
- σ_{nom} [MPa] represents the analytical failure stress, calculated considering only the reduced cross section given by the presence of holes. The values of σ_{nom} are the ones listed in Table 29.

The stress concentration factors induced by the different hole diameters are shown in the following table and were calculated considering the real radius shape. It must be highlighted that smaller holes origin greater stress concentration factors (and therefore greater stress near the hole).

| hole \varnothing [mm] | σ_{\max} [MPa] | σ_{nom} [MPa] | $k_t = \sigma_{\max} / \sigma_{\text{nom}}$ [-] |
|-------------------------|-----------------------|-----------------------------|---|
| 2.7 | 110 | 55.21 | 1.99 |
| 3.5 | 110 | 61.89 | 1.78 |
| 4.5 | 110 | 72.40 | 1.52 |

Table 30: Stress concentration factor calculation for the samples with single holes

As mentioned previously the stress concentration factors can also be evaluated using the charts presented in several structural mechanics book such as Pilkey et al., 2008 [58] The chart for a regular tube or cylinder with a transverse single hole is presented in Figure 118.

The use of the mentioned charts needs the knowledge of the geometrical parameters of the structure such as external diameter (D), internal diameter (d_i) and hole diameter (d) in order to calculate the parameters d/D , d_i/D which allow the evaluation of k_t . The parameters characterizing the studied cases are presented in the following table.

| d [mm] | d_i [mm] | D [mm] | d/D | d_i/D |
|--------|------------|--------|-------------|-------------|
| 2.7 | 4* | 14** | 0.19 | 0.29 |
| 3.5 | | | 0.25 | |
| 4.5 | | | 0.32 | |

Table 31: Parameters for the evaluation of the stress concentration through the use of the charts.

** and **: since the bone and bone marrow canal do not have a regular shape an approximated value was measured from the CAD model*

The result of the stress concentration evaluation using the chart of Figure 118 gives:

- $k_t \approx 2.1$ for the 2.7 mm hole
 - $k_t \approx 2.05$ for the 3.5 mm hole
 - $k_t \approx 2.0$ for the 4.5 mm hole
- } Confirmation of the fact that smaller holes generate higher stress concentration

It can be seen that the k_t values estimated from the chart are not the same as the values calculated analytically. This difference is mainly caused by the use of the chart which refers to the bending of a regular hollow cylinder with one transverse hole which is a not completely comparable situation with the actual radius bone. For this reason the k_t values calculated in Table 30 were considered the most correct parameters in describing the true stress situation on the structure since they are characterized by fewer approximations, mainly because the “true shape” was taken into account.

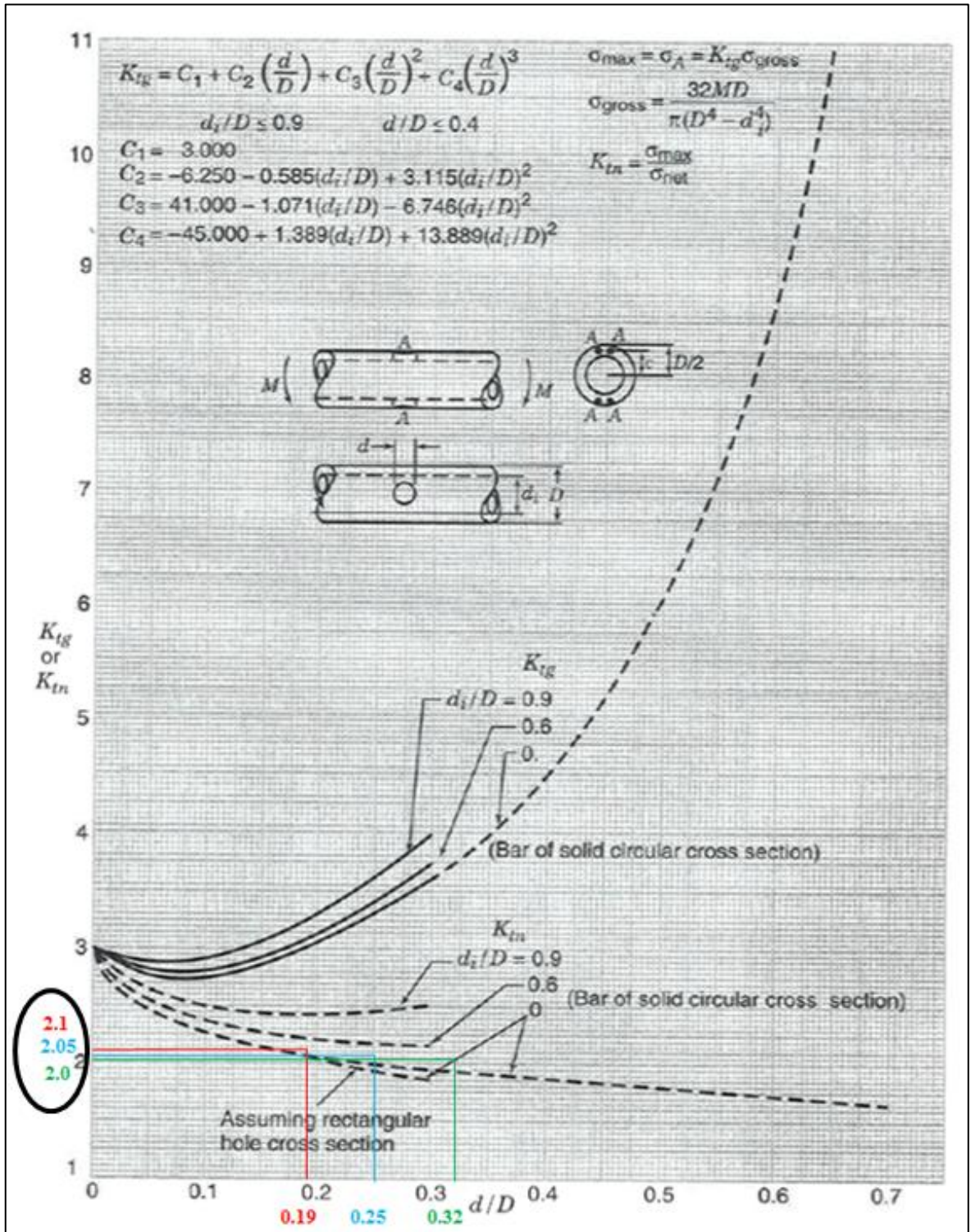


Figure 118: Chart for the evaluation of stress concentration factor in presence of a tube or cylinder with transverse hole (modified from [58])

The last consideration regards the stiffness of the samples with one hole which appeared for each group similar to the one of the noHoles sample (Figure 109). This aspect indicates that one single hole does not appear to influence importantly the relationship between force and displacement of the structure which behaves in a similar manner as when no discontinuity is present (a part, obviously, from the level of force and displacement at failure).

In conclusion, the tests on samples with one single hole showed only slight differences in terms of risk of re-fracture between different groups. The calculated safety coefficients α assumed, in fact, similar values meaning that the presence of a 2.7 mm, 3.5 mm or 4.5 mm hole does not change in an evident way the possibility of failure of the bone.

As already described, this is caused by the fact that large holes generate higher stress than small holes because of a smaller moment of inertia; oppositely the stress concentration caused by the geometrical discontinuity given by large holes is lower than in presence of small holes. The sum of these two components leads to a similar situation in terms of force to failure, displacement to failure and energy to failure for all the samples analyzed characterized by single holes.

However, the slightly safer case within the analyzed situations and when the radius is subject to bending is in presence of the hole left after removal of a 2.7 mm screw ($\alpha_{2.7\text{mm}} = 0.175 > \alpha_{3.5\text{mm}} = 0.164 > \alpha_{4.5\text{mm}} = 0.152$).

The above discussed simulations were followed by several ones performed on the radius bone with *multiple holes* left in consequence of the removal of different plates and screws. This section of the work would permit the evaluation of an actually possible situation in terms of holes present on a patient's radius in the immediate period after plate removal.

The first aspect noticed (Figure 110) regarded the significantly decreased energy to failure of these samples in comparison to the simulation performed on the intact bone model. This was, of course, an expected result since the reduced cross section and the stress concentration induced by holes causes, as explained for the single hole samples, a higher risk of failure.

It was also noticed that the energy to failure was lower compared to the one present in the samples with a single hole. This aspect was probably due to the fact that having six holes in six different locations increases the chances of reducing an already weaker cross section of the intact bone. This consideration can be verified, for example, by comparing the location of the max principal stress in the samples HybSYK3.5mm and HybLCP3.5mm (Figure 119). It can be noticed that the maximum principal stress appeared in correspondence of the first hole from the distal epiphysis for the HybSYK3.5mm and on the second hole from the distal portion of the bone for the HybLCP3.5mm, even if the dimension of the holes are the same.

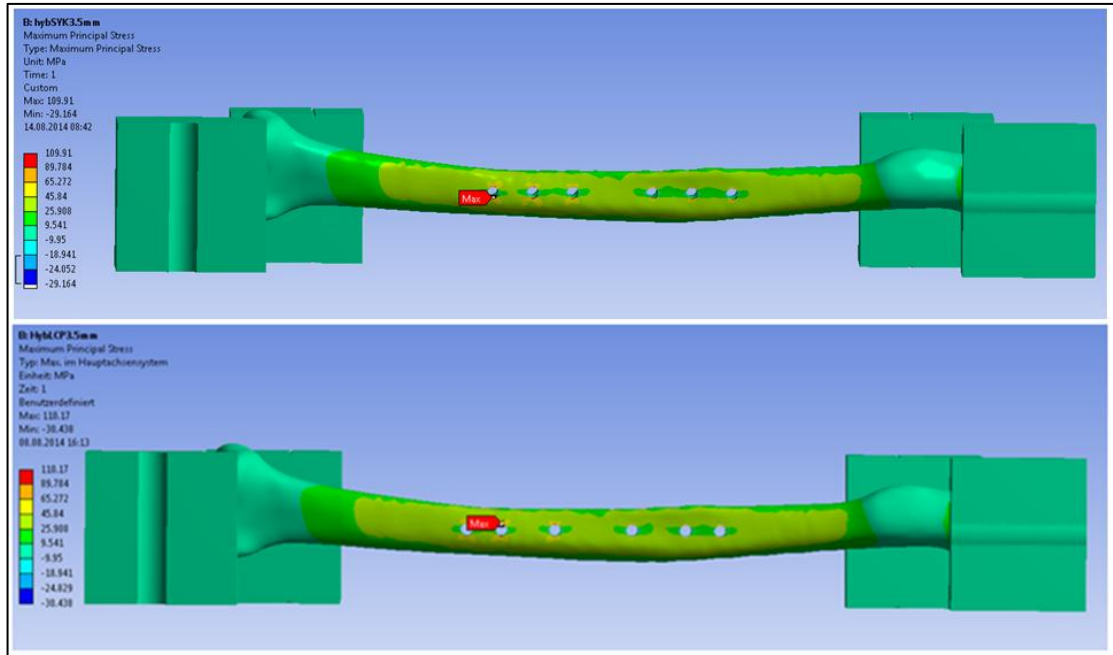


Figure 119: Different maximum principal stress location in the HybSYK3.5mm (top) and HybLCP3.5mm (bottom) models

This difference in terms of location of the maximum stress (and of the probable failure point) is caused by the different position of the screws due to the different design of the plate. As can be seen in the following image, in fact, in the hybrid configuration the Stryker Variax 7 hole plate and the DePuy Synthes LCP 7 hole plate present a different distance between each hole and the center of the plate which corresponds, as described in the design section (Chapter 2.2.1), to the center of the bone. The different distances implicate that screws are placed in zones characterized by diverse cross section since the radius and bone marrow canal have an irregular shape. For these two groups the zones characterized by maximum stress (first distal hole for HybSYK3.5mm and second distal hole for HybLCP3.5mm) are the areas where the smaller cross section was measured (Table 32).

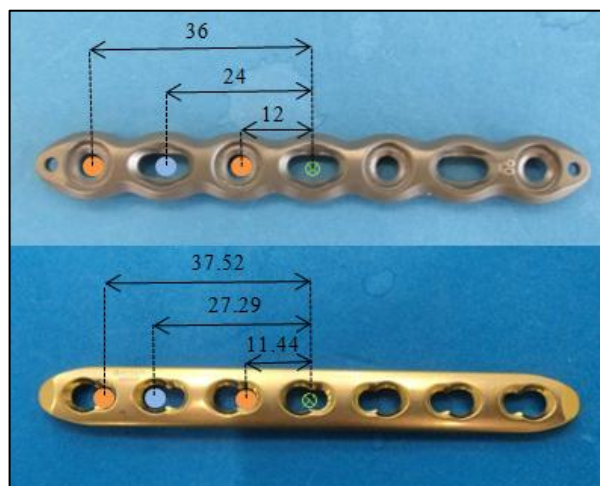


Figure 120: Distance between the center and the holes in the hybrid configurations.

Top: Hybrid Stryker; Bottom: Hybrid LCP

● : locking screws; ● : cortex/bone screws; ⊗ : plate center

| Group | Hole # | Cross Section [mm ²] |
|--------------|--------------|----------------------------------|
| HybSyk3.5 mm | 1 - distal | 108.93 |
| | 2 | 110.46 |
| | 3 | 112.98 |
| | 4 | 120.27 |
| | 5 | 122.23 |
| | 6 – proximal | 120.13 |
| HybLCP3.5 mm | 1 – distal | 110.12 |
| | 2 | 109.23 |
| | 3 | 113.10 |
| | 4 | 119.02 |
| | 5 | 123.55 |
| | 6 - proximal | 118.65 |

*Table 32: Cross section measurement for the groups HybSyk3.5 mm and HybLCP3.5 mm.
The minimum cross section for each group is highlighted*

The analysis just described showed that there might be a higher risk of re-fracture when choosing to implant a screw in one location instead than in another one since the bone is characterized by a not regular shape.

A further analysis of results showed that the distal portion of the radius is the most critical area in terms of risk of re-fracture when screws are removed after plate fixation. This aspect can be evidenced for each screw pattern and screw dimension and as example the following case (HybSYK3.5mm) is presented.

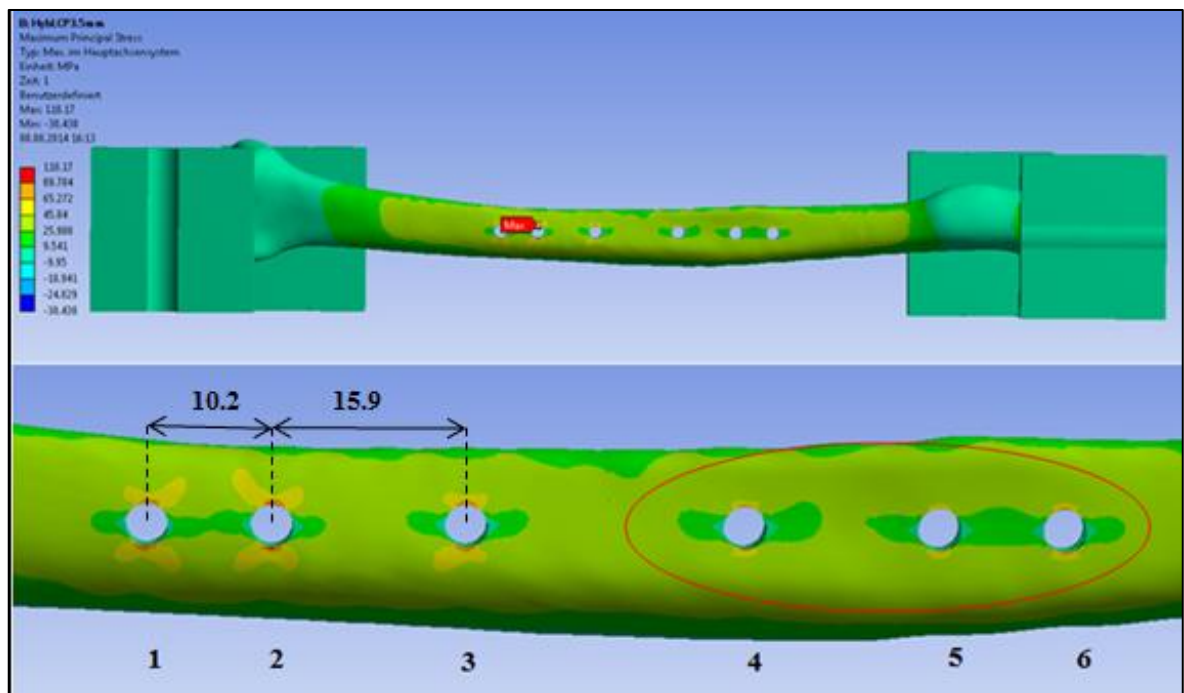


Figure 121: Maximum principal stress for HybLCP3.5mm

Analyzing Figure 121 it can be noticed that the three proximal holes (right holes) present lower principal stresses compared to the three most distal holes (left holes) since the area characterized by yellow and orange color is significantly smaller. Since this happens for all the analyzed groups it can be surely stated that the distal portion of the radius shaft is the most critical in reference to failure, at least when bending is applied. The situation appears to be very different in comparison to the sample with no holes where the greater stress was noticed on the most proximal portion of the bone.

Another aspect which was noticed comparing the above presented stress results (HybLCP3.5mm) with the ones obtained with other screw patterns is the reduction of stress that sometimes appears between holes (more evidently in the proximal side of the shaft). In the above presented image this behavior can be seen in the space between holes 1-2 and between holes 5-6 where the stress is characterized by a dark green (lower stress than between holes 2-3 and 4-5). A confirmation of such finding is presented for the model HybSYK3.5mm in Figure 122 and for the model StdLCP3.5mm in Figure 123. The arrows indicate the mentioned zones of stress reduction. In the distal region this effect was noticed when the distance between holes was approximately smaller than 12 mm, in case of 3.5 mm holes.

Even if the zone of maximum stress (area of most probable failure) does not appear influenced by this effect it is always better to have wider areas characterized by lower stresses.

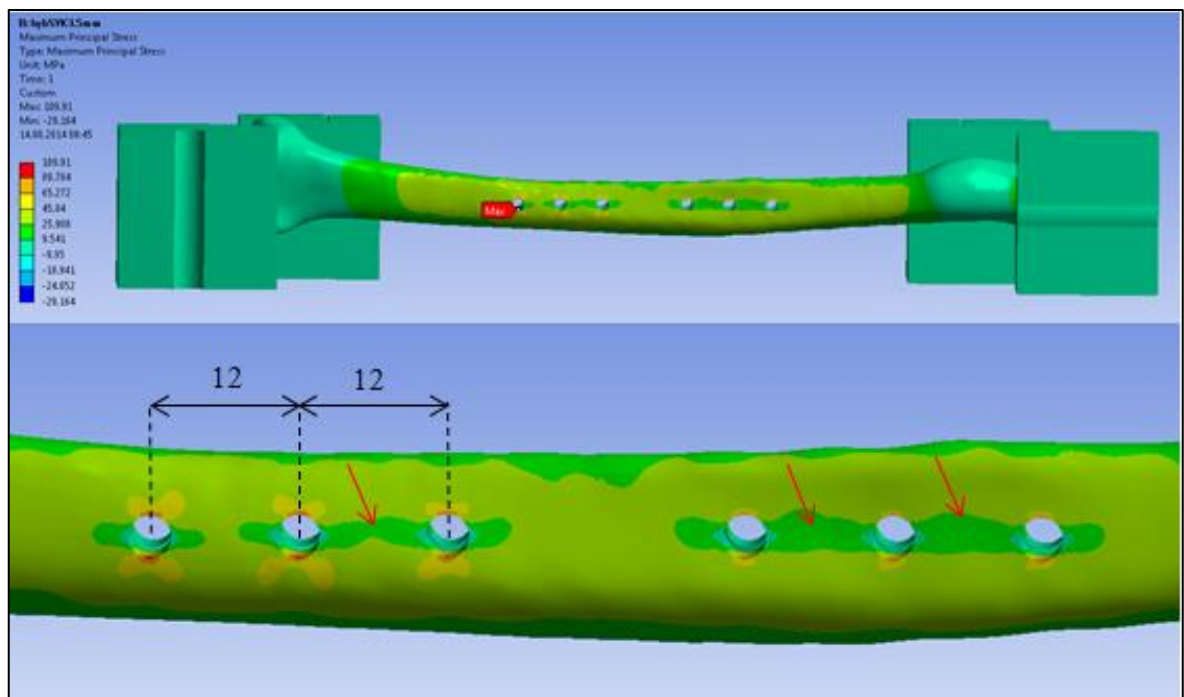


Figure 122: Stress distribution for the HybSYK3.5mm model. Indicated by arrows are the zones of stress reduction in the space between holes

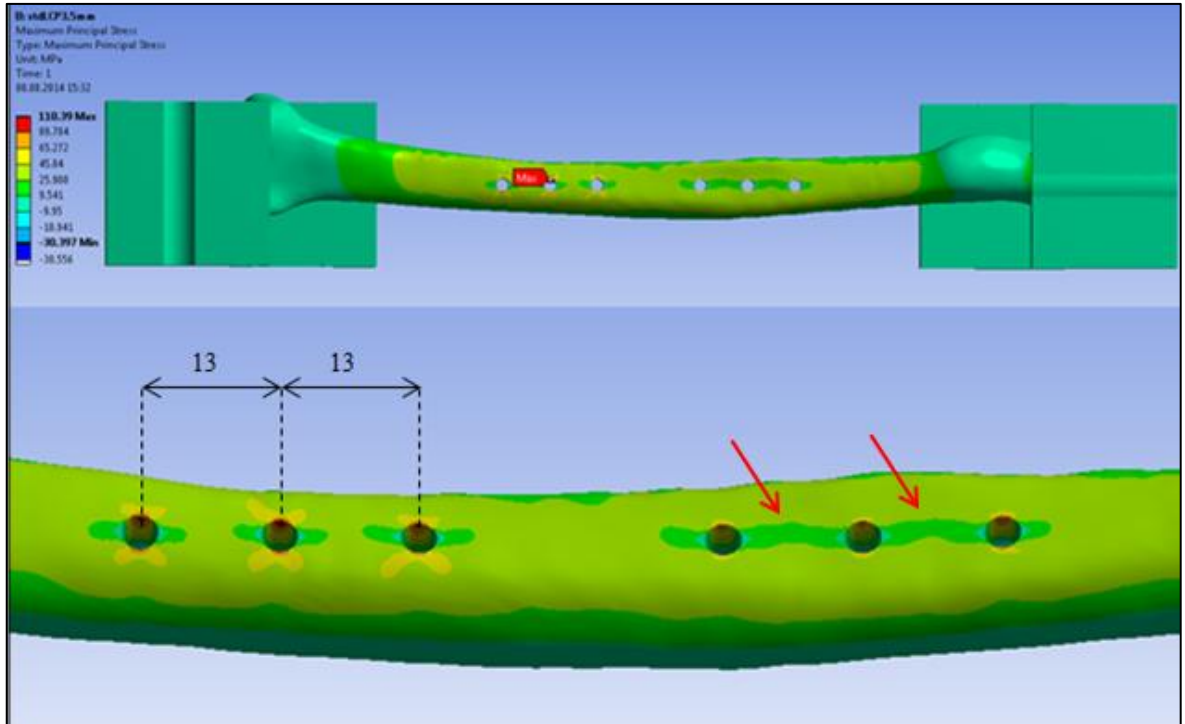


Figure 123: Stress distribution for the StdLCP3.5mm model.

For 2.7 mm screws the distance probably needs to be even smaller in order to obtain the described stress reduction behavior since, as evident in Figure 124, the dark green region is scarcely present between holes, also in correspondence of the proximal region which in the other cases shows a much more evident reduced principal stress.

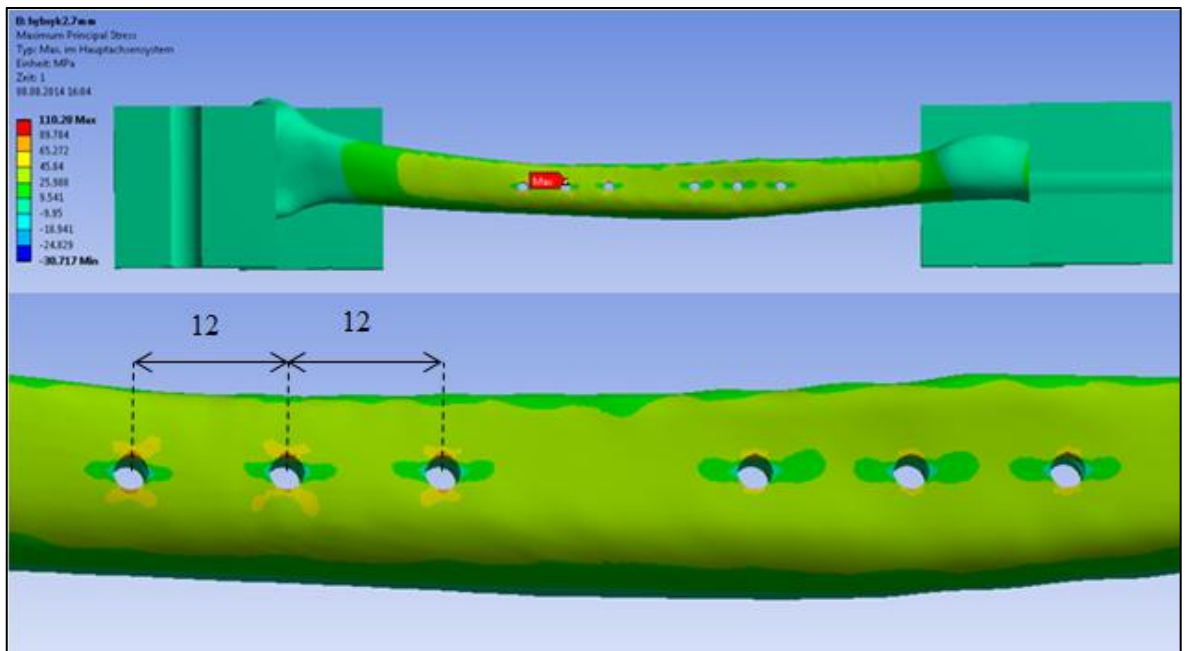


Figure 124: Stress distribution for the HybSYK2.7mm model.

Results presented in Figure 110 also evidence that the samples with multiple holes show a lower stiffness compared to the intact bone. This is also an expected finding since the presence of multiple holes tends to weaken the structure which will then show an increased deformation capability in correspondence of the application of the same forces. To be evidenced is the fact that the stiffness of the samples with smaller holes (2.7 mm in this case) is higher than the one with larger holes (3.5 mm and 4.5 mm).

Regarding the major goal of this investigation the following considerations were made. The models which presented 3.5 mm screws appear all the same in terms of safety since α assumes in each case the value of 0.129. The different position of the holes, therefore, does not influence the strength of the structure.

The model with 2.7 mm multiple holes represents the best situation in terms of risk of re-fracture when bending is applied (higher energy to failure and higher safety coefficient) while the model which presents multiple 4.5 mm holes is the weakest and therefore the energy to failure and α assume lower values. This last statement confirms literature data since a lower energy to failure, compared to the groups with smaller holes, was calculated (higher failure risk).

Differences in regards to the risk of re-fracture are present but they are not significantly evident ($\alpha_{\text{HybSYK2.7mm}} = 0.142 > \alpha_{\text{Multiple3.5mm}} = 0.129 > \alpha_{\text{HybSYK4.5mm}} = 0.119$).

All the analyzed results with single or multiple holes were obtained through a finite element analysis performed assigning to the cortical bone material linear, isotropic and brittle properties.

In reality the situation is more complex since the cortical bone exhibits viscoelastic properties (the material is sensitive to strain rate and to the duration of the applied loads), anisotropic behavior (mechanical properties vary in regards to the direction of evaluation) and ductile or brittle failure mode in dependence to the strain rate applied. [90] The reasons why the cortical bone was modeled in a simpler way were presented in Chapter 3.

The outcome of the computational simulations was not expected to be numerically exactly the same as what would happen in reality but it was believed it would highlight correctly the geometrical influence of different holes and hole patters in the risk of re-fracture of the radius after hardware removal, which is exactly the aim of this work.

The loading applied to the bone, in both the experimental and computational tests, was a pure bending in the shaft region. This situation causes one side of the bone to be in tension and one side to be in compression. The applied loading pattern is an approximation of what happens in reality and it was chosen since it represented a worst case and allowed to manage an easy performance of the experimental and computational tests. Physiologically, the action of the muscles also generates some compression (in a stepwise trend as shown in Figure 51) which permits the release of a part of tension on the volar surface and the addition of some compression on the opposite side. This pattern would probably lead to higher energy to failure (safer situation) during loading since the most critical stress (tension driven) is lowered. This is one of the reasons why the performed tests can be considered as worst case. The other reasons were already described in the test definition presented in Chapter 2.1.2.

4.2 Conclusions

The work performed had the aim of evaluating the influence of the screw removal in the re-fracture risk of the radius bone.

In particular a computational analysis was performed on samples with one single hole of different diameters in order to verify the dimension influence on the static resistance of the bone structure. The major finding was that the energy to failure decreased significantly in presence of any hole (-80%) compared to the situation when no hole was present on the bone model.

The slightly safer situation in terms of re-fracture risk, when a 4-point bending tests is performed, was given by the presence of the 2.7 mm hole. However, the energy to failure, force to failure and safety coefficient did not highlight extremely important differences when 2.7 mm, 3.5 mm and 4.5 mm single holes were present.

The comparison in terms of safety factor for the samples with a single hole is presented in the following image.

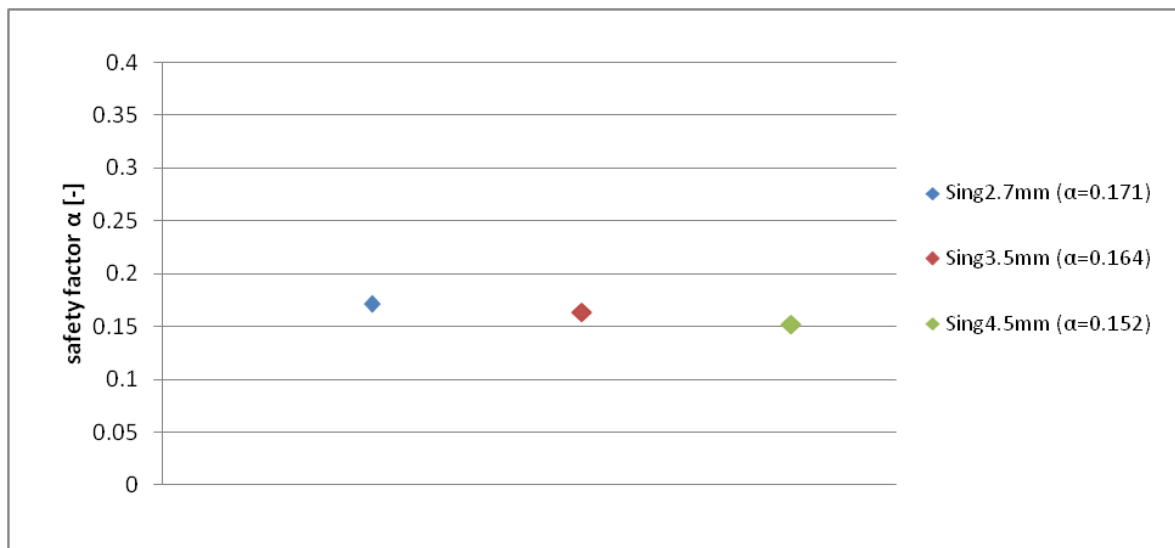


Figure 125: Comparison between the safety factor α for the samples with one single hole. (Min possible $\alpha = 0$; Max possible $\alpha = 1$)

The evaluations involving radius models with multiple holes were done, instead, for analyzing the behavior of the structure in presence of different hole patterns during a bending loading in order to have an idea of what could happen in a real situation involving a patient subject to the removal of plate and screws from the forearm. This evaluation was made through an experimental test and a computational test. It must be highlighted that experimental test and computational test performed on the radius with multiple holes are not completely comparable since, as presented in the previous chapters, the test setup, loading conditions, etc presented some diversities. Differences can be seen for example in the failure location of the computational and of the experimental samples with multiple holes (distal and proximal area of the shaft respectively) and also in the results of the calculation of the safety factor α which does not appear exactly the same for the experimental and the computational tests (Figure 126).

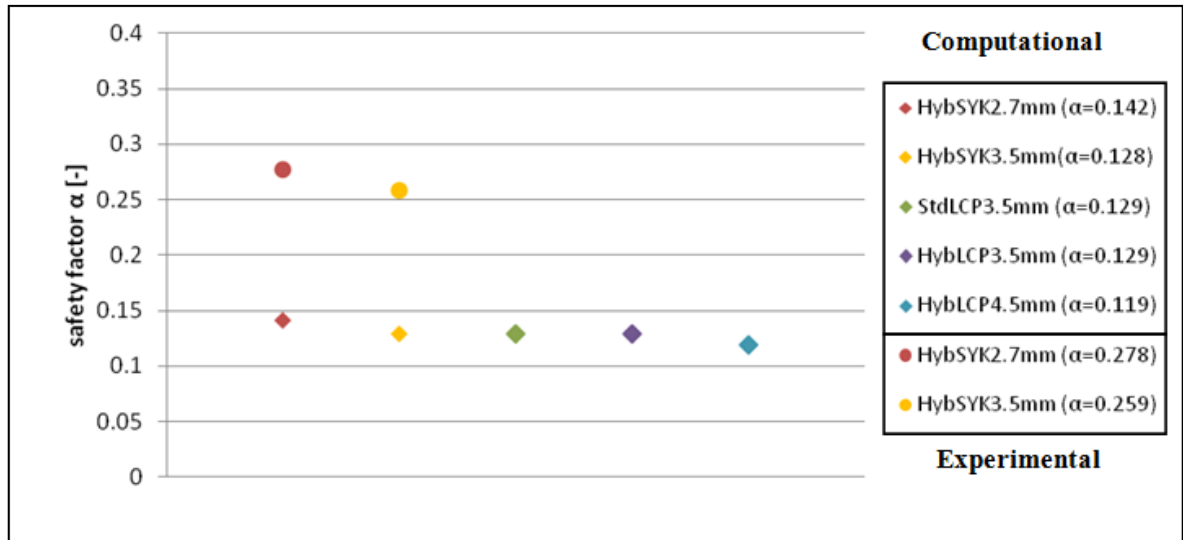


Figure 126: Comparison between the safety factor α for the samples with multiple holes obtained from the computational and experimental tests (Min possible $\alpha = 0$; Max possible $\alpha = 1$)

However, the results of both tests showed that the slightly safer situation was the one which presented 2.7 mm screws since the calculated energy to failure and safety factor were the highest. The relationship between groups HybSYK2.7mm and HybSYK3.5mm appears similar in both experimental and computational analysis. In fact the difference between the two safety factors is 7% and 10% respectively for the experimental and computational tests.

The differences in terms of all the analyzed parameters, and therefore in terms of safety factor, are probably due to the different approaches used for the experimental and computational analysis since it has not been possible for multiple reasons (time, expenses, etc) to uniform the tests.

The main aspects of diversity regarded:

- **Material:** the computational test was performed assigning to the model a single material (cortical bone) while the experimental samples are made of two materials (epoxy and PU foam). The mechanical properties of the different materials are different and, therefore, the behavior of the samples during mechanical testing was different.
- **Shape:** the computational samples were characterized by an anatomical shape also in regards to the bone marrow canal which showed an increasing dimension towards the epiphysis of the bone (Figure 112). The experimental samples had, instead, a constant 5 mm bone marrow canal throughout the radius length.
- **Hole orientation:** the computational samples (and samples designed for test 1) presented an alignment of the axis of the holes with the direction of application of the force since, as described in Chapter 2, it was considered a worst case loading. The experimentally tested samples did not show this alignment since the plate was positioned less precisely and the volar surface of the bone was not exactly perpendicular to the force when the sample was mounted on the 4-point bending jig.
- **Bone positioning:** the computational model (and samples designed for test 1) allowed an extremely reproducible placement of the sample (see Figure 67) while the experimental test had more chances of inserting imprecisions while positioning the bone on the 4-point bending jig since no coupling was present.

Despite these differences both experimental and the computational tests showed an important reduction of the energy to failure (70% - 80%) and of the force to failure (40% – 60%) when holes were present on the radius bone shaft subject to a 4-point bending test. It must be kept in mind that the test performed, as stated previously, did not represent exactly a physiological situation but an extreme loading case.

This finding is important since it proves that during the period after plate removal the bone is actually heavily weakened and it should be paid attention in performing stressful activities for the forearm since its capability of adsorbing forces and displacements is limited. This is valid for every plate and every type of screw implanted and consequently removed, even for the 2.7 mm screws which represent the safer situation.

4.3 Future developments

The future developments of the presented work could touch different points for both experimental and computational tests in order to obtain more precise and realistic results.

Regarding the *experimental test* the future developments would be directed in order to more precisely manage to perform the implant of plate and screws and the 4-point bending test. This would require for example the design and construction of specific couplings which would guarantee the correct alignment and orientation of the sample in every phase. An initial design (see Figure 127 and Figure 128) was started but could not be brought to the production phase because of time issues.

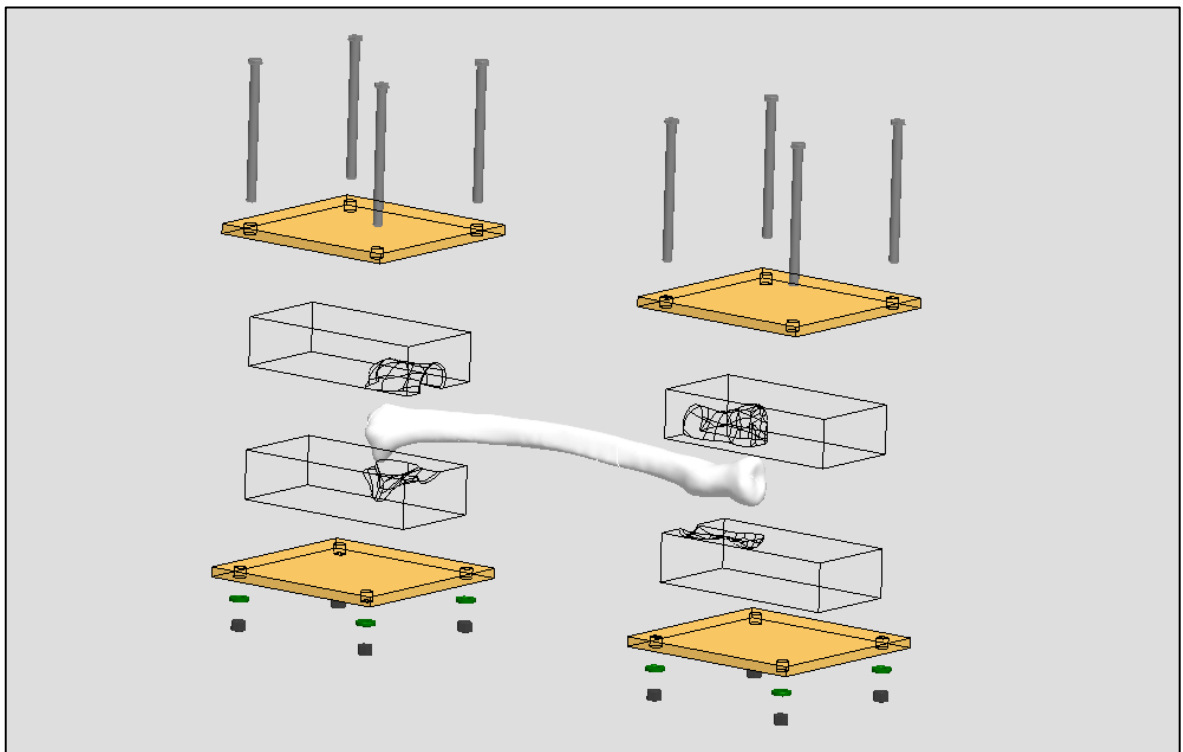


Figure 127: Exploded view of the possible future couplings for a more precise preparation and testing of the Sawbones® bone models



Figure 128: Testing mode of the possible future setup

As a continuation of the experimental work performed it would also make sense to test the configurations which were not managed to be tested. This would allow a complete comparison of the computational – experimental results which could confirm that the relationship between different screw patterns is the one noticed and described in Figure 126. It would also eventually allow confirming that the gap between experimental and computational results is only due to the differences in test samples, test setup, test performance, etc.

With regards to the *computational analysis* the greatest improvements could be made in order to achieve a much more realistic model to simulate.

This improvement would involve for example the material definition. In fact, as explained in Chapter 3, the cortical bone was assumed for simplicity as an ideal linear, isotropic and brittle material. An interesting continuation of the work would therefore be the definition of more realistic properties which could more precisely simulate the actual behavior of the bone. This would inevitably lead to a higher number of iterations performed by the software and therefore to a greater computational time.

The material refinement should also be accompanied by a more physiological definition of the loading pattern on the bone. This task would require the analysis of a great number of movements and actions performed with the forearm until a worst case could be defined. The resulting loading would not comprehend only bending but compression, torsion and shear would also probably be present as well. This improvement looks eventually to be more feasible from a computational perspective rather than from an experimental point of view for the reason that building a setup which can apply all the mentioned loads can be very complicated.

The effort to go towards a more realistic condition would also require the consideration of the holes left by the screws not only as simple cylinders. The actual shape of the screws could be easily cut out from the bone model using CAD software and the eventual influence of the shape of the thread in generating high stresses could be verified.

A further aspect that could be evaluated through the use of computational tools is the eventual existence of a screw configuration that allows minimizing the risk of re-fracture of the radius in the period successive to the reduction of a shaft fracture. The reduction of the stress distribution in areas of the bone discussed in Chapter 4.1.2 would need the performance of further studies and simulation in order to understand in detail the parameters that effectively drive this phenomenon which in literature is called “shadow effect”.

The “shadow effect” usually refers to the voluntary insertion of notches/holes/grooves in a body in order to lower the stress concentration that appears on the tested samples. Therefore problems of stress concentration can be solved by removing material instead of adding material.

In the specific case of the radius bone with holes the limitation of stress concentration could maybe be performed by avoiding sudden changes of cross section (the use of gradual increasing screws is an example) or by placing the holes at a calculated distance [80] This last described mode of reducing σ was already noticed in the computational test (and discussed in 4.1.2) where different distance between holes produced different stress levels in the region between them.

Attachment 1

Bended Beams [80]

Considering a polar coordinate system $\rho - \theta$ with origin in the center of curvature C the following dimensions can be defined (see Figure 129).

- z : distance of the generic fiber from the neutral axis;
- z_g : distance of the barycenter from the neutral axis;
- ρ : radius of curvature of the generic fiber;
- ρ_n : radius of curvature of the fiber in correspondence of the neutral axis;
- ρ_g : radius of curvature of the fiber in correspondence of the baricentral axis;
- θ : angular position of the generic section

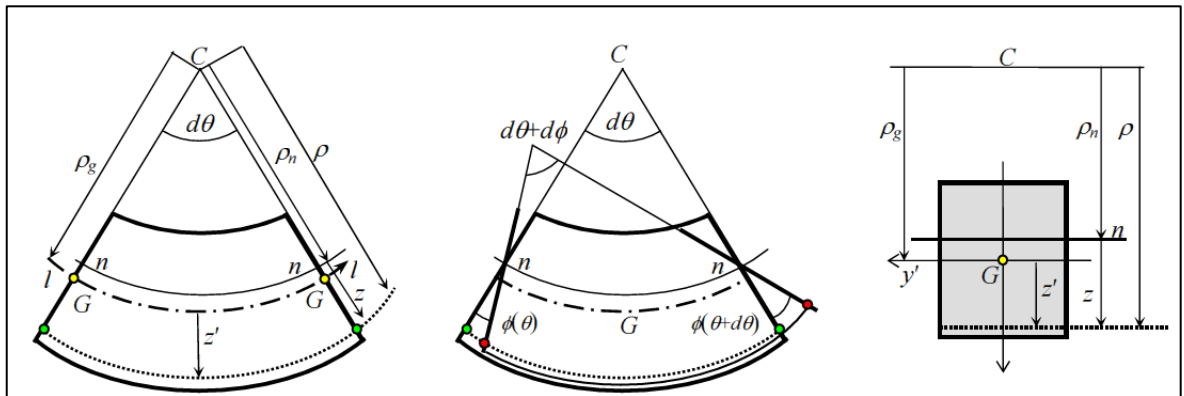


Figure 129: Curved Beams. Left: reference system; Center: cross sections rotations and lengthening of the generic fiber; Right: cross section [80]

The relationship between the coordinates relative to the center of rotation and to the neutral axis is the following:

$$z = \rho - \rho_n \quad (1)$$

Considering M the bending moment applied to the beam, the normal stress to the cross section has a null resultant (2 left) and a bending moment equal to the following relationship (2 right):

$$N = \int_A \sigma \, dA = 0 \quad M = \int_A z \sigma \, dA \quad (2)$$

Considering a fiber positioned between two sections at an angular distance of $d\theta$, distant ρ from the center of curvature and z from the neutral axis, whose initial length is $l = \rho \cdot d\theta$. After the deformation the cross sections of the beam rotate of $\phi(\theta)$ around the neutral axis in correspondence of which the fiber maintains its original length.

The relative rotation of the the sections is $d\varphi = (\theta+d\theta) - \varphi(\theta)$ and the consequent lengthening of the fiber distant z from the neutral axis results $dl = z * d\varphi$.

The deformation of the fiber is therefore given by the following equation:

$$\varepsilon = \frac{dl}{d} = \frac{d\varphi * z}{d\theta * \rho} = \frac{d\varphi}{d\theta} \frac{z}{\rho_n + z} \quad (3)$$

From relations (2 - right) and (3) it is possible to derive:

$$\sigma = E \varepsilon = E \frac{d\varphi * z}{\theta * \rho} \quad (4)$$

Equation (4) gives a relation between the stress in one point, the distance z from the neutral axis, the curvature ρ and the function $d\varphi / d\theta$.

In presence of a curved beam the neutral axis is not barycentric also when a simple flexion is applied. In fact, from (2 - left) and (4) the following relation is obtained.

$$N = E \frac{d\varphi}{d\theta} \int_A \frac{z}{\rho} dA = 0 \quad (5)$$

Equation (5) is verified for:

$$\int_A \frac{z}{\rho} dA = 0 \quad (6)$$

The position of the neutral axis can be extracted from (6):

$$\int_A \frac{z}{\rho} dA = \int_A \frac{\rho - \rho_n}{\rho} dA = -\rho_n \int_A \frac{1}{\rho} dA - \int_A dA = 0 \quad (7)$$

And it can be obtained solving the following integral:

$$\rho_n = \frac{A}{\int_A \frac{1}{\rho} dA} \quad (8)$$

Solving equation (8) is also possible to demonstrate that the neutral axis is always shifted towards the center of rotation of the bended beam.

The definition of the stress trend on the cross section can be made using equations (2 - right) and (4):

$$M = \int_A z \sigma dA = E \frac{d\varphi}{d\theta} \int_A \frac{z^2}{\rho} dA \quad (9)$$

Remembering (1), the argument of the integral can be written as:

$$\frac{z^2}{\rho} = \frac{z(\rho - \rho_n)}{\rho} = z - \frac{\rho_n z}{\rho} \quad (10)$$

Inserting (10) in (9):

$$M = E \frac{d\varphi}{d\theta} \left(\int_A z \, dA - \rho_n \int_A \frac{z}{\rho} \, dA \right) \quad (11)$$

The first integral gives:

$$\int_A z \, dA = A z_g \quad (12)$$

The second integral is zero (see equation (5)).

Equation (11) becomes:

$$M = E \frac{d\varphi}{d\theta} A z_g \quad (13)$$

This can be re-written as:

$$E \frac{d\varphi}{d\theta} = \frac{M_y}{A z_g} \quad (14)$$

Substituting (14) in equation (4):

$$\sigma = \frac{M z}{A z_g \rho} = \frac{M}{A z_g} \frac{z_i}{\rho_n + z} \quad (15)$$

The stress trend is hyperbolic. The superior and inferior edges are subject to the stresses:

$$\sigma = \frac{M z_s}{A z_g \rho_s} \quad \sigma = \frac{M z_i}{A z_g \rho_i} \quad (16)$$

The stress on the superior or inferior surface is a tension or compression stress in dependence to the moment applied but the maximum stress is always located on the edge nearest to the center of curvature.

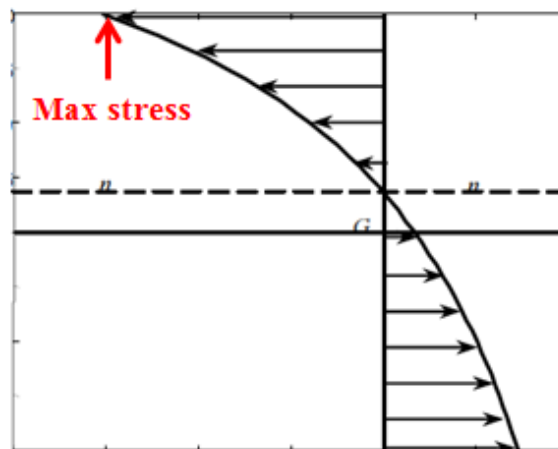



Figure 130: Stress trend on the cross section of the bended beam [80]

Attachment 2

PA GF material data sheet



Lasersintern (SLS)

Materialien

| Eigenschaften / Eigenschappen / Properties | PA | PA GF | Rigid GF | DuraForm Flex inf. | Einheit / Eenheid / Unit |
|--|------|-------|----------|--------------------|-----------------------------|
| Bruchdehnung / Rek bij breuk / Elongation at Break | 18 | 9 | 4 | 151 | % |
| Biege E-Modul / Buig E-Modulus / Flexural modulus | 1500 | 2900 | 2450 | 7,8 | MPa |
| Zugfestigkeit / Treksterkte / Tensile strength | 48 | 51 | 45 | 2,3 | MPa |
| Zugmodul / Trek E-modulus / Tensile modulus | 1650 | 3200 | 3400 | 9,2 | MPa |
| Dichte (gesintert) / Hardheid (laser-gesinterd) / Hardness (lasersintered) | 0,93 | 1,22 | 1,45 | 0,44 | g/cm ³ |
| Schmelztemperatur / Smelttemperatuur / Melting temperature | 176 | 176 | 180 | 192 | °C |
| Kerbschlagzähigkeit / Kerfslagsterkte / Izod impact | 4,4 | 4,2 | - | - | KJ/m ² |

Die realen Werte können je nach Aufbaurichtung und Charge des Pulvers von den angegebenen Werten abweichen.
De exacte waardes kunnen afhankelijk van de opbouwrichting en de Charge van het poeder afwijken.
The actual values are depending on building direction and powder charge

Deutschland
CNC Speedform AG • Dammstraße 54-56 • 33824 Werther • Tel.: 05203/9748-0 • Fax: 05203/9748-20 • Mail: sales@cnc-ag.de

Niederlande
CNC Speedform AG • P.O. Box 72 • 7580 AB Losser • Tel.: +31 (0)53 - 53618 - 19 • Fax: +31 (0)53 - 53618 - 20 • Mail: sales-nl@cnc-ag.de
www.cnc-ag.de

Attachment 3

The results of the experimental test 1 on the PA GF samples are presented below.

The samples which reached failure are listed in black. The max force reached is the force to failure of the samples and the max displacement reached represents the displacement to failure.

The samples which did not reach failure are listed in grey. The values of force to failure, displacement to failure and energy to failure were not possible to evaluate since the limit of displacement of the rollers was reached and the measurement had to be stopped.

| Tested Group | Sample# | Failure mode | Stiffness [N/mm] | Max reached force [N] | Max reached displacement [mm] | Energy to failure [Nmm] |
|--------------|---------------|------------------|------------------|-----------------------|-------------------------------|-------------------------|
| No Holes | 1 | Brittle breakage | 112.59 | 1648.99 | 14.24 | 11813.12 |
| | 2 | No-failure | 82.61 | 890.93 | 14.05 | - |
| | 3 | No-failure | 105.43 | 1273.42 | 13.58 | - |
| | 4 | No-failure | 74.15 | 1047.53 | 13.63 | - |
| | 5 | No-failure | 104.07 | 1210.73 | 13.36 | - |
| | 6 | Brittle breakage | 135.63 | 1072.22 | 8.50 | 5071.37 |
| | Median | | 104.07 | 1648.99 | 14.24 | 8442.25 |
| SingLCP3.5mm | 1 | Brittle breakage | 153.23 | 997.69 | 6.76 | 3529.96 |
| | 2 | No-failure | 73.63 | 1082.33 | 13.84 | - |
| | 3 | No-failure | 113.07 | 1222.65 | 13.91 | - |
| | 4 | Brittle breakage | 88.58 | 940.68 | 10.58 | 5187.37 |
| | 5 | Brittle breakage | 128.77 | 873.9 | 7.37 | 3589.74 |
| | 6 | Brittle breakage | 117.59 | 1022.38 | 10.17 | 5579.45 |
| | Median | | 115.33 | 969.19 | 8.77 | 5383.41 |
| SingSYK3.5mm | 1 | Brittle breakage | 85.33 | 936.93 | n/a | 5143.75 |
| | 2 | Brittle breakage | 149.22 | 982.25 | 6.90 | 3613.28 |
| | 3 | Brittle breakage | 132.99 | 861.38 | 8.80 | 4334.17 |
| | 4 | Brittle breakage | 108.41 | 975.4 | 10.18 | 5330.04 |
| | 5 | Brittle breakage | 134.14 | 898.74 | 8.67 | 4544.94 |
| | 6 | Brittle breakage | 143.9 | 895.28 | 7.25 | 3610.17 |
| | Median | | 133.57 | 917.84 | 8.67 | 4439.55 |
| SingLCP4.5mm | 1 | No-failure | 72.39 | 1095.23 | 13.97 | - |
| | 2 | No-failure | 78.21 | 1061.58 | 13.38 | - |
| | 3 | Brittle breakage | 84.83 | 1108.56 | 12.38 | 6265.10 |
| | 4 | No-failure | 87.51 | 1110.08 | 13.81 | - |
| | 5 | No-failure | 97.33 | 1158.75 | 13.81 | - |
| | 6 | No-failure | 70.32 | 1231.05 | 13.88 | - |
| | Median | | 81.52 | 1108.56 | 12.38 | 6265.10 |
| SingSYK2.7mm | 1 | Brittle breakage | 149.73 | 1203.51 | 8.70 | 5476.31 |
| | 2 | No-failure | 73.325 | 1017.37 | 13.93 | - |
| | 3 | No-failure | 77.22 | 987.10 | 14.24 | - |
| | 4 | No-failure | 98.07 | 1184.82 | 13.56 | - |

| | | | | | | |
|-------------|---------------|------------------|---------------|----------------|--------------|----------------|
| | 5 | Brittle breakage | 83.63 | 814.29 | 10.46 | 4487.93 |
| | 6 | No-failure | 110.92 | 922.45 | 14.08 | - |
| | Median | | 90.85 | 1008.9 | 9.58 | 4982.12 |
| HybSYK3.5mm | 1 | No-failure | 76.74 | 991.27 | 12.85 | - |
| | 2 | No-failure | 95.91 | 1021.69 | 14.22 | - |
| | 3 | Brittle breakage | 83.62 | 1173.58 | 12.67 | 6870.76 |
| | 4 | No-failure | 73.60 | 868.44 | 13.50 | - |
| | 5 | No-failure | 54.79 | 995.72 | 13.17 | - |
| | 6 | Brittle breakage | 119.33 | 1036.66 | 10.10 | 5695.00 |
| | Median | | 80.18 | 1008.71 | 11.39 | 6282.88 |
| HybLCP3.5mm | 1 | No-failure | 60.81 | 1116.63 | 13.99 | - |
| | 2 | No-failure | 71.88 | 1324.55 | 13.61 | - |
| | 3 | No-failure | 57.48 | 1074.86 | 13.63 | - |
| | 4 | No-failure | 69.37 | 990.41 | 13.74 | - |
| | 5 | No-failure | 67.77 | 982.81 | 13.24 | - |
| | 6 | Brittle breakage | 65.054 | 1116.14 | 13.53 | 6373.21 |
| | Median | | 65.064 | 1116.14 | 13.53 | 6373.21 |
| StdLCP3.5mm | 1 | Brittle breakage | 103.53 | 984.78 | 10.89 | 5868.39 |
| | 2 | No-failure | 97.85 | 1461.41 | 13.68 | - |
| | 3 | Brittle breakage | 98.60 | 940.34 | 10.01 | 4646.34 |
| | 4 | Brittle breakage | 95.57 | 989.29 | 11.26 | 5940.18 |
| | 5 | Brittle breakage | 94.63 | 1095.27 | 11.77 | 6652.33 |
| | 6 | Brittle breakage | 90.58 | 989.02 | 11.25 | 5526.31 |
| | Median | | 95.57 | 989.02 | 11.25 | 5868.39 |
| HybSYK2.7mm | 1 | Brittle breakage | 86.46 | 1023.63 | 11.83 | 6302.28 |
| | 2 | No-failure | 91.41 | 1185.13 | 13.94 | - |
| | 3 | No-failure | 68.90 | 1063.90 | 13.58 | - |
| | 4 | No-failure | 91.84 | 1177.04 | 13.67 | - |
| | 5 | No-failure | 68.24 | 977.98 | 13.29 | - |
| | 6 | Brittle breakage | 127.37 | 1047.16 | 8.94 | 4874.80 |
| | | | 88.94 | 1035.40 | 10.39 | 5588.54 |

Table 33: Complete results of the experimental tests on PA GF samples

Attachment 4

Validation model noHoles:

| displacement [mm] | experimental force [N] | computational force [N] | percentage difference |
|-------------------|------------------------|-------------------------|-----------------------|
| 0 | 0 | 0 | 0 |
| 0.8119 | 172.073 | 160.347 | -6.814549639 |
| 1.6238 | 355.22 | 320.7 | -9.717921288 |
| 2.4357 | 531.65 | 481.05 | -9.517539735 |
| 3.2476 | 708.22 | 641.4 | -9.434921352 |
| 4.0595 | 879.88 | 801.76 | -8.87848343 |
| 4.8714 | 1037.97 | 962.11 | -7.308496392 |
| 5.6833 | 1228.67 | 1122.48 | -8.642678669 |
| 6.4952 | 1410.37 | 1282.84 | -9.042308047 |
| 7.3071 | 1545.64 | 1443.2 | -6.627675267 |
| 8.119 | 1704.63 | 1603.58 | -5.927972639 |

Table 34: Validation results for the sample noHoles

Validation model SingSYK2.7mm:

| displacement [mm] | experimental force [N] | computational force [N] | percentage difference |
|-------------------|------------------------|-------------------------|-----------------------|
| 0 | 0 | 0 | 0 |
| 0.626 | 112.7 | 122.476 | 8.674356699 |
| 1.252 | 248.805 | 244.96 | -1.54538695 |
| 1.878 | 379.04 | 367.43 | -3.063001266 |
| 2.504 | 510.39 | 489.91 | -4.012617802 |
| 3.13 | 641.23 | 612.4 | -4.49604666 |
| 3.756 | 761.56 | 734.88 | -3.503335259 |
| 4.382 | 918.72 | 857.37 | -6.67776907 |
| 5.008 | 1032.44 | 979.86 | -5.092789896 |
| 5.634 | 1131.45 | 1102.35 | -2.571920986 |
| 6.26 | 1242.91 | 1224.84 | -1.453846216 |

Table 35: Validation results for the sample SingSYK2.7mm

Attachment 5

Detailed results of the statistical analysis

Case Processing Summary

| Group | Cases | | | | | | |
|-------------------------|-------------|---------|---------|---------|-------|---------|--------|
| | Valid | | Missing | | Total | | |
| | N | Percent | N | Percent | N | Percent | |
| Max Force [N] | NoHoles | 6 | 100.0% | 0 | 0.0% | 6 | 100.0% |
| | HybSYK2.7mm | 6 | 100.0% | 0 | 0.0% | 6 | 100.0% |
| | HybSYK3.5MM | 6 | 100.0% | 0 | 0.0% | 6 | 100.0% |
| Max Displacement [mm] | NoHoles | 6 | 100.0% | 0 | 0.0% | 6 | 100.0% |
| | HybSYK2.7mm | 6 | 100.0% | 0 | 0.0% | 6 | 100.0% |
| | HybSYK3.5MM | 6 | 100.0% | 0 | 0.0% | 6 | 100.0% |
| Stiffness [N/mm] | NoHoles | 6 | 100.0% | 0 | 0.0% | 6 | 100.0% |
| | HybSYK2.7mm | 6 | 100.0% | 0 | 0.0% | 6 | 100.0% |
| | HybSYK3.5MM | 6 | 100.0% | 0 | 0.0% | 6 | 100.0% |
| Energy-to-failure [Nmm] | NoHoles | 6 | 100.0% | 0 | 0.0% | 6 | 100.0% |
| | HybSYK2.7mm | 6 | 100.0% | 0 | 0.0% | 6 | 100.0% |
| | HybSYK3.5MM | 6 | 100.0% | 0 | 0.0% | 6 | 100.0% |

Table 36: Statistics case processing summary

Descriptives

| Group | Statistic | Std. Error | |
|----------------------------------|----------------------------------|-------------|-----------|
| Max Force [N] | Mean | 3975.0317 | 68.52494 |
| | 95% Confidence Interval for Mean | Lower Bound | 3798.8827 |
| | | Upper Bound | 4151.1806 |
| | 5% Trimmed Mean | 3970.2674 | |
| | Median | 3981.0250 | |
| | Variance | 28174.003 | |
| | Std. Deviation | 167.85113 | |
| | Minimum | 3789.85 | |
| | Maximum | 4245.97 | |
| | Range | 456.12 | |
| | Interquartile Range | 286.71 | |
| | Skewness | .600 | .845 |
| | Kurtosis | .196 | 1.741 |
| | HybSYK2.7mm | Mean | 2275.4100 |
| 95% Confidence Interval for Mean | | Lower Bound | 2131.2142 |
| | | Upper Bound | 2419.6058 |
| 5% Trimmed Mean | | 2268.8289 | |
| Median | | 2250.0150 | |
| Variance | | 18879.635 | |
| Std. Deviation | | 137.40318 | |
| Minimum | | 2138.91 | |
| Maximum | | 2530.37 | |
| Range | | 391.46 | |
| Interquartile Range | | 187.48 | |
| Skewness | | 1.526 | .845 |
| Kurtosis | | 2.884 | 1.741 |
| HybSYK3.5MM | | Mean | 2207.5433 |
| | 95% Confidence Interval for Mean | Lower Bound | 2085.6451 |
| | | Upper Bound | 2329.4416 |
| | 5% Trimmed Mean | 2210.4820 | |
| | Median | 2246.0050 | |
| | Variance | 13492.215 | |
| | Std. Deviation | 116.15599 | |
| | Minimum | 2027.84 | |
| | Maximum | 2334.35 | |
| | Range | 306.51 | |
| | Interquartile Range | 209.98 | |
| | Skewness | -.808 | .845 |
| | Kurtosis | -.694 | 1.741 |

| | | | | | | | | | |
|-----------------------|-------------|----------------------------------|---------------------|----------------------------------|----------------------------------|-------------|----------|----------|--|
| Max Displacement [mm] | NoHoles | Mean | | 5.8800 | .29693 | | | | |
| | | 95% Confidence Interval for Mean | Lower Bound | 5.1167 | | | | | |
| | | | Upper Bound | 6.6433 | | | | | |
| | | 5% Trimmed Mean | | 5.8850 | | | | | |
| | | Median | | 6.0300 | | | | | |
| | | Variance | | .529 | | | | | |
| | | Std. Deviation | | 7.2732 | | | | | |
| | | Minimum | | 4.98 | | | | | |
| | | Maximum | | 6.69 | | | | | |
| | | Range | | 1.71 | | | | | |
| | | Interquartile Range | | 1.47 | | | | | |
| | | Skewness | | -.337 | .845 | | | | |
| | | Kurtosis | | -2.126 | 1.741 | | | | |
| | | HybSYK2.7mm | HybSYK2.7mm | Mean | | 3.1200 | .13510 | | |
| | | | | 95% Confidence Interval for Mean | Lower Bound | 2.7727 | | | |
| | | | | | Upper Bound | 3.4673 | | | |
| | | | | 5% Trimmed Mean | | 3.0983 | | | |
| | | | | Median | | 2.9650 | | | |
| | | | | Variance | | .110 | | | |
| Std. Deviation | | | | 3.3094 | | | | | |
| Minimum | | | | 2.89 | | | | | |
| Maximum | | | | 3.74 | | | | | |
| Range | | | | .85 | | | | | |
| Interquartile Range | | | | .47 | | | | | |
| Skewness | | | | 1.747 | .845 | | | | |
| Kurtosis | | | | 2.745 | 1.741 | | | | |
| HybSYK3.5MM | HybSYK3.5MM | | | Mean | | 3.0167 | .09632 | | |
| | | | | 95% Confidence Interval for Mean | Lower Bound | 2.7691 | | | |
| | | | | | Upper Bound | 3.2643 | | | |
| | | | | 5% Trimmed Mean | | 3.0191 | | | |
| | | | | Median | | 3.0400 | | | |
| | | | | Variance | | .056 | | | |
| | | Std. Deviation | | 2.3594 | | | | | |
| | | Minimum | | 2.70 | | | | | |
| | | Maximum | | 3.29 | | | | | |
| | | Range | | .59 | | | | | |
| | | Interquartile Range | | .47 | | | | | |
| | | Skewness | | -.253 | .845 | | | | |
| | | Kurtosis | | -1.734 | 1.741 | | | | |
| | | Stiffness [N/mm] | NoHoles | Mean | | 882.7467 | 20.34429 | | |
| | | | | 95% Confidence Interval for Mean | Lower Bound | 830.4500 | | | |
| | | | | | Upper Bound | 935.0433 | | | |
| | | | | 5% Trimmed Mean | | 883.4230 | | | |
| | | | | Median | | 874.9950 | | | |
| | | | | Variance | | 2483.342 | | | |
| Std. Deviation | | | | 49.83314 | | | | | |
| Minimum | | | | 804.01 | | | | | |
| Maximum | | | | 949.31 | | | | | |
| Range | | | | 145.30 | | | | | |
| Interquartile Range | | | | 73.97 | | | | | |
| Skewness | | | | -.332 | .845 | | | | |
| Kurtosis | | | | .605 | 1.741 | | | | |
| HybSYK2.7mm | HybSYK2.7mm | | | Mean | | 795.9117 | 15.17856 | | |
| | | | | 95% Confidence Interval for Mean | Lower Bound | 756.8939 | | | |
| | | | | | Upper Bound | 834.9294 | | | |
| | | | | 5% Trimmed Mean | | 795.7174 | | | |
| | | | | Median | | 796.9550 | | | |
| | | | | Variance | | 1382.332 | | | |
| | | | Std. Deviation | | 37.17973 | | | | |
| | | | Minimum | | 752.65 | | | | |
| | | | Maximum | | 842.67 | | | | |
| | | | Range | | 90.02 | | | | |
| | | | Interquartile Range | | 78.88 | | | | |
| | | | Skewness | | -.014 | .845 | | | |
| | | | Kurtosis | | -1.706 | 1.741 | | | |
| | | | HybSYK3.5MM | HybSYK3.5MM | Mean | | 794.5850 | 11.10515 | |
| | | | | | 95% Confidence Interval for Mean | Lower Bound | 766.0383 | | |
| | | | | | | Upper Bound | 823.1317 | | |
| | | | | | 5% Trimmed Mean | | 793.8333 | | |
| | | | | | Median | | 791.8050 | | |
| | | | | | Variance | | 739.946 | | |
| Std. Deviation | | | | | 27.20195 | | | | |
| Minimum | | | | | 763.69 | | | | |
| Maximum | | | | | 839.01 | | | | |
| Range | | | | | 75.32 | | | | |
| Interquartile Range | | | | | 47.36 | | | | |
| Skewness | | | | | .736 | .845 | | | |
| Kurtosis | | | | | .318 | 1.741 | | | |

| Energy-to-failure [Nmm] | NoHoles | Mean | 13187.9600 | 960.62158 |
|----------------------------------|-------------|------|-------------|-----------|
| 95% Confidence Interval for Mean | Lower Bound | | 10718.6036 | |
| | Upper Bound | | 15657.3164 | |
| 5% Trimmed Mean | | | 13152.5383 | |
| Median | | | 13180.6900 | |
| Variance | | | 5536762.944 | |
| Std. Deviation | | | 2353.03271 | |
| Minimum | | | 10577.51 | |
| Maximum | | | 16436.00 | |
| Range | | | 5858.49 | |
| Interquartile Range | | | 4763.15 | |
| Skewness | | | .170 | .845 |
| Kurtosis | | | -1.449 | 1.741 |
| | HybSYK2.7mm | Mean | 3662.0567 | 275.31689 |
| 95% Confidence Interval for Mean | Lower Bound | | 2954.3321 | |
| | Upper Bound | | 4369.7813 | |
| 5% Trimmed Mean | | | 3619.2180 | |
| Median | | | 3416.9700 | |
| Variance | | | 454796.323 | |
| Std. Deviation | | | 674.38589 | |
| Minimum | | | 3128.21 | |
| Maximum | | | 4967.00 | |
| Range | | | 1838.79 | |
| Interquartile Range | | | 814.91 | |
| Skewness | | | 1.934 | .845 |
| Kurtosis | | | 3.950 | 1.741 |
| | HybSYK3.5mm | Mean | 3418.5755 | 193.86157 |
| 95% Confidence Interval for Mean | Lower Bound | | 2920.2385 | |
| | Upper Bound | | 3916.9125 | |
| 5% Trimmed Mean | | | 3418.2371 | |
| Median | | | 3512.1150 | |
| Variance | | | 225493.861 | |
| Std. Deviation | | | 474.86194 | |
| Minimum | | | 2858.29 | |
| Maximum | | | 3984.95 | |
| Range | | | 1126.66 | |
| Interquartile Range | | | 977.06 | |
| Skewness | | | -.312 | .845 |
| Kurtosis | | | -1.845 | 1.741 |

Table 37: Descriptive statistics for each variable of each tested groups. Mean value and standard deviation are highlighted

| Ranks | | | | |
|-------------------------|-------------|-----------|--------------|-------|
| Group | N | Mean Rank | Sum of Ranks | |
| Energy-to-failure [Nmm] | NoHoles | 6 | 9.50 | 57.00 |
| | HybSYK2.7mm | 6 | 3.50 | 21.00 |
| Total | 12 | | | |

| Test Statistics ^a | | | | Energy-to-failure [Nmm] |
|--------------------------------|------|-------------------------|-------------|-------------------------|
| Mann-Whitney U | | | | .000 |
| Wilcoxon W | | | | 21.000 |
| Z | | | | -2.882 |
| Asymp. Sig. (2-tailed) | | | | .004 |
| Exact Sig. [2*(1-tailed Sig.)] | | | | .002 ^b |
| Monte Carlo Sig. (2-tailed) | Sig. | | | .002 ^c |
| | | 95% Confidence Interval | Lower Bound | .001 |
| | | | Upper Bound | .003 |
| Monte Carlo Sig. (1-tailed) | Sig. | | | .001 ^c |
| | | 95% Confidence Interval | Lower Bound | .000 |
| | | | Upper Bound | .001 |

a. Grouping Variable: Group
 b. Not corrected for ties.
 c. Based on 10000 sampled tables with starting seed 624387341.

| Ranks | | | | |
|-------------------------|-------------|-----------|--------------|-------|
| Group | N | Mean Rank | Sum of Ranks | |
| Energy-to-failure [Nmm] | NoHoles | 6 | 9.50 | 57.00 |
| | HybSYK3.5MM | 6 | 3.50 | 21.00 |
| Total | 12 | | | |

| Test Statistics ^a | | | | Energy-to-failure [Nmm] |
|--------------------------------|------|-------------------------|-------------|-------------------------|
| Mann-Whitney U | | | | .000 |
| Wilcoxon W | | | | 21.000 |
| Z | | | | -2.882 |
| Asymp. Sig. (2-tailed) | | | | .004 |
| Exact Sig. [2*(1-tailed Sig.)] | | | | .002 ^b |
| Monte Carlo Sig. (2-tailed) | Sig. | | | .003 ^c |
| | | 95% Confidence Interval | Lower Bound | .002 |
| | | | Upper Bound | .003 |
| Monte Carlo Sig. (1-tailed) | Sig. | | | .002 ^c |
| | | 95% Confidence Interval | Lower Bound | .001 |
| | | | Upper Bound | .002 |

a. Grouping Variable: Group
 b. Not corrected for ties.
 c. Based on 10000 sampled tables with starting seed 334431365.

| Ranks | | | | |
|-------------------------|-------------|-----------|--------------|-------|
| Group | N | Mean Rank | Sum of Ranks | |
| Energy-to-failure [Nmm] | HybSYK2.7mm | 6 | 6.67 | 40.00 |
| | HybSYK3.5MM | 6 | 6.33 | 38.00 |
| Total | 12 | | | |

| Test Statistics ^a | | | | Energy-to-failure [Nmm] |
|--------------------------------|------|-------------------------|-------------|-------------------------|
| Mann-Whitney U | | | | 17.000 |
| Wilcoxon W | | | | 38.000 |
| Z | | | | -.160 |
| Asymp. Sig. (2-tailed) | | | | .873 |
| Exact Sig. [2*(1-tailed Sig.)] | | | | .937 ^b |
| Monte Carlo Sig. (2-tailed) | Sig. | | | .937 ^c |
| | | 95% Confidence Interval | Lower Bound | .932 |
| | | | Upper Bound | .941 |
| Monte Carlo Sig. (1-tailed) | Sig. | | | .469 ^c |
| | | 95% Confidence Interval | Lower Bound | .459 |
| | | | Upper Bound | .479 |

a. Grouping Variable: Group
 b. Not corrected for ties.
 c. Based on 10000 sampled tables with starting seed 1502173562.

Table 38: Mann-Whitney- U Test results in regards to the parameter “ENERGY TO FAILURE”
 The p-values are highlighted in red

| Ranks | | | | |
|---------------|-------------|-----------|--------------|-------|
| Group | N | Mean Rank | Sum of Ranks | |
| Max Force [N] | NoHoles | 6 | 9.50 | 57.00 |
| | HybSYK2.7mm | 6 | 3.50 | 21.00 |
| | Total | 12 | | |

| Test Statistics ^a | | | | Max Force [N] |
|--------------------------------|-------------------------|-------------|--|-------------------|
| Mann-Whitney U | | | | .000 |
| Wilcoxon W | | | | 21.000 |
| Z | | | | -2.882 |
| Asymp. Sig. (2-tailed) | | | | .004 |
| Exact Sig. [2*(1-tailed Sig.)] | | | | .002 ^b |
| Monte Carlo Sig. (2-tailed) | Sig. | | | .002 ^c |
| | 95% Confidence Interval | Lower Bound | | .001 |
| | | Upper Bound | | .003 |
| Monte Carlo Sig. (1-tailed) | Sig. | | | .001 ^c |
| | 95% Confidence Interval | Lower Bound | | .000 |
| | | Upper Bound | | .001 |

a. Grouping Variable: Group
 b. Not corrected for ties.
 c. Based on 10000 sampled tables with starting seed 112562564.

| Ranks | | | | |
|---------------|-------------|-----------|--------------|-------|
| Group | N | Mean Rank | Sum of Ranks | |
| Max Force [N] | NoHoles | 6 | 9.50 | 57.00 |
| | HybSYK3.5MM | 6 | 3.50 | 21.00 |
| | Total | 12 | | |

| Test Statistics ^a | | | | Max Force [N] |
|--------------------------------|-------------------------|-------------|--|-------------------|
| Mann-Whitney U | | | | .000 |
| Wilcoxon W | | | | 21.000 |
| Z | | | | -2.882 |
| Asymp. Sig. (2-tailed) | | | | .004 |
| Exact Sig. [2*(1-tailed Sig.)] | | | | .002 ^b |
| Monte Carlo Sig. (2-tailed) | Sig. | | | .002 ^c |
| | 95% Confidence Interval | Lower Bound | | .001 |
| | | Upper Bound | | .003 |
| Monte Carlo Sig. (1-tailed) | Sig. | | | .001 ^c |
| | 95% Confidence Interval | Lower Bound | | .001 |
| | | Upper Bound | | .002 |

a. Grouping Variable: Group
 b. Not corrected for ties.
 c. Based on 10000 sampled tables with starting seed 221623949.

| Ranks | | | | |
|---------------|-------------|-----------|--------------|-------|
| Group | N | Mean Rank | Sum of Ranks | |
| Max Force [N] | HybSYK2.7mm | 6 | 7.17 | 43.00 |
| | HybSYK3.5MM | 6 | 5.83 | 35.00 |
| | Total | 12 | | |

| Test Statistics ^a | | | | Max Force [N] |
|--------------------------------|-------------------------|-------------|--|-------------------|
| Mann-Whitney U | | | | 14.000 |
| Wilcoxon W | | | | 35.000 |
| Z | | | | -.641 |
| Asymp. Sig. (2-tailed) | | | | .522 |
| Exact Sig. [2*(1-tailed Sig.)] | | | | .539 ^b |
| Monte Carlo Sig. (2-tailed) | Sig. | | | .539 ^c |
| | 95% Confidence Interval | Lower Bound | | .576 |
| | | Upper Bound | | .595 |
| Monte Carlo Sig. (1-tailed) | Sig. | | | .293 ^c |
| | 95% Confidence Interval | Lower Bound | | .284 |
| | | Upper Bound | | .302 |

a. Grouping Variable: Group
 b. Not corrected for ties.
 c. Based on 10000 sampled tables with starting seed 303130861.

**Table 39: Mann-Whitney- U Test results in regards to the parameter “MAX FORCE”
 The p-values are highlighted in red**

| Ranks | | | | |
|-----------------------|-------------|-----------|--------------|-------|
| Group | N | Mean Rank | Sum of Ranks | |
| Max Displacement [mm] | NoHoles | 6 | 9.50 | 57.00 |
| | HybSYK2.7mm | 6 | 3.50 | 21.00 |
| Total | | 12 | | |

| Test Statistics ^a | | | | Max Displacement [mm] |
|--------------------------------|------|-------------------------|-------------|-----------------------|
| Mann-Whitney U | | | | .000 |
| Wilcoxon W | | | | 21.000 |
| Z | | | | -2.882 |
| Asymp. Sig. (2-tailed) | | | | .004 |
| Exact Sig. [2*(1-tailed Sig.)] | | | | .002 ^b |
| Monte Carlo Sig. (2-tailed) | Sig. | | | .002 ^c |
| | | 95% Confidence Interval | Lower Bound | .001 |
| | | | Upper Bound | .003 |
| Monte Carlo Sig. (1-tailed) | Sig. | | | .001 ^c |
| | | 95% Confidence Interval | Lower Bound | .001 |
| | | | Upper Bound | .002 |

a. Grouping Variable: Group
b. Not corrected for ties.
c. Based on 10000 sampled tables with starting seed 92208573.

| Ranks | | | | |
|-----------------------|-------------|-----------|--------------|-------|
| Group | N | Mean Rank | Sum of Ranks | |
| Max Displacement [mm] | NoHoles | 6 | 9.50 | 57.00 |
| | HybSYK3.5MM | 6 | 3.50 | 21.00 |
| Total | | 12 | | |

| Test Statistics ^a | | | | Max Displacement [mm] |
|--------------------------------|------|-------------------------|-------------|-----------------------|
| Mann-Whitney U | | | | .000 |
| Wilcoxon W | | | | 21.000 |
| Z | | | | -2.882 |
| Asymp. Sig. (2-tailed) | | | | .004 |
| Exact Sig. [2*(1-tailed Sig.)] | | | | .002 ^b |
| Monte Carlo Sig. (2-tailed) | Sig. | | | .003 ^c |
| | | 95% Confidence Interval | Lower Bound | .002 |
| | | | Upper Bound | .004 |
| Monte Carlo Sig. (1-tailed) | Sig. | | | .001 ^c |
| | | 95% Confidence Interval | Lower Bound | .001 |
| | | | Upper Bound | .002 |

a. Grouping Variable: Group
b. Not corrected for ties.
c. Based on 10000 sampled tables with starting seed 1335104164.

| Ranks | | | | |
|-----------------------|-------------|-----------|--------------|-------|
| Group | N | Mean Rank | Sum of Ranks | |
| Max Displacement [mm] | HybSYK2.7mm | 6 | 6.83 | 41.00 |
| | HybSYK3.5MM | 6 | 6.17 | 37.00 |
| Total | | 12 | | |

| Test Statistics ^a | | | | Max Displacement [mm] |
|--------------------------------|------|-------------------------|-------------|-----------------------|
| Mann-Whitney U | | | | 16.000 |
| Wilcoxon W | | | | 37.000 |
| Z | | | | -.320 |
| Asymp. Sig. (2-tailed) | | | | .749 |
| Exact Sig. [2*(1-tailed Sig.)] | | | | .818 ^b |
| Monte Carlo Sig. (2-tailed) | Sig. | | | .823 ^c |
| | | 95% Confidence Interval | Lower Bound | .815 |
| | | | Upper Bound | .830 |
| Monte Carlo Sig. (1-tailed) | Sig. | | | .412 ^c |
| | | 95% Confidence Interval | Lower Bound | .402 |
| | | | Upper Bound | .421 |

a. Grouping Variable: Group
b. Not corrected for ties.
c. Based on 10000 sampled tables with starting seed 329836257.

Table 40: Mann-Whitney- U Test results in regards to the parameter “MAX DISPLACEMENT”
The p-values are highlighted in red

| Ranks | | | | |
|------------------|-------------|-----------|--------------|-------|
| Group | N | Mean Rank | Sum of Ranks | |
| Stiffness [N/mm] | NoHoles | 6 | 9.17 | 55.00 |
| | HybSYK2.7mm | 6 | 3.83 | 23.00 |
| Total | 12 | | | |

| Test Statistics ^a | | | | Stiffness [N/mm] |
|--------------------------------|------|-------------------------|-------------|-------------------|
| Mann-Whitney U | | | | 2.000 |
| Wilcoxon W | | | | 23.000 |
| Z | | | | -2.562 |
| Asymp. Sig. (2-tailed) | | | | .010 |
| Exact Sig. [2*(1-tailed Sig.)] | | | | .009 ^b |
| Monte Carlo Sig. (2-tailed) | Sig. | | | .008 ^c |
| | | 95% Confidence Interval | Lower Bound | .007 |
| | | | Upper Bound | .010 |
| Monte Carlo Sig. (1-tailed) | Sig. | | | .005 ^c |
| | | 95% Confidence Interval | Lower Bound | .003 |
| | | | Upper Bound | .006 |

a. Grouping Variable: Group
 b. Not corrected for ties.
 c. Based on 10000 sampled tables with starting seed 1535910591.

| Ranks | | | | |
|------------------|-------------|-----------|--------------|-------|
| Group | N | Mean Rank | Sum of Ranks | |
| Stiffness [N/mm] | NoHoles | 6 | 9.17 | 55.00 |
| | HybSYK3.5MM | 6 | 3.83 | 23.00 |
| Total | 12 | | | |

| Test Statistics ^a | | | | Stiffness [N/mm] |
|--------------------------------|------|-------------------------|-------------|-------------------|
| Mann-Whitney U | | | | 2.000 |
| Wilcoxon W | | | | 23.000 |
| Z | | | | -2.562 |
| Asymp. Sig. (2-tailed) | | | | .010 |
| Exact Sig. [2*(1-tailed Sig.)] | | | | .009 ^b |
| Monte Carlo Sig. (2-tailed) | Sig. | | | .008 ^c |
| | | 95% Confidence Interval | Lower Bound | .006 |
| | | | Upper Bound | .009 |
| Monte Carlo Sig. (1-tailed) | Sig. | | | .004 ^c |
| | | 95% Confidence Interval | Lower Bound | .003 |
| | | | Upper Bound | .005 |

a. Grouping Variable: Group
 b. Not corrected for ties.
 c. Based on 10000 sampled tables with starting seed 1993510611.

| Ranks | | | | |
|------------------|-------------|-----------|--------------|-------|
| Group | N | Mean Rank | Sum of Ranks | |
| Stiffness [N/mm] | HybSYK2.7mm | 6 | 6.67 | 40.00 |
| | HybSYK3.5MM | 6 | 6.33 | 38.00 |
| Total | 12 | | | |

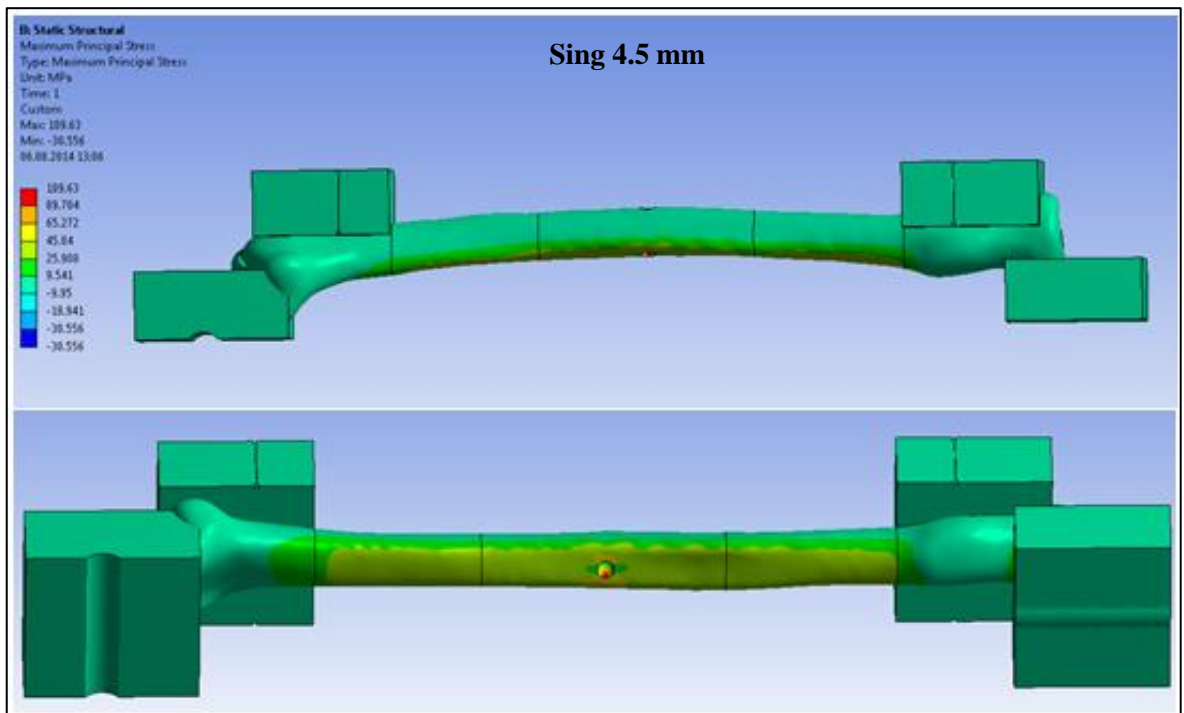
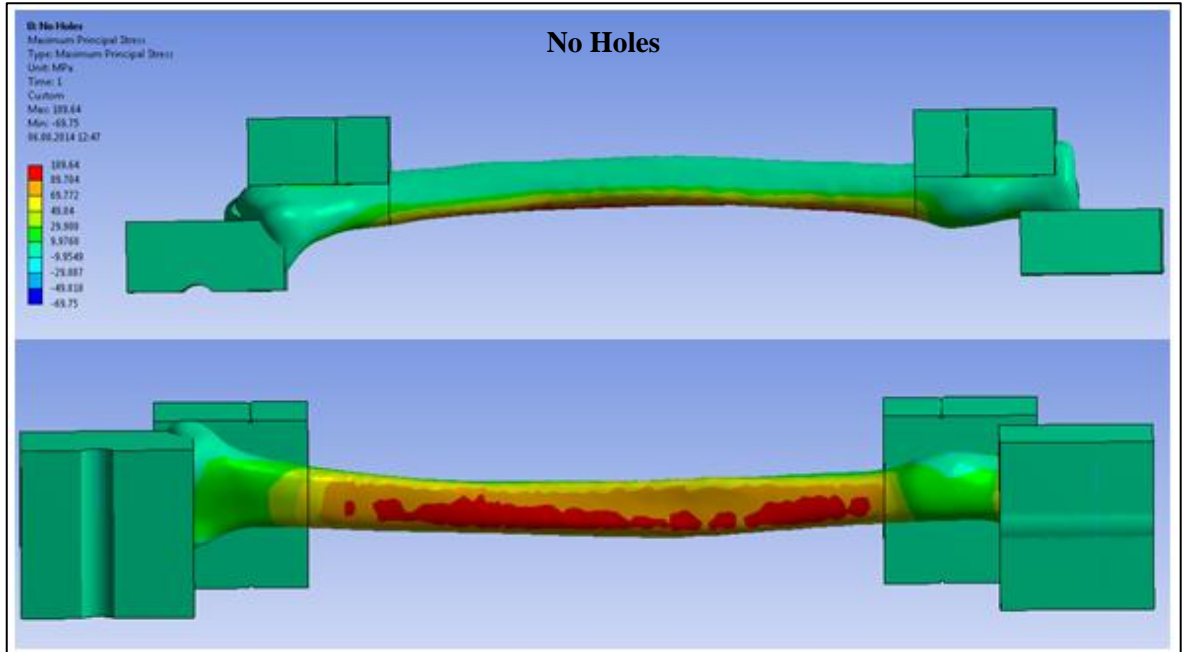
| Test Statistics ^a | | | | Stiffness [N/mm] |
|--------------------------------|------|-------------------------|-------------|-------------------|
| Mann-Whitney U | | | | 17.000 |
| Wilcoxon W | | | | 38.000 |
| Z | | | | -.160 |
| Asymp. Sig. (2-tailed) | | | | .873 |
| Exact Sig. [2*(1-tailed Sig.)] | | | | .937 ^b |
| Monte Carlo Sig. (2-tailed) | Sig. | | | .941 ^c |
| | | 95% Confidence Interval | Lower Bound | .936 |
| | | | Upper Bound | .946 |
| Monte Carlo Sig. (1-tailed) | Sig. | | | .477 ^c |
| | | 95% Confidence Interval | Lower Bound | .467 |
| | | | Upper Bound | .486 |

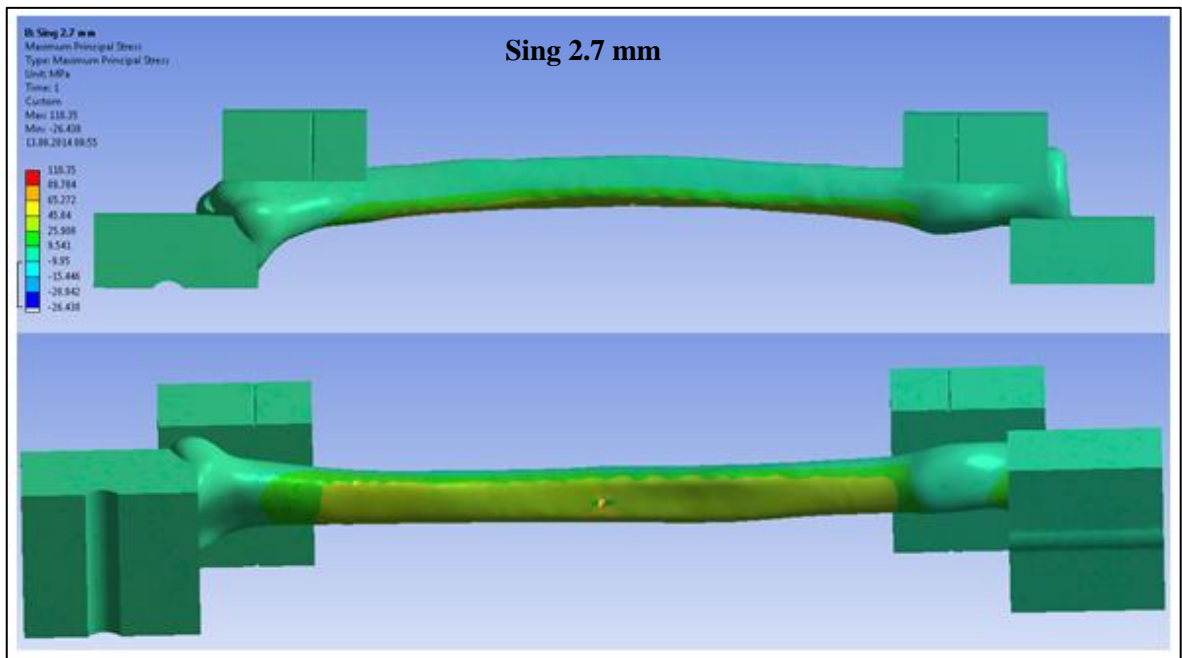
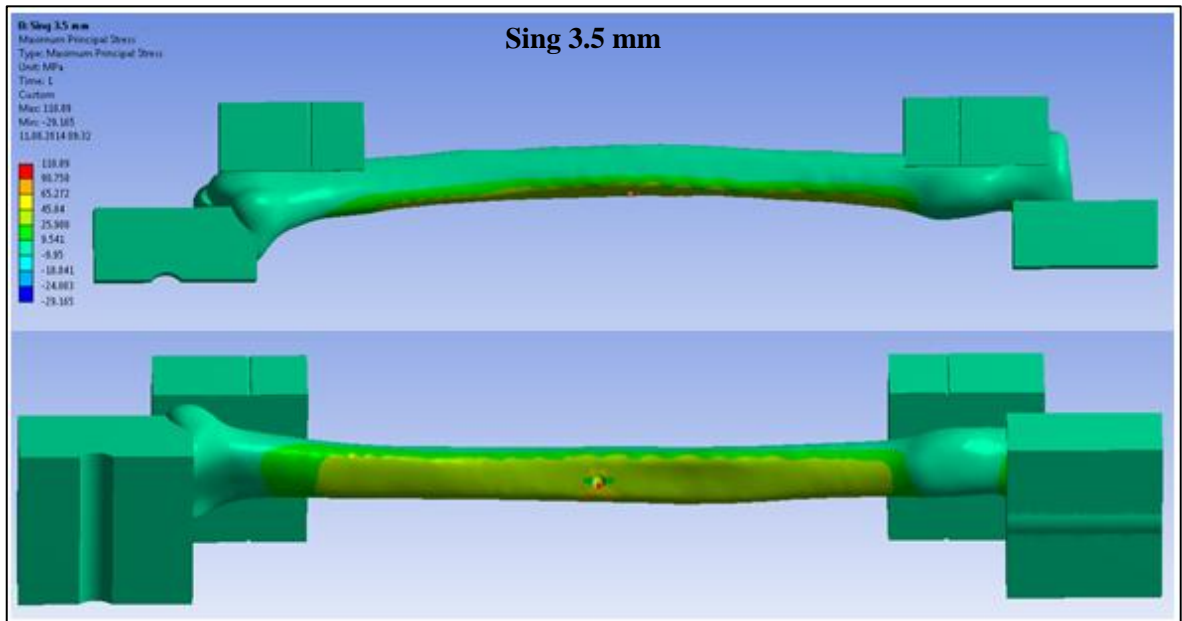
a. Grouping Variable: Group
 b. Not corrected for ties.
 c. Based on 10000 sampled tables with starting seed 1241531719.

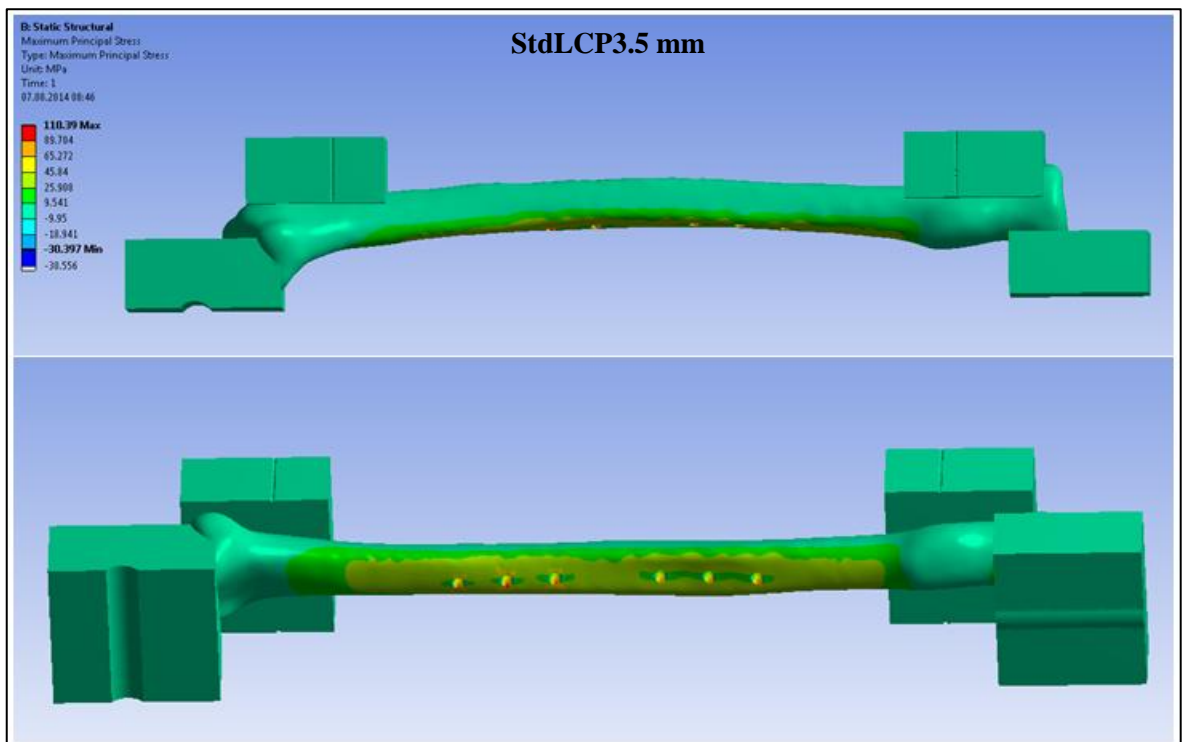
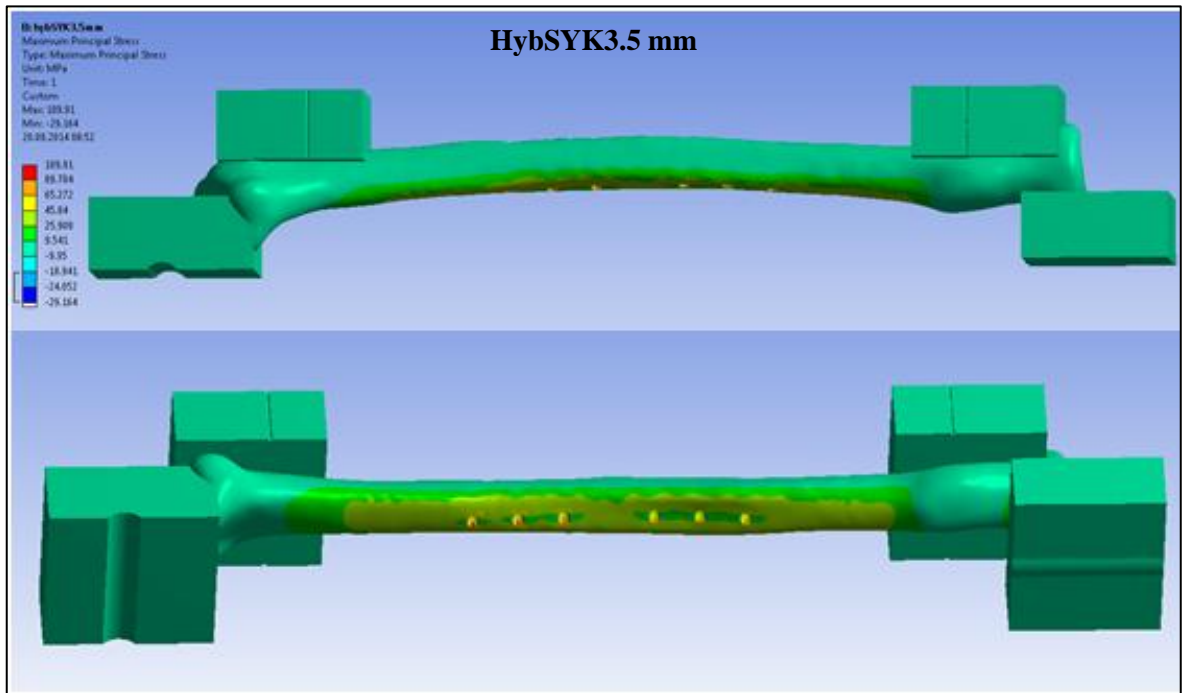
Table 41: Mann-Whitney- U Test results in regards to the parameter “STIFFNESS”
The p-values are highlighted in red

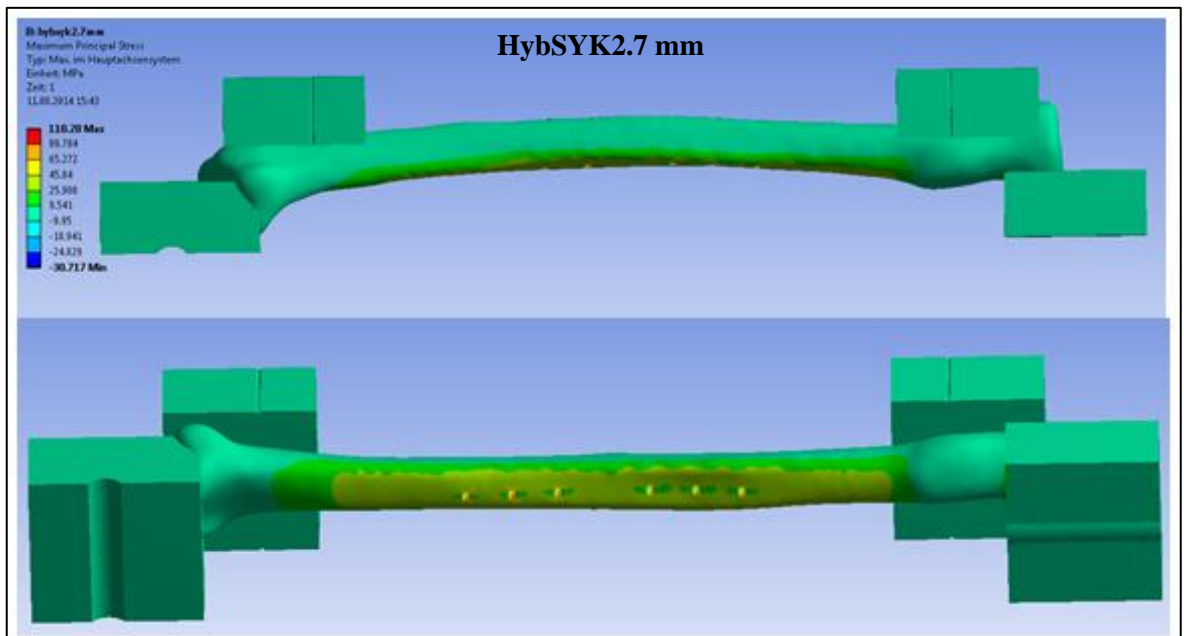
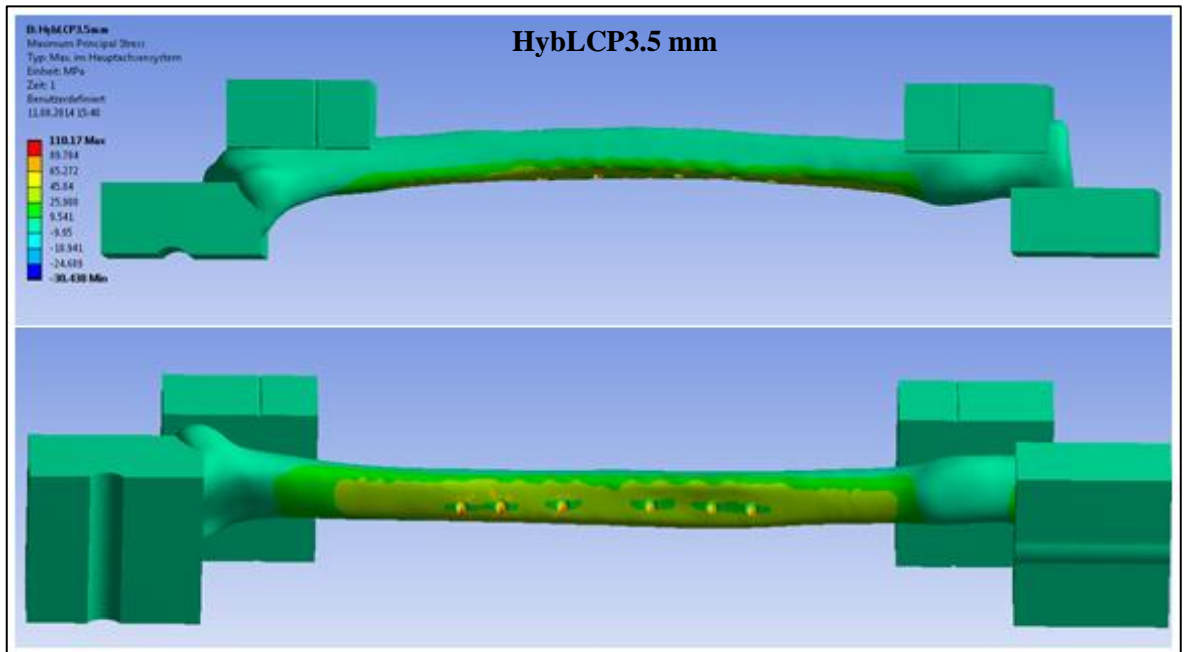
Attachment 6

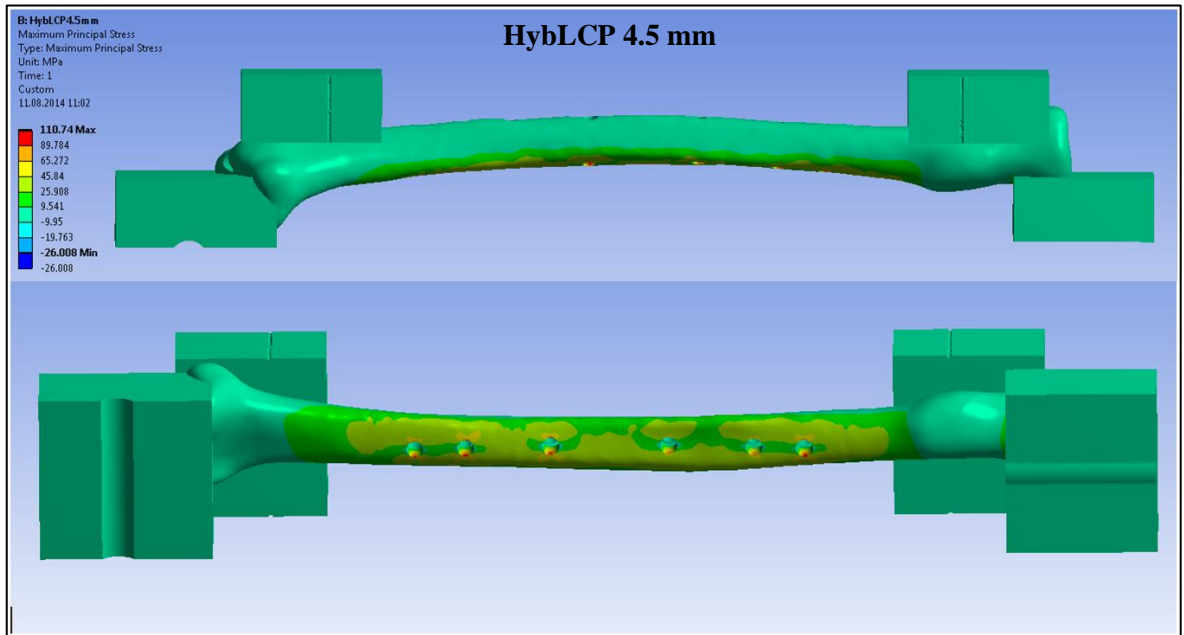
Computational Outputs











Bibliography

- [1] E. Marieb, J. Mallatt and P. Wilhelm, "Human Anatomy (5th ed.)", San Francisco: Pearson Benjamin Cummings, 2008.
- [2] T. White and P. Folkens, "The human bone manual", Elsevier, 2005.
- [3] A. Halim, "Human Anatomy: Volume I: Upper Limb And Thorax", I. K. International Pvt Ltd, 2008.
- [4] C. Clemente, "Anatomy: A Regional Atlas of the Human Body (5th ed.)", Philadelphia: Lippincott Williams & Wilkins, 2007.
- [5] J. Shaaban, G. giakas, M. Bolton, R. Williams, L. S. P. Wicks and C. Lees, "The load bearing characteristics of the forearm: pattern of axial and bending force transmitted through ulna and radius," *Journal of hand surgery*, Vols. 31-B, no. 3, pp. 274-279, 2006.
- [6] N. V. Kulkarni, "Clinical Anatomy for Students: Problem Solving Approach", Jaypee Brothers, 2007.
- [7] P. La Stayo and M. Lee, "The forearm complex: Anatomy, biomechanics and clinical considerationsJ," *Journal of hand therapy*, vol. 19, pp. 137-145, 2006.
- [8] "Collection of anatomical images and fracture radiographies - www.quizlet.com," 2014. [Online]. [Accessed 11 June 2014].
- [9] H. Gray, "Gray's Anatomy of the human body", Philadelphia: Les & Febiger, 1918.
- [10] A. Rumian, "Elbow Anatomy - www.shoulderandelbowspecialist.co.uk -," [Online]. [Accessed 25 06 2014].
- [11] "Anatomical images collection - www.studyblue.com," 2014. [Online]. [Accessed 10 June 2014].
- [12] P. Tsai and N. Pakasima, "The distal radioulnar joint," *Bulletin of the NYU hospital for joint diseases*, vol. 67, no. 1, pp. 90-96, 2009.
- [13] Department of Radiology University of Medicine - Washington , "www.rad.washington.edu," [Online]. [Accessed 10 June 2014].
- [14] W. Platzer, "Color Atlas of human anatomy, Vol1: Locomotor system", Thieme, 2004.
- [15] E. van Oudenaarde and R. A. Oostendorp, "Functional relationship between the abductor pollicis longus and abductor pollicis brevis muscles: an EMG analysis," *J. Anat*, vol. 186 (Pt 3), p. 509–515, 1995.
- [16] "Muscle images - www.kenhub.com," [Online]. [Accessed 2014 June 11].
- [17] D. Slutski and A. Osterman, *Fractures and Injuries to the Distal Radius and Carpus*, Saunders, 2008.
- [18] B. Pereira, "Biomechanics of forearm stabilisers," in *Ph.D Thesis*, 2004.
- [19] S. Marshall and B. Browner, "Sabiston textbook of surgery: the biological basis of modern surgical practice", Elsevier, 2012.
- [20] T. Rüedi and W. Murphy, "AO principles of fracture management", Thieme, 2000.

- [21] Orthopaedic trauma association committee for coding and classification, "'Fracture and dislocation compendium'," *Journal of Orthopaedic Trauma*, vol. 10, pp. v-ix, 1996.
- [22] J. Kellam and L. Audigè, "Fracture classification - www.aofoundation.org," [Online].
- [23] R. Bucholz, J. Heckman, C. Court-Brown and P. Tornetta, "Rockwood and Green's Fractures in Adults", 2009.
- [24] Journal of Orthopaedic Trauma, "Number 10 Supplement," *Journal of Orthopaedic Trauma*, vol. 21, pp. S23-S26, 2007.
- [25] D. Heim, S. Luria, R. Mosheiff and Y. Weil, "Forearm shaft fractures - www.aofoundation.org," [Online]. [Accessed 25 June 2014].
- [26] W. Black and J. Becker, "Common forearm fractures in adults," *American Family Physiscian*, vol. 80, no. 10, pp. 1096-1102, 2009.
- [27] J. Stannard, A. Schmidt and P. Gregor, "Surgical Treatment of Orthopaedic Trauma", Thieme, 2007.
- [28] P. DeLuca, R. Newington, R. Lindsey and P. Ruwe, "Refracture of bones of the forearm after the removal of compression plates," *The journal of bone and joint surgery*, vol. 70, no. 9, pp. 1372-1376, 1988.
- [29] J.-P. Wang, F.-Y. Chiu, C.-M. Chen and T.-H. Chen, "Surgical treatment of open diaphyseal fractures of both the radius and ulna," *Journal of the Chinese Medical Association*, vol. 68, no. 8, pp. 379-382, 2005.
- [30] R. Hertel, M. Pisan, S. Lambert and F. Ballmer, "Plate osteosynthesis of diaphyseal fractures of the radius and ulna," *Injury*, vol. 27, no. 8, pp. 545-548, 1996.
- [31] M. Chapmann, J. Gordon and A. Zissimos, "'Compression-plate fixation of acute fractures of the diaphyses of the radius and ulna'," *The Journal of Bone and Joint Surgery*, Vols. 71-A, no. 2, pp. 159-169, 1989.
- [32] S. Wei, C. Born, A. Abene, A. Ong and R. Hayada, "Diaphyseal forearm fractures treated with and without bone graft," *The journal of trauma: Injury, infection and critical care*, vol. 46, no. 6, pp. 1045-1048, 1999.
- [33] E. Schemitsch and R. Richards, "The effect of malunion on functional outcome after plate fixation of fractures of both bones of the forearm in adults," *Journal of bone and joint surgery*, Vols. 74-A, no. 7, pp. 1068-1078, 1992.
- [34] C. Sfeir, L. Ho, B. Doll, K. Azari and J. Hollinger, "Fracture repair," in *Bone redeneration and repair: biology and clinical application*, Humana Press, pp. 21-24.
- [35] P. Schmittenebecher, "State of the art treatment of forearm shaft fractures," *Injury*, vol. 36, pp. A25-A34, 2005.
- [36] E. Lindvall and H. Sagi, "Selective screw placement in forearm compression plating: results of 75 consecutive fractures stabilized with 4 cortices of screw fixation on either side of the fracture," *Journal of Orthopaedic Trauma*, vol. 20, no. 3, p. 157163, 2006.
- [37] M. Wagner, "General principles for the clinical use of LCP," *Injury*, vol. 34, pp. B31-B42, 2003.
- [38] D. Miller and T. Goswami, "A review of locking compression plate biomechanics and their advantages as internal fixators in fracture healing," *Clinical Biomechanics*, vol. 22, pp. 1049-1062, 2007.

- [39] R. Greiwe and M. Archdeacon, "Locking plate technology," *Journal of knee surgery*, vol. 20, no. 1, pp. 50-55, 2007.
- [40] S. Perren, "Evolution of the internal fixation of long bone fractures," *The Journal of bone and joint surgery*, Vols. 84-B, no. 8, pp. 1093-1110, 2002.
- [41] J. Doornink, D. Fitzpatrick, S. Boldhaus, S. Madey and M. Bottlang, "Effects of hybrid plating with locked and nonlocked screws on the strength of locked plating constructs in the osteoporotic diaphysis," *The journal of trauma injury, infection and critical care*, vol. 69, no. 2, pp. 411-417, 2010.
- [42] Stryker Trauma & Extremities, *VariAx Compression plating system - Operative Technique*.
- [43] M. Müller, M. Allgöwer, R. Schneider und H. Willenegger, *Manula of internal fixation*, Springer, 1995.
- [44] "Collection of Orthopaedical Implants - www.orthopedic-implants.net -," [Online]. [Accessed 4 07 2014].
- [45] L. Anderson, D. Sisk, R. Tooms and W. Park, "Compression-plate fixation in acute diaphyseal fractures of the radius and ulna," *Journal of Bone and Joint Surgery*, Vols. 57-A, no. 3, pp. 287-297, 1975.
- [46] K. Egol, K. Koval and J. Zuckerman, "Handbook of fractures", Lippincott Williams & Wilkins, 2010.
- [47] A. ElMaraghy, M. ElMaraghy, M. Nousiainen, R. Richards and H. Schemitsch, "Influence of the number of cortices on the stiffness of plate fixation of diaphyseal fractures," *Journal of Orthopaedic Trauma*, vol. 15, no. 3, pp. 186-191, 2001.
- [48] W. Eglseder, L. Jasper, C. Davis and S. Belkoff, "A biomechanical evaluation of lateral plating of distal radial shaft fractures," *The Journal of hand surgery*, vol. 28A, no. 6, pp. 959-963, 2003.
- [49] S. Hidaka and R. Gustillo, "Refracture of the forearm after plate removal," *Journal of Bone and Joint Surgery*, Vols. 66-A, no. 8, pp. 1241-1243, 1984.
- [50] J. Rosson and J. Shearer, "Refracture after the removal of plates from the forearm," *Journal of bone and joint surgery*, Vols. 73-B, no. 3, p. 415-417, 1991.
- [51] K. Rumball and M. Finnegan, "Refracture after forearm plate removal," *Journal of Orthopaedic Trauma*, vol. 4, no. 2, pp. 124-129, 1990.
- [52] R. Sanders, G. Haidukewych, T. Milne, J. Dennis and L. Latta, "Minimal versus maximal plate fixation techniques of the ulna: the biomechanical effect of number of screws and plate length," *Journal of orthopaedic trauma*, vol. 16, no. 3, pp. 166-171, 2002.
- [53] s. M. Nasab, N. Sarrafan and S. Sabahi, "Four-screw fixation vs conventional fixation for diaphyseal fractures of the forearm," *Trauma Monthly*, vol. 17, no. 1, pp. 245-249, 2012.
- [54] Stryker Trauma and Extremities, "VariAx Compression Plating System-Operative Technique".
- [55] A. Burestein, J. Currey, V. Frankel, K. Heiple, P. Lunseth and J. Vesseley, "Bone strength: the effect of screw holes," *Journal of bone and joint surgery*, Vols. 54-A, no. 6, pp. 1143-1156, 1972.
- [56] B. Johnson and L. Fallat, "The effect of screw holes on bone strength," *Journal of foot & ankle surgery*, vol. 36, no. 6, pp. 446-451, 1997.
- [57] J. Rosson, W. Murphy, C. Tonge and J. Shearer, "Healing of residual screw holes after plate

- removal," *Injury*, vol. 22, no. 5, pp. 383-384, 1991.
- [58] W. Pilkey and D. Pilkey, "Peterson's Stress concentration factors", John Wiley & sons, 2008.
- [59] "Encyclopedia - www.the freedictionary.com," [Online].
- [60] "Engineers handbook - ww.engineershandbook.net," [Online]. [Accessed 22 July 2014].
- [61] J. Rosson, J. Egan, J. Shearer and P. Monro, "Bone weakness after the removal of plates and screws. Cortical atrophy or screw holes?," *Journal of bone and joint surgery*, Vols. 73-B, no. 2, pp. 283-286, 1991.
- [62] C. Wheelers, "Wheelers textbook of orthopaedics", Duke orthopaedics, 2011.
- [63] J. Roberts, S. Grindel, B. Rebholz and M. Wang, "Biomechanical evaluation of locking plate radial shaft fixation: unicortical locking fixation versus mixed bicortical and unicortical fixation in a sawbone model," *Journal of hand surgery*, vol. 32A, no. 7, pp. 971-975, 2007.
- [64] Synthes, *Small Fragment Locking compression plate (LCP) system. Stainless steel and titanium. Technique guide*.
- [65] M. Pierce, G. Bertocci, E. Vogeley and M. Moreland, "Evaluating long bone fractures in children: a biomechanical approach with illustrative cases," *Child abuse & Neglect*, vol. 28, pp. 505-524, 2004.
- [66] M. Alms, "Fracture mechanics," *Journal of bone and joint surgery*, vol. 43B, no. 1, pp. 162-166, 1961.
- [67] D. A. Nehme, "Adult humerus fractures - www.arabbones.com -," [Online]. [Accessed 2014].
- [68] D. Stanley, I. A. Trail and A. Amis, "Biomechanics of the elbow," in *Operative Elbow Surgery*, Elsevier, 2012, pp. 29-44.
- [69] V. Frankel and M. Nordin, *Basic biomechanics of the skeletal system*, Philadelphia: Lea & Febiger, 1980.
- [70] F. Ekenstam, A. Palmer and R. Glisson, "The load on the radius and ulna in different positions of the wrist and forearm. A cadaver study," *Acta Orthopaedica Scandinavica*, vol. 55, pp. 363-365, 1984.
- [71] A. Palmer and F. Werner, "Biomechanics of the distal radioulnar joint," *Clinical orthopaedics and related research*, vol. 187, pp. 26-35, 1984.
- [72] Stryker Osteosynthesis, "TI2753/10 Biomechanical model loads on the distal radius and ulna," 2010.
- [73] M. Winemaker, S.Chinchalkar, R. Richards, J. Johnson, D. Chess and G. King, "Load relaxation and forces with activity in hoffman external fixators: a clinical study in patients with colles' fractures," *The Journal of hand surgery*, vol. 23A, no. 5, pp. 926-932, 1998.
- [74] M. Leunissen, "Biology for biological engineering - www.soe.uoguelph.ca-," [Online]. [Accessed 25 June 2014].
- [75] N. Berme, *Biomechanics of normal and pathological human articulating joints*, Kluwer, 1980.
- [76] A. Naito, Y.-J. Sun, M. Yajima, H. Fukamachi and K. Ushikoshi, "Electromyographic study of the elbow flexors and extensors in a motion of forearm pronation/supination while maintaining elbow flexion in humans," *Journal of experimental medicine*, vol. 186, pp. 267-277, 1998.
- [77] A. Amis, D.Dowson and V.Wright, "Elbow joint force predictions for some strenuous isometric actions," *Journal of Biomechanics*, vol. 13, pp. 765-775, 1980.

- [78] Y. An and R. Draughn, *Mechanical testing of bone and bone-implant interface*, CRC Press, 2000.
- [79] J. Collins, *Mechanical design of machine elements and machines*, Wiley & Sons, 2003.
- [80] G. Petrucci, "www.unipa.it/giovanni.petrucci/Disp/," 04 February 2013. [Online]. [Accessed 02 July 2014].
- [81] M. Gardner, R. Brophy, D. Campbell, A. Mahajan, T. Wright, D. Helfet and D. Lorich, "The mechanical behavior of locking compression plates compared with dynamic compression plates in a cadaver radius model," *Journal of orthopedic trauma*, vol. 19, no. 9, pp. 597-603, 2005.
- [82] CNC Speedform, "www.cnc-speedform.de," [Online]. [Accessed 02 July 2014].
- [83] Synthes, *Large fragment LCP Instrument and implant set. Part of the Synthes locking compression plate (LCP) system*.
- [84] Sawbones, "Bone materials - www.sawbones.com," [Online].
- [85] Stryker Osteosynthesis, "DQI 30-504 V1.0 - Usage of SPSS and samplepower in design verification and validation," 2010.
- [86] A. Field, *Discovering statistics using IBM SPSS statistics - 4th edition -*, Sage Publications, 2013.
- [87] G. Dhatt, G. Touzot and E. Lefrancois, *Finite element method*, Wiley, 212.
- [88] G. Pennati, *Lessons of Biomechanical Constructions - Politecnico di Milano*, 2013-2014.
- [89] Wang, E.; Nelson, T.; R.Rauch - CAD-FEM GmbH, "Back to elements - Tetrahedra vs hexaedra," Munich.
- [90] Stryker Osteosynthesis, "DQI 30-508: Bone and bone simulation materials: characteristics and use in testing".
- [91] University of Cambridge, "Mechanical properties of bone - <http://www.cam.ac.uk>," [Online]. [Accessed 22 07 2014].
- [92] University of Idaho, "Properties of Biological Materials - <http://www.uidaho.edu/>," [Online]. [Accessed 06 August 2014].
- [93] R. Narayan, *Biomedical Materials*, Springer, 2009.
- [94] M. Bureau, J. Denault and J. Legaux, "Implantable biomimetic prosthetic bone". Patent W02006074556A1.
- [95] Q.Chen, C.Zhu and G.Thouas, "Progress and challenges in biomaterials used for bone tissue engineering: bioactive glasses and elastomeric composites," *Progress in Biomaterials*, vol. 1, no. 2, pp. 1-22, 2012.
- [96] T. Keaveny, E. Morgan and O. Yeh, "Chapter 8: Bone mechanics," in *Standard handbook of biomedical engineering and design*, McGraw-Hill, 2004, pp. 8.1-8.23.
- [97] P. Vena and R. Contro, *Lessons of Computational Biomechanics 2013-2014 - Finite element method - Politecnico di Milano -*.